

**MODE OF ACTION OF TWO AUREOLIC ACID  
ANTIBIOTICS AND CHELERYTHRINE - A CHEMICAL  
BIOLOGY APPROACH**

*By*

**SHREYASI DUTTA**

**LIFE05201104001**

**Saha Institute of Nuclear Physics, Kolkata**

*A thesis submitted to the*

*Board of Studies in Life Sciences*

*In partial fulfillment of requirements*

*for the Degree of*

**DOCTOR OF PHILOSOPHY**

*of*

**HOMI BHABHA NATIONAL INSTITUTE**



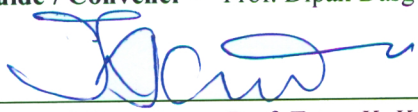





**May, 2014**

# Homi Bhabha National Institute<sup>1</sup>

## Recommendations of the Viva Voce Committee

As members of the VivaVoce Committee, we certify that we have read the dissertation prepared by **Ms. Shreyasi Dutta** entitled "Mode of action of two aureolic acid antibiotics Mithramycin and Chromomycin A3 and Chelerythrine – a chemical biology approach" and recommend that it may be accepted as fulfilling the thesis requirement for the award of Degree of Doctor of Philosophy.

	15/09/14
<b>Chairman</b> - Prof. Dipak Dasgupta	Date:
	15/09/14
<b>Guide / Convener</b> - Prof. Dipak Dasgupta	Date:
	15/9/14
<b>External Examiner</b> - Prof. Tapas K. Kundu	Date:
<b>Member 1</b> - Prof. Rahul Banerjee	Date:
	15/9/14
<b>Member 2</b> - Prof. Dhananjay Bhattacharyya	Date:
	15/9/2014
<b>Member 3</b> - Prof. Pradeep Parrack	Date:
	15-09-14

Final approval and acceptance of this thesis is contingent upon the candidate's submission of the final copies of the thesis to HBNI.

I hereby certify that I have read this thesis prepared under my direction and recommend that it may be accepted as fulfilling the thesis requirement.

Date: 15.09.2014.

Place: Kolkata

  
Guide

<sup>1</sup> This page is to be included only for final submission after successful completion of viva voce.

## **STATEMENT BY AUTHOR**

This dissertation has been submitted in partial fulfillment of requirements for an advanced degree at Homi Bhabha National Institute (HBNI) and is deposited in the Library to be made available to borrowers under rules of the HBNI.

Brief quotations from this dissertation are allowable without special permission, provided that accurate acknowledgement of source is made. Requests for permission for extended quotation from or reproduction of this manuscript in whole or in part may be granted by the Competent Authority of HBNI when in his or her judgment the proposed use of the material is in the interests of scholarship. In all other instances, however, permission must be obtained from the author.



Shreyasi Dutta

## **DECLARATION**

I, hereby declare that the investigation presented in the thesis has been carried out by me. The work is original and has not been submitted earlier as a whole or in part for a degree / diploma at this or any other Institution / University.



Shreyasi Dutta



## List of publications arising from the thesis

### Journal

#### (a) Published

1. "Spectroscopic and calorimetric approach to understand the molecular basis of self-association of aureolic acid antibiotic, Chromomycin A3", Shreyasi Dutta, Shibojyoti Lahiri and Dipak Dasgupta, *Open Journal of Biophysics*, **2014**, 4, 66-82.
2. "Association of antitumor antibiotic Mithramycin with  $Mn^{2+}$  and the potential cellular targets of Mithramycin after association with  $Mn^{2+}$ ", Shreyasi Dutta, Shibojyoti Lahiri, Amrita Banerjee, Shriya Saha and Dipak Dasgupta, *Journal of Biomolecular Structure and Dynamics*, **2014**, DOI: 0.1080/07391102.2014.887031

#### (b) Communicated

1. "Association of Chelerythrine with chromatin," Shreyasi Dutta, Amrita Banerjee, Sulagna Sanyal, Chandrima Das and Dipak Dasgupta

### Conference presentations

1. "Association of antitumor antibiotic Mithramycin and Chromomycin A3 with  $Mn^{2+}$ ", Shreyasi Dutta and Dipak Dasgupta, *Recent advances in chemical and physical biology*, 2012, Saha Institute of Nuclear Physics, Kolkata.
2. "Association of Mithramycin with essential trace element  $Cu^{2+}$  and its interaction with metalloenzymes Cu/Zn Superoxide dismutase (SOD1) and metallo  $\beta$ -Lactamase (MBL)", Shibojyoti Lahiri, Shreyasi Dutta and Dipak Dasgupta, *Recent advances in chemical and physical biology*, 2012, Saha Institute of Nuclear Physics, Kolkata.
3. "Chemical biology of the additional therapeutic potential of aureolic acid group of antibiotics", Shibojyoti Lahiri, Shreyasi Dutta, P. Grihanjali Devi, and Dipak Dasgupta, *EMBO Conference Series Chemical Biology*, 2012, EMBL Heidelberg, Germany.
4. "Association of antitumor antibiotics Mithramycin with  $Mn^{2+}$  and biological significance of the association", Shreyasi Dutta and Dipak Dasgupta, *Photosciences: Contemporary Challenges and Future Perspectives*, 2013, Jadavpur University, Kolkata.



Shreyasi Dutta

## **DEDICATION**

*I dedicate this thesis to my beloved parents without whom none of my success would be possible.*

## ACKNOWLEDGEMENTS

At the memorable moment of submitting my doctorate thesis, I take an opportunity to warmly acknowledge all those, who have inspired and motivated me throughout my journey both academically and personally. First and foremost I offer my sincere gratitude to my mentor and research supervisor Professor Dipak Dasgupta for deft guidance, valuable suggestions, constructive criticism and academic support. I sincerely acknowledge the research facility, infrastructure and funding provided by my institute, Saha Institute of Nuclear Physics. I also acknowledge CSIR, Govt. of India, for providing me fellowship to pursue my research work. I am thankful to all my doctoral committee members, Prof. Pradeep Parrack (Bose institute), Prof. Rahul Banerjee (SINP) and Prof. Dhananjay Bhattacharyya (SINP), for their careful and timely revision and valuable comments for improving the work. Thanks are also due to Prof. Milan K Sanyal, ex-Director, SINP and Prof. Bikas K Chakrabarti, Director, SINP, who gave me this opportunity to work under the patronages of this esteemed institution towards fulfillment of my degree. No task can be successful without an immediate congenial environment. I want to thank my previous and current lab members; Shibojyoti da, Parijat di, Sudipta di, Suman da, Saptarni and Amrita; for sharing numerous experiences, in experimental successes as well as troubleshooting problems, and for their friendship. A special thanks to Amrita and Saptarni for their extended unconditional help at the n<sup>th</sup> hour.

On the personal front, words are not enough to thank Baba and Ma for making me what I am. Last but not the least I would reserve my heartiest thanks for my husband, Soumya, for being my pillar of strength through thick and thin and loving me for who I am.

# CONTENTS

	<b>Page No.</b>
<b>SYNOPSIS</b>	i - xxii
<b>LIST OF FIGURES</b>	xxiii - xxix
<b>LIST OF TABLES</b>	xxx - xxxi
<b>LIST OF SCHEMES</b>	xxxii
<b>CHAPTER 1:</b> Introduction	1 - 35
<b>CHAPTER 2:</b> Difference in the ionization properties of two aureolic acid antibiotics mithramycin and chromomycin A <sub>3</sub>	36 - 54
<b>CHAPTER 3:</b> Molecular basis of self association of aureolic acid antibiotic, chromomycin A <sub>3</sub>	55 - 81
<b>CHAPTER 4:</b> Association of antitumor antibiotic mithramycin with Mn <sup>2+</sup> and the potential cellular targets of mithramycin after association with Mn <sup>2+</sup>	82 - 116
<b>CHAPTER 5:</b> Structural basis of the association of plant alkaloid chelerythrine with different DNA sequences and chromatin components	117 - 156
<b>CHAPTER 6:</b> Summary	157 - 160
<b>REFERENCES</b>	161 - 183

# Synopsis

---

## PREAMBLE:

The term ‘antibiotic’ refers to any natural/synthetic /semi synthetic compound that inhibits the growth of microorganisms. Antibiotics are specific products of metabolism, or their modifications with high physiological activity against individual groups of microorganisms (virii, bacteria, fungi, algae, protozoa) or against malignant tumors, that can selectively slow down or completely inhibit their growth [1]. Since the above definition has certain limitations e.g. it neither gives the idea, at which stage of metabolism antibiotics are formed or nor does it tell about the specificity of their activities. Therefore, we suggest the definition of antibiotic as follows: antibiotics are the final metabolic products from specific species produced below basal level in quantity and/or the synthetic analogous or modifiers with physiological activity against other cells or specific groups of microorganisms. Antibiotics could be classified on the basis of biosynthetic origin such as natural, semi synthetic, and synthetic.

Screening of natural products synthesized by microbes has led to the discovery of a number of growth-inhibiting compounds that have proved to be clinically useful in cancer chemotherapy. Many of these antibiotics bind to DNA with base specificity and inhibit one or more DNA-templated phenomena.

*Streptomyces* is known to be the largest antibiotic-producing genus [2]. The history of antibiotics derived from the genus *Streptomyces* begins with the discovery of the first antibiotic isolated from bacteria, ‘streptothricin’, in 1942. After two years ‘streptomycin’ came, this triggered systematic screening of antibiotics from this genus. The aureolic acid group of antibiotics is a family of compounds isolated from various strains of *Streptomyces sp.* The group comprises antitumor agents namely Mithramycin, Chromomycin A3, olivomycin, chromocyclo mycin, UCH9 and durhamycin [3]. The agents inhibit growth and multiplication of several tumour cell lines, and they also act on Gram-positive bacteria. Some of the members of this family have clinical applications, and they are used for the treatment of certain tumours and Paget’s bone disease.

Plants have also been extensively used in traditional medicines which have been in existence for thousands of years. World Health Organization has estimated that still approximately 80 % of the world’s inhabitants rely mainly on traditional medicines for

---

---

their primary health care. Alkaloids are nitrogen-containing secondary metabolites produced mostly by plants, fungi and bacteria [4]. The first medically useful example of an alkaloid was morphine, isolated in 1805 from the opium poppy *Papaver somniferum*. The search for anti-cancer agents from plant sources started in the 1950s with the discovery and development of the vinca alkaloids, vinblastine and vincristine. Benzo[c]phenanthridine alkaloids are a family of tetracyclic aromatic compounds, isolated mainly from the Rutaceae, Papaveraceae, and Fumariaceae plants [5]. Many of these alkaloids with isoquinoline moiety show a wide range of pharmacological properties including anti-tumor activity. The physical and molecular basis of interaction of benzophenanthridine alkaloids with nucleic acid structures have been a subject of extensive study in the recent past.

Biologically active substances from bacteria and plants provide inspiration, challenges and opportunities for the biologists including the medical community. Knowledge of their chemical properties has contributed immensely in understanding the mode of their biological action. The representative aureolic acid antibiotics Mithramycin and Chromomycin A3, isolated from bacterial sources, exert their biological actions through their ability to bind DNA. However, plant alkaloid Chelerythrine has been reported to be highly specific inhibitor of protein kinase C [6]. In this dissertation, I have investigated the chemical biology of the action of the aforementioned antibiotics.

## AIMS:

- To investigate the difference in ionisation properties of the two aureolic acid antibiotics, Mithramycin and Chromomycin A3
  - To characterize the self association of Chromomycin A3 in neutral and anionic forms
  - To study the association of antitumor antibiotic, Mithramycin, with  $Mn^{2+}$ , an essential micronutrient and the potential cellular targets after association with  $Mn^{2+}$
  - To investigate the binding of plant alkaloid Chelerythrine with DNA having different base sequences and DNA in chromatin assembly.
-

---

The broad objective of the thesis is chemical biology based approach to throw light on the mode of action of the antibiotics mentioned above.

**ORGANISATION OF THESIS:** The work embodied in this thesis is divided into the following chapters: Chapter 1 is the introduction with a comprehensive survey of the literature related to the present work. Chapter 2 contains the results describing the difference in the ionisation properties of the two aureolic acid antibiotics, Mithramycin and Chromomycin A3. Chapter 3 states the results to study the molecular basis of self-aggregation of both neutral and anionic forms of Chromomycin A3. Chapter 4 reports the association of antitumor antibiotic Mithramycin with the essential micronutrient,  $Mn^{2+}$  and the potential cellular target(s) of the resulting complex. In Chapter 5 molecular basis of the association of plant alkaloid chelerythrine with calf thymus DNA and different polynucleotides such as poly(dG-dC), poly(dA-dT), poly(dG).poly(dC) and poly(dA).poly(dT) is described. In this chapter we have also reported the association of chelerythrine with components of chromatin assembly. Chapter 6 summarizes the work and the conclusions obtained therefrom.

### **Chapter 1: Introduction**

Exploration of natural products from uncultured soil microorganisms is a branch of science which unites chemistry and biology. The attraction in this field lies in the vast diversity of unknown soil microorganism and the chemical affluence that they are thought to contain. Cultured soil microorganisms are the most common source of antibiotics and other therapeutic agents of any group of organisms [7]. The glyco-antibiotics aureolic acid family is produced by *Streptomyces* species. Aureolic acid group of antitumor antibiotics consists of mithramycin, chromomycin A3, olivomycin, chromocyclomycin, UCH9 and durhamycin [3, 8]. Structurally, the aureolic acid antibiotics belong to the family of the aromatic polyketides. All the members of the family are intense yellow in colour, hence the name ‘aureolic’. Except chromocyclomycin, all of them consist of a tricyclic chromophore with one or two aliphatic side chains (aglycone). Two representative aureolic acid antibiotics

---



Mithramycin (MTR) and Chromomycin A3 (CHR) (Figure 1) share the same aglycone moiety and differ only in some of the sugars attached to them. Initially, MTR and CHR were used for their antibiotic activity against gram-positive bacteria. But various studies with these antibiotics have proposed that they bind to DNA in presence of different bivalent metal

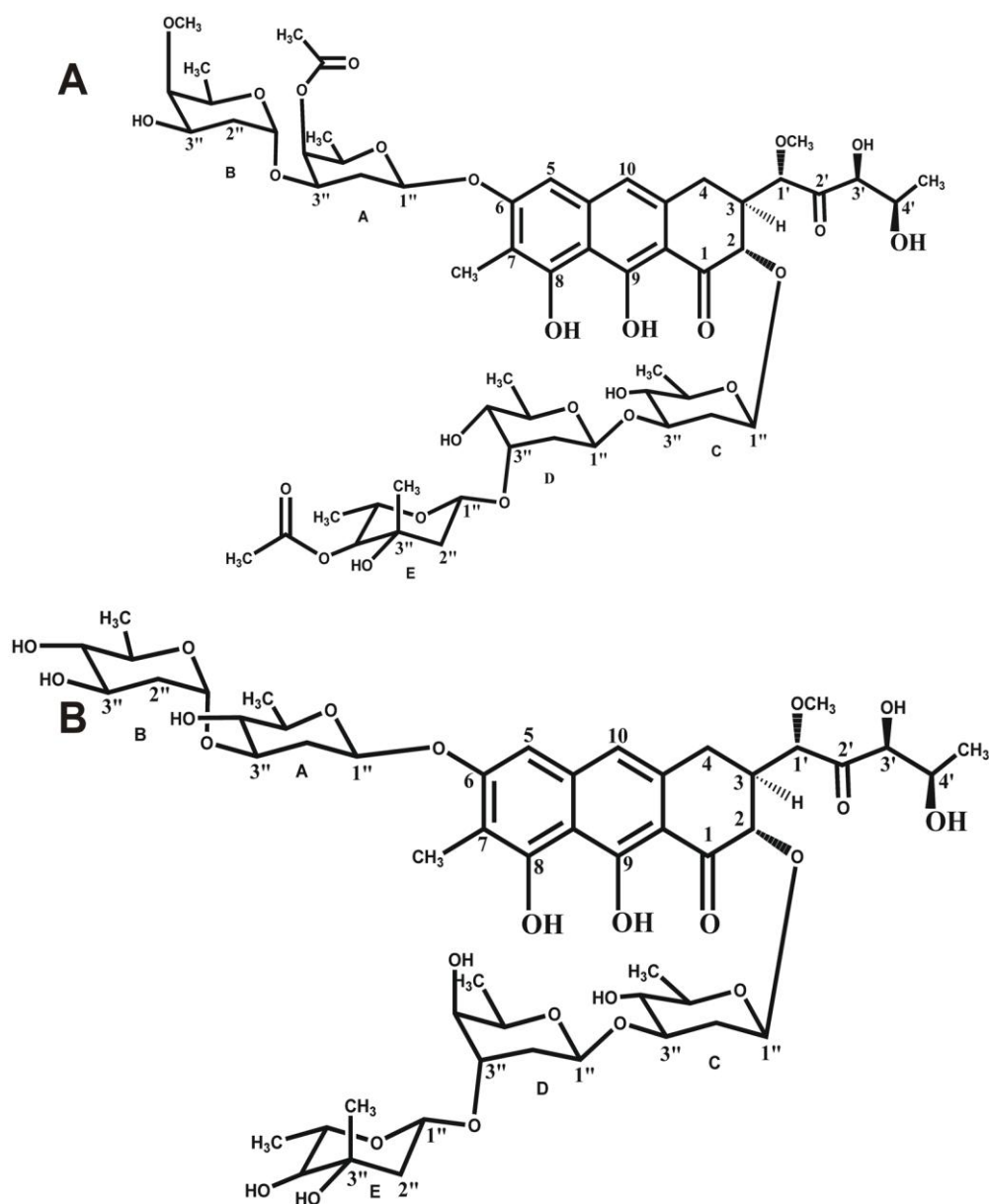


**Figure 1. Chemical Structures of antibiotics (A) Structure of Chromomycin A3 (B) Structure of Mithramycin**

ions, like  $\text{Mg}^{2+}$ ,  $\text{Zn}^{2+}$ ,  $\text{Ni}^{2+}$ ,  $\text{Co}^{2+}$ ,  $\text{Fe}^{2+}$  [9, 10]. Thus they inhibit DNA-dependent RNA synthesis both *in vivo* and *in vitro* via reversible interaction with (G.C)-rich DNA. Metal ions play a key role in the actions of aureolic acid antibiotics. Research has shown significant progress in utilization of transition metal complexes as drugs to treat variety of diseases and disorders. It is well established that manganese ( $\text{Mn}^{2+}$ ) is an important trace element required by all organisms in various cellular processes, including metabolism and oxidative stress defense. We have examined  $\text{Mn}^{2+}$  binding property of Mithramycin (MTR) to study the possibility of using it in conditions of hypermanganism [11].

Plants are sources of diverse phytochemicals, classified into various families such as alkaloids, flavinoids and isothiocyanates, with potential medicinal properties. Alkaloids are nitrogen containing bases found mainly in plants, but also to a lesser extent in microorganism and animals. They consist of one or more nitrogen atoms in the heterocyclic ring, usually as primary, secondary, or tertiary amines. Presence of amine group confers basicity to the alkaloids. Benzo[c]phenanthridine alkaloids are a family of tetracyclic aromatic compounds, isolated mainly from the Rutaceae, Papaveraceae, and Fumariaceae plants. This group of alkaloids possesses potent anticancer and antimicrobial properties. The benzo[c]phenanthridines have interesting structure with an isoquinoline part. Chelerythrine is a benzo[c]phenanthridine alkaloid isolated from an herb called greater celandine (*Chelidonium majus*) [5]. It has been used as an inhibitor of protein kinase C (PKC) for many years. Chelerythrine is believed to be a potential anticancer agent but its mechanism of action has not been fully elucidated. The potential anticancer activities of chelerythrine may be attributed to its binding to chromosomal DNA. In this thesis we have characterized the association of Chelerythrine with various sequences of template DNA and chromatin assembly by employing spectroscopic and calorimetric techniques.

---

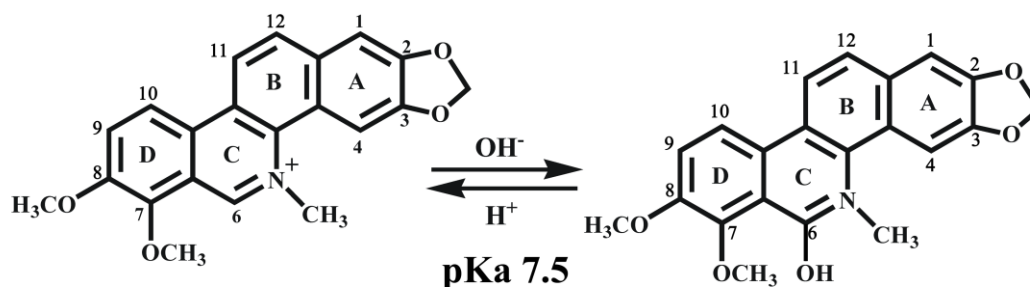


**Figure 2.** Chemical structures of cationic and neutral forms of Chelerythrine

## **Chapter 2: Difference in the ionisation properties of two aureolic acid antibiotics**

### **Mithramycin and Chromomycin A3**

#### **Background:**

Mithramycin and Chromomycin A3 have similar structures with identical tricyclic chromophore in which a 5 member aliphatic side chain is attached to C3 position and a methyl group to C7 position. In both antibiotics a trisaccharide and a disaccharide moiety is attached at C2 and C6 positions, respectively. In spite of the same core chromomycinone ring with the structurally identical aglycone moiety (Figure 1), the ionization constants of the two antibiotics, CHR and MTR, differ by two units. MTR has the reported  $pK_a$  of 5.0, while CHR has a  $pK_a$  of 7.0 [9, 12].

#### **Objective:**

It is interesting from the chemical perspective to know the basis of such difference in ionizations constants. In this chapter, we have adopted spectroscopic approaches such as different optical and NMR techniques to probe the difference. This has been supplemented with isothermal titration calorimetry to throw light upon the energetic aspect of the difference.

#### **Results:**

1. I have monitored the ionization profiles of hydroxyl groups present in C8 and C9 positions by means of optical spectroscopic methods such as absorbance, fluorescence

---

and CD. A plot of emission intensity at 540 nm ( $F_{540}$ ) versus pH gives the  $pK_a$  values of MTR and CHR as 5.5 and 7.0, respectively (Figure 3).

2. Notable differences are obtained in absorption spectrum of MTR and CHR, like hypochromicity and red-shift over the entire pH range. Below pH 5.0 the spectra have broad peaks and are red shifted. On the other hand, spectra at and above pH 5.0 are characterized by an isosbestic point.

3. At pH 8.0, MTR and CHR have two exciton coupling-type CD bands at 285 nm and 435 nm, while CD spectra of MTR and CHR at pH 3.0 are radically different (Figure 4). For MTR, there is an exciton coupling- type split CD bands with very low ellipticity value at ~315 nm and a broad band at ~ 415 nm. In case of CHR, two bands with lower ellipticity value were observed at 287 nm and 440 nm at pH 3.0. Due to protonation of the chromophore present in both antibiotics at lower pH, the interaction of the oligosaccharide moieties with the chromophore may change, leading to an alteration of the chiroptical environment.

4. Heats of ionisation of MTR and CHR were determined from calorimetric method. Heat of ionization of MTR (~9.4 kcal/ mol) is higher than that of CHR (~3.0 kcal/ mol) (Figure 4). In MTR the trisaccharide chain has more hydrophilic surface. It leads to the possibility of more hydrogen bond formation between the aglycone and the trisaccharide chain, which may alter during the ionization process. Therefore a greater number of H-bonds are formed/ broken leading to a higher heat of ionization. In case of CHR, the hydrophobic surface of these trisaccharide chains is more compared to that of MTR. So, less number of H-bond is formed/ broken, hence the lower value of heat of ionization.

5. We have done 1D  $^1\text{H}$  NMR at different pH for both MTR and CHR. In contrast to the higher pH, a broadening in the spectra characterizes the NMR spectra. The most notable feature is that the peaks corresponds to aromatic protons are so broadened at low pH that they became indistinguishable with the base line, which provides support for our proposition that for both MTR and CHR at pH 3.0 protonation at C1 carbonyl oxygen, which leads to the exchange of aromatic proton with solvent water molecule.

---

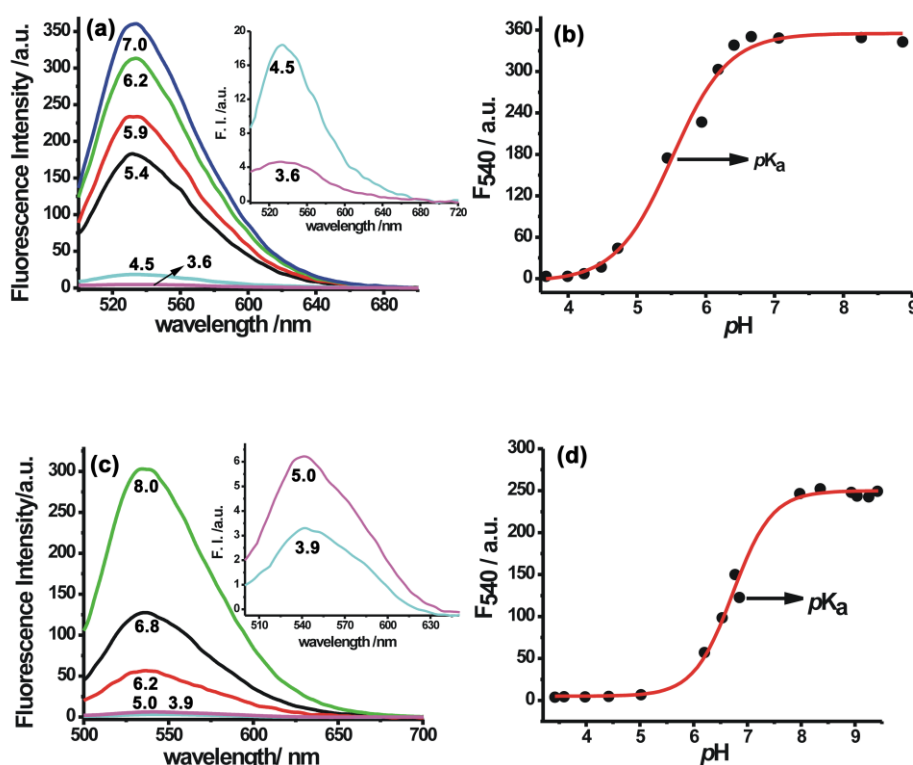


**Figure 3. Determination of pH by fluorescence spectroscopy:** Optical spectra of MTR and CHR in unbuffered deionized water adjusted to different pH by means of addition of HCl or NaOH at 25°C : (a) Fluorescence spectra of MTR at different pH values indicated in the spectra (b) pH-dependence of MTR fluorescence emission measured at 540nm ( $\lambda_{\text{excitation}} = 470\text{nm}$ ) (c) Fluorescence spectra of CHR at different pH values indicated in the spectra (d) pH-dependence of CHR fluorescence emission measured at 540nm ( $\lambda_{\text{excitation}} = 470\text{nm}$ ). The pH values are those measured after dissolving the antibiotic and adjusting the pH.

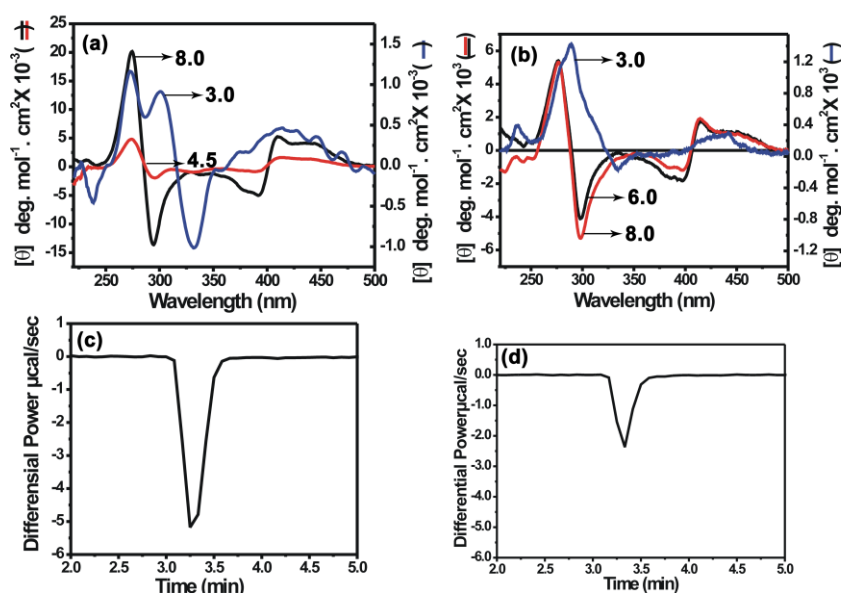


**Figure 4. CD spectra and ionisation energies of the antibiotics:** (a) Normalised CD spectra for MTR (10 µM) at pH 8.0(black), pH 4.5 (red) and pH 3.0 (blue) (b) Normalised CD spectra for CHR (10 µM) at pH 8.0(red), pH 6.0 (black) and pH 3.0 (blue) at 25°C. (c) Injection of 5 µM MTR (1.82 mM) at pH 4.0 to 20mM Tris-HCl buffer pH 9.0. (d) Injection of 5 µM CHR (1.82 mM) at pH 7.0 to 20mM Tris-HCl buffer pH 9.0 at 25°C.

---

### **Chapter 3: Molecular basis of self association of aureolic acid antibiotic, Chromomycin A3**

#### **Background:**

Micro-organisms protect themselves from the toxic action of antibiotics they produce by developing self-defense mechanisms and they are highly resistant to that specific antibiotic. Chromomycin A3 is an antitumor antibiotic produced by *Streptomyces griseus*, earlier used for the treatment of Paget's disease of bones and testicular carcinoma under the trade name of toyomycin. Currently the clinical use of CHR is discontinued due to its cytotoxicity. However, it is widely used in karyotyping and painting of the cell nucleus. The self-association antibiotics would play an important role in its storage outside the bacterial cell wall, biological action and gene expression from *Streptomyces griseus*.

#### **Objective:**

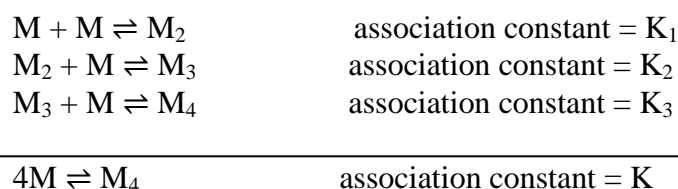
Previous reports from our laboratory have shown that anionic form of Mithramycin self-associates extensively. Chromomycin A3 has a  $pK_a$  of 7.0. At physiological pH, it therefore, has a mixed population of anionic and neutral forms. Here I have examined the self-association of CHR in aqueous solution both in neutral and in anionic forms by means of spectroscopic (absorbance, fluorescence and CD) and calorimetric (ITC) techniques.

#### **Results:**

1. Absorbance studies have been carried out for CHR at two different concentrations in pH 5.0 and pH 9.0 buffers respectively. Non overlap of the spectra in both buffers over the concentration range, 2  $\mu$ M-60  $\mu$ M, indicates the aggregation of CHR both in neutral and anionic forms.
  2. To detect the self-aggregation of neutral and anionic CHR in aqueous buffers of pH 5.0 and pH 9.0 at low concentration range (1  $\mu$ M -7  $\mu$ M), the fluorescence emission spectra and intensity at 540 nm, were measured as a function of CHR concentration. At this concentration range of CHR there is an increase in the normalized fluorescence
-

spectra in both buffers (pH 5.0 and pH 9.0). Deviation from linearity of the fluorescence intensity values at 540 nm as a function of CHR concentration (Figure 5 and 6) is another feature arising from self-aggregation of neutral and anionic forms of CHR in low concentration.

**3.** The chiro-optical properties of CHR in buffers of pH 5.0 and 9.0 as a function of input concentration have been investigated to study the self association of neutral and anionic CHR. I have plotted the observed ellipticity at 413 nm for the neutral drug and 444 nm for anionic drug as a function of input concentration of CHR. The resulting plot shows three breaks over the entire concentration range in each case. The results suggest that there are four types of species present over the total concentration range as follows:



with three association constants, denoted as  $K_1$ ,  $K_2$ , and  $K_3$  (where  $K = K_1 \times K_2 \times K_3$ ).  $M$ ,  $M_2$ ,  $M_3$ , and  $M_4$  represent the monomer, dimer, trimer, and tetramer of CHR, respectively. The dissociation constants are calculated from the break points (Table 1). The apparent dissociation constant for dimerisation process ( $K_d^1$ ) of anionic CHR is three fold lower than that of neutral CHR. It means that ionization leads to oligomerization of CHR at low concentration. With increase in concentration, the dimer further associates to form trimer and tetramer for both, neutral as well as anionic CHR. Formation of tetramer from trimer is associated with a relatively lower affinity.

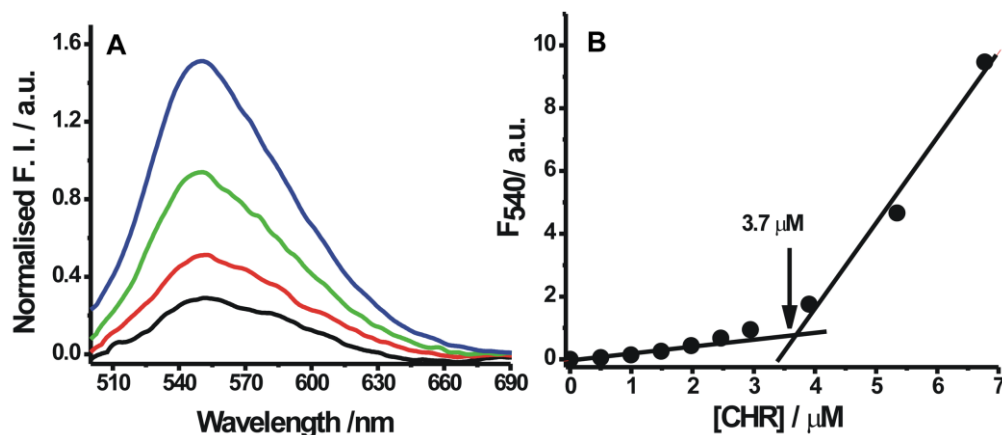


**Figure 5. Fluorescence studies of neutral form** (A) Fluorescence spectra (normalized per micromolar concentration of CHR) of neutral CHR, 2.5  $\mu\text{M}$  (black), 3.9  $\mu\text{M}$  (red), 5.4  $\mu\text{M}$  (green) and 10  $\mu\text{M}$  (blue) in 20 mM sodium acetate acetic acid buffer pH 5.0 at 25  $^{\circ}\text{C}$  (B) Fluorescence intensity at 540 nm is plotted against different concentration in 20mM sodium acetate acetic acid buffer pH 5.0 at 25  $^{\circ}\text{C}$ .

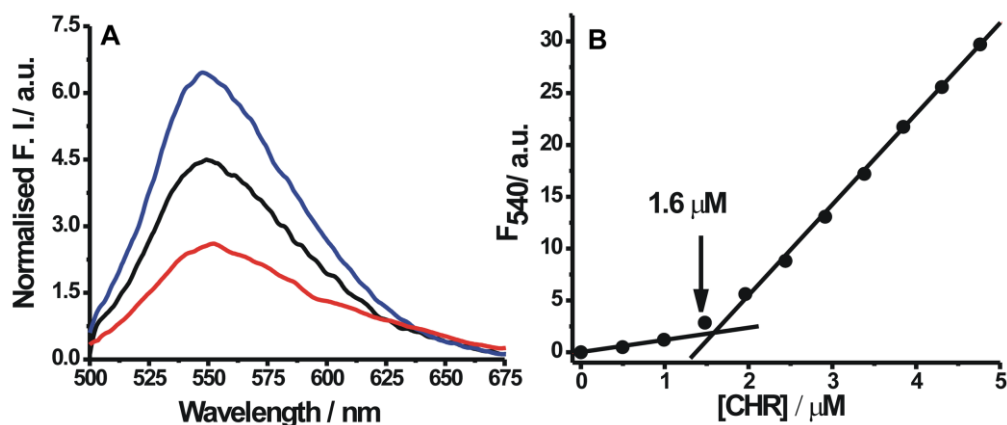


**Figure 6. Fluorescence studies of anionic form** (A) Fluorescence spectra (normalized per micromolar concentration of CHR) of anionic CHR, 1  $\mu\text{M}$  (red), 2  $\mu\text{M}$  (black), 3.5  $\mu\text{M}$  (blue) in 20 mM Tris-HCl buffer pH 9.0. (B) Fluorescence intensity at 540nm plotted against different concentration in 20 mM Tris-HCl buffer pH 9.0 at 25  $^{\circ}\text{C}$ .

4. The molar heat of dilution has been measured at different concentrations corresponding to dimer and trimer formation of neutral and anionic CHR in isothermal titration calorimetry (ITC) method. From the isotherms we have seen that neutral CHR



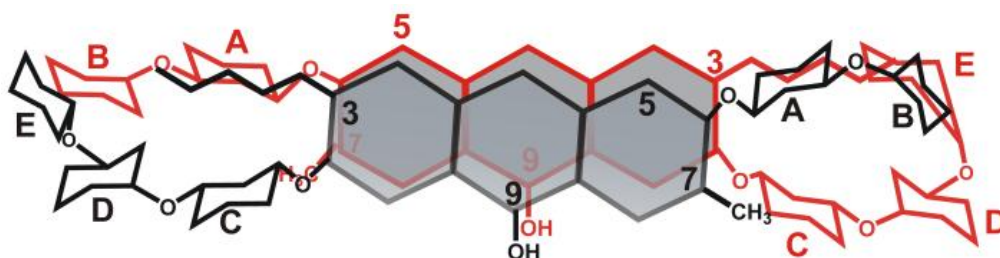
aggregates at  $\sim 10 \mu\text{M}$  concentration whereas the anionic CHR aggregates at much lower concentrations.

**Table 1.** Apparent dissociation constants values for the multiple equilibria of CHR and MTR in neutral and anionic forms at  $25^\circ\text{C}$ .

Reaction	Dissociation Constant of CHR at pH 5.0 (neutral form)	Dissociation Constant of CHR at pH 9.0 (anionic form)	Dissociation Constant of MTR at pH 3.0 (neutral form)
$\text{M} + \text{M} \rightleftharpoons \text{M}_2$	$K_1^{\text{d}} = 43.4 \text{ nM}$	$K_1^{\text{d}} = 14.5 \text{ nM}$	$K_1^{\text{d}} = 411 \text{ nM}$
$\text{M}_2 + \text{M} \rightleftharpoons \text{M}_3$	$K_2^{\text{d}} = 212.8 \mu\text{M}$	$K_2^{\text{d}} = 204.5 \mu\text{M}$	$K_2^{\text{d}} = 11 \text{ nM}$
$\text{M}_3 + \text{M} \rightleftharpoons \text{M}_4$	$K_3^{\text{d}} = 5.78 \mu\text{M}$	$K_3^{\text{d}} = 0.33 \mu\text{M}$	$K_3^{\text{d}} = 7.4 \text{ nM}$

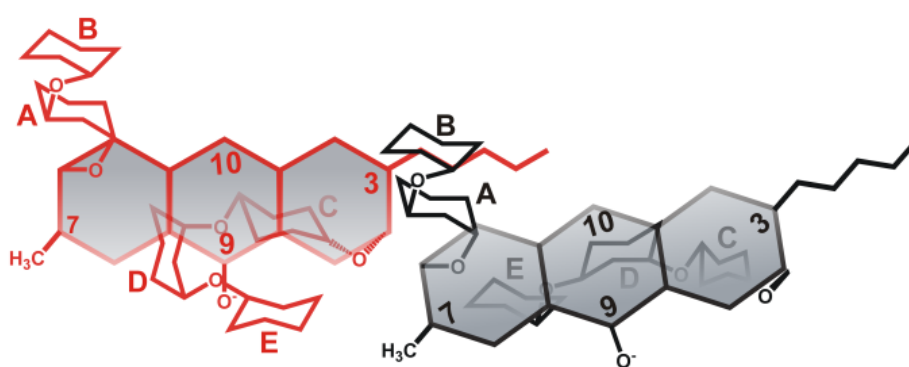
5. Chemical shift values of anionic and neutral CHR (at pH 8.0 and pH 6.0 respectively) have been assigned using 1D and 2D (through bond connectivity-TOCSY and through space connectivity-NOESY) NMR spectra. Chemical shift values of C5-H and C10-H of both forms do not show any NOESY contacts apart from those arising from the protons of the same molecule. Involvement of the aromatic region and therefore, role of stacking interactions in the process of aggregation of anionic/ neutral CHR appears a remote possibility, because there is no concentration dependent upfield shift of the aromatic protons. Involvement of the aliphatic region of the anionic CHR molecule can be determined from the NOESY contacts of different C-atoms of the aliphatic side chain at C3. An examination of shows that C1'-OCH<sub>3</sub> ( $\delta = 3.218$ ) develops NOESY contacts with both C5''-CH<sub>3</sub> ( $\delta = 1.196$ ) and A-ring acetyl group protons ( $\delta = 2.035$ ) (Figure 9B). C3'-H ( $\delta = 3.785$ ) builds NOESY contacts with C1''-H (A-ring) ( $\delta = 5.473$ ) as well as A-ring acetyl group protons ( $\delta = 2.035$ ) and C4'-CH<sub>3</sub> is spatially close to many sugar atoms. These NOESY contacts between the protons could not arise from the same molecule as that would involve a severe steric hindrance and conformational stress. Therefore the anionic CHR molecules are mutually oriented in such a way that the di-saccharide moiety of one molecule lies over the aliphatic side

chain at C3. To minimize the electrostatic repulsion arising from two anionic molecules aliphatic chain of one molecule comes close to the aglycone of another molecule. This is probably reflected in the NOESY contact between C10-H and C4'-H.



**Scheme 1.** Association of neutral CHR molecules

6. The aliphatic side chain develops NOESY contacts with a number of protons of the di-saccharide moiety as is exemplified by NOE cross peaks between C1'-OCH<sub>3</sub> ( $\delta = 3.221$ ) and A-ring acetyl group protons ( $\delta = 2.039$ ) in neutral form of CHR. In contrast to anionic form of CHR, aliphatic side chain of neutral CHR does not form any NOE contacts with the aglycone. C1'-OCH<sub>3</sub> aliphatic side chain also develops NOE contacts with B- ring C3''-H ( $\delta = 3.763$ ) and B-ring C5''-CH<sub>3</sub> ( $\delta = 1.198$ ), which is possible if two neutral CHR molecule arrange themselves so that aliphatic side chain of one molecule lies over the di saccharide moiety of another (scheme 2).



**Scheme 2.** Association of anionic CHR molecule

---

## **Chapter 4: Association of antitumor antibiotic Mithramycin with $Mn^{2+}$ and the potential cellular targets of mithramycin after association with $Mn^{2+}$**

### **Background:**

Mithramycin (plicamycin, MTR) is a naturally occurring anticancer antibiotic isolated from *Streptomyces plicatus*. It has been used clinically for many years to treat testicular carcinoma and hypercalcemia in patients with metastatic bone lesions. The anticancer property was ascribed to the inhibitory effect of MTR on DNA replication and transcription during macromolecular biosynthesis. MTR was found to inhibit the binding of transcription factor *Sp1* to its promoter, which in turn leads to gene transcription modulation of different genes, including *c-myc*, and *ha-ras*, as well as anti-apoptotic genes. Moreover, MTR has been found to cross the blood-brain barrier and is in its preclinical trials in Huntington's disease (HD). Structural analysis revealed that, MTR binds to minor groove of DNA around GC-rich sequences only in the presence of bivalent metal ions such as  $Mg^{2+}$ ,  $Zn^{2+}$ ,  $Co^{2+}$ ,  $Fe^{2+}$  etc.

### **Objective:**

Considering the complex formation ability of MTR with the metal ions, I have studied by means of different spectroscopic and calorimetric techniques its binding ability with  $Mn^{2+}$  in view of the important biological roles of the metal ion. I have also examined plausible targets of the resultant antibiotic :  $Mn^{2+}$  complex inside the cell.

### **Results:**

1. Association of MTR with  $Mn^{2+}$  is characterized by absorption, fluorescence and CD spectroscopy. Upon addition of  $Mn^{2+}$  there is a decrease in absorbance at 400 nm and appearance of a new absorption band at around 440 nm, which is the signature of complex formation of MTR with the metal ion. The presence of an isosbestic point at 413nm suggests the formation of a single type of complex under equilibrium condition over the input concentration range of  $Mn^{2+}$ . Quenching of fluorescence intensity is associated with broadening of the fluorescence emission spectrum of MTR upon addition of increasing concentration of  $Mn^{2+}$ . In the visible CD spectra, the double

---

bands at 415 nm and 450 nm in free MTR are replaced by a broad band around 450 nm as a result of an increase in the input concentration of  $\text{Mn}^{2+}$ . In the near UV CD spectra there is an inversion of the signature CD band of MTR at 274 nm as the concentration of  $\text{Mn}^{2+}$  increases. The apparent dissociation constant,  $K_d^{\text{app}}$ , evaluated from three methods (Figure 7, Table 2).

2. The rate and kinetic nature of the association of MTR with  $\text{Mn}^{2+}$  were measured by absorption, fluorescence and CD methods. It follows first-order kinetics with

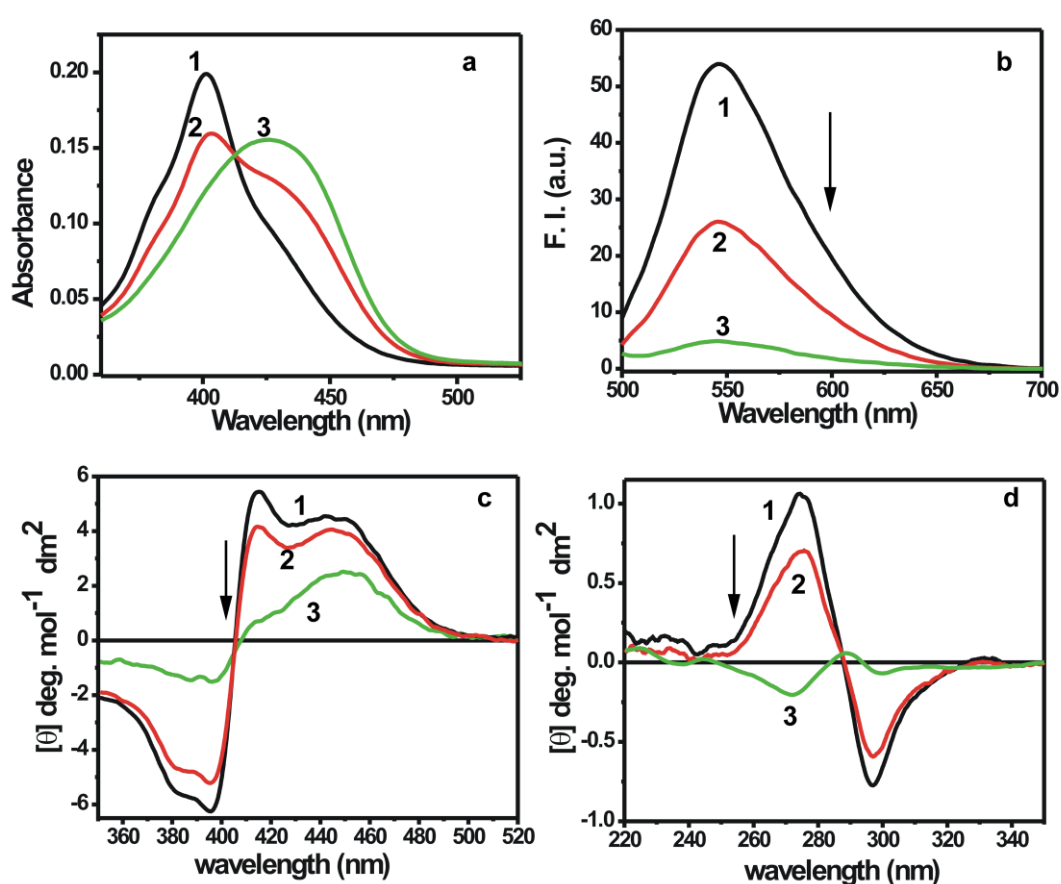


**Figure 7.** Association of MTR with  $\text{Mn}^{2+}$  in 20 mM Tris-HCl pH 8.0 at 25°C (a) Absorption spectra of MTR alone (20  $\mu\text{M}$ , curve 1), MTR incubated with 135  $\mu\text{M}$  of  $\text{Mn}^{2+}$  (curve 2) and 900  $\mu\text{M}$  of  $\text{Mn}^{2+}$  (curve 3) in the visible (360-550 nm) region. (b) Change in fluorescence emission ( $\lambda_{\text{ex}} = 470$  nm) spectrum (500-700 nm) of MTR (20  $\mu\text{M}$ , curve 1), MTR incubated with 135  $\mu\text{M}$  of  $\text{Mn}^{2+}$  (curve 2) and 900  $\mu\text{M}$  of  $\text{Mn}^{2+}$  (curve 3). (c) Visible (350-520 nm) CD spectra of MTR alone (20  $\mu\text{M}$ , curve 1), MTR incubated with 135  $\mu\text{M}$  of  $\text{Mn}^{2+}$  (curve 2) and 900  $\mu\text{M}$  of  $\text{Mn}^{2+}$  (curve 3). (d) Near UV (220-350 nm) CD spectra of MTR alone (20  $\mu\text{M}$ , curve 1), MTR incubated with 135  $\mu\text{M}$  of  $\text{Mn}^{2+}$  (curve 2) and 900  $\mu\text{M}$  of  $\text{Mn}^{2+}$  (curve 3).

---

comparable rate constants obtained from the time dependent changes in absorbance at 440 nm, fluorescence emission intensity at 540 nm and ellipticity at 275 nm.

**3.** The enthalpy change for the binding of MTR with  $\text{Mn}^{2+}$  is obtained from isothermal titration calorimetry (ITC) method. Apparent dissociation constant ( $K_d^{\text{app}}$ ) obtained from ITC and spectroscopic methods are comparable (137  $\mu\text{M}$  from spectroscopic method and 132  $\mu\text{M}$  from ITC). Changes in enthalpy ( $\Delta H$ ) and entropy ( $\Delta S$ ) determined from ITC show that complex formation between MTR and  $\text{Mn}^{2+}$  is predominantly enthalpy driven and the reaction is exothermic in nature.

**4.** Interaction of  $[(\text{MTR})_2 \text{Mn}^{2+}]$  complex with DNA is characterized by spectroscopic method (absorption, fluorescence and CD). The features of these changes are (i) red-shifting and broadening of the peaks and (ii) an increase in the absorbance beyond 410 nm of the spectrum of free MTR, which is similar to the earlier observations in case of  $\text{Mg}^{2+}$  and  $\text{Zn}^{2+}$  complexes. Quenching of fluorescence of the complex occurs due to their interactions with DNA. CD spectroscopy has been employed to show the change in conformation of the complex due to binding with DNA. There is a marked increase in the positive band for  $[(\text{MTR})_2 \text{Mn}^{2+}]$  upon binding to DNA. The apparent dissociation constant,  $K_d^{\text{app}} = 54 \mu\text{M}$ , was measured using both non linear curve fitting analysis and Scatchard plot.

**5.** The apparent dissociation constant for  $[(\text{MTR})_2 \text{Mn}^{2+}]$  complex with poly(dG-dC) is 43  $\mu\text{M}$  suggesting higher affinity than calf thymus DNA.

**6.** Association of  $[(\text{MTR})_2 \text{Mn}^{2+}]$  complex with Chromatin is determined by absorption spectroscopy. The apparent dissociation constant is 298  $\mu\text{M}$ . This is as expected lower than that for calf thymus DNA. This indicates that the presence of histones reduces the accessibility of the ligand for chromosomal DNA.

**7.** Interaction of MTR with  $\text{Mn}^{2+}$  containing metallo-enzyme, MnSOD was determined by different spectroscopic method. The change in visible absorption spectra upon addition of two different concentrations of MnSOD indicates formation of complex between the two. Increase in intensity of the fluorescence emission spectra of MTR in presence of MnSOD further supports the conclusion. Plausible reason for this increase

---

**Table 2. Affinity of MTR for  $\text{Mn}^{2+}$  *in vitro***

Apparent dissociation constant ( $K_d^{\text{app}}$ ) and true dissociation constant ( $K_D$ ) values for the association of MTR with  $\text{Mn}^{2+}$ .  $2(\text{MTR}) + \text{Mn}^{2+} \rightleftharpoons [(\text{MTR})_2 \text{Mn}^{2+}]$

Complex	Method used	Apparent dissociation constant, $K_d^{\text{app}}$ ( $\mu\text{M}$ )
[(MTR) <sub>2</sub> Mn <sup>2+</sup> ]	Absorbance at 440nm	111
	Fluorescence at 540nm	137
	CD at 274nm	193

in fluorescence intensity is the change of microenvironment of the fluorophore of MTR upon interaction with MnSOD. The formation of the complex between MTR and MnSOD is further confirmed from the significant alteration of CD spectrum of MTR upon addition of MnSOD.

### **Chapter 5: Structural basis of the association of plant alkaloid Chelerythrine with different DNA sequences and chromatin components**

#### **Background:**

In the last few years, clinical trials using plant-derived drugs for prevention and treatment of tumors have become increasingly prevalent in cancer therapy. Quaternary benzo[c]phenanthridine alkaloids (QBAs) affect eukaryotic cells in many ways and several cellular targets for their action have recently been established. The interaction of compounds with organelles and other intracellular targets depends on both cellular permeability and intracellular distribution. Chelerythrine is an important member of 2,3,7,8-tetrasubstituted quaternary benzo[c]phenanthridine alkaloids and present in plants such as Chinese herbs, *M. cordata* and *C. majus*. Chelerythrine have been reported to exert cell growth-inhibitory effects via the induction of apoptosis in a variety of cancer cells. Chelerythrine is known as a specific protein kinase C inhibitor

and potent anticancer drug. However, a number of recent studies indicate that PKC-independent mechanisms might be also responsible for its potential anticancer property. Although substantial work has progressed in evaluating the drug potential of chelerythrine, yet a biophysical characterization of the effect of the molecule on DNA and chromatin is still wanting.

**Objective:**

My objective is to understand the mode of interaction of chelerythrine with DNA and chromatin assembly. Different spectroscopic and calorimetric methods were employed to characterize the association of chelerythrine with DNA and chromatin assembly. To investigate the effect of association of chelerythrine upon various DNA sequences, different polynucleotides namely poly(dG-dC), poly(dG).poly(dC), poly(dA-dT) and poly(dA).poly(dT) have been used.

**Results:**

1. Association of Chelerythrine (CHL) with DNA and polynucleotides were characterized by absorbance and fluorescence spectroscopy. Absorbance spectra of free CHL are altered in presence of DNA/polynucleotide. The sets of spectra are characterized by the presence of isosbestic points originating from the equilibrium between free and bound CHL molecule. In contrast to the absorption spectral change, alteration in fluorescence property of the ligand is sensitive to the nature of the DNA/polynucleotide. Fluorescence intensity of CHL enhances upon association with calf thymus DNA, poly(dA-dT) and poly(dA).poly(dT). On the other hand, quenching of the fluorescence entails the association of the ligand with poly(dG-dC) and poly(dG).poly(dC).

2. The apparent dissociation constants for ctDNA, poly(dG-dC), poly(dG).poly(dC) and poly(dA-dT) complexed with CHL are comparable. In contrast, the same is ~3.5 fold higher for poly(dA).poly(dT)-CHL complex. Binding stoichiometry for the association of CHL and (G.C) specific polynucleotides are comparable (Table 3) whereas those are higher for (A.T) specific polynucleotides.

---

3. Binding parameters of CHL to DNA/ polynucleotides obtained from the ITC experiments show that, both enthalpy and entropy contribute in a favorable way to the negative free energy change associated with the complex formation with the notable

**Table 3:** Dissociation constant, stoichiometry and free energy change for the interaction of different DNA sequences with CHL in 10 mM potassium phosphate pH 6.8 at 25 °C obtained from spectrofluoremetric titration.

System	Apparent dissociation constant, $K_d^{app}$ ( $\mu$ M)	Stoichiometry	$\Delta G$ (kcal/mol)
Chromosomal DNA -CHL	$16.6 \pm 1.6$	5.0	$-(5.13 \pm 0.5)$
Poly(dG-dC) - CHL	$12.6 \pm 1.1$	3.4	$-(6.68 \pm 0.4)$
Poly(dG).poly(dC) - CHL	$13.01 \pm 1.1$	3.8	$-(6.66 \pm 0.3)$
Poly(dA-dT) - CHL	$12.9 \pm 1.0$	5.6	$-(6.67 \pm 0.3)$
Poly(dA).poly(dT) - CHL	$46.1 \pm 0.02$	11.6	$-(5.91 \pm 0.01)$

exception of poly(dA).poly(dT). Negative enthalpic contribution indicates non-covalent interaction such as stacking and hydrogen bonding which stabilizes the complex between DNA/polynucleotides and CHL. In case of all DNA/ polynucleotides, entropy is found to play a positive role in the association with CHL. Positive entropic contribution could be ascribed to the release of water molecules present in the minor groove of the DNA/ polynucleotides through which CHL access the macromolecule which has been proved from the EtBr displacement assay experiments.

4. Conformational changes induced in the DNA/polynucleotide structure due to association with CHL molecule have been monitored by CD experiments. In all cases binding to CHL led to an induced CD band at the absorption region of CHL. In case of calf thymus DNA, poly(dG-dC) and poly(dA-dT) characteristic CD spectra of B-form of duplexes with large positive bands in 260-290nm region and a negative band at 248nm result from the association. CHL decreases the ellipticity of the of the positive and negative bands of poly(dG).poly(dC) and poly(dA).poly(dT) upon binding to them.



---

**5.** Association of CHL with chromatin components such as chromatin, chromatosome and chromosomal DNA was determined by spectroscopic and calorimetric method. Absorption and fluorescence spectra of free CHL alter in presence of increasing concentrations of chromatin/chromatosome/chromosomal DNA. Affinity constants of CHL with chromatin and its components (chromatosome and chromosomal DNA) are determined from spectroscopic and calorimetric studies. CHL has higher affinity for chromosomal DNA compare to chromatin and chromatosome. The effect of CHL on the structure of native chromatin, chromatosome and chromosomal DNA was examined by CD spectroscopy. Appearance of induced CD band in the absorbance region of optically inactive CHL demonstrates CHL-polymer association.

## **Chapter 6: Summary**

The present thesis is an attempt to understand the mode of action of two aureolic acid antibiotics, Mithramycin and Chromomycin A3 and one plant alkaloid Chelerythrine from chemical biology point of view. MTR and CHR are weak acids of  $pK_a$  5.0 and 7.0 respectively. In our study we have described the difference in ionisation properties of Mithramycin and Chromomycin A3 using spectroscopic and calorimetric techniques. Different sugars and specific modifications of the sugars are responsible for the different ionisation property of MTR and CHR. Many bioactive natural products are glycosylated compounds in which the sugar moieties are essential for their biological activity. Biosynthesis of chromomycin A3 requires two acetylation steps and one methylation step which contribute to the biological activity of it. Presence of different sugars and specific modifications in CHR entails for this distinctive activities.

Our study has also characterized the oligomerisation ( $n = 2$  to  $4$ ) of neutral and anionic forms of CHR in buffers of pH 5 and 9. Dimerisation of neutral and anionic forms of CHR starts at much lower concentrations ( $< 10 \mu\text{M}$ ) compared to MTR, whereas tetramerisation is the predominant process for MTR in both neutral as well as anionic form.  $^1\text{H}$  NMR studies have revealed that, sugar moieties attached to their aglycone part in CHR and MTR play key roles in the self association process. The difference in the sugar substituents present in CHR and MTR give rise to the alteration of self

---

---

aggregation pattern in aqueous solution though in both processes hydrophobic interaction is an important.

Mithramycin forms single type of complex (antibiotic: metal = 2:1) with  $\text{Mn}^{2+}$ . Calorimetric study shows that the reaction is exothermic in nature and enthalpy driven at room temperature. MTR- $\text{Mn}^{2+}$  complex bind to double helical DNA via minor groove with GC base specificity. Our study also shows that MTR binds to  $\text{Mn}^{2+}$ -containing metalloenzyme Manganese superoxide dismutase (MnSOD) without inhibiting its enzymatic activity.

From the studies with plant alkaloid chelerythrine with various DNA sequences, namely poly(dG-dC), poly(dG).poly(dC), poly(dA-dT), poly(dA).poly(dT) and calf thymus DNA, we have observed that Association of CHL with polynucleotide is sequence dependent. Chelerythrine exhibits different fluorescence properties in presence of (A.T) and (G.C) containing polynucleotides. Thermodynamic parameters for the association of CHL with different sequences of DNA except poly(dA).pol(dT), suggest that both enthalpy and entropy contribute in a favorable way to the negative free energy change associated with complex formation. In our study we have also characterized the association of chelerythrine with different levels of chromatin structure. Presence of associated histone proteins in chromatin and chromatosome has a negative effect upon DNA-binding potential of chelerythrine.

---

---

## References

- [1] N.S. Egorov, Antibiotics: A scientific approach, MIR publishers 1985.
  - [2] P.M. Dewick, Medicinal natural products: a biosynthetic approach, John Wiley & Sons
  - [3] F. Lombo, N. Menendez, J.A. Salas, C. Mendez, The aureolic acid family of antitumor compounds: structure, mode of action, biosynthesis, and novel derivatives, *Appl Microbiol Biotechnol* 73 (2006) 1-14.
  - [4] M.G. Watve, R. Tickoo, M.M. Jog, B.D. Bhole, How many antibiotics are produced by the genus *Streptomyces*?, *Arch Microbiol* 176 (2001) 386-390.
  - [5] M. Maiti, G.S. Kumar, Biophysical aspects and biological implications of the interaction of benzophenanthridine alkaloids with DNA, *Biophysical Reviews* 1 (2009) 119-129.
  - [6] J.M. Herbert, J.M. Augereau, J. Gleye, J.P. Maffrand, Chelerythrine is a potent and specific inhibitor of protein kinase C, *Biochem Biophys Res Commun* 172 (1990) 993-999.
  - [7] J. Handelsman, M.R. Rondon, S.F. Brady, J. Clardy, R.M. Goodman, Molecular biological access to the chemistry of unknown soil microbes: a new frontier for natural products, *Chemistry & biology* 5 (1998) R245-R249.
  - [8] J.R. Rohr, C. Mendez, J.A. Salas, The biosynthesis of aureolic acid group antibiotics, *Bioorganic Chemistry* 27 (1999) 41-54.
  - [9] P. Aich, R. Sen, D. Dasgupta, Role of magnesium ion in the interaction between chromomycin A3 and DNA: binding of chromomycin A3-Mg<sup>2+</sup> complexes with DNA, *Biochemistry* 31 (1992) 2988-2997.
  - [10] M.H. Hou, A.H. Wang, Mithramycin forms a stable dimeric complex by chelating with Fe(II): DNA-interacting characteristics, cellular permeation and cytotoxicity, *Nucleic Acids Res* 33 (2005) 1352-1361.
  - [11] S. Montes, M. Alcaraz-Zubeldia, P. Muriel, C. Rios, Striatal manganese accumulation induces changes in dopamine metabolism in the cirrhotic rat, *Brain Res* 891 (2001) 123-129.
  - [12] R. Nayak, M. Sirsi, S.K. Podder, Role of magnesium ion on the interaction between chromomycin A(3) and deoxyribonucleic acid, *FEBS Lett* 30 (1973) 157-162.
-

## LIST OF FIGURES

Figure No.	Figure caption	Page No.
Figure 1.1	Classes of DNA-interactive agents and their molecular interactions with DNA	5
Figure 1.2	Chemical structures of aureolic acid group of antibiotics	10
Figure 1.3	Genetic organization of the chromomycin A3 gene cluster and its comparison with the mithramycin gene cluster	11
Figure 1.4	Proposed pathway of the biosynthesis of premithramycinone moiety	13
Figure 1.5	Proposed pathway of the glycosylation of premithramycinone B moiety	14
Figure 1.6	Final step of biosynthesis of mithramycin	16
Figure 1.7	Transportation of $Mn^{2+}$ across the cell	23
Figure 1.8	$Mn^{2+}$ -induced dopamine oxidation	26
Figure 1.9	Classification of naturally occurring benzo[c]phenanthridine alkaloids	29
Figure 2.1	Chemical structure of chromomycin A3 and mithramycin	37
Figure 2.2	Optical spectra of MTR and CHR in unbuffered deionized water adjusted to different pH by means of addition of HCl or NaOH at room temperature: Fluorescence spectra of (a) MTR and (c) CHR at different pH values indicated in the spectra. pH-dependence of (b) MTR and (d) CHR on fluorescence emission measured at 540 nm ( $\lambda_{\text{excitation}} = 470\text{nm}$ )	42
Figure 2.3	Normalized absorption spectra (molar extinction coefficient) of (a) MTR (20 $\mu\text{M}$ ) and (b) CHR (20 $\mu\text{M}$ ) at different pH values indicated in the spectra. Absorption spectra of the antibiotics were recorded in unbuffered synergy water adjusted to different pH by means of addition of HCl or NaOH at 25 $^{\circ}\text{C}$	43
Figure 2.4	(a) CD spectra for MTR (10 $\mu\text{M}$ ) at pH 8.0( <i>black</i> ), pH 4.5 ( <i>red</i> ) and pH 3.0 ( <i>blue</i> ) (b) CD spectra for CHR (10 $\mu\text{M}$ ) at pH 8.0( <i>red</i> ), pH 6.0 ( <i>black</i> ) and pH 3.0 ( <i>blue</i> ) at 25 $^{\circ}\text{C}$	44
Figure 2.5	(a) Injection of 5 $\mu\text{l}$ MTR (1.82 mM) at pH 4.0 to 20 mM Tris-HCl buffer pH 9.0. (b) Injection of 5 $\mu\text{l}$ CHR (1.82 mM) at pH 7.0 to 20 mM Tris-HCl buffer pH 9.0 at 25 $^{\circ}\text{C}$	45
Figure 2.6	Overlay of full scale 1D NMR spectra of 1 mM MTR at pH 8.0 and pH 3.0 at 25 $^{\circ}\text{C}$	46
Figure 2.7	Overlay of full scale 1D NMR spectra of 1 mM CHR at pH 8.0 and pH 3.0 at 25 $^{\circ}\text{C}$	47
Figure 3.1	Chemical structure of chromomycin A3	56
Figure 3.2	Absorption spectra of neutral CHR, 7.7 $\mu\text{M}$ ( <i>black</i> ) and 59 $\mu\text{M}$	61

	(red) in (a) 20 mM sodium acetate acetic acid buffer pH 5.0 and (b) in 20 mM Tris-HCl buffer pH 9.0 at 25 °C	
Figure 3.3	(a) Fluorescence spectra (normalized per micromolar concentration of CHR) of neutral CHR, 2.5 $\mu$ M (black), 3.9 $\mu$ M (red), 5.4 $\mu$ M (green) and 10 $\mu$ M (blue) in 20 mM sodium acetate acetic acid buffer pH 5.0; (b) Fluorescence intensity at 540 nm plotted against different CHR concentration in 20 mM sodium acetate acetic acid buffer pH 5.0; (c) Fluorescence spectra (normalized per micromolar concentration of CHR) of anionic CHR, 1 $\mu$ M (red), 2 $\mu$ M (black), 3.5 $\mu$ M (blue) in 20 mM Tris-HCl buffer pH 9.0; (d) Fluorescence intensity at 540nm ( $F_{540}$ ) plotted against different concentration in 20 mM Tris-HCl buffer pH 9.0. All experiments are performed at 25 °C	62
Figure 3.4	(a) CD spectra of CHR, 37 $\mu$ M (black), 102 $\mu$ M (red), 241 $\mu$ M (green) and 378 $\mu$ M (blue) in 20 mM sodium acetate acetic acid buffer pH 5.0 (b) CD spectra of CHR, 46 $\mu$ M (black), 120 $\mu$ M (red), 217 $\mu$ M (green) and 305 $\mu$ M (blue) in 20 mM Tris-HCl buffer pH 9.0. CD spectra were recorded at 25 °C	63
Figure 3.5	Change in observed ellipticity of CHR at 413 nm as a function of its concentration in 20 mM sodium acetate acetic acid buffer pH 5.0 at 25°C	64
Figure 3.6	Change in observed ellipticity of CHR at 444 nm wavelength as a function of its concentration in 20 mM Tris-HCl buffer pH 9.0 at 25°C	64
Figure 3.7	Calorimetric titration of anionic CHR in 20 mM Tris-HCl, pH 9.0 ( $\blacktriangledown$ ), neutral CHR in 20 mM sodium acetate acetic acid buffer pH 5.0 ( $\blacktriangle$ ) and neutral MTR in 20 mM citric acid citrate buffer at pH 3.0 ( $\bullet$ ) at 25 °C. The final concentration in the cell ranges from 1 $\mu$ M to 30 $\mu$ M	68
Figure 3.8	NOESY spectra of CHR (1 mM) in 20 mM phosphate buffer, pH 8.0 at 25°C showing the cross-peak between (a) C10-H and C4'-H (6.058, 3.087), (b) C1'-OCH <sub>3</sub> and C5''-CH <sub>3</sub> (3.218, 1.196) and C1'-OCH <sub>3</sub> and A-ring -COCH <sub>3</sub> (3.218, 2.035) (c) C3'-H and A C1''-H (3.785, 5.473) and C3'-H and A-ring -COCH <sub>3</sub> (3.785, 2.035)	72
Figure 3.9	2D NMR of neutral form: NOESY spectra of CHR (1 mM) in 20 mM phosphate buffer, pH 6.0 at 25°C showing the cross-peak between (a) C1'-OCH <sub>3</sub> and A-ring -COCH <sub>3</sub> (3.221, 2.039) (b) C1'-OCH <sub>3</sub> and B-ring C3''-H (3.221, 3.763) (c) C1'-OCH <sub>3</sub> and B-ring C5''-H (3.221, 1.198)	74
Figure 4.1	Chemical structure of mithramycin	82
Figure 4.2	(a) Absorption spectra of MTR alone (20 $\mu$ M, <i>black</i> ) incubated with 135 $\mu$ M of Mn <sup>2+</sup> ( <i>red</i> ) and 900 $\mu$ M of Mn <sup>2+</sup> ( <i>green</i> ) in the	100

visible (360-550 nm) region (b) Change in fluorescence emission ( $\lambda_{\text{ex}} = 470$  nm) spectrum (500-700 nm) of MTR (20  $\mu\text{M}$ , *black*) incubated with 135  $\mu\text{M}$  of  $\text{Mn}^{2+}$  (*red*) and 900  $\mu\text{M}$  of  $\text{Mn}^{2+}$  (*green*). (c) Visible (350-520nm) CD spectra of MTR alone (20  $\mu\text{M}$ , *black*) incubated with 135  $\mu\text{M}$  of  $\text{Mn}^{2+}$  (*red*) and 900  $\mu\text{M}$  of  $\text{Mn}^{2+}$  (*green*) (d) Near UV (220-350nm) CD spectra of MTR alone (20  $\mu\text{M}$ , *black*) incubated with 135  $\mu\text{M}$  of  $\text{Mn}^{2+}$  (*red*) and 900  $\mu\text{M}$  of  $\text{Mn}^{2+}$  (*green*) in 20 mM Tris-HCl pH 8.0 at 25°C. The experiments were performed in 20 mM Tris-HCl pH 8.0 at 25°C

- Figure 4.3 (a) Plot of fraction bound MTR against input  $[\text{Mn}^{2+}]$  obtained from spectrophotometric (■), spectrofluorometric (O) and circular dichroic ( $\Delta$ ) titrations in 20 mM Tris-HCl pH 8.0 at 25°C. Absorbance, fluorescence ( $\lambda_{\text{ex}} = 470$  nm) and molar ellipticity were measured at 400 nm, 540 nm and 274 nm, respectively (b) Continuous variation plot of association of MTR with  $\text{Mn}^{2+}$  101
- Figure 4.4 (a) Overlay of the kinetic traces of MTR (10  $\mu\text{M}$ ) with  $\text{Mn}^{2+}$  (300  $\mu\text{M}$ ) measured by absorption ( $\lambda = 440$  nm, *black*), fluorescence ( $\lambda = 540$  nm, *red*) and circular dichroism ( $\lambda = 275$  nm, *green*) spectroscopy. (b) Plot of logarithm of initial rate against the logarithm of different concentrations of MTR (5, 10, 15 and 20  $\mu\text{M}$ ) for the complex formation with  $\text{Mn}^{2+}$  (300  $\mu\text{M}$ ) (c) Plot of logarithm of initial rate against the logarithm of different concentrations of  $\text{Mn}^{2+}$  (80, 100 and 150  $\mu\text{M}$ ) for the complex formation with MTR (10  $\mu\text{M}$ ) (d) Plot of logarithm of rate constant  $\ln k$  against  $1/T$  at different temperatures (15, 20, 25, 30 and 35°C) in 20 mM Tris-HCl pH 8.0 102
- Figure 4.5 (a) Thermogram for the association of MTR (75  $\mu\text{M}$ ) with  $\text{Mn}^{2+}$  (2.5 mM) at 25°C in 20 mM Tris-HCl, pH 8.0. The top panel presents the real time data and the lower panel shows the normalized enthalpy change for the reaction. The solid line through the data points represents the best fit curve for the titration; (b) Plot of  $\ln (1/K_d^{\text{app}})$  versus  $1/T$  at different temperatures (10, 15, 20, 25, 30 and 35°C) for the complex formation between MTR and  $\text{Mn}^{2+}$  in 20 mM Tris-HCl, pH 8.0 104
- Figure 4.6 (a) Change in visible absorption spectra of  $[(\text{MTR})_2\text{Mn}^{2+}]$  (20  $\mu\text{M}$  MTR + 1 mM  $\text{Mn}^{2+}$ , *black*) alone and in the presence of chromosomal DNA 17  $\mu\text{M}$  (*red*), 81  $\mu\text{M}$  (*green*), 294  $\mu\text{M}$  (*blue*) and 365  $\mu\text{M}$  (*cyan*) respectively; (b) Change in fluorescence emission spectra of  $[(\text{MTR})_2\text{Mn}^{2+}]$  (20  $\mu\text{M}$  MTR + 1 mM  $\text{Mn}^{2+}$ , *black*) alone and in presence of chromosomal DNA (11  $\mu\text{M}$ , *red*; 57  $\mu\text{M}$  *green*; 119  $\mu\text{M}$ , *magenta*; 220  $\mu\text{M}$ , *navy* and 331  $\mu\text{M}$ , *cyan*) respectively; (c) Change in CD spectra of MTR (20  $\mu\text{M}$ ) (*black*) and  $[(\text{MTR})_2\text{Mn}^{2+}]$  (20  $\mu\text{M}$  MTR + 1 mM  $\text{Mn}^{2+}$ , *red*) alone and in presence of chromosomal DNA (20  $\mu\text{M}$ , *green*; 131  $\mu\text{M}$ , *blue* and 353  $\mu\text{M}$ , *cyan*), respectively in 20 mM Tris-HCl pH 8.0 at 25°C 105

Figure 4.7	(a) Plot of fraction bound of $[(\text{MTR})_2 \text{Mn}^{2+}]$ versus [Chromosomal DNA] as obtained from absorbance (at 400 nm, ●), fluorescence emission (at 540 nm, ■) and CD (at 450 nm, ▲) (b) Scatchard plot for the association of $[(\text{MTR})_2 \text{Mn}^{2+}]$ with chromosomal DNA from absorbance (at 400 nm) (c) Plot of fraction bound $[(\text{MTR})_2 \text{Mn}^{2+}]$ complex against poly(dG-dC) (■) and poly(dA-dT) (●) as obtained from spectrofluorometric method. All the experiments were performed in 20 mM Tris-HCl pH 8.0 at 25°C	106
Figure 4.8	(a) Absorption spectra of $[(\text{MTR})_2 \text{Mn}^{2+}]$ (20 $\mu\text{M}$ MTR +1 mM $\text{Mn}^{2+}$ , <i>curve 1</i> ) alone and in presence of chromatin (56 $\mu\text{M}$ , <i>curve 2</i> , 111 $\mu\text{M}$ , <i>curve 3</i> , 272 $\mu\text{M}$ , <i>curve 4</i> and 529 $\mu\text{M}$ , <i>curve 5</i> ) in the visible (380-510 nm) region (b) Curve fitting analysis to evaluate dissociation constant for the association of $[(\text{MTR})_2 \text{Mn}^{2+}]$ with chromatin using absorbance method ( $\lambda_{\text{abs}} = 440 \text{ nm}$ ). Experiments were performed in 20 mM Tris-HCl pH 8.0 at 25 °C	107
Figure 4.9	(a) Change in visible absorption spectra of MTR alone (3 $\mu\text{M}$ MTR, <i>black</i> ) in the presence of MnSOD (3 $\mu\text{M}$ , <i>red</i> ; 5 $\mu\text{M}$ , <i>blue</i> ); (b) Change in fluorescence emission ( $\lambda_{\text{ex}} = 470 \text{ nm}$ ) spectrum of MTR alone (10 $\mu\text{M}$ , <i>black</i> ) in presence of MnSOD (4 $\mu\text{M}$ , <i>red</i> , 10 $\mu\text{M}$ , <i>green</i> ) (c) Change in CD spectra of MTR alone (5 $\mu\text{M}$ , <i>black</i> ) in presence of MnSOD (5 $\mu\text{M}$ , <i>red</i> ) in 20 mM Tris-HCl pH 8.0 at 25 °C (d) Change in rate of pyrogallol (0.2 mM, <i>black</i> ) autoxidation in presence of MnSOD (100 nM, <i>red</i> ), MnSOD incubated with MTR (10 $\mu\text{M}$ , <i>green</i> ; 20 $\mu\text{M}$ , <i>blue</i> and 50 $\mu\text{M}$ , <i>cyan</i> ) in 20 mM Tris-cacodylate pH 8.2 at 25 °C	108
Figure 5.1	Chemical structure of cationic/iminium and neutral /alkanolamine forms of chelerythrine	117
Figure 5.2	(a) Absorption spectra of CHL alone (10 $\mu\text{M}$ , <i>black</i> ) and in presence of increasing concentrations of chromosomal DNA, 10 $\mu\text{M}$ ( <i>red</i> ), 24 $\mu\text{M}$ ( <i>green</i> ) and 104 $\mu\text{M}$ ( <i>blue</i> ); (b) Absorption spectra of CHL alone (10 $\mu\text{M}$ , <i>black</i> ) in presence of increasing concentrations of poly(dG-dC), 10 $\mu\text{M}$ ( <i>red</i> ), 24 $\mu\text{M}$ ( <i>green</i> ) and 104 $\mu\text{M}$ ( <i>blue</i> ); (c) Absorption spectra of CHL alone (10 $\mu\text{M}$ , <i>black</i> ) upon addition of poly(dG).poly(dC), 10 $\mu\text{M}$ ( <i>red</i> ), 24 $\mu\text{M}$ ( <i>green</i> ) and 104 $\mu\text{M}$ ( <i>blue</i> ); (d) Absorption spectra of CHL alone (5 $\mu\text{M}$ , <i>black</i> ) upon addition of poly(dA-dT), 10 $\mu\text{M}$ ( <i>red</i> ), 24 $\mu\text{M}$ ( <i>green</i> ) and 104 $\mu\text{M}$ ( <i>blue</i> ); (e) Absorption spectra of CHL alone (5 $\mu\text{M}$ , <i>black</i> ) upon addition of poly(dA).poly(dT), 10 $\mu\text{M}$ ( <i>red</i> ), 24 $\mu\text{M}$ ( <i>green</i> ) and 104 $\mu\text{M}$ ( <i>blue</i> ). Experiments were performed in 10 mM potassium phosphate buffer pH 6.8 at 25°C	128
Figure 5.3	(a) Fluorescence spectra of CHL alone (5 $\mu\text{M}$ , <i>black</i> ) upon addition of chromosomal DNA, 10 $\mu\text{M}$ ( <i>red</i> ), 24 $\mu\text{M}$ ( <i>green</i> ), 80 $\mu\text{M}$ ( <i>blue</i> ) and 104 $\mu\text{M}$ ( <i>orange</i> ); (b) Fluorescence spectra of CHL alone (10 $\mu\text{M}$ , <i>black</i> ) in presence of increasing concentrations of poly(dG-dC), 10 $\mu\text{M}$ ( <i>red</i> ), 24 $\mu\text{M}$ ( <i>green</i> ), 80 $\mu\text{M}$ ( <i>blue</i> ) and 104 $\mu\text{M}$ ( <i>orange</i> ); (c) Fluorescence spectra of	129

CHL alone (10  $\mu\text{M}$ , *black*) upon addition of poly(dG).poly(dC) , 10  $\mu\text{M}$  (*red*), 24  $\mu\text{M}$  (*green*), 80  $\mu\text{M}$  (*blue*) and 104  $\mu\text{M}$  (*orange*); (d) Fluorescence spectra of CHL alone (5  $\mu\text{M}$ , *black*) in presence of increasing concentrations of poly (dA-dT), 10  $\mu\text{M}$  (*red*), 24  $\mu\text{M}$  (*green*), 80  $\mu\text{M}$  (*blue*) and 104  $\mu\text{M}$  (*orange*); (e) Fluorescence spectra of CHL alone (5 $\mu\text{M}$ , *black*) in presence of increasing concentrations of poly(dA).poly(dT), 10  $\mu\text{M}$  (*red*), 24  $\mu\text{M}$  (*green*), 80  $\mu\text{M}$  (*blue*) and 104  $\mu\text{M}$  (*orange*). Experiments were performed in 10 mM potassium phosphate buffer pH 6.8 at 25 $^{\circ}\text{C}$

Figure 5.4	Binding isotherms (●) for the association of CHL and (a) chromosomal DNA (b) poly(dG-dC) (c) poly(dG).poly(dC), (d) poly(dA - dT), (e) poly(dA).poly(dT) in 10 mM potassium phosphate buffer pH 6.8 at 25 $^{\circ}\text{C}$ . <b>Insets:</b> Corresponding isotherms showing the binding stoichiometry, obtained from the break in the straight lines representing the linear fit of the initial and final few data points	130
Figure 5.5	Representative ITC profiles for the titration of (a) chromosomal DNA (b) poly(dG-dC) (c) poly(dG).poly(dC) (d) poly(dA-dT) and (e) poly(dA).poly(dT) into 25 $\mu\text{M}$ solution of CHL in 10 mM potassium phosphate buffer pH 6.8 at 25 $^{\circ}\text{C}$	133
Figure 5.6	Energetics of the association of CHL with DNA/ polynucleotides in 10 mM potassium phosphate buffer pH 6.8 at 25 $^{\circ}\text{C}$ as determined from ITC	134
Figure 5.7	Variation of enthalpy change ( $\Delta H$ , ●), entropy change ( $-T\Delta S$ , ■) and free energy change ( $\Delta G$ , ▼) are plotted as a function of temperature for the association of CHL with (a) chromosomal DNA (c) poly(dG-dC) (e) poly(dG).poly(dC) (g) poly(dA-dT) and (i) poly(dA).poly(dT). Enthalpy-entropy compensation plot(●) for association of CHL with (b) chromosomal DNA (d) poly(dG-dC) (f) poly(dG).poly(dC) (h) poly(dA-dT) and (j) poly(dA).poly(dT)	134
Figure 5.8	Observed CD spectra of (a) chromosomal DNA alone (100 $\mu\text{M}$ , <i>black</i> ) in presence of increasing concentrations of CHL 15 $\mu\text{M}$ ( <i>red</i> ), 35 $\mu\text{M}$ ( <i>blue</i> ), and 60 $\mu\text{M}$ ( <i>green</i> ); (b) poly(dG-dC) alone (100 $\mu\text{M}$ , <i>black</i> ) in presence of increasing concentrations of CHL, 6 $\mu\text{M}$ ( <i>red</i> ), 15 $\mu\text{M}$ ( <i>green</i> ) and 35 $\mu\text{M}$ ( <i>blue</i> ); (c) poly(dG).poly(dC) alone (100 $\mu\text{M}$ , <i>black</i> ) in presence of increasing concentrations of CHL, 25 $\mu\text{M}$ ( <i>red</i> ), 40 $\mu\text{M}$ ( <i>blue</i> ) and 60 $\mu\text{M}$ ( <i>green</i> ); (d) poly(dA-dT) alone (100 $\mu\text{M}$ , <i>black</i> ) in presence of increasing CHL concentrations, 10 $\mu\text{M}$ ( <i>red</i> ), 20 $\mu\text{M}$ ( <i>green</i> ) and 40 $\mu\text{M}$ ( <i>blue</i> ); (e) poly(dA).poly(dT) (100 $\mu\text{M}$ , <i>black</i> ) in presence of increasing CHL concentrations, 15 $\mu\text{M}$ ( <i>red</i> ), 25 $\mu\text{M}$ ( <i>green</i> ) and 40 $\mu\text{M}$ ( <i>blue</i> ). All experiments were performed in 10 mM potassium phosphate buffer pH 6.8 at 25 $^{\circ}\text{C}$	136
Figure 5.9	Basis spectra obtained from CCA analysis of CD spectra of DNA	137



	/ polynucleotide in 10 mM potassium phosphate buffer pH 6.8 at 25 °C: left hand panel (a, c, e, g and i) are components 1 and 2 obtained from the CCA analysis of the observed CD spectrum. <b>Note:</b> Right hand scales of these plots show the observed ellipticity of induced CD band from CHL. Percentage populations of the components 1 and 2 for (b) chromosomal DNA (d) poly(dG-dC) (f) poly(dG).poly(dC) (h) poly(dA-dT) and (j) poly(dA).poly(dT) are plotted as a functions of CHL concentration	
Figure 5.10	EtBr displacement assay of CHL from EtBr-DNA / polynucleotide complex in 10 mM potassium phosphate buffer pH 6.8 at 25 °C	138
Figure 5.11	(a) Absorption spectra of CHL (10 µM) with 45 µM of chromatin, chromatosome, nucleosome and chromosomal DNA (b) Fluorescence spectra of CHL (5 µM, <i>black</i> ) in presence of 45 µM of chromatin ( <i>red</i> ), chromatosome ( <i>green</i> ), nucleosome ( <i>brown</i> ) and chromosomal DNA ( <i>blue</i> ) in 10 mM potassium phosphate buffer pH 6.8 at 25 °C	139
Figure 5.12	Binding isotherm obtained from fluoremetric titration of CHL with (a) chromatin (b) chromatosome (c) nucleosome core particle (d) chromosomal DNA in 10 mM potassium phosphate buffer pH 6.8 at 25 °C. <i>Inset</i> Corresponding isotherms show the stoichiometry values obtained from the break in the straight lines representing the linear fit of the initial and final few data points	140
Figure 5.13	Representative ITC profiles for the titration of (a) chromatin (b) chromatosome (c) nucleosome (d) chromosomal DNA with CHL in 10 mM potassium phosphate buffer pH 6.8 at 25 °C	142
Figure 5.14	CHL (50 µM) induced conformational changes of 100 µM of (a) chromatin (b) chromatosome (c) chromosomal DNA in 10 mM potassium phosphate buffer pH 6.8 at 25 °C (d) Induced CD bands obtained as a result of interaction of chromatin components with CHL	143
Figure 5.15	(a) Effect of CHL on the hydrodynamic size of chromatin monitored by DLS: Intensity statistics of 10 measurements each was plotted for chromatin (500µM) in presence of increasing concentrations of CHL. Error bars indicate standard deviations. (b) Agarose gel electrophoresis to study effect of chelerythrine on chromatosome structure: chromatosome samples (1 mM DNA base) were incubated with CHL at 37 °C for different time points at CHL/ DNA base ratios indicated in the figure, post-stained with Sybr green and analyzed on 1.5% agarose gel. Fresh chromatosome sample (lane 1) and chromatosome incubated with buffer at 37 °C for 3 hrs (lane 2) serve as negative controls.	144
Figure 5.16	Optimized structures of the (a) DNA double helix for d(ATATAT) <sub>2</sub> sequence with a site of intercalation created at the	154

central AT step and (b) CHL. The nature of electron density around each atom is shown by color code.

- Figure 5.17 (a) Optimized structures of CHL showing its propeller twisted form (b) molecular modeled structure of d(TATATA)<sub>2</sub> along with CHL, showing how easily the propeller twisted ligand can remain at the intercalation site 155
-

## LIST OF TABLES

Table No.	Table caption	Page No.
Table 1.1	Natural products in clinical use	4
Table 1.2	Mode of action of various anticancer antibiotics	9
Table 1.3	Different disease condition related to $Mn^{2+}$	25
Table 3.1	Apparent dissociation constants values for the multiple equilibria of CHR and MTR in both neutral and anionic forms at 25 °C	66
Table 3.2	Chemical shift values of protons of anionic CHR (100 $\mu$ M and 1 mM) in 20 mM Phosphate Buffer, pH 8.0 at 25 °C	69
Table 3.3	NOESY contacts of protons of anionic CHR (1 mM) in 20 mM Phosphate buffer, pH 8.0 at 25 °C	70
Table 3.4	Chemical shift values of protons of neutral CHR (100 $\mu$ M and 1 mM) in 20 mM sodium phosphate buffer, pH 6.0 at 25 °C	73
Table 3.5	Chemical shift values of protons of neutral CHR (100 $\mu$ M and 1 mM) in 20 mM sodium phosphate buffer, pH 6.0 at 25 °C	75
Table 4.1	Affinity of MTR for $Mn^{2+}$ in vitro: Apparent dissociation constant ( $K_d^{app}$ ) and true dissociation constant ( $K_D$ ) values for the association of MTR with $Mn^{2+}$	101
Table 4.2	Rate constant ( $k$ ) for the association of MTR (10 $\mu$ M) with $Mn^{2+}$ (300 $\mu$ M) at 25°C	103
Table 4.3	Thermodynamic parameters for the association of MTR with $Mn^{2+}$ in 20 mM Tris HCl buffer, pH 8.0 at 25°C	104
Table 4.4	Binding parameters for the interaction of $(MTR)_2Mn^{2+}$ with chromatin and chromosomal DNA in 20 mM Tris-HCl buffer, pH 8.0 at 25°C	106
Table 5.1	Summary of absorption properties of CHL after binding with DNA/polynucleotides in 10 mM potassium phosphate pH 6.8 at 25°C	117
Table 5.2	Summary of fluorescence properties of CHL after binding with DNA/ polynucleotides in 10 mM K-Phosphate pH 6.8at 25 °C	129
Table 5.3	Dissociation constant, stoichiometry and free energy change for the interaction of different DNA sequences with CHL in 10 mM potassium phosphate pH 6.8 at 25°C obtained from spectrofluorimetric titration	131
Table 5.4	Thermodynamic parameters for the association DNA/ polynucleotide with CHL by isothermal titration calorimetry in 10 mM potassium phosphate buffer pH 6.8 at 25°C	133
Table 5.5	Binding parameters obtained from fluorescence studies for the	140

---

	association of CHL with chromatin, chromatosome, nucleosome and chromosomal DNA at 25°C	
Table 5.6	Thermodynamic parameters obtained from ITC experiments for the association of CHL with chromatin and its components in 10 mM K-phosphate (pH 6.8) at 25 °C	143

---

---

**LIST OF SCHEMES**

<b>Scheme No.</b>	<b>Scheme caption</b>	<b>Page No.</b>
Scheme 2.1	Ionic equilibrium between neutral and anionic forms of MTR/ CHR	49
Scheme 2.2	Resonance stabilization of protonated form of aglycone moiety present in MTR and CHR	50
Scheme 2.3	Resonance stabilization of mono-anionic forms of MTR /CHR above neutral pH	51
Scheme 2.4	Intramolecular hydrogen bond formation between aglycon moiety and trisaccharide chain in MTR	52
Scheme 3.1	Association of neutral chromomycin A3 molecules	75
Scheme 3.2	Association of anionic chromomycin A3 molecule	79

---

# Chapter 1

## Introduction

## **1. INTRODUCTION**

### **1.1. Antibiotics**

The word ‘antibiotic’ (literally means ‘against life’) was first coined by Selman Waksman in 1942 (Waksman, 1941). Antibiotics are chemical substances formed by microorganisms that can inhibit the growth of bacteria or even destroy them and other microorganisms (Waksman et al., 1958). However, the above definition fails to differentiate between antibiotic substances and other metabolites of the microorganisms which also have antibiotic properties but are not considered as antibiotics. Moreover, it denotes only the substances produced by microorganisms, but antibiotics are also produced by higher plants and animals. The latest definition of antibiotics given so far is “antibiotics are specific products of metabolism, or their modifications with high physiological activity against individual groups of microorganisms (virii, bacteria, fungi, algae, protozoa) or against malignant tumors, that can selectively slow down or completely inhibit their growth” (Egorov, 1985). This definition covers most of the major features of antibiotics and clears the anomaly of the definition given by Waksman. However, this definition neither tells about the stage of metabolism from which antibiotics are formed nor about their specificity of their activity. Therefore the modified definition of antibiotics could be as follows: antibiotics are the final metabolic products from specific species produced below basal level in quantity and/or the synthetic analogous or modifiers with high physiological activity against other cells or specific groups of microorganisms. Along with the anti-metabolic activities, it can selectively slow down or completely inhibit the growth of cancer cells. Physiologically, an antibiotic may work at different levels of cellular metabolism via interaction with one or more cellular organelles.

---

## 1.2. Antibiotics from natural products

Nature has been a source of medicinal agents for thousands of years and continues to be an abundant source of novel chemotypes and pharmacophores. In 1895, Vincenzo Tiberio, physician of the University of Naples discovered that, a mold (*Penicillium*) in water well had an antibacterial action (Elder, 1970). After this initial chemotherapeutic compound proved effective, others pursued similar lines of inquiry, but it was not until in 1928 that Alexander Fleming observed antibiosis against bacteria by a fungus of the genus *Penicillium* (Fleming, 1929). Following the success of penicillin, drug companies and research groups soon accumulated large microorganism culture collections in order to discover new antibiotics (Elder, 1970, Lax, 2004, Wainwright, 1990, Mann, 1999). Subsequently, a new area of science has emerged, which is the exploration of natural products from previously uncultured soil microorganisms (Handelsman et al., 1998). The approach involves directly accessing the genomes of soil organisms that cannot be, or have not been, cultured by isolating their DNA, cloning it into culturable organisms and screening the resultant clones for the production of new chemicals. The notable number of bioactive molecules isolated from soil microbe actinomycetes reflects their historical importance in antibiotic discovery (Baltz, 2005, Baltz, 2006). In 2001, Watve et al.(Watve et al., 2001) estimated that the order Actinomycetales had produced ~3,000 known antibiotics (90% of those from *Streptomyces*, an Actinomycetales genus) from the first report of streptothricin in 1942. *Streptomyces* is the largest antibiotic-producing genus in the microbial world discovered so far (Clardy et al., 2006).

Plants have also played an important role as a source of effective anti-cancer agents (Hartwell, 1982). Over 60% of currently used anti-cancer agents are derived in one way

---



or another from natural sources, including plants, marine organisms and micro-organisms (Cragg and Newman, 2004, Newman et al., 2003). Clinical, pharmacological and chemical studies of the traditional medicines, which were derived predominantly from plants, were the basis of most early medicines such as aspirin, morphine, quinine, and pilocarpine. Table 1.1 shows some examples of naturally occurring agents that are currently used in clinical practice. The first agents which proceed into clinical use for cancer were the so-called 'vinca' alkaloids, vinblastine (VLB) and vincristine (VCR), isolated from the Madagascar periwinkle, *Catharanthus roseus* G. Don. (Apocynaceae) (Gueritte and Fahy, 2005). They have shown anticancer activity against lymphocytic leukaemia in mice. Recently semisynthetic analogs of these alkaloids, vinorelbine (VRLB) and vindesine (VDS) are used in combination with other chemotherapeutic drugs for the treatment of a variety of cancers, including leukemias, lymphomas, advanced testicular cancer, breast and lung cancers, and Kaposi's sarcoma (Cragg and Newman, 2005). Another important addition to the plant derived chemotherapeutic agents is the taxanes (Kingston, 2005). Paclitaxel initially was isolated from the bark the Pacific Yew, *Taxus brevifolia* Nutt. (Taxaceae) (Cragg, 1998). It is used in the treatment of breast, ovarian and non-small cell lung cancer (NSCLC)(Cseke et al., 2006). Other examples of antitumor compounds currently in clinical trials include ingenol 3-O-angelate a derivative of the polyhydroxy diterpenoid ingenol isolated from the sap of *Euphorbia peplus* which is a potential chemotherapeutic agent for skin cancer (Kedei et al., 2004, Gillespie et al., 2004). The introduction of active agents derived from both microbes and plants, into the collection of cancer chemotherapeutics has changed the natural history of many types of human cancer. Some of the plant derived agents are now stimulating renewed interest with help of advanced technologies, which failed earlier in clinical studies.

---

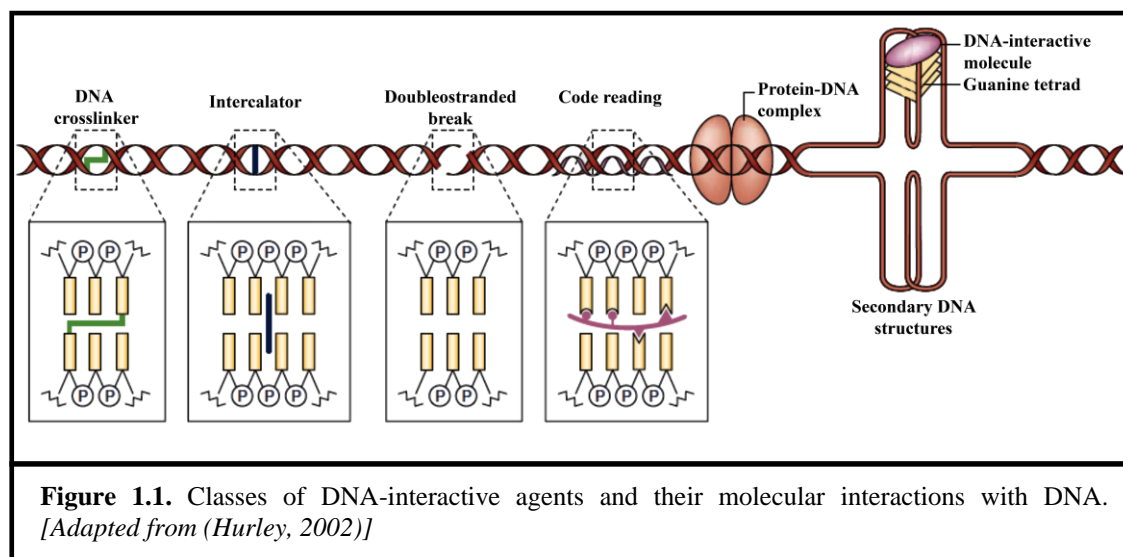
**Table 1.1.** *Natural products in clinical use*

<b>Drugs</b>	<b>Clinical use</b>	<b>Mechanism of action</b>	<b>Source</b>
<b>Aspirin</b>	Analgesic, anti-inflammatory	Inhibition of cyclooxygenase (COX)	Plant
<b>Atropine</b>	Pupil dilator	Antagonist of acetylcholine at muscarinic receptors at post-ganglionic parasympathetic region	Plant
<b>Caffeine</b>	Stimulant	Adenosine receptor antagonist	Plant
<b>Codeine</b>	Analgesic, antitussive	Opioid receptor agonist	Plant
<b>Digoxin</b>	For atrial fibrillation and Congestive Heart Failure	Inhibition of the Na <sup>+</sup> /K <sup>+</sup> ATPase membrane pump	Plant
<b>Eugenol</b>	Toothache	Reduces excitability of sensory nerves (increased K <sup>+</sup> efflux and reduced Ca <sup>2+</sup> influx)	Plant
<b>Morphine</b>	Analgesic	Opioid receptor agonist	Plant
<b>Pilocarpine</b>	Glaucoma	Muscarinic receptor agonist	Plant
<b>Quinine</b>	Anti-malarial	Inhibition of protein synthesis in the malaria parasite	Plant
<b>Taxol</b>	Anticancer agent	Antimitotic agent (binds to and stabilizes microtubules)	Plant
<b>Penicillin</b>	Antibiotic	Inhibition of synthesis of cell wall peptidoglycan	Microbe
<b>Cyclosporin A</b>	Immunosuppressant	Inhibition of clonal proliferation of T lymphocytes (via inhibition of lymphokine production)	Microbe
<b>Tetracyclin</b>	Antibiotic	Inhibition of protein synthesis by binding to the ribosome 30S subunit	Microbe

[Adapted from (da Rocha et al., 2001)]

### 1.3. Modes of action of anticancer antibiotics

Microbial products and several plant derived natural products have come up as one of the most important source of anticancer antibiotics (Dias et al., 2012). Many of these antibiotics recognise specific sites in DNA causing damage/ modifications in DNA strand (Figure 1.1). The structure of the DNA molecule makes it a versatile target for anticancer antibiotics, as it has a negatively charged phosphate backbone, hydrogen bond forming bases in the major and minor groove (Saenger, 1984). Additionally, DNA is polymorphic and has various confirmations such as double helix, hairpins, holliday junctions, triple helices and quadruplexes (Blackburn, 2006). DNA binding antibiotics can recognise these structural diversities and specifically bind to them. Based on the different mechanism of DNA recognition by the ligands, they can be classified into two groups: (a) covalently interacting anticancer antibiotics and (b) non-covalently interacting anticancer antibiotics.



#### 1.3.1. Covalently interacting anticancer antibiotics:

Some antibiotics can bind to DNA via reactive groups to a specific binding site in DNA to cause covalent modification or degradation (Paloma et al., 1994, Uesugi and

Sugiura, 1993). DNA damage from these antibiotics can occur in any cell cycle phase. But cells tend to arrest in S-phase or G2-phase of the cell cycle in cells with p53 and Rb pathway lesions as the result of defective checkpoint mechanisms in cancer cells. Covalent modifications can be of different types; such as (i) DNA strand scission (single/ double) (ii) crosslink the two strands of DNA (iii) adduct formation with bases of DNA (iv) modification of DNA bases. Several types of covalently interacting anticancer antibiotics are shown in Table 1.2.

### **1.3.2. Non-covalently interacting anticancer antibiotics**

Interaction of antibiotics with DNA is always initiated by non-covalent recognitions involving coulomb forces, van der Waal interactions, hydrogen bonding, and stacking interactions. Based on the geometry of the small molecule-DNA complex the non-covalent interactions can be divided into two groups; such as (1) intercalation between base pairs and (2) groove binding (Ghosh et al., 2010, Lerman, 1961). In case of intercalation, planer aromatic rings or heterocycles or carbocycles are inserted into the base pairs of DNA resulting extension of DNA helix. The complex between antibiotics and DNA is stabilized by  $\pi$ - $\pi$  stacking interaction. An intercalator can also induce unwinding of DNA double helix in order to accommodate itself in the DNA base pairs. Several types of intercalators have been identified with diverse chemical structures (Myers et al., 1988, Gianni et al., 1983). These are monointercalators and bisintercalators. A list of different types of intercalators is given in Table 1.2. Another possible way by which small molecule can interact with DNA helix is via major groove or minor groove of DNA (Table 1.2). The major/minor grooves of DNA are of immense structural and chemical significance (Chaires, 1997, Spolar and Record Jr, 1994). Presence of different hydrogen bond donors and acceptors in the minor and

---

major grooves allows for sequence readout by these groups of small molecules. Binding of small molecules via major/ minor groove of DNA could lead to widening of the minor groove. Sometimes it can also induce bending in DNA helix.

### **1.3.3. Dual mode of binding (chromosomal DNA and histones) for DNA-binding small molecules**

It is well established that in eukaryotic nucleus DNA does not exist free in solution, but is compacted in the form of chromatin with several histones and non-histone proteins (Kornberg and Lorch, 1999, Fletcher and Hansen, 1996). The first level of compaction occurs when DNA is wrapped around a histone octamer to form the repeating subunit nucleosome. Nucleosome is composed of 145–147 bp of DNA, wrapped around an octamer of histone proteins in 1.65 turns of a left-handed superhelix (Kornberg, 1977, McGhee and Felsenfeld, 1980, Luger et al., 1997). Tandemly arranged nucleosome cores further assemble into higher-order structures that are stabilized by the linker histone. As a result, the mode of interaction of DNA with small molecules in the chromatin context is more complicated as compared to free DNA. In the chromatin context, small molecules that interact via non-covalent forces may bind to either chromosomal DNA or chromosomal proteins. A number of molecules have been reported that bind to both DNA and histones. Example includes plant alkaloid sanguinarine (Selvi B et al., 2009), ethidium bromide and propidium iodide (Banerjee et al., 2014), anthracycline antibiotics daunomycin (Rabbani et al., 1999), and mitoxantrone etc (Hajihassan and Rabbani-Chadegani, 2011). All of them are well-established DNA intercalators. Reports from our laboratory have shown that sanguinarine binds to core histone in solution causing chromatin aggregation with DNA release (Selvi B et al., 2009). However, classical intercalators, ethidium bromide and

---

propidium iodide, cause chromatin compaction and disrupt the structural integrity of chromatosome upon binding to chromosomal DNA and histone octamer (Banerjee et al., 2014). The biological consequence of the dual-binding mode of these small molecules including some antibiotics in the cell might have far-ranging consequence, since they may be potential epigenetic modulators.

#### **1.4. Aureolic Acid Antibiotics**

Members of the aureolic acid group of antibiotics have been discovered by different groups since their initial identification in 1950s (Lombo et al., 2006a). Small, but distinct group of the aureolic acid antibiotics are produced by various *Streptomyces* Sp. (Figure 1.2). The first member of this family, mithramycin, was isolated from *Streptomyces argillaceus* American Type Culture Collection (ATCC) 12956 (Grundy et al., 1953, Sensi et al., 1958, Rao et al., 1962). The family also includes chromomycins (Sato et al., 1960), olivomycins (Brazhnikova et al., 1962), chromocyclomycin (Blumauerová et al., 1976), UCH9 (Ogawa et al., 1998), and durhamycin A (Jayasuriya et al., 2002). All these compounds have intense yellow colour and fluoresce under UV light, hence the name ‘aureolic’ (Lombo et al., 2006a). Structurally, these compounds belong to the large and important family of the glycosylated aromatic polyketides. The aglycons of this family consist of a tricyclic aromatic moiety, which is connected with one or two aliphatic side chains of variable chain length (Sastry and Patel, 1993, Wohlert et al., 1999). However, chromocyclomycin is the exception as it has tetracyclic aromatic moiety in its aglycone part. In all family members, two oligosaccharide chains containing 2,6-dideoxysugar are bound to the aromatic polyketide moiety (Figure 1.2).

---

**Table 1.2.** Mode of action of various anticancer antibiotics. [Modified from (Hurley, 2002)]

	Mode of interaction	Anticancer antibiotics	Species
Covalent modification	Single-strand breakage (SSB)	Neocarzinostatin (NCS) group of antibiotics	<i>Streptomyces macromomyceticus</i>
	Double-strand breakage (DSB)	Calicheamicin $\gamma 1$	<i>Micromonospora echinospora</i>
	Single/Double-strand breakage	Esperamicin A1	<i>Actinomadura verrucosopora</i> .
	Single/Double-strand breakage	C-1027	<i>Streptomyces globisporus</i> C-1027
	Single-strand breakage (SSB)	Dynemicin A	<i>Micromonospora chernisa</i>
	Single/Double-strand breakage	Bleomycin	<i>Streptomyces verticillus</i>
	Double-strand breakage	Pleomycin	<i>Streptomyces verticillus</i>
	Alkylation of DNA and crosslinking DNA strands	Mitomycin C	<i>Streptomyces caespitosus</i>
	sequence-specific DNA alkylation	Tomamaycin	<i>Streptomyces achromogenes</i>
	Adduct formation with DNA	Sibiromycin	<i>Streptosporangium sibiricum</i>
	Adduct formation with DNA	Anthramycin	<i>Streptomyces refuineus</i>
Non-covalent interaction	Monointercalator	Doxorubicine/ Daunomycin	<i>Streptomyces peucetius</i>
		Actinomycin D	<i>Streptomyces pervulus</i>
		Arugomycin	<i>Streptomyces violochromogenes</i>
		Nogalamycin	<i>Streptomyces nogelater</i>
		Pluramycin	<i>Streptomyces pluricologrescens</i>
		Steffimycin D	<i>Streptomyces steffisburgensi</i>
	Bisintercalator	Triostin A	<i>Streptomyces triostinicus</i>
		Echinomycin	<i>Streptomyces lasaliensis</i> , <i>Streptomyces triostinicus (minor)</i>
		Quinomycin	<i>Streptomyces lasaliensis</i>
	Groove binder	Netropsin	<i>Streptomyces netropsis</i>
		Distamycin	<i>Streptomyces distallicus</i>

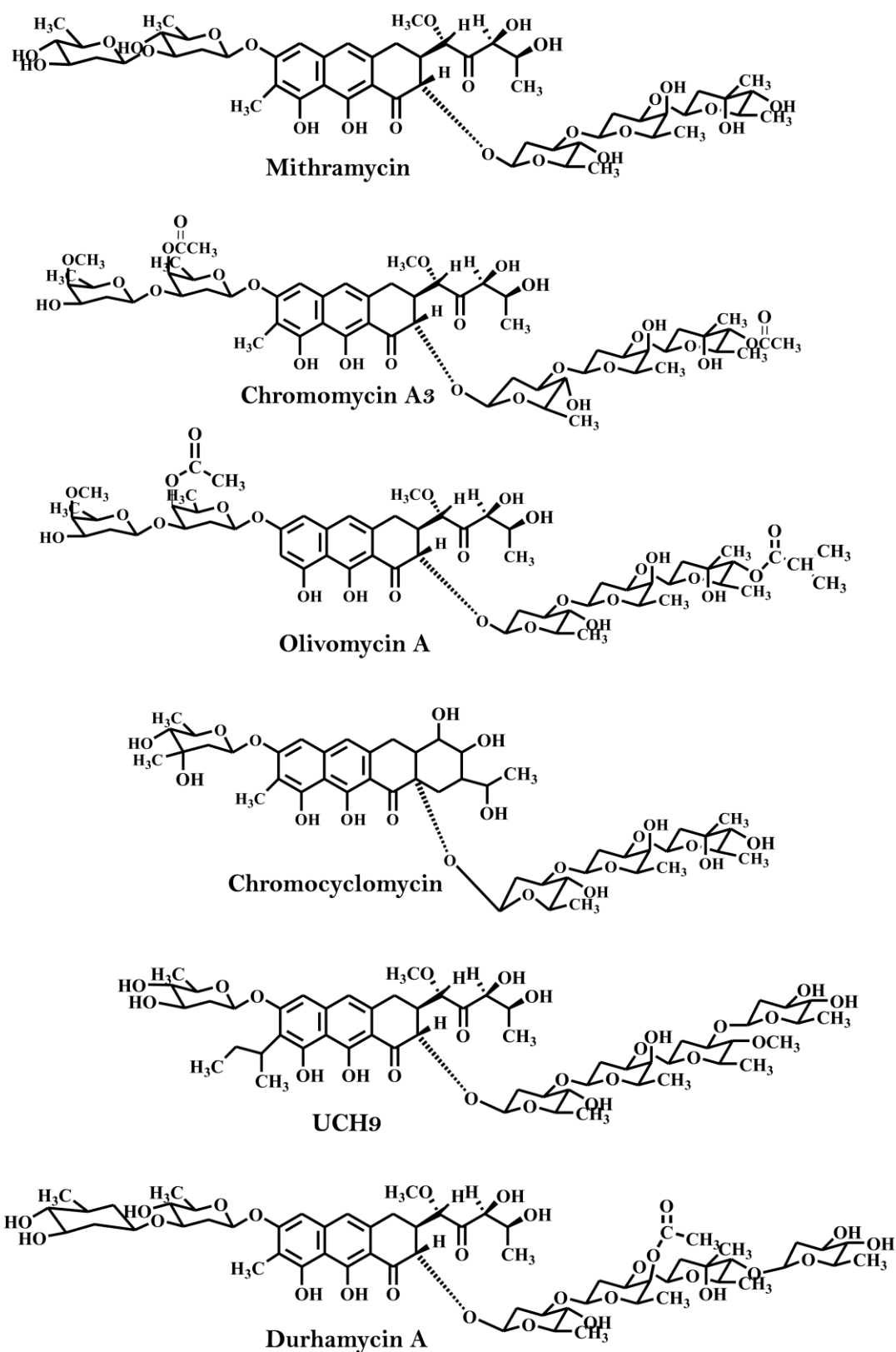
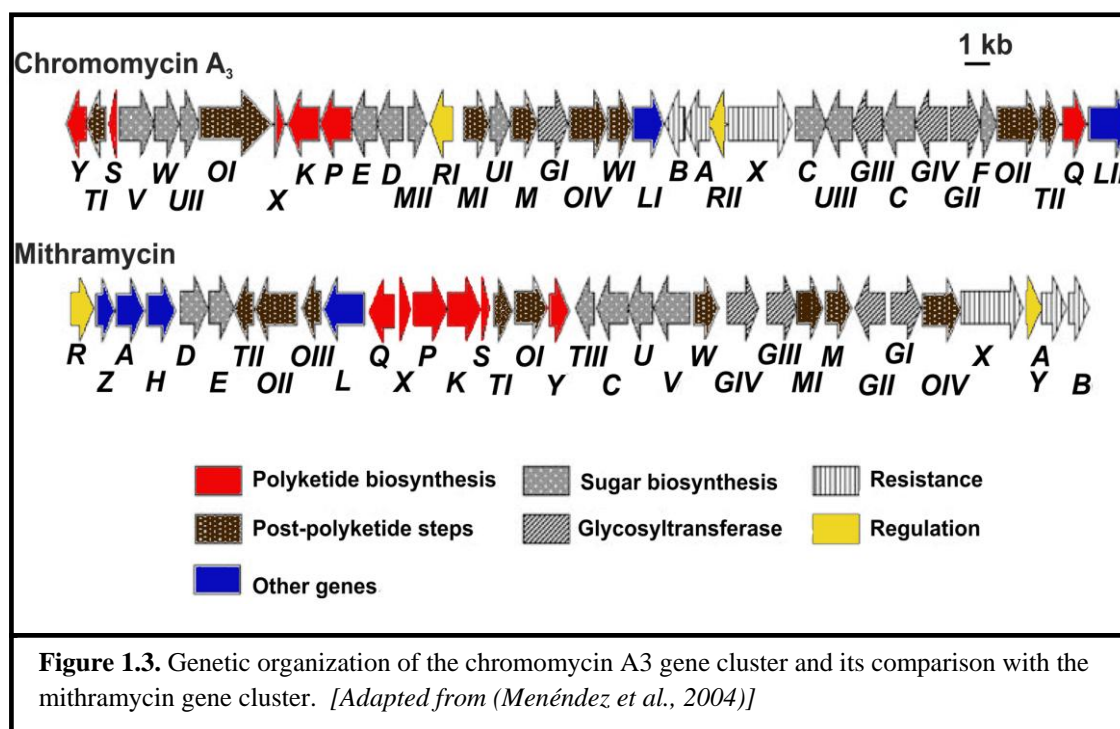


**Figure 1.2.** Chemical structures of aureolic acid group of antibiotics



### 1.4.1 Biosynthesis of mithramycin and chromomycin A<sub>3</sub>

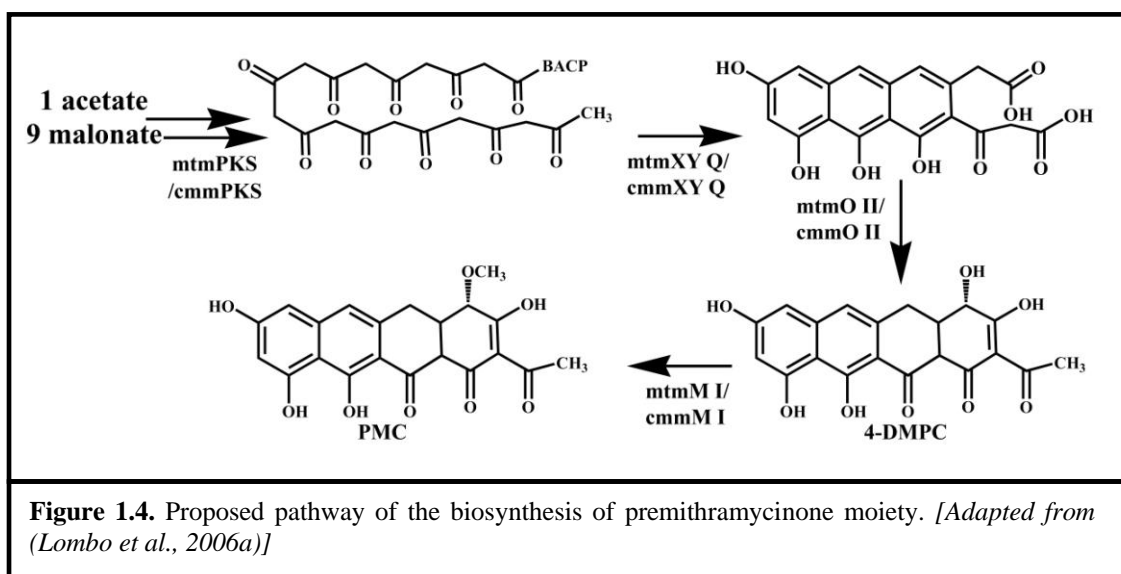
The biosynthesis gene clusters of mithramycin and chromomycin A<sub>3</sub> have been isolated and characterized (Figure 1.3) (Menéndez et al., 2004, Lombó et al., 1999). In spite of the high structural similarity between mithramycin and chromomycin A<sub>3</sub>, the genetic organization of both gene clusters is highly different. The accepted borders of the chromomycin cluster are genes coding for a cyclase and an aromatase (Menéndez et al., 2004). However, genes encoding regulatory and resistance functions enclose the cluster for mithramycin (Lombó et al., 1999), which favour the hypothesis of convergent evolution for the generation in both antitumor compounds. The biosynthetic pathway of formation of MTR and CHR progress through various important steps; such as (a) formation of premithramycinone (PMC), (b) glycosylation of tetracyclic intermediate, (c) conversion of tetracyclic intermediate into tricyclic compound and finally, (e) tailoring modifications.



#### 1.4.1.1. Biosynthesis of premithramycinone moiety

The biosynthesis of MTR and CHR progress through a common intermediate called, premithramycinone (PMC)(Montanari and Rosazza, 1990, Rohr, 1992). It is the last non-glycosylated intermediate in the MTR/CHR biosynthesis pathway (Figure 1.4). PMC consists of a polyketide backbone, which is characteristic for aureolic acid group. The polyketide backbone is synthesized through the condensation of one acetyl-CoA and nine malonyl-CoA units by type II polyketide synthase (PKS) (Künzel et al., 1997, Blanco et al., 1996). Type II PKS from a mithramycin producer, *S. argillaceus* (ATCC 12596) contains several genes like, *mtmP* ( $\beta$ -ketoacylsynthase), *mtmK* (chain length factor), and *mtmS* (acyl carrier protein) (Hopwood, 1997, Hopwood and Sherman, 1990, Katz and Donadio, 1993, Hutchinson and Fujii, 1995). Similar genes for chromomycin A3 biosynthesis pathway have been also identified and sequenced and they are *cmmP*, *cmmK* and *cmmS* respectively (Menéndez et al., 2004). Action of all these genes generate a linear decaetide which is further aromatized in the first two rings by the *mtmQ/cmmQ* aromatase and cyclized at the third ring by the *mtmY/cmmY* cyclase (Lozano et al., 2000, Prado et al., 1999b, Lombó et al., 1996). Then, the action of the *mtmOII/ cmmOII* oxygenase introduces two hydroxyl groups (Prado et al., 1999a) and the *mtmX/cmmX* cyclase carries out the cyclization at the fourth ring, which generates the first tetracyclic intermediate, 4-demethylpremithramycinone (4-DMPC) (Figure 1.4) (Lozano et al., 2000). This compound is methylated by the *mtmMI/cmmMI* O-methyltransferase, giving rise to PMC (Lombo et al., 1997). PMC plays a key role in the biosynthesis of all aureolic acid compounds. In spite of structural differences between members of the group, the early stages are the same, leading to the formation of this crucial intermediate PMC.

---



#### 1.4.1.2. Glycosylation of PMC in the mithramycin biosynthesis pathway

The glycosylation of PMC is the second stage of the biosynthesis of MTR. In order to determine the sequence of incorporation of the disaccharide and the trisaccharide to PMC, different mutants were generated by independent inactivation of four genes encoding glycosyltransferases (*mtmGI*, *mtmGII*, *mtmGIII*, and *mtmGIV*) (Figure 1.5) (Blanco et al., 2000, Gonzalez et al., 2001, Menendez et al., 2006b). Different compounds with variable number of sugar moiety attached to the PMC are formed. They differ in the number of sugar units in the trisaccharide and lack the disaccharide moiety. Main inferences can be drawn from these observations are (a) the disaccharide is transferred to the aglycon as a unit, (b) the trisaccharide is transferred to the aglycon sequentially before the disaccharide unit and (c) *mtmMII* transfer the methyl group to the C9 position of PMC after the first sugar unit of the trisaccharide chain has been attached (Figure 1.5) (Remsing et al., 2002, Menendez et al., 2006a, Blanco et al., 2000). Thus another important intermediate premithramycinone B is formed.



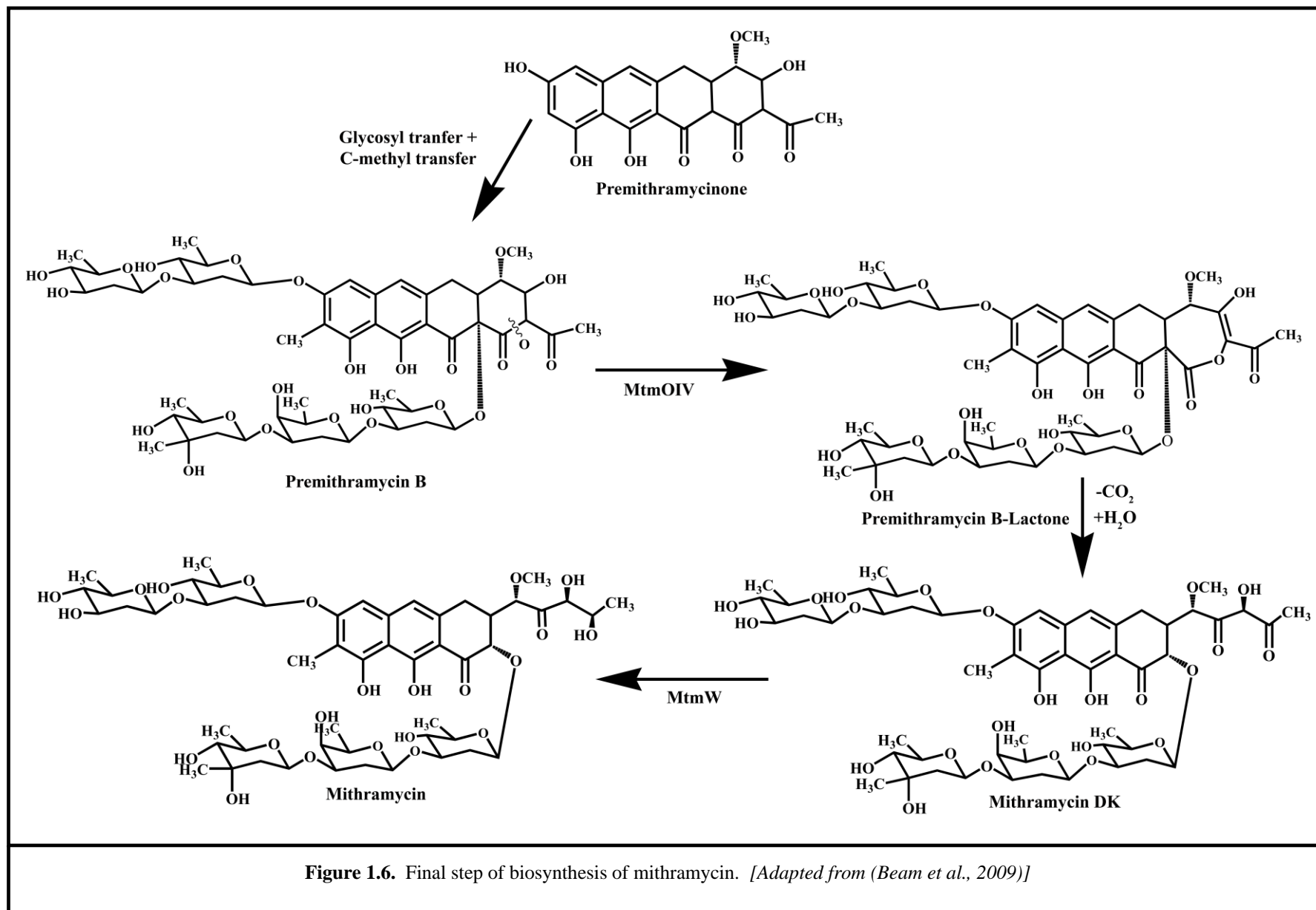
#### 1.4.1.3. Conversion of premithramycinone B to active tricyclic compound

The final step of MTR biosynthesis pathway is the opening of the fourth ring of the premithramycinone B. Interestingly, premithramycin B did not show detectable antibiotic or antitumor activity, thus suggesting that the opening of the fourth ring becomes essential to generate biologically active compounds (Rodríguez et al., 2003, Gibson et al., 2005). MtmOIV oxidatively cleaves the fourth ring via a Baeyer- Villiger reaction to generate the characteristic tricyclic aglycone core and highly functionalized pentyl side chain of MTR (Figure 1.6) (Menéndez et al., 2004, Prado et al., 1999a). Recent studies have shown the three-dimensional structure of MtmOIV by X-ray crystallography (Beam et al., 2009). The Baeyer-Villiger reaction leads to lactone opening followed by decarboxylation. As a result of this reaction, a 4'-ketomithramycin is generated, which is further reduced to form the 4'-hydroxyl group of the thereby formed pentyl side chain by MtmW (ketoreductase) to give rise the fully activated MTR (Wang et al., 2012).

#### 1.4.1.4. Glycosylation of premithramycin B in chromomycin pathway

Previous reports show that the producer organisms of MTR and CHR (*S. argillaceus* and *S. griseus subsp. griseus* respectively) are highly resistant to their own product (Lombo et al., 2006a). But interestingly producer organisms do not show cross-resistance in spite of the close structural similarity in MTR and CHR. Unique pattern of sugars in CHR confer altered activity of CHR (Menendez et al., 2006b). Glycosyltransferases *cmmGIV* and *cmmGIII* sequentially attach sugars (D-olivose) to the tetracyclic compound PMC to produce premithramycin A2. The third deoxysugar of the trisaccharide is a branched chain sugar (L-chromose B) connected by the action of glycosyltransferase *cmmGIV*. This leads to the formation of 9-demethyl-

---



prechromomycin A3. The last two D-oliose sugars are sequentially incorporated by *cmmGII* and *cmmGI* (Menéndez et al., 2004, Remsing et al., 2003).

#### **1.4.1.5. Tailoring modifications of the sugars in CHR biosynthesis pathway**

Once the sugars are transferred to the aglycon, they undergo further tailoring modifications, such as two acetylations and one methylation (Menendez et al., 2004). *CmmA* and *cmmMIII* enzymes are responsible for catalysing these tailoring modifications. *CmmMIII* methyltransferase acts before the *CmmA* acyltransferase. Interestingly, in spite of the existence of two acetyl groups in chromomycin A3, only one acyltransferase *cmmA* was found in the chromomycin cluster and it is capable of acting on both L- and D-sugars (sugars E and A). The acetylation steps are considered as crucial enzymatic events during chromomycin biosynthesis, as these acetylation steps are essential to convert less active biosynthetic intermediates (dideacetylated chromomycin) into a totally active compound (chromomycin A3) (Menendez et al., 2004). To survive during the production phase of CHR producer organism activates the final product in the vicinity of the cell membrane. The protein *cmmA* has several trans-membrane domains which is the characteristic of membrane-embedded proteins. This supports the view that the acetylation events take place linked with the cell membrane. However, a recent report showed that the fully functionalized substrate, prechromomycin is the preferred substrate for the critical oxygenase *cmmOIV* (Bosserman et al., 2011). This observation ruled out the earlier proposition that O-acetylation and O-methylation occur at the very end of the chromomycin A3 biosynthesis. The accumulation of completely acetylated and methylated prechromomycin compounds in *CmmOIV*-minus mutant indicates that modifications on the sugar residues take place prior to *cmmOIV* reaction.

---

### 1.4.2. Effects of mithramycin and chromomycin

#### 1.4.2.1. Antitumor property

Initially, MTR and CHR were isolated due to their antibiotic activity against Gram-positive bacteria (Lombo et al., 2006b). Later their antitumor properties acquired interest. MTR/CHR exerts their antitumor property upon binding to DNA helix via minor groove in regions with high GC content (Waring, 1981, Katahira et al., 1998, Goldberg and Friedman, 1971). Presence of bivalent metal ions like  $Mg^{2+}$ ,  $Zn^{2+}$ ,  $Fe^{2+}$  is prerequisite for MTR/CHR to bind DNA (Chakraborty et al., 2008, Devi et al., 2009, Aich and Dasgupta, 1995, Aich et al., 1992). Complexes of MTR/CHR with bivalent metal ions are the DNA binding ligands (Devi et al., 2007, Hou and Wang, 2005, Lu et al., 2009). Deoxysugars provide the stabilization of MTR/CHR- $M^{2+}$  complexes with the DNA (Sastry et al., 1995, Keniry et al., 2000). The sequence specificity of MTR/CHR- $M^{2+}$  complexes is the consequence of H-bond formation of between guanosine base in the DNA helix and the hydroxyl groups present in the aglycone part present in MTR/CHR (Sastry and Patel, 1993). Association of MTR/CHR with DNA leads to the inhibition of DNA dependent RNA synthesis (Wakisaka et al., 1963, Ward et al., 1965). Hence they exhibit antitumor properties towards various cancer cells. Proto-oncogene *c-myc*, containing G.C rich promoter, plays important role in cellular proliferation and differentiation. MTR inhibits *c-myc* expression in both differentiating and non-differentiating cells upon binding to *c-myc* promoter regions, in particular P1 and P2 regions (Snyder et al., 1991, Blume et al., 1991, Albertini et al., 2006). Moreover, MTR directly blocks the binding of the transcription factor *Spl* to the P1 promoter region thereby inhibit the expression of angiogenic gene (Black et al., 2001). MTR has been used clinically in the treatment of some cancer like testicular carcinoma (Fletcher, 1973, Kennedy and Torkelson, 1995), chronic myelogenous leukemia (CML)

---



(Koller et al., 1985, Koller and Miller, 1986), brain tumors (Kennedy et al., 1968) and pancreatic cancer (Jia et al., 2007, Jia et al., 2010, Gao et al., 2011, Yuan et al., 2007) in combination with other compounds.

Aberrant DNA hypermethylation on promoter region of tumor-suppressor genes (TSGs) play key role in cancer initiation and progression. Recent studies have also shown that MTR inhibits the enzymatic action of DNA methyltransferase (DNMT), thereby prevents hypermethylation of CpG islands present in different TSGs (Lin et al., 2007). It has been also shown that MTR can not only bind to DNA but can also directly bind to DNMT1 and deplete the protein.

#### **1.4.2.2. Role in neuro-protection**

MTR and CHR are potent inhibitors of neuronal apoptosis (Chatterjee et al., 2001). They are among the few anticancer antibiotics which can penetrate the blood-brain barrier. MTR increased the survival of a transgenic mouse model of Huntington's disease (HD) (R6/2) by 29.1% (Ferrante et al., 2004). Additionally, MTR improves functional motor performance and improves brain neuropathological sequelae. Different mechanisms have been proposed to explain the neuro -protection activity of MTR and CHR. MTR/CHR can inhibit glutathione depletion induced Sp1/Sp3 DNA binding to DNA (Chatterjee et al., 2001). Binding of Sp1/Sp3 to DNA induce oxidative stress in embryonic cortical neurons. MTR/CHR can inhibit enhanced DNA binding of these transcription factors to the GC rich promoter in DNA and thereby inhibit the oxidative-stress induced apoptosis of neurons. Another possibility for the neuroprotective mechanism of MTR is that it can alter the epigenetic modifications of histone. Increased histone H3 lysine 9(H3K9) methylation leads to transcriptional repression in HD (Ryu et al., 2006). MTR prevents the hypermethylation by inhibiting

---

the enzymatic action of histone methyl transferase (HMT). Pathogenesis of various neurodegenerative diseases is also associated with endoplasmic reticulum (ER) stress. MTR exerts strong neuro-protective effect against ER stress-induced cell death in organotypic hippocampal slice cultures (OHCs), however the mechanism is not fully understood (Kosuge et al., 2011). MTR decreases the development of behavioural sensitization and dopaminergic neurotoxicity in mice after repeated administration of methamphetamine (METH), an addictive stimulant associated with memory loss, aggression, psychotic symptoms and potential heart and brain damage (Hagiwara et al., 2009). Furthermore, recent studies have shown that MTR decreases basal as well as cigarette smoke-induced expression of ABCG2 gene, which is responsible for proliferation, migration of lung and oesophageal cancer cells (Zhang et al., 2012).

#### **1.4.2.3. Role in bone remodelling**

MTR treatment to patients with advanced Paget's disease brings about significant beneficial effects (Russell and Lentle, 1974, Condon et al., 1971). Paget's disease is a disorder that involves abnormal bone destruction and regrowth, which ultimately leads to deformity. MTR alters the calcium metabolism and ameliorates the symptoms of patients with Paget's disease. Moreover, MTR has been also used for hypercalcemia associated with malignancy. MTR directly inhibits osteoclastic bone resorption in the *in vitro* bone slice assay (Esbrit and Hurtado, 2002, Hall et al., 1993).

Matrix metalloproteinases (MMPs) are zinc-dependent endopeptidases, which are known to cleave collagens and aggrecan of cartilage extracellular matrix. Overexpression of MMPs leads to degeneration of articular cartilage. MTR can downregulate the expression of MMP genes without affecting the function of mitogen-activated protein kinases (MAPKs) (Liacini et al., 2005).

---

#### **1.4.2.4. Role in fetal haemoglobin (HbF) production**

Several DNA binding drugs are capable of augmenting HbF levels in humans, for example tallimustine and some cisplatin analogs (Bianchi et al., 2001, Bianchi et al., 2000). They can regulate the gene expression by modifying DNA-protein complex formation. Various reports have shown that MTR and CHR are potential inducers of erythroid differentiation and in human leukemic K562 cell line (Bianchi et al., 2001). Sequence specific binding of MTR/CHR leads to the increase in expression of  $\gamma$ -globin gene (Fibach et al., 2003, Bianchi et al., 2001). As a result, MTR and CHR can increase the HbF production in erythroid precursor cells from healthy human subjects as well as from  $\beta$ -thalassemia patients.

### **1.5. Importance of transition metals ion in biology**

Transition metal ions are essential to diverse biological processes in cell (Reyes-Caballero et al., 2011). Inherent properties of a metal ion dictate its role in a specific biological process. Transition metal ions are essential cofactors for oxidation–reduction, electron transfer, hydrolytic and acid–base reactions. They are important structural elements, which stabilize protein folding. Among first row transition metals  $\text{Zn}^{2+}$  is unique as it plays a dual function in cell. It can act as a structural element and a catalytic cofactor. For example,  $\text{Zn}^{2+}$  stabilizes diverse “zinc-finger” proteins (Berg and Godwin, 1997, S  n  que et al., 2009, Auld, 2001). On the other hand,  $\text{Zn}^{2+}$  is an essential cofactor of many hydrolytic enzymes, including proteases, phosphatases, esterases and deacetylases, where it functions as a Lewis acid to activate a water molecule for catalysis (Auld, 2001). Other transition metal ions like  $\text{Mn}^{2+}$ ,  $\text{Fe}^{2+}$ ,  $\text{Ni}^{2+}$ ,  $\text{Cu}^{2+}$  are also important cofactors of various enzymes. For instance, superoxide dismutases (SODs) which are ubiquitous enzymes found in virtually all cells and

---

oxygen-tolerant organisms (Perry et al., 2010). They have a wide array of metals in their catalytic sites to catalyse the dismutation reaction. The stomach pathogen *Helicobacter pylori* has  $\text{Ni}^{2+}$  as a cofactor for the enzyme urease, which allows this organism to colonize the acidic gastric lumen (Ermler et al., 1998). The precise control of cytoplasmic metal ion concentrations is termed as metal homeostasis, which includes metallochaperones, metal importers, and metal fluxing transporters. All of them play vital roles in regulating metal bioavailability (Giedroc and Arunkumar, 2007).

### 1.5.1. Biological significance of manganese ion

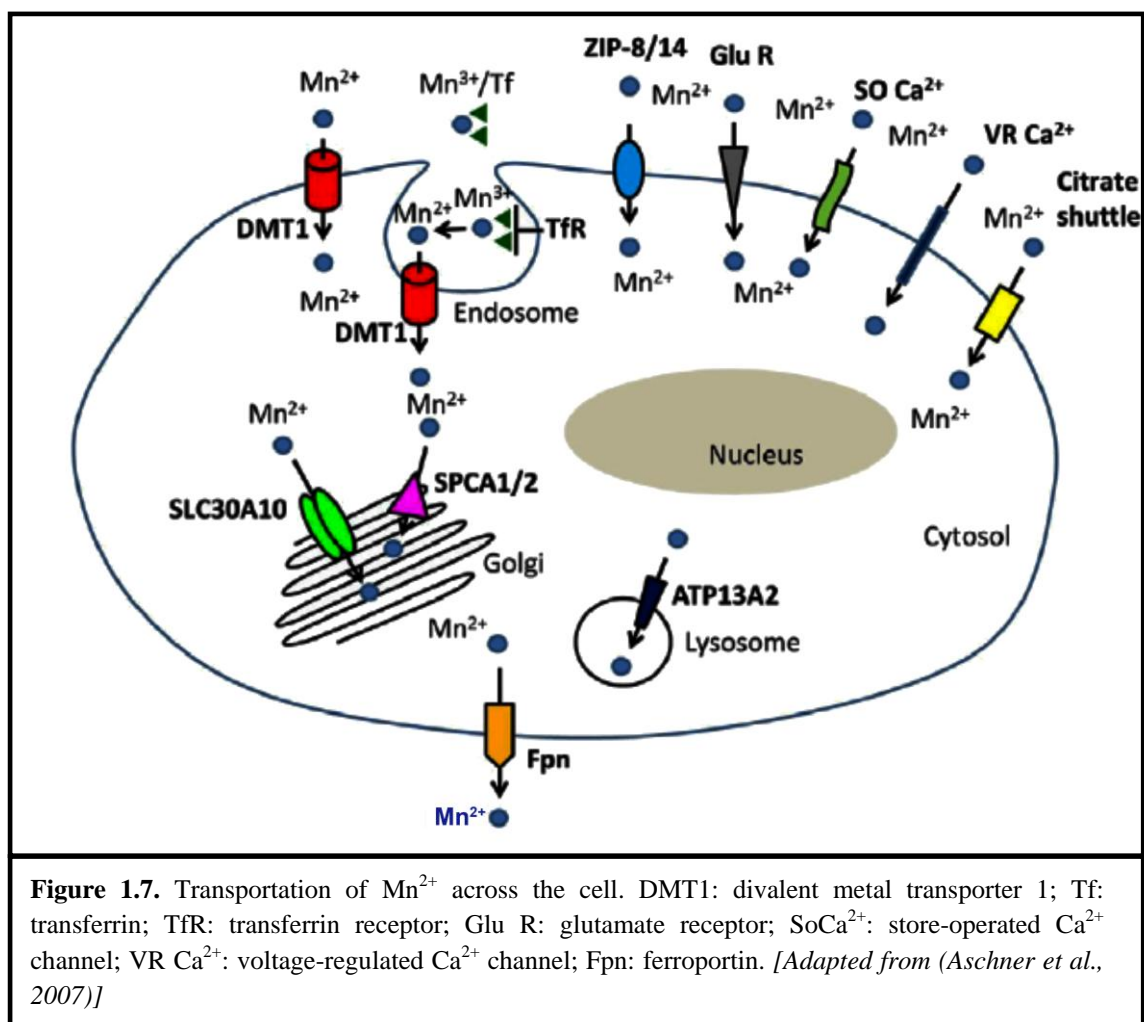
Manganese ( $\text{Mn}^{2+/3+}$ ) is an essential trace element which is required for the function of a variety of enzymes like oxidoreductases, transferases, hydrolases etc (Takeda, 2003, Aschner et al., 2005, Aschner et al., 2007). Stable tissue levels are maintained by tight homeostatic control of intestinal absorption and biliary excretion of  $\text{Mn}^{2+}$  (Aschner et al., 2005). In all human tissues, 0.3 to 2.9  $\mu\text{g}$  of  $\text{Mn}^{2+}$  per gram of wet tissue are required for homeostatic regulation. The liver, kidney, pancreas, bone, and basal ganglia and cerebellum of brain are particularly rich in  $\text{Mn}^{2+}$ .

### 1.5.2. Metabolism of manganese

***Uptake of Manganese:*** Manganese is absorbed into the enterocyte in the proximal small bowel via the divalent metal transporter 1 (DMT1) (Sacher et al., 2001). Once absorbed into the portal circulation, the main proportion of  $\text{Mn}^{2+}$  (80%) is bound to  $\beta$ -globulin and albumin. Certain portion of absorbed  $\text{Mn}^{2+}$  is oxidized to  $\text{Mn}^{3+}$  by ceruloplasmin and bound to transferrin (Tf) (Aschner et al., 2007).

---

**Manganese transportation:** The exact mechanisms of  $\text{Mn}^{2+/3+}$  transportation in various organs are not well understood. Three possible routes have been proposed for the uptake of  $\text{Mn}^{2+/3+}$  into the central nervous system, such as (i) entry across the cerebral capillaries at the blood brain barrier (BBB) (ii) crossing the choroid plexus into the cerebrospinal fluid (CSF) (iii) direct intra-axonal uptake via olfactory or trigeminal presynaptic nerve endings (Aschner et al., 2005, Yokel and Crossgrove, 2004). One major contributor of  $\text{Mn}^{2+/3+}$  - transport to the brain is DMT1 (via Tf-dependent and Tf-independent pathways) (Figure 1.7).



In the Tf-dependent pathway,  $Mn^{3+}$  binds to Tf with high affinity (Au et al., 2008, Guilarte et al., 2006). Next, the Tf– $Mn^{3+}$  complex binds to the Tf receptor (TfR) at the plasma membrane, which leads to the internalization of the Tf–TfR complex into endosomal vesicles. The endosomal V-ATPase facilitates acidification of the vesicle and leads to release of the metal, followed by conversion of  $Mn^{3+}$  to  $Mn^{2+}$ . In the Tf-independent pathway DMT1 has been suggested to transfer  $Mn^{2+}$  at the BBB (Crossgrove et al., 2003).

ZIP-8 and ZIP-14 are also important for  $Mn^{2+}$ -transportation in other organs, like duodenum, liver lungs, and kidney. Studies on the function of ZIP-8 and ZIP-14 have shown that they also play vital role in the absorption of  $Mn^{2+}$  in the liver and the proximal tubule in the kidney (Girijashanker et al., 2008, He et al., 2006).

***Manganese efflux from cell:*** The cytoplasmic Fe exporter Fpn has been shown to act as an effective mediator of  $Mn^{2+}$  efflux from cell (Yoon et al., 2011, Madejczyk and Ballatori, 2012). SLC30A10, belongs to cation ( $M^{2+}$ ) diffusion facilitator family, has also been identified as an important contributor in the regulation of  $Mn^{2+}$  homeostasis.

### 1.5.3. Manganese toxicity

Homeostasis of  $Mn^{2+}$  is very important for human as well as for bacteria. Experimental models have suggested that low levels of  $Mn^{2+}$  cause poor bone growth, skeletal abnormalities, ataxia, and abnormal glucose tolerance (Keen et al., 1998, Friedman et al., 1987). However,  $Mn^{2+}$  overload causes a well-recognized condition known as “manganism.” Manganism has been extensively characterized (Couper, 1837, Rodier, 1955). This Parkinson like syndrome can be divided in three overlapping stages (Roth, 2009). Emotional and cognitive disturbances with abnormal fine motor coordination are

---

observed in initial stage. Second stage is associated with psychiatric illnesses, speech disorder and mask-like facial expression. During the final stage, patients develop disabling limb rigidity, dystonia, impairment of balance and a characteristic cock-walk gait (Huang et al., 1997).

**Table 1.3.** Different disease condition related to  $Mn^{2+}$

$Mn^{2+}$ deficiency	Excess $Mn^{2+}$
Growth retardation and skeletal deformities	<b>Manganism:</b>  <u>Stage 1:</u> emotional and cognitive disturbances with abnormalities in fine motor coordination  <u>Stage 2:</u> profound psychiatric illnesses, speech disorder and mask-like facial expression  <u>Stage 3:</u> disabling limb rigidity, dystonia, impairment of balance, and a characteristic cock-walk gait
Ataxia	
Abnormal glucose metabolism	
Pancreatic dysfunction	
Elevated blood pressure	
Atherosclerosis	
Reduced protein metabolism	
Reduced immune function	
Infertility	
Selenium deficiency	
Depressed activity of mammary glands in nursing mothers	
Mitochondrial abnormalities	

### 1.5.3.1. Mechanism of neurotoxicity

Understanding of biochemical mechanisms associated with  $Mn^{2+}$  neurotoxicity progressed at rapid rate, which are as follows.

**Alteration of dopamine transmission:**  $Mn^{2+}$  neurotoxicity causes abnormal presynaptic dopaminergic signalling and decrease dopamine (DA) release while preserving the integrity of the neurons (Guilarte et al., 2006). Recent report has suggested that excess  $Mn^{2+}$  accumulates in the basal ganglia, which affects DA neurotransmission (Roth et al., 2013). Furthermore, it has been suggested that in basal ganglia areas in brain,  $Mn^{2+}$  is converted to  $Mn^{3+}$  and thereby oxidise extra cellular DA which may cause oxidative

injury and degeneration of dopaminergic neurons after uptake via DA transporter (Figure 1.8) (Farina et al., 2013).

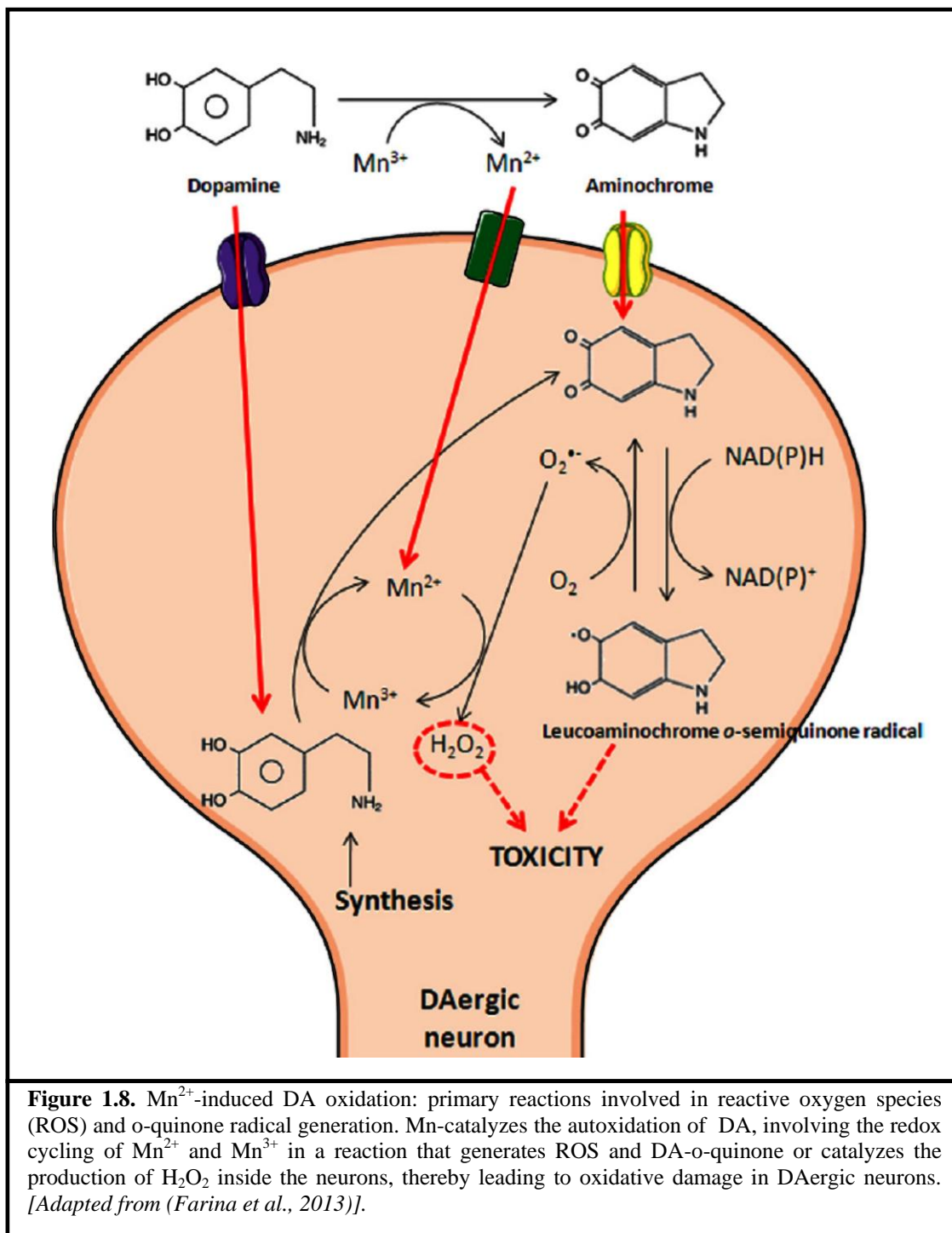


**Figure 1.8.** Mn<sup>2+</sup>-induced DA oxidation: primary reactions involved in reactive oxygen species (ROS) and o-quinone radical generation. Mn-catalyzes the autooxidation of DA, involving the redox cycling of Mn<sup>2+</sup> and Mn<sup>3+</sup> in a reaction that generates ROS and DA-o-quinone or catalyzes the production of H<sub>2</sub>O<sub>2</sub> inside the neurons, thereby leading to oxidative damage in DAergic neurons. [Adapted from (Farina et al., 2013)].



***Production of reactive oxygen species:*** Excess  $\text{Mn}^{2+}$  produces reactive oxygen species (ROS) and thereby enhanced oxidative stress in cell (Graham, 1978). The most common ROS include the superoxide radical ( $\text{O}_2^{\cdot-}$ ), hydrogen peroxide ( $\text{H}_2\text{O}_2$ ) and hydroxyl radical ( $\text{OH}^{\cdot}$ ) which are potential agents to damage of nucleic acids, proteins, and phospholipids.  $\text{Mn}^{2+}$  preferentially concentrates in mitochondria as it can bind to ATP (Martinez-Finley et al., 2013).  $\text{Mn}^{2+}$  directly interferes with the production of ROS which in turn leads to the inhibition of oxidative phosphorylation. In the first step of ROS production, superoxide radical ( $\text{O}_2^{\cdot-}$ ) is converted to  $\text{H}_2\text{O}_2$  by the  $\text{Mn}^{2+}$  and Cu/Zn superoxide dismutase enzymes; present in the mitochondria and cytoplasm respectively.  $\text{H}_2\text{O}_2$  can be further converted to  $\text{OH}^{\cdot}$  in the presence of  $\text{Mn}^{2+}$  or other transition metals (Gavin et al., 1992, Goldstein et al., 1993, Martinez-Finley et al., 2013).

***Alters  $\text{Ca}^{2+}$  homeostasis:*** In mitochondria  $\text{Mn}^{2+}$  can replace  $\text{Ca}^{2+}$  by occupying its binding site (Farina et al., 2013, Martinez-Finley et al., 2013). This induces of a process called mitochondrial permeability transition (MPT), which causes increased solubility of the mitochondrial membrane for ions and protons. Thus inner membrane potential of mitochondria decreases, which leads to mitochondrial swelling and cell death through apoptosis (Rao and Norenberg, 2004).

***Hinder glutamine transportation:*** Glutamine has variety of biochemical function such as protein synthesis, regulating acid-base balance and transportation of ammonia in blood (Sidoryk-Wegrzynowicz et al., 2011). Excess  $\text{Mn}^{2+}$  inhibits the expression of specific glutamine transporters causing reduced uptake of glutamine (Aschner et al., 2007). As a consequence, extracellular glutamate level increases which leads to neuronal excitability (Farina et al., 2013).

---

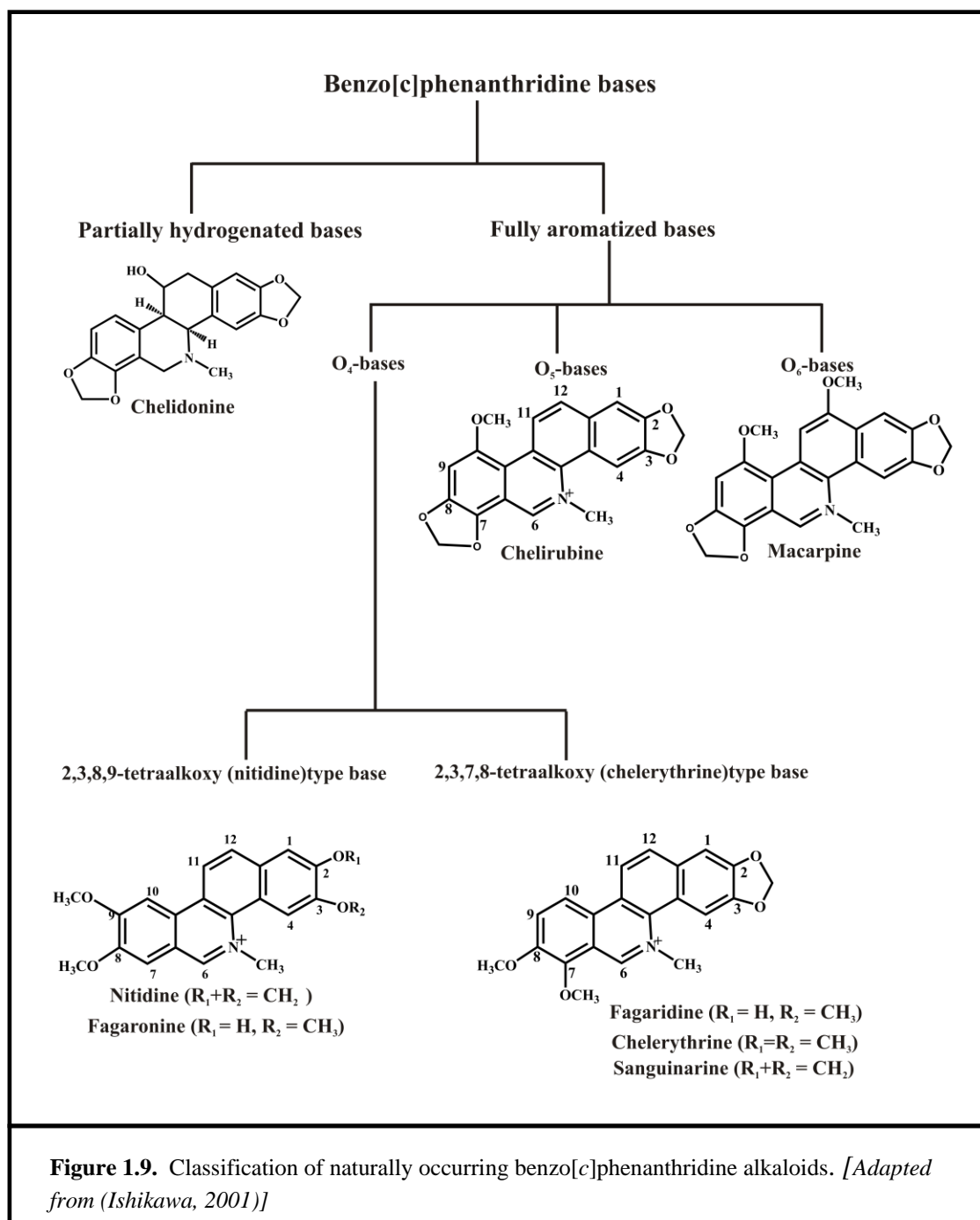
## 1.6. Alkaloids

The alkaloids are organic nitrogenous bases found mainly in plants, but also to a lesser extent in microorganism and animals. The name alkaloid is originated from alkali. Usually several nitrogen atoms present in heterocyclic ring form primary, secondary, tertiary or quaternary amines and confer basicity to the alkaloids (Dewick, 2011). Alkaloids are often classified according to the nature of their nitrogen-containing structure, e.g. pyrrolidine, piperidine, quinoline, isoquinoline, indole, pyrrolizidine, etc (Evans, 2009). Alkaloids have traditionally been of interest due to their pronounced and various physiological activities in animals and humans. The biological activity of many alkaloids is often dependent on the amine functional group, which can transform into a quaternary system by protonation at physiological pHs (Southon and Buckingham, 1989).

### 1.6.1 Benzo[c]phenanthridine alkaloids

Benzo[c]phenanthridine alkaloids are tetracyclic aromatic compounds containing an isoquinoline structure (Ishikawa, 2001). Naturally occurring benzo[c]phenanthridine bases are structurally classified into five categories based on both their oxidation level and the number of oxygen functionalities as shown in Figure 1.9 (Ishikawa, 2001). The isolations of impure forms of benzo[c]phenanthridine alkaloids started date back to the first half of the 19<sup>th</sup> century (Ishikawa, 2001). Since then, several others have been found mostly in the plant families like Papaveraceae, Fumariaceae and Rutaceae (Krane et al., 1984). Some of these alkaloids have attracted much attention because of their anti-inflammatory (Lenfeld et al., 1981), antimicrobial (Mitscher et al., 1977, Navarro and Delgado, 1999, Odebiyi and Sofowora, 1979), antitumour (Nakanishi et al., 1998, Stermitz et al., 1975, Stermitz et al., 1973), antiviral effects (Sethi, 1979).

---



Benzo[c]phenanthridine alkaloids are highly reactive biological reducing agents and also act as nucleophiles. They have pseudobase, aminal, pseudoalcoholate and iminium forms depending on the different solvent conditions (Eldin and Jencks, 1995, Nakanishi et al., 2000, Parenty et al., 2004, Yoshida et al., 1999). Consequently, these different chemical forms will have different effects in biological systems.

### 1.6.2. Chelerythrine

Chelerythrine (CHL) is a 2,3,7,8-tetrasubstituted quaternary benzo[c]phenanthridine alkaloids (QBA), isolated from chinese herbs, *Chelidonium majus* L. and *Macleaya cordata* (Malikova et al., 2006a). *Chelidonium majus* L. or ‘greater celandine’ is a rich source of biologically active substances used for the treatment of various diseases. The most effective alkaloids of this plant are protopine, chelidonine, coptisine, sanguinarine, allocryptopine, chelerythrine, etc. Various analytical techniques such as high-performance liquid chromatography (HPLC) or capillary electrophoresis (CE) are used to separate and quantify currently available alkaloids (Kursinszki et al., 2006, Lee et al., 2007, Fabre et al., 2000).

CHL exerts wide spectrum of biological activities, e.g. from antimicrobial, antifungal, anti-inflammatory and cytotoxicity against various human cancer cell lines (Zdarlova et al., 1997). Chemically, chelerythrine can interconvert between the cationic vs. neutral forms (i.e. hydroxide adduct /pseudobase) (Malikova et al., 2006a). Thus it can penetrate the cell membrane in the form of nonpolar pseudobase. In the cationic form, the iminium bond,  $C_6=N^+$  is susceptible to nucleophilic attack and plays a key role in inhibition of SH-proteins (Slaninova et al., 2001). CHL affect eukaryotic cells in many ways and several cellular targets for its action have recently been established. However, the exact molecular mechanisms for biological activities of CHL are still not known.

#### 1.6.2.1. Effect of chelerythrine on tumour cells

The cytotoxic effects of CHL were evaluated in various human tumour cell lines such as breast cancer cells MCF7 and MCF7ADR (resistant to adriamycin), colon cancer cells H29, brain cancer cells DaOY, prostate cancer cells LnCaP, some chemo-radio resistant oral tumor cell lines SQ-20B, JSQ-3, SCC-35 and SCC61 to assess its

---

spectrum of activity (Kemeny-Beke et al., 2006, Yamamoto et al., 2001, Chan et al., 2003). It exerts cell growth-inhibitory effects via the induction of apoptosis in a variety of cancer cells.

Apoptosis is a term used to describe the terminal morphological and biochemical events seen in programmed cell death (Wyllie, 1997). Cells undergoing programmed cell death are characterized by morphological changes, including cellular shrinkage, plasma and nuclear membrane leaking, organelle re-localization and compaction, nuclear DNA condensation with or without fragmentation, and hyper-segmentation of nuclear chromatin of irregular size (Orrenius, 1995). There are three mechanisms involved in the apoptotic process: (i) receptor-ligand mediated mechanism, (ii) mitochondrial pathway and (iii) mechanism in which the endoplasmic reticulum plays a central role (McConkey et al., 1996). All three mechanisms activate caspases which are responsible for the characteristic morphological changes observed during apoptosis (Thornberry and Lazebnik, 1998). The caspase-cascade system plays a vital role in the induction, transduction and amplification of intracellular apoptotic signals (Mancini et al., 1998). CHL decreases the mitochondrial potential and disrupts the interaction between anti-apoptotic protein Bcl-XL and pro-apoptotic protein Bax in human neuroblastoma SH-SY5Y and human leukemia HL-60 cells, which stimulate the release of cytochrome c from mitochondria (Chan et al., 2003). Cytochrome c participates in the assembly of the apoptosome resulting in the activation of caspase-9 which subsequently activates the effector caspase-3 followed by cleavage of the caspase-3 substrate PARP (Poly ADP ribose polymerase) and subsequent DNA degradation and apoptotic death.

CHL exerts its antitumor effect in part through the induction of apoptosis mediated by inhibition of protein kinase C (PKC) (Herbert et al., 1990) followed by activation of

---

sphingomyelinase, and induction of ceramide production. It has been reported that CHL directly inhibits PKC in a concentration dependent manner.

CHL (1  $\mu\text{M}$ ) causes cell cycle arrest in G1 phase and at higher concentration (5  $\mu\text{M}$ ) increases the cell population in G2/M phase for HL-60 cells (Sherr and Roberts, 1999, Malikova et al., 2006b). It induces cell cycle arrest followed by apoptosis in a p53 independent pathway as HL-60 cells lack tumour suppressor p53. It is also reported that in human prostate cancer DU-145 cells with mutated p53, chelerythrine increases expression of p21<sup>Waf1/Cip1</sup> and p27<sup>Kip1</sup>, which are the key regulators of cell cycle progression and function through inhibition of the cyclin/cdk activities (Malikova et al., 2006b). p27<sup>Kip1</sup> bind to cyclin-CDK complexes to inhibit their catalytic activity and induce cell-cycle arrest (Coqueret, 2003).

Production of reactive oxygen species (ROS) is known to play an essential role in apoptosis through release of cytochrome c from mitochondria (Von Harsdorf et al., 1999). CHL induces rapid morphological changes and cell death in cultured cardiac myocytes in a concentration dependent manner (Yamamoto et al., 2001). It has been reported that fluorescence property of CHL changes when it enters into the cell. Since CHL has a pK<sub>a</sub> of 7.5 and many tumour cells have an intracellular pH of 7.1–7.3 and an acidic extracellular environment, not much pseudobase would be formed under these physiological conditions (Von Harsdorf et al., 1999). Therefore it is more likely that reduced dihydroiminium form of CHL enters into the cell and produces superoxide anion and hydrogen peroxide (H<sub>2</sub>O<sub>2</sub>) upon reaction with various cellular reducing agents such as NADH. The production of large amounts of H<sub>2</sub>O<sub>2</sub> leads to the rapid apoptosis in a p53-independent pathway (Maulik et al., 1999).

---

## 1.7. Aims and scope

Aureolic acid group of antibiotics was first isolated from *Streptomyces sp* in India, USA and erstwhile Soviet Union (Calabresi and Parks 1985, Grundy et al., 1953, Sensi et al., 1958, Rao et al., 1962). They were originally intended for use as antibiotic to treat bacterial diseases (Lombo et al., 2006a, Walberg et al., 1999). However, it was later shown that their potential application could be extended to therapy in various types of cancer such as chronic myeloid leukemia, testicular carcinoma and embryonal cell carcinoma (Kennedy and Torkelson, 1995, Koller and Miller, 1986). In fact they were later tried more in cancer chemotherapy. Mithramycin (MTR) and chromomycin (CHR) are two antibiotics which belong to this class of antibiotics. Numerous studies have demonstrated that, they exhibit antitumor activity via inhibition of DNA – templated phenomenon. MTR is currently under trial as human medicine for Ewing sarcomas (Gaspar et al., 2012). However, clinical use of CHR is discontinued because it is more cytotoxic compared to MTR (Lombo et al., 2006b). Presently, CHR is widely used in karyotyping and painting of the cell nucleus (Sahar and Latt, 1978). From the perspective of chemical biology, it indicates that in spite of similar chemical structure MTR/CHR may have different chemical features which lead to different biological activities. The major objective of the first three chapters of the thesis is to correlate their chemical and structural properties with biological functions inside the target cells.

Keeping in view the above, we have addressed the following aspects in the first three chapters of the present thesis: 1) Difference in the ionization property of two structurally similar antibiotics, MTR and CHR 2) Self-association of CHR in its anionic and neutral forms 3) Binding of MTR to bivalent metal ion,  $Mn^{2+}$  and association of the resulting complex with chromatin/chromosomal DNA. We have also examined the

---

effect of metal ion ( $\text{Mn}^{2+}$ ) binding potential of MTR upon an important enzyme, manganese superoxide dismutase.

Scope of this part of the thesis includes the development of new therapeutic strategies, where, aureolic acid antibiotics could be used more effectively, based on the knowledge acquired from the above studies. Current studies on the combinatorial biosynthesis of MTR/CHR open the possibility of new analogs with improved pharmacological and toxicological properties. It may create new therapeutics with broad spectrum of use and diminished cytotoxicity.

Plants are another enriched source of anticancer agents with potential as human medicine. Chelerythrine (CHL) is such a benzophenanthridine class of alkaloids isolated from the roots of *Chelidonium majus L* (Matkar et al., 2008). CHL induces apoptosis in different malignant cell lines. The mechanism by which it mediates apoptosis still remains controversial. In the present thesis we have studied the mode of action of plant alkaloid chelerythrine from chemical biology point of view. CHL has a planar aromatic structure with  $\text{pK}_a$  of 7.5 (Kulp et al., 2011). Therefore, under physiological condition it may interconvert between the cationic/ iminium form and neutral/ alkanolamine form. There are few preliminary reports on the interaction of CHL with dsDNA. Since in eukaryotes DNA is wrapped around histone proteins to form a nucleoprotein complex, chromatin; we have studied the association of CHL with various structural levels of chromatin in chapter 5. Additionally, we have studied the molecular basis of sequence selectivity of CHL by using different polynucleotides like poly(dG-dC), poly(dG).poly(dC), poly(dA-dT) and poly(dA).poly(dT). The study has enabled us to quantify the binding energetics associated with chelerythrine-DNA/ polynucleotide complex formation and predict the overall structure of the complex. Overall, the work presented in the last chapter advances our knowledge on the

---



interaction of CHL to ds DNA, both alone and as a potential intracellular target in the cell. Understanding this yet unexplored property of CHL might serve as an initial effort of employing it as a lead compound in anticancer drug development.

---

# Chapter 2

---

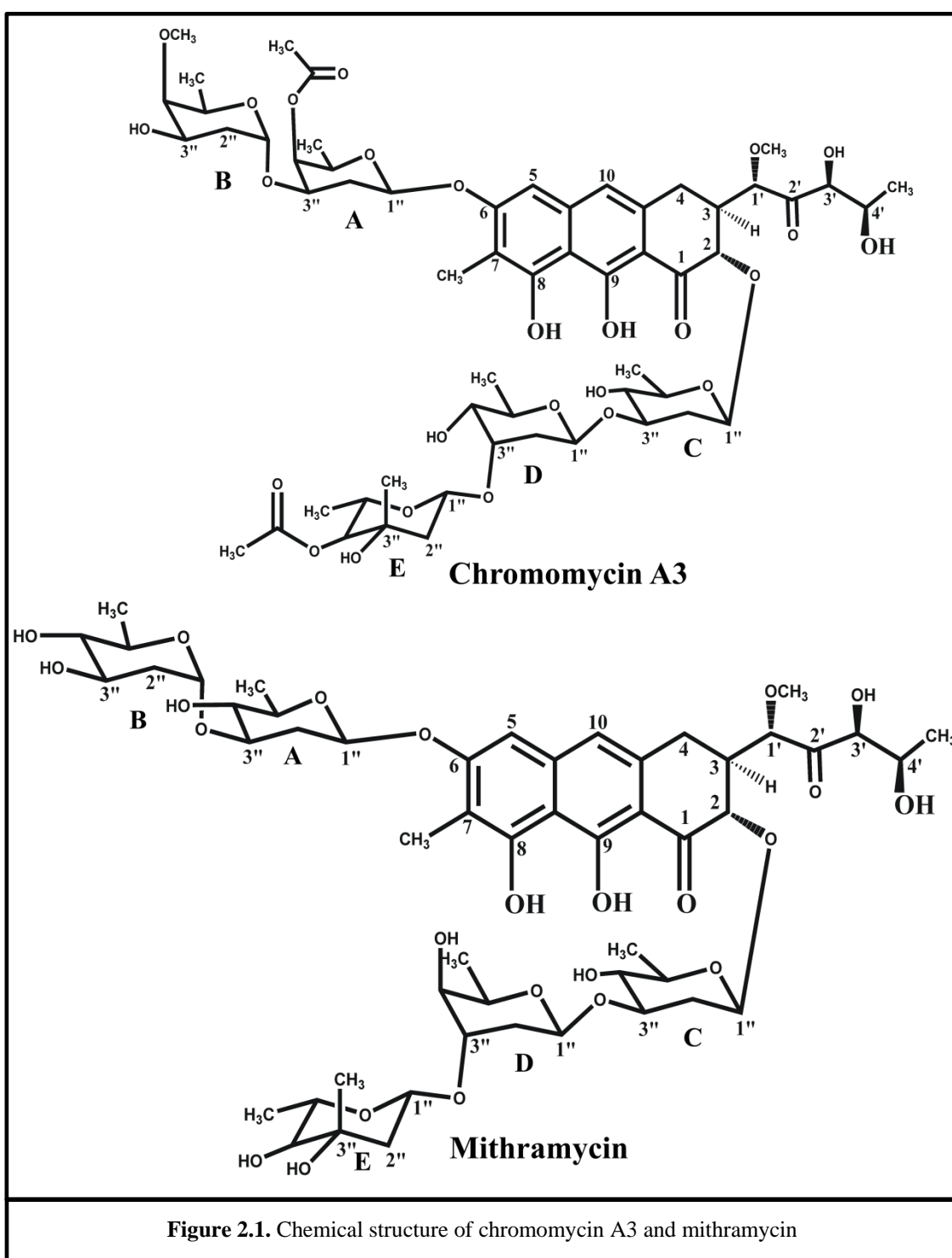
**Difference in the ionization  
properties of two aureolic acid  
antibiotics Mithramycin and  
Chromomycin A3**

## 2.1. INTRODUCTION

The aureolic acid group of antitumor antibiotics comprises of mithramycin (MTR), chromomycin A3 (CHR), olivomycin, chromocyclomycin, UCH9 and durhamycin A (Rohr et al., 1999, Jayasuriya et al., 2002). They inhibit the growth of gram-positive bacteria (Walberg et al., 1999). In addition, they have antitumor activity. The antitumor property has been ascribed to their potential to bind DNA and thereby inhibiting DNA-templated phenomena such as expression of proto-oncogenes like *c-myc* (Snyder et al., 1991). The interesting observation is that they exhibit large differences (>100- fold) in their toxicity towards cultured cells from different species (Singh and Gupta, 1985). Among these antibiotics MTR is under clinical trial as human medicine (Gaspar et al., 2012), though initially after their discovery the antitumor properties of both CHR and MTR were studied extensively in different cell lines.

Structurally, all members of the family consist of a tricyclic chromophore (except chromocyclomycin) which is glycosylated at two different positions with oligosaccharides of different chain lengths. Among this group of antibiotics, MTR and CHR have similar structures with identical tricyclic chromophores, which are attached to a 5 member aliphatic side chain at C3 position and methyl group at C7 position (Bosserman et al., 2011, Beam et al., 2009). In both antibiotics trisaccharide and disaccharide moieties are attached at C2 and C6 positions, respectively (Figure 2.1). In spite of the same core chromomycinone ring, preliminary reports show that the ionization constants of the two antibiotics, CHR and MTR, differ by two units. MTR has the reported  $pK_a$  of 5.0, while CHR has a  $pK_a$  of 7.0 (Nayak et al., 1975, Aich and Dasgupta, 1995). It is interesting from the chemical perspective to know the basis of such difference in ionization constants. It might help to throw light on the effect of

---



the sugars upon the physico-chemical property of the antibiotics. Though there are preliminary reports of the  $pK_a$ 's of the two antibiotics, the estimation of these values were not done in depth. Here we have adopted spectroscopic approaches such as optical and NMR techniques to probe the difference. This has been supplemented with

isothermal titration calorimetry to throw light upon the energetic aspect of the difference. The following considerations also emphasize the necessity of the above studies from the perspective to understand their activities under *in vivo* conditions.

---

## 2.2. MATERIALS AND METHODS

### 2.2.1. Materials

CHR, MTR, hydrochloric acid, sodium hydroxide, tris, sodium acetate, acetic acid, citric acid, sodium citrate, disodium hydrogen phosphate and sodium dihydrogen phosphate are ACS grade chemicals from Sigma Chemical Co., USA. All solutions were prepared in Milli-Q (Synergy, Millipore, USA.) water after filtration through a 0.1  $\mu\text{m}$  filter. CHR and MTR were dissolved in deionized water. Concentrations were determined from absorbance measurements at 405 nm ( $\epsilon_{405} = 8800 \text{ M}^{-1} \text{ cm}^{-1}$ ) (Aich et al., 1992) for CHR and at 400nm ( $\epsilon_{400} = 10000 \text{ M}^{-1} \text{ cm}^{-1}$ ) (Aich and Dasgupta, 1995) for MTR in 20 mM Tris-HCl (pH 8.0) within the linear range of concentration, 10-20  $\mu\text{M}$ .

### 2.2.2. Methods

All absorption spectra were recorded in a Cecil 7500 UV-visible spectrophotometer at 25 °C using cuvettes of 1 cm path length. Fluorescence spectra in different pH values were recorded in a Perkin-Elmer LS55 luminescence spectrometer with a thermostatted cuvette holder at 25 °C. The fluorescence emission intensity has been monitored over the range, 500 nm to 700 nm, when excitation wavelength is 470 nm. The fluorescence intensity at 540 nm was recorded as a function of pH to determine the  $\text{pK}_a$  of the antibiotics. CD spectra of the antibiotics at different pH were recorded over the range 500 nm to 220 nm in a Bio Logic Science Instruments, France using cuvettes of 1 cm path length. Data were analysed using the inbuilt Bio-Kine 32 V4.49-1 software.

---

**2.2.2.1. Determination of ionization constant:**

The pH induced structural change of MTR and CHR was used to determine the  $pK_a$  of these antibiotics. Fluorescence spectra of MTR and CHR in unbuffered deionized water adjusted to different pH upon addition of HCl or NaOH was recorded. Fluorescence intensities of MTR and CHR at 540 nm ( $F_{540}$ ) are plotted against different pH to determine the  $pK_a$  of the molecule.

**2.2.2.2. Estimation of heat of ionization by isothermal titration calorimetry:**

Heats of ionization CHR and MTR were measured in iTC200 microcalorimeter (MicroCal Inc., U.S.A.) using the built-in Microcal LLC ITC software. A single injection in the multiple injection mode was used to determine heat of ionisation for both antibiotics. As MTR has a reported  $pK_a$  of 5.0 (Aich and Dasgupta, 1995), neutral form of MTR solution was obtained at pH 4.0. To determine the heat of ionization of MTR, 5  $\mu$ l of MTR (1.82 mM in deionized water) was injected into the cell containing 20 mM Tris-HCl, pH 9.0. Heat of dilution of solution pH 4.0 to pH 9.0 was subtracted from the heat change obtained from dilution of MTR pH 4.0 into pH 9.0. Similarly, to get the heat of ionisation of CHR ( $pK_a$  7.0), it (1.82 mM in deionized water) was taken in the syringe and injected (5  $\mu$ l) into the cell containing 20 mM Tris-HCl, pH 9.0. As a control the same amount of water was injected into the buffer and the corresponding heat change was subtracted from the heat change obtained from the dilution of CHR. All experiments were performed at 25 °C with the syringe at a stirring speed of 800 rpm. All solutions were filtered and degassed extensively before each experiment.

---

**2.2.2.3. NMR spectroscopic measurements:**

1D  $^1\text{H}$  NMR spectra for 1 mM CHR and 1 mM MTR at different pH values were recorded in a Bruker Spectrospin 500MHz NMR instrument at 25°C. 10%  $\text{D}_2\text{O}$  was used for external locking. A mixing time of 400 ms was used in each case. 2D  $^1\text{H}$  NMR (TOCSY and NOESY) spectra were recorded for MTR (1 mM) and CHR (1 mM). All samples were prepared in 20 mM potassium phosphate buffer (pH 8.0). Data were analyzed using Bruker TopSpin 1.3 software.

---



## 2.3. RESULTS

### 2.3.1. Determination of $pK_a$ of mithramycin and chromomycin A3

We monitored the ionization profiles of hydroxyl groups (OH) present in C8 and C9 positions in MTR and CHR by means of spectroscopic methods such as absorbance, fluorescence and CD. Fluorescence spectra of MTR and CHR at different pH, ranging from 3.0 to 10.0 are shown in Figures 2.2 (a) and (c). Fluorescence emission intensities of these antibiotics below pH 5.0 were considerably low compared to higher pH.

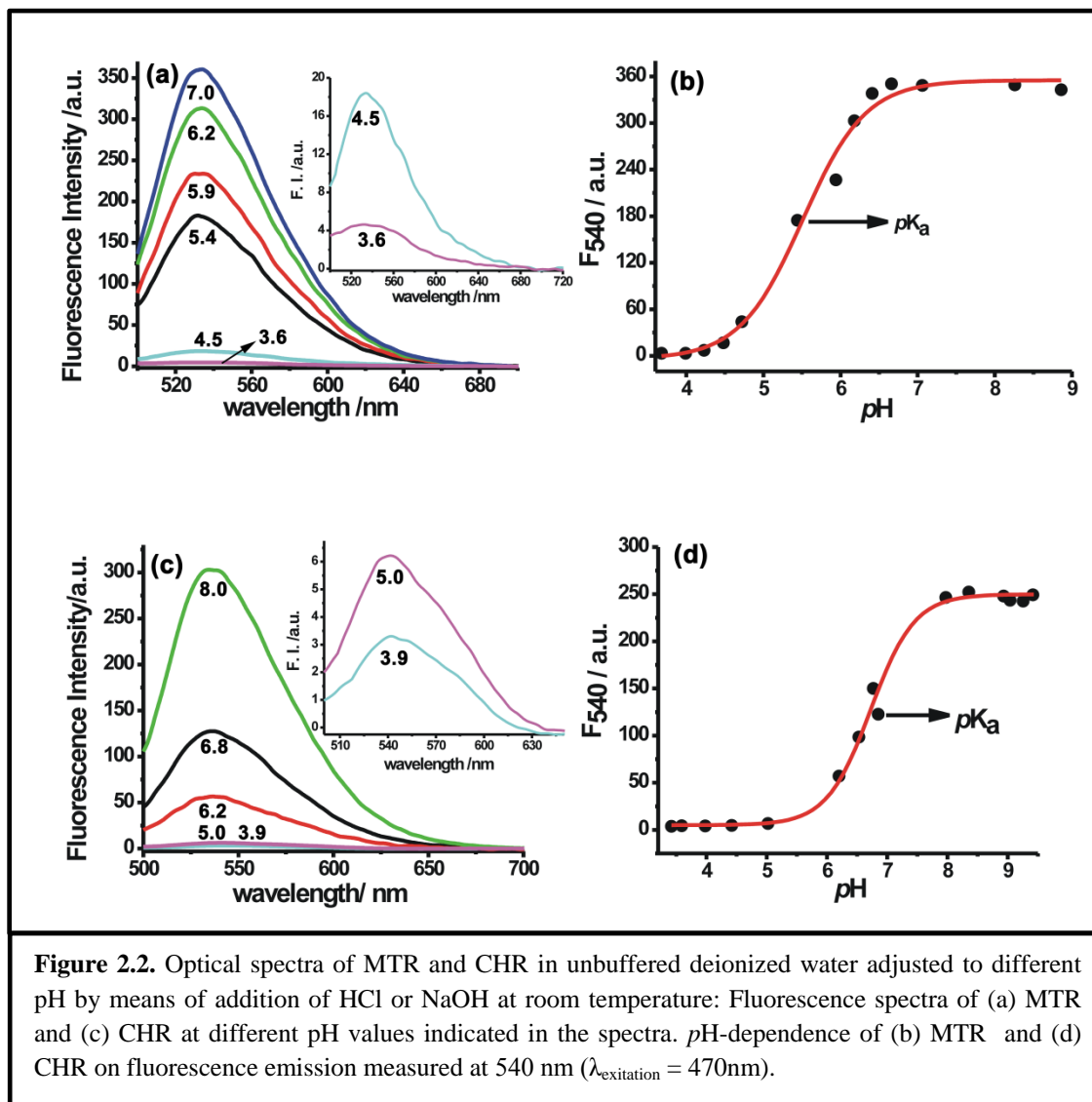
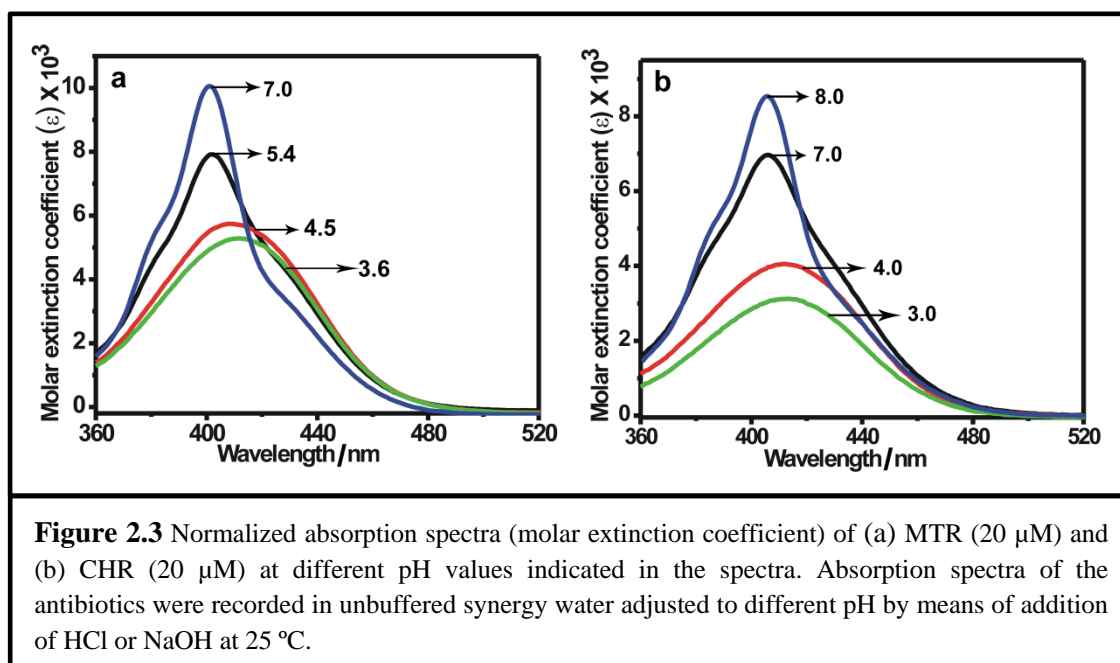


**Figure 2.2.** Optical spectra of MTR and CHR in unbuffered deionized water adjusted to different pH by means of addition of HCl or NaOH at room temperature: Fluorescence spectra of (a) MTR and (c) CHR at different pH values indicated in the spectra. pH-dependence of (b) MTR and (d) CHR on fluorescence emission measured at 540 nm ( $\lambda_{\text{excitation}} = 470\text{nm}$ ).

A plot of emission intensity at 540 nm ( $F_{540}$ ) versus pH (Figures 2.2 (b) and (d)), provides the  $pK_a$  values of MTR and CHR as 5.5 and 7.0, respectively. The values agree well with the reported values (Nayak et al., 1975, Aich and Dasgupta, 1995). It is worth mentioning that none of the previous report was obtained from a number of fluorescence intensity values as reported in the current study.

### 2.3.2. Absorbance of mithramycin and chromomycin A3 in different pH

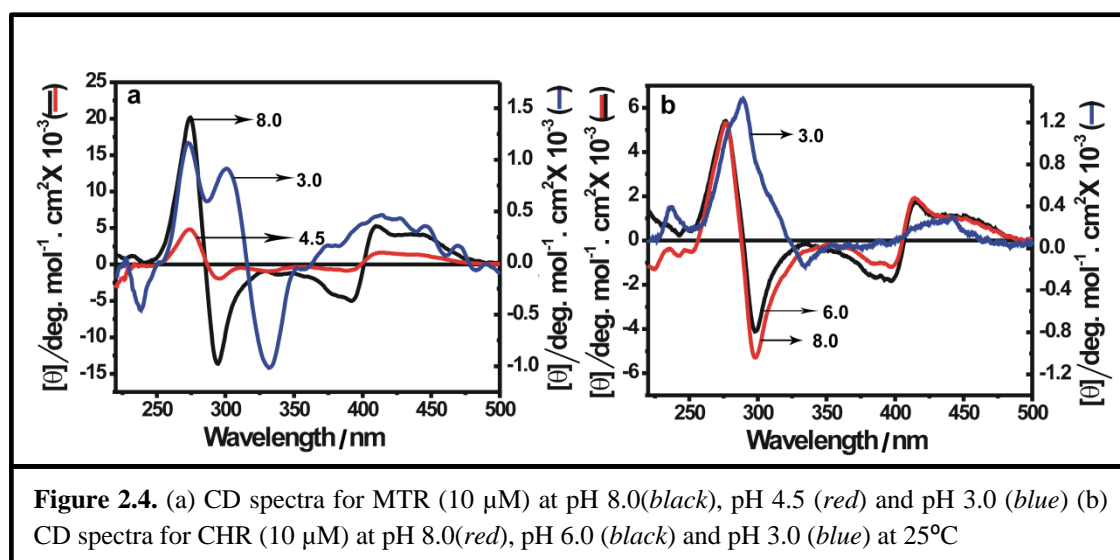
The absorption spectra of the two antibiotics at different pH values are shown in Figures 2.3(a) and (b). Remarkable differences like hypochromicity and red-shift in the nature of the absorption spectrum over the entire pH range characterize the spectra in both cases. The overall spectra can be grouped into two classes in the pH range, below 5 and above. Below pH 5.0 the spectra have broad peaks; on the other hand, spectra above pH 5.0 are characterized by the presence of relatively sharper peaks and isosbestic points. In the acidic pH range all the peaks of MTR and CHR are red-shifted.



Specifically, the absorption spectra of MTR at lower pH (4.5 and 3.6) are broadened and there is a red shift of 10 nm at the absorption maxima compared to the absorption spectra obtained at higher pH (Figure 2.3a). Similar broadening and red shift of absorption maxima (7 nm) is also observed for absorption spectra of CHR at pH 4.0 and 3.4.

### 2.3.3. Circular dichroism studies at different pH

To study the pH induced changes of MTR and CHR we have also recorded the CD spectra at different pH values (Figure 2.4). As MTR has a  $pK_a$  of 5.5, CD spectra of MTR at pH 4.5 and 8.0 correspond to the neutral and anionic forms respectively (Figure 2.4a). Similarly, CD spectra of CHR at pH 6.0 and 8.0 correspond to the neutral and anionic forms of CHR ( $pK_a = 7.0$ ), respectively (Figure 2.4b).

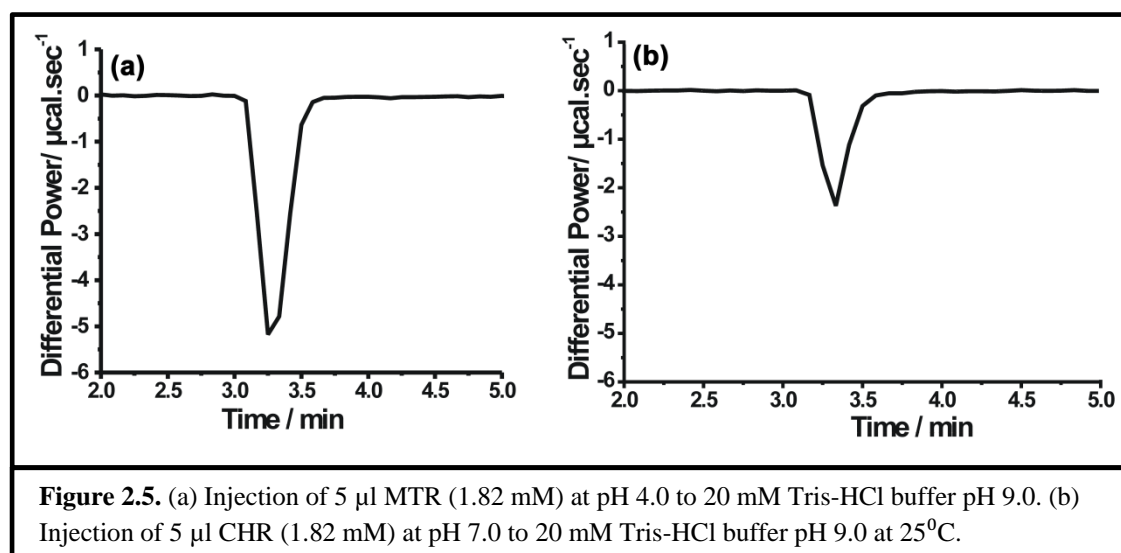


Above the ionisation pH, MTR and CHR have two exciton coupling-type CD bands; one is centered at 285 nm and another at 435 nm. These molar ellipticity values agree well with earlier reports obtained for both MTR and CHR (Aich and Dasgupta, 1995, Aich et al., 1992, Demicheli et al., 1991). But CD spectra of MTR and CHR at pH 3.0

are radically different from the spectra obtained at higher pH values. For MTR, there is an exciton coupling- type split CD bands with very low ellipticity value at  $\sim 315$  nm and a broad band at  $\sim 415$  nm, (Figure 2.4a). In case of CHR at pH 3.0, two bands with lower ellipticity value were observed at 287 nm and 440 nm. The interaction between excited states of chromophores in chiral environments give CD spectra with split Cotton effects.

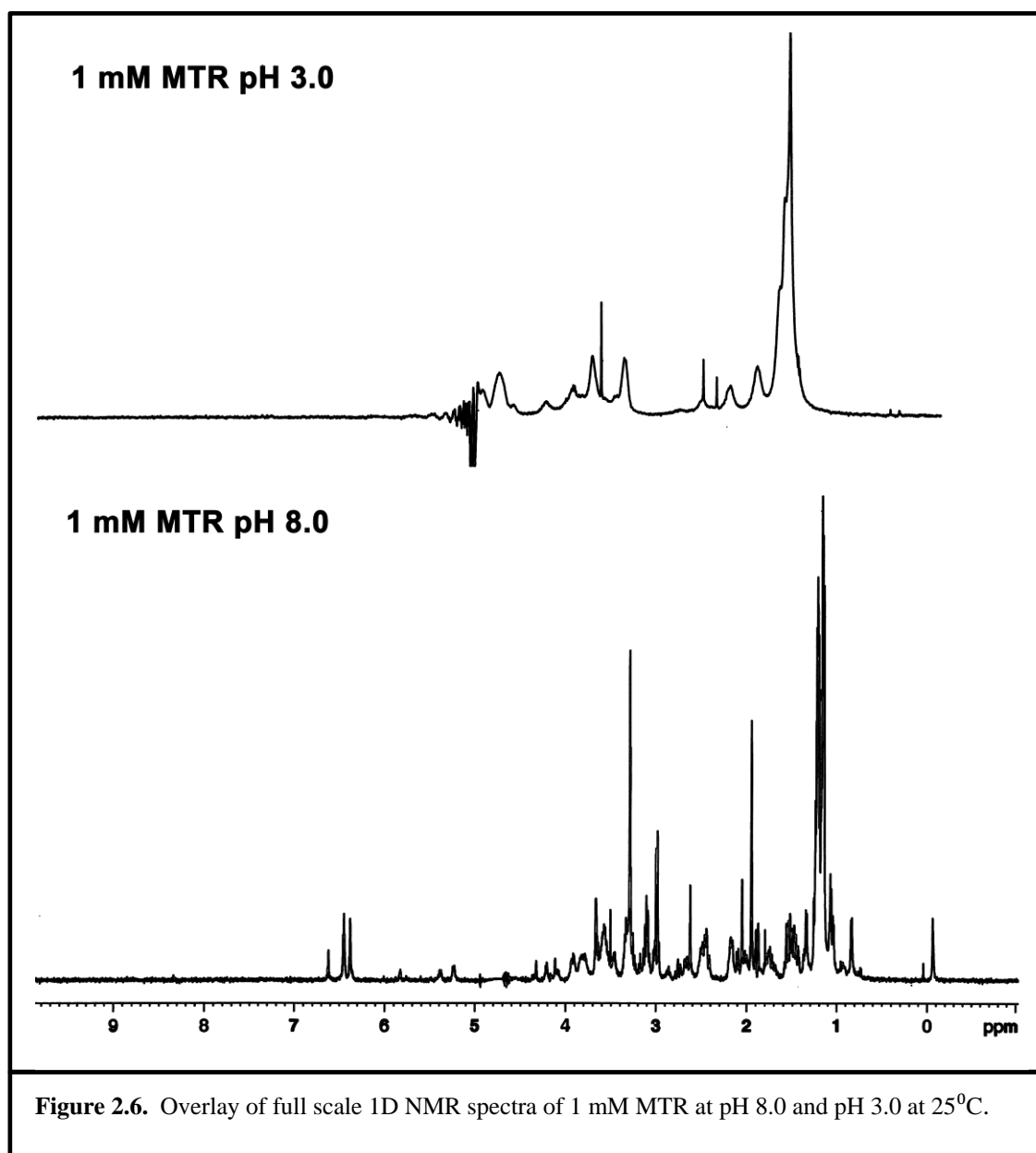
### 2.3.4. Estimation of heat of ionization

Calorimetric method was employed to determine the heats of ionization of MTR and CHR. Figures 2.5(a) and (b) show the heat change profile for MTR and CHR. Heat of ionization of MTR and CHR were determined to be 9.4 kcal/ mol and 3.0 kcal/ mol, respectively.

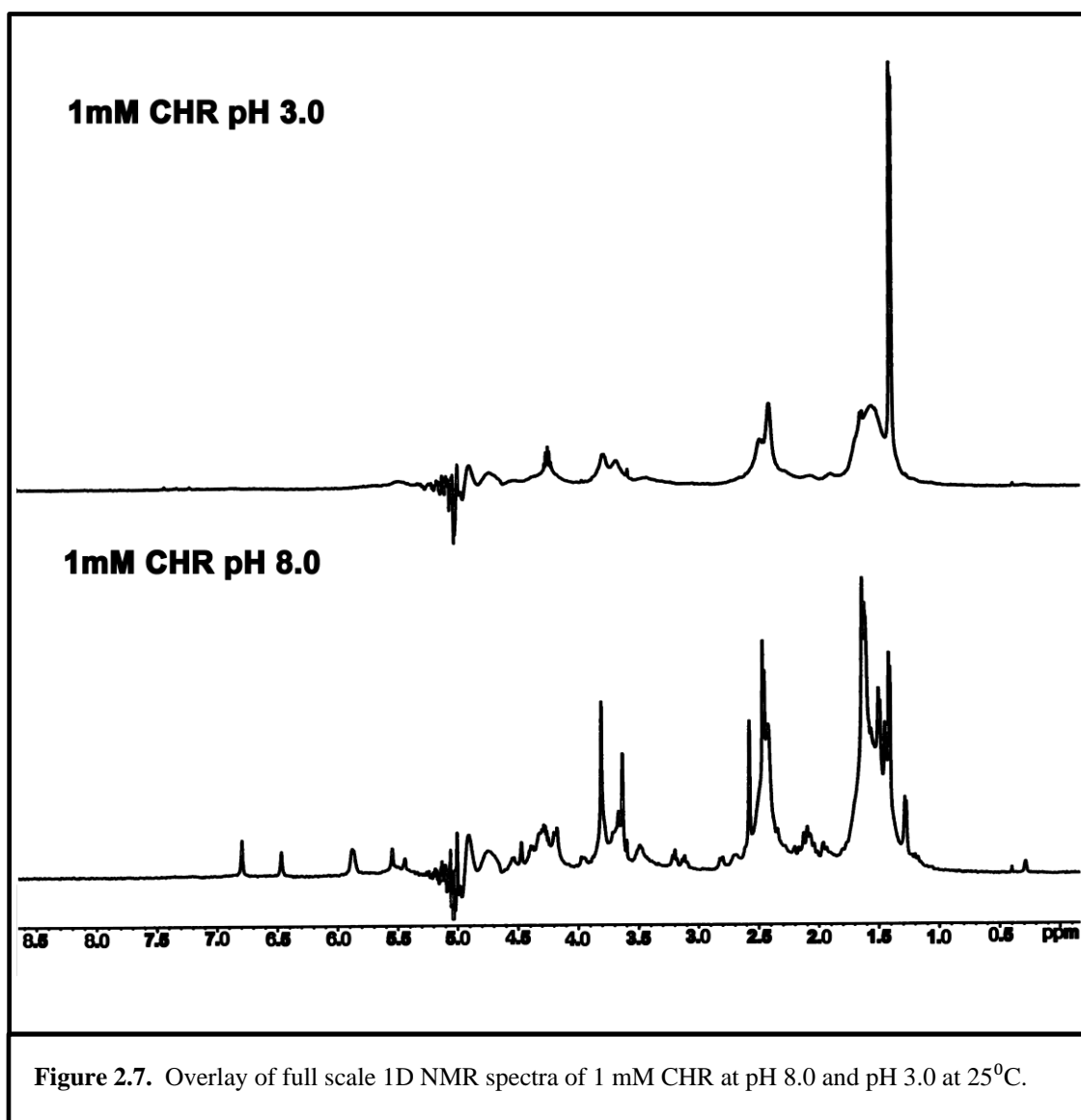


### 2.3.5. NMR spectroscopic measurements

To check the observations of spectroscopic and calorimetric measurements, we have done 1D and 2D  $^1\text{H}$  NMR in different buffer systems for both MTR and CHR. Chemical shift values of anionic CHR and MTR (at pH 8.0) have been assigned using 1D and 2D (through bond connectivity-TOCSY and through space connectivity-NOESY) NMR spectra.



Chemical shift values of anionic CHR and MTR (at pH 8.0) have been assigned using 1D and 2D (through bond connectivity-TOCSY and through space connectivity-NOESY) NMR spectra.



The chemical shift values of different protons present in the drug are found to be in good agreement with previously reported NMR data for the structural elucidation of MTR and CHR (Devi et al., 2007, Lahiri et al., 2012, Gao and Patel, 1989). However, at lower pH, a broadening in the spectra characterizes the NMR spectra of MTR and CHR compared to the higher pH range. In addition, the most notable feature is that the

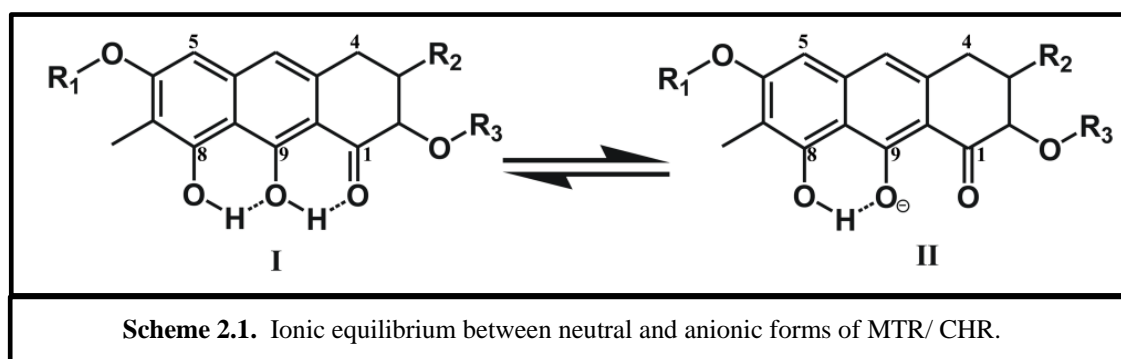
peaks corresponds to aromatic protons are so broadened that they became indistinguishable with the base line (Figures 2.6 and 2.7).

---

## 2.4. DISCUSSION

MTR and CHR have the same aglycone moiety with different sugar substituents at C2 and C6 positions (Rohr et al., 1999). Basic structure of the aglycone (Figure 2.1) suggest that one of the ionizable hydroxyl groups present in C8 and C9 position would dissociate above neutral pH (Nayak et al., 1975). The  $pK_a$  values of MTR and CHR determined by spectroscopic methods (absorbance, fluorescence and circular dichroism) are 5.5 and 7.0, respectively, which are in accordance with previous reports.

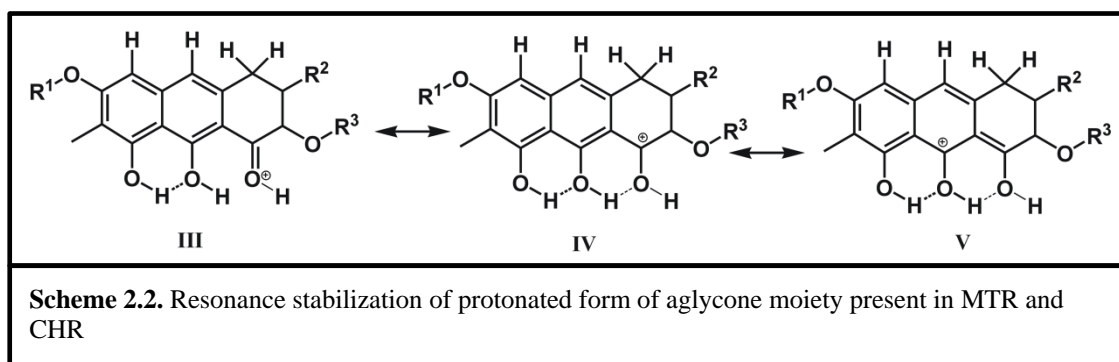
The difference in the absorption spectra of MTR and CHR in acidic and neutral pH can be ascribed to the formation of altered molecular species as proposed below. Presence of an isosbestic points in the absorption spectra of MTR and CHR in the pH range 5.0 and above could be ascribed to equilibria, I and II, where I is the neutral form and II is the anionic form (*Scheme 2.1*).



The broadening of absorption spectra and red shift of absorption maxima of MTR and CHR at lower pH could be attributed to the possibility of protonation at C1 carbonyl oxygen (III, *Scheme 2.2*) for both antibiotics at pH 4.0 or less, which leads to strong intra-molecular hydrogen bonding among the adjacent phenolic –OH groups with an

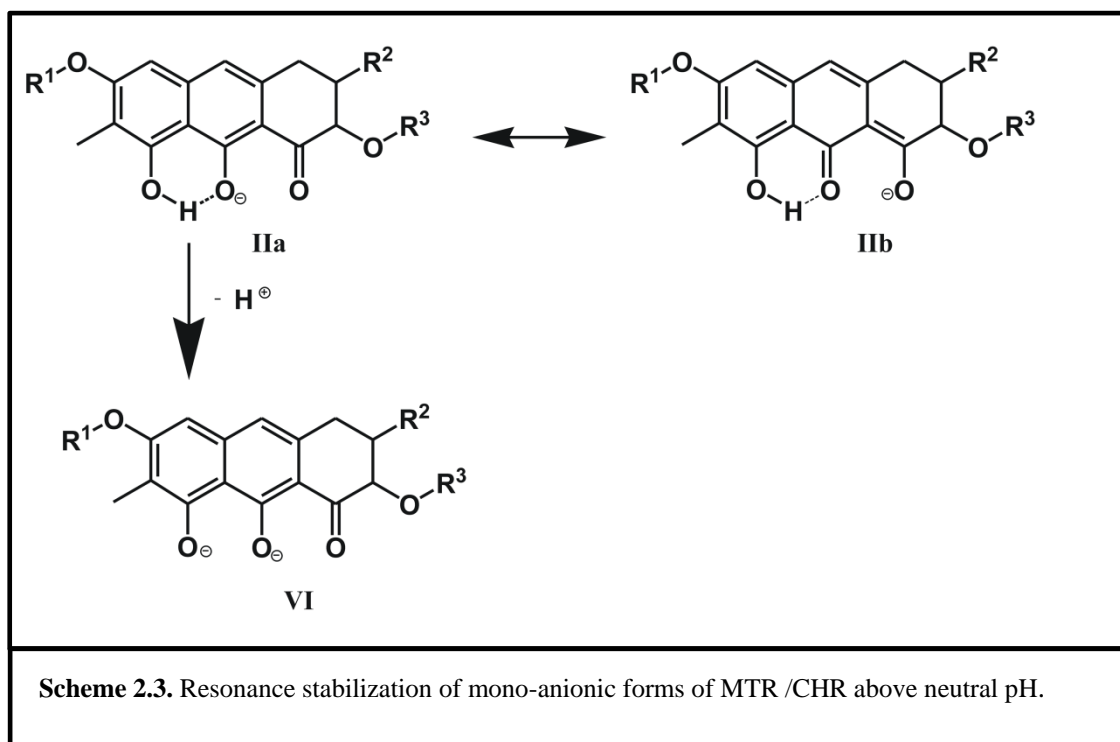


overall positive charge over aromatic part of the antibiotics (IV and V, *Scheme 2.2*). Since the transition dipole moment ( $\mu$ ) for absorption is directly related to the electronic state of a molecule, cationic forms of MTR and CHR have different absorption spectra than the same observed for neutral and anionic forms. Formation of such protonated forms of the antibiotics involving a six membered stable hydrogen bonded ring might give rise to the change in the behavior of excited state of the chromophore (Upadrashta and Wurster, 1988). The extensive quenching of fluorescence intensity of MTR and CHR at 540 nm ( $\lambda_{\text{ex}} = 470$  nm) at lower pH (pH 3.0 to 4.0) can occur as a consequence.



Although MTR and CHR have two dissociable protons (from the phenolic groups at C8 and C9 positions); we could not detect any second ionization phenomenon. This observation suggests that form II (*Scheme 2.1*) is intramolecularly hydrogen bonded and resonance stabilized (*Scheme 2.3*). It leads to the molecule being less susceptible to further de-protonation to achieve form VI (*Scheme 2.3*) (Upadrashta and Wurster, 1988).

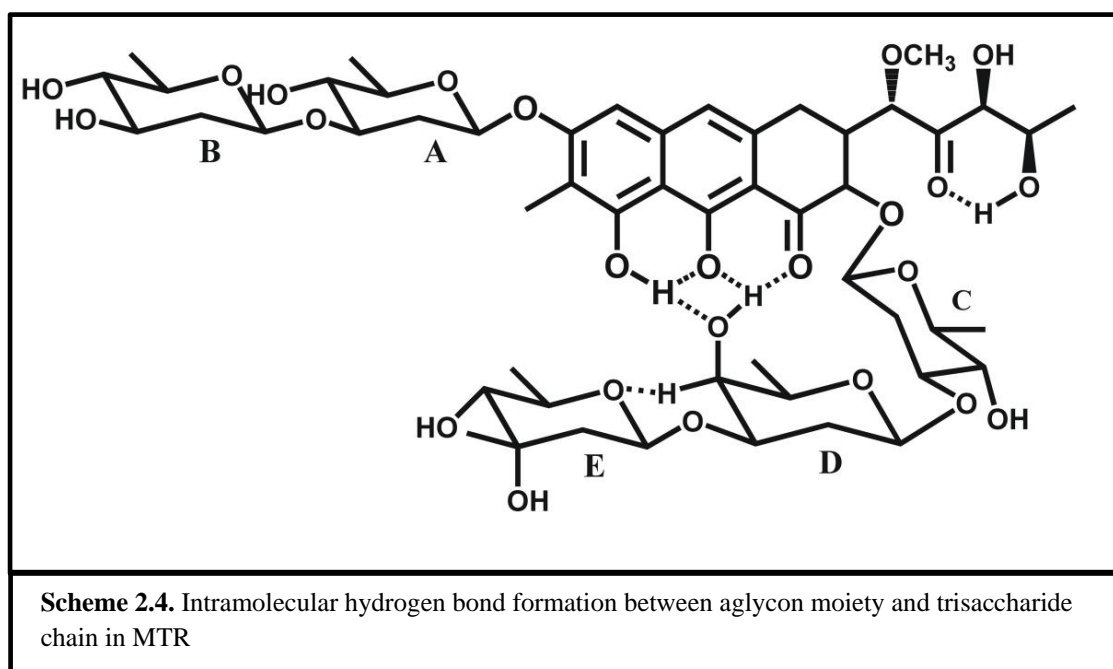
Structural alterations of various ionization states of MTR and CHR are monitored with CD spectroscopy. Similar to the observations obtained from absorption and fluorescence spectroscopy, CD spectra of MTR and CHR in pH 3.0 are drastically



different from the CD spectra obtained at higher pH values. At pH 3.0, the chromophores of the antibiotics get protonated. As a result, the interaction of the oligosaccharide moieties with chromophores may change leading to an alteration of the chiroptical environment, which leads to the change of overall CD spectra of MTR and CHR at pH 3.0.

Heat of ionisation of MTR is higher than that of CHR. This can be explained by the fact that MTR and CHR have different sugar moieties present in the trisaccharide chain linked at C2 positions. In MTR the trisaccharide chain consists of D-olivose (sugar C), D-oliose (sugar D) and D-mycarose (sugar E) (Beam et al., 2009), which has more hydrophilic surface. It leads to the possibility of more hydrogen bond formation

between the aglycone and the trisaccharide chain, as shown in scheme 2.4, which may alter during the ionization process. Therefore a greater number of H-bonds are formed/broken, which leads to a higher heat of ionization. In case of CHR, the trisaccharide chain consists of D-olivose (sugar C), D-olivose (sugar D) and 4-O-acetyl-L-chromose (sugar E) (Menendez et al., 2004). The hydrophobic surface of these trisaccharide sugars is more compared to those of MTR. So, less number of H-bond is formed/broken; hence the lower value of heat of ionisation.



By spectroscopic methods such as absorption, fluorescence and CD, we have shown that at lower pH values (3.0 to 4.0) electronic state and the chiral environment around the chromophore is different. Heat of ionisation obtained from isothermal calorimetric method suggests that the number of H-bond between the chromophore and the oligosaccharide chain or between chromophore and the solvent molecule is different for MTR and CHR. In order to gain in-depth knowledge about the chemical structure of

various ionization states of the antibiotics we have done 1D and 2D proton NMR studies. At lower pH values, broadening of NMR spectra of MTR and CHR leads to the loss of most of the information about the structure and orientation of MTR and CHR in pH 3.0. However, broadening of the spectra for both MTR and CHR at pH 3.0 provides support to our proposition of protonation at C1 carbonyl oxygen, which leads to the exchange of aromatic proton with solvent water molecule.

Absorption and distribution of an antibiotic molecule involve its passage across cell membranes. Physico-chemical properties of antibiotic molecules influence transport of it across the cell membranes. The mechanism by which the antibiotic molecules pass membranes depends on its molecular size and shape, degree of ionisation, state of aggregation and relative lipid solubility of its ionized and neutral forms. The neutral molecules are usually lipid soluble and can diffuse across the cell membrane. In contrast, the ionized molecules are unable to penetrate the cell membrane in absence of active transport system due to their low lipid solubility. MTR and CHR are weak acids of  $pK_a$  5.5 and 7.0 respectively. In the present study we have observed that MTR and CHR have different ionisation properties. Therefore the trans-membrane distribution of these antibiotics will differ to a significant extent in different tissues. Presence of different sugars and specific modifications in CHR entails for this distinctive behaviour. Overall, different sugars and specific modifications of the sugars are responsible for the different ionisation properties of MTR and CHR.

Many bioactive natural products are glycosylated compounds in which the sugar moieties are essential for their biological activity. Only some cases, sugars undergo further tailoring modifications once they have been transferred to the aglycon, for

---

example, O-methylations in L-olivose sugar during biosynthesis of oleandomycin from *Streptomyces antibioticus* (Rodriguez et al., 2001). But sugar tailoring modification by acetylation is less common. The chromomycin biosynthesis requires two acetylation steps and one methylation step. The dideacetylated chromomycin shows low biological activity compared with the acetylated compound (i.e. Chromomycin A3) (Menendez et al., 2004). In contrast, MTR does not require any tailoring modification for its full biological activity.

---

# Chapter 3

**Molecular basis of self  
aggregation of neutral and  
anionic Chromomycin A3**

### 3.1. INTRODUCTION

Chromomycin A3 (CHR) is an antitumor antibiotic produced by *Streptomyces griseus* (Figure 3.1) (Calabresi et al., 1991, Lombo et al., 2006). It belongs to the aureolic acid family of antibiotics. It was earlier used for treatment of Paget's disease and testicular carcinoma under the trade name of toyomycin (Reynolds et al., 1976). Currently the clinical use of CHR is discontinued due to its cytotoxicity (Lombo et al., 2006). However, it is widely used in karyotyping and painting of the cell nucleus (Sahar and Latt, 1978). The antitumor properties of CHR are ascribed to its inhibitory effects on replication and transcription processes during macromolecular biosynthesis (Goldberg and Friedman, 1971). In the presence of bivalent metal ion, like  $Mg^{2+}$ , it can bind to minor groove of DNA at GC-rich nucleotide sequence (Aich et al., 1992) and thereby down regulates the expression of many cancer-related genes that bear GC-rich motifs in their promoter regions, such as the *c-myc* proto-oncogene (Snyder et al., 1991). Apart from these antitumor activities, CHR also acts as a potent inhibitor of neuronal apoptosis induced by oxidative stress and can induce erythroid differentiation of K562 cells by binding to the human  $\gamma$ -globin promoter (Fibach et al., 2003). CHR has also been shown in our laboratory to inhibit the enzyme activity of Zn(II)-containing metalloenzymes (Devi et al., 2009).

CHR contains a tricyclic aglycone with a  $\beta$ -ketophenol chromophore, which is attached to two aliphatic side chains at C3 and C7 position and different oligosaccharide moieties via O-glycosidic linkages. The disaccharide is attached to C6 position of the anthracene ring whereas the trisaccharide is attached to the C2 position (Lombo et al., 2006). The trisaccharide unit of CHR consists of D-olivose (sugar C and sugar D) and 4-O-cetyl-L-chromose B (sugar E). The disaccharide unit consists of 4-O-acetyl-D-oliose (sugar A) and 4-O-methyl-D-oliose (sugar B) linked via glycosidic linkages.

---

Micro-organisms protect themselves from the toxic action of antibiotics they produce, by developing self-defense mechanisms and they are highly resistant to that specific antibiotic. Therefore, the self-association of these antibiotics would play an important role in its storage, biological action and gene expression. CHR is structurally similar to mithramycin (MTR), as they have the same aglycone and aliphatic side chain but differ in four out of five sugars attached to the aglycone (Lombo et al., 2006, Bosserman et al., 2011, Beam et al., 2009). Previous reports from our laboratory have shown that anionic form of MTR self-associates extensively (Lahiri et al., 2008). CHR has a  $pK_a$  of 7.0 (Nayak et al., 1975). At physiological pH, it therefore, has a mixed population of anionic and neutral forms. Here we have examined the self-association of CHR in aqueous solution both in neutral and in anionic forms by means of spectroscopic (absorbance, fluorescence and CD) and calorimetric (ITC) techniques to characterize



the self-association property of CHR and provide a molecular basis of the aggregation. Structural analysis of the process of aggregation has been studied by nuclear magnetic resonance (NMR) spectroscopy, which has helped to elucidate the mode of self-association of the CHR molecules in different ionization states.

---

## 3.2. MATERIALS AND METHODS

### 3.2.1. Materials

CHR, hydrochloric acid, Tris, sodium acetate, acetic acid, disodium hydrogen phosphate and sodium dihydrogen phosphate were obtained from Sigma Chemical Co., USA. All solutions were prepared in Milli-Q (Synergy, Millipore, USA) water after filtration through a 0.1  $\mu\text{m}$  filter. Unless mentioned separately, all spectroscopic and ITC experiments were performed in 20 mM Tris-HCl (pH 9.0) and 20 mM sodium acetate-acetic acid buffer (pH 5.0). For the NMR experiments, 20 mM sodium phosphate buffer at pH 8.0 and 20 mM sodium phosphate buffer at pH 6.0 were used. CHR was dissolved in Milli-Q water and the concentration was checked from absorbance measurements at 405 nm in 20 mM Tris-HCl (pH 8.0) using the extinction coefficient ( $\epsilon_{405}$ )  $8800 \text{ M}^{-1} \text{ cm}^{-1}$  (Aich et al., 1992) within the linear range of concentration, 10-20  $\mu\text{M}$ .

### 3.2.2. Methods

#### 3.2.2.1. Absorption spectroscopy

All absorbance spectra were recorded in a Cecil 7500 UV-visible spectrophotometer (DataStream CE 7000 Series software) at 25  $^{\circ}\text{C}$ . Absorbance spectra of neutral and anionic forms of CHR were taken in 20 mM Sodium acetate-acetic acid buffer (pH 5.0) and 20 mM Tris-HCl (pH 9.0), respectively at 25  $^{\circ}\text{C}$  in quartz cuvettes of 1 cm path length. For comparison, the spectra shown in the results contain normalized absorbance

---

$(A/A_{\max})$  as a function of wavelength, where  $A$  is the absorbance and  $A_{\max}$  is the absorbance at the peak.

### **3.2.2.2. Fluorescence spectroscopy**

Fluorescence spectra of CHR at different concentrations and in different pH were recorded in a Perkin-Elmer LS55 luminescence spectrometer with a thermostatted cuvette holder at 25 °C. The excitation wavelength is 470 nm and fluorescence emission intensity has been monitored over the range, 500 nm to 700 nm. Intensity at 540 nm was noted as a function of input concentration to study the self-association. The excitation wavelength of 470 nm was chosen to avoid photochemical degradation of CHR during the fluorescence measurements as mentioned in a previous report (Aich et al., 1992). Fluorescence measurements were done in cuvettes of different path length with absorbance upper limit of 0.02 to detect self-association.

### **3.2.2.3. Circular Dichroism spectroscopy**

We have employed CD spectroscopy to monitor the self-association of CHR as a function of its concentration. CD spectra were recorded in a Bio Logic Science Instruments, France using cuvettes of 1 cm path length for lower concentration and 0.2 cm path length for higher concentration range. Data were analyzed using the inbuilt Bio-Kine 32 V4.49-1 software. The change of ellipticity as a function of concentration has been plotted at different wavelengths, where the changes in CD were most pronounced for the two systems.

---

#### **3.2.2.4. Isothermal Titration Calorimetry**

The heat of dilution CHR was measured in a VP-ITC micro-calorimeter (MicroCal Inc., USA) using the built-in Microcal LLC software with Origin 7.0. CHR was taken in the syringe (299  $\mu$ M) and injected into the cell containing 20 mM Tris-HCl (pH 9.0) and 20 mM sodium acetate-acetic acid buffer (pH 5.0). All experiments were performed at 25 °C with the syringe at a stirring speed of 307 rpm. All solutions were filtered and degassed extensively before each experiment. Corrected enthalpies were calculated after subtracting the enthalpy change due to mixing of the buffers in each case.

#### **3.2.2.5. $^1\text{H}$ NMR Spectroscopy**

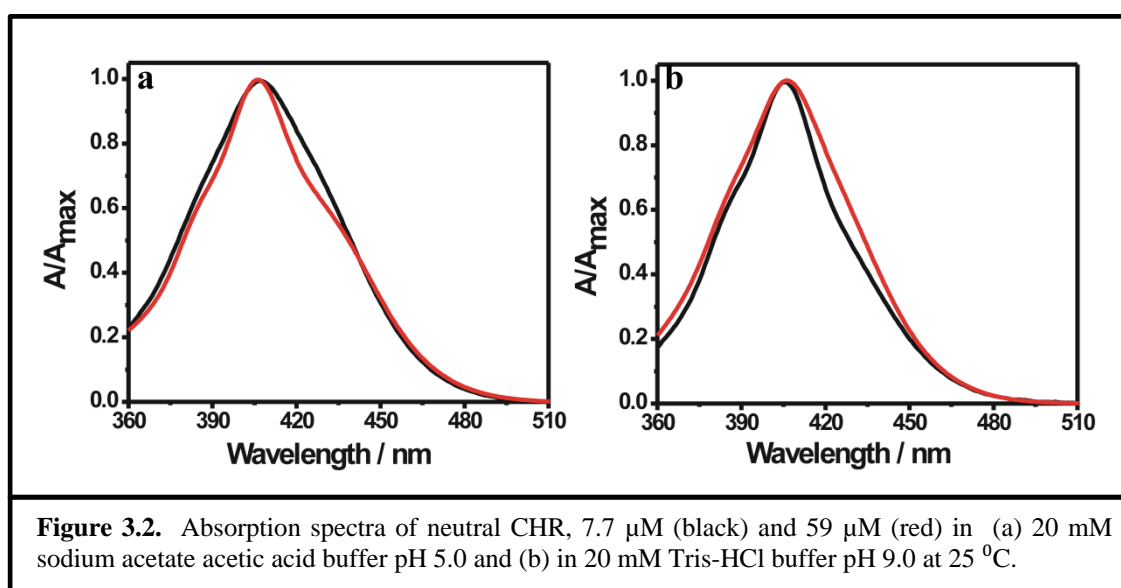
1D  $^1\text{H}$  NMR spectra for 100  $\mu$ M CHR and 1 mM CHR and 2D  $^1\text{H}$  NMR (Total Correlation Spectroscopy (TOCSY) and Nuclear Overhauser Effect Spectroscopy (NOESY)) spectra for 1 mM CHR were recorded in a Bruker Spectrospin 500MHz NMR machine at 25 °C. 10% D<sub>2</sub>O was used for external locking. The 2D spectra were recorded for ~16 hour. A mixing time of 400 ms was used in each case. Samples were prepared in 20 mM sodium phosphate buffer (pH 8.0 and pH 6.0). Data were analyzed using Bruker TopSpin 3.1 software.

---

### 3.3. RESULTS

#### 3.3.1. Absorbance studies for chromomycin in neutral and anionic forms

The absorption spectra of CHR at two different concentrations in pH 5.0 and pH 9.0 buffers are shown in Figures 3.2a and b, respectively. The nonoverlap of the spectra in both buffers over the concentration range, 2.0  $\mu\text{M}$ -60  $\mu\text{M}$ , indicates the aggregation of CHR both in neutral and anionic forms. At pH 5.0 there is a broadening of the spectra of the neutral form at low concentration which become sharper with the increase in concentration. In contrast, the absorption spectra of the anionic CHR at pH 9.0 broadened with the increase in concentration. Such difference could arise from the difference in the geometry of aggregation of the two forms leading to a difference in the relative orientation of the chromophores. We have not noticed any such deviation from linearity for the  $[(\text{CHR})_2 \text{Mg}^{2+}]$  complex at pH 9.0 in presence of 10 mM  $\text{Mg}^{2+}$  in this concentration range.



### 3.3.2. Fluorescence measurements of CHR in neutral and anionic form

To detect the self-aggregation of neutral and anionic CHR in aqueous buffers of pH 5.0 and pH 9.0 at low concentration range of 1  $\mu\text{M}$  to 7  $\mu\text{M}$ , the fluorescence emission spectra and intensity at 540 nm were measured as a function of CHR concentration. At this concentration range of CHR there is an increase in the normalized fluorescence spectra in both buffers (pH 5.0 and pH 9.0) (Figures 3.3).

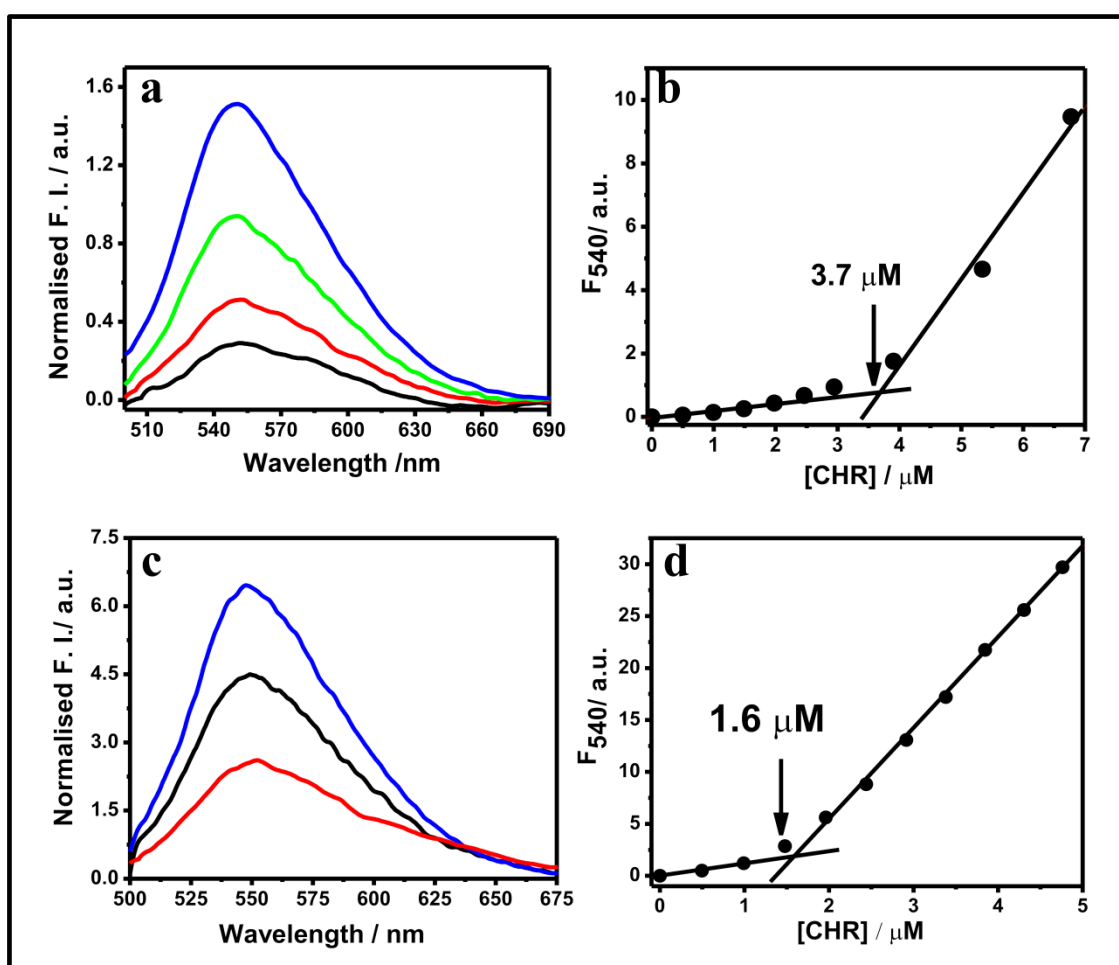
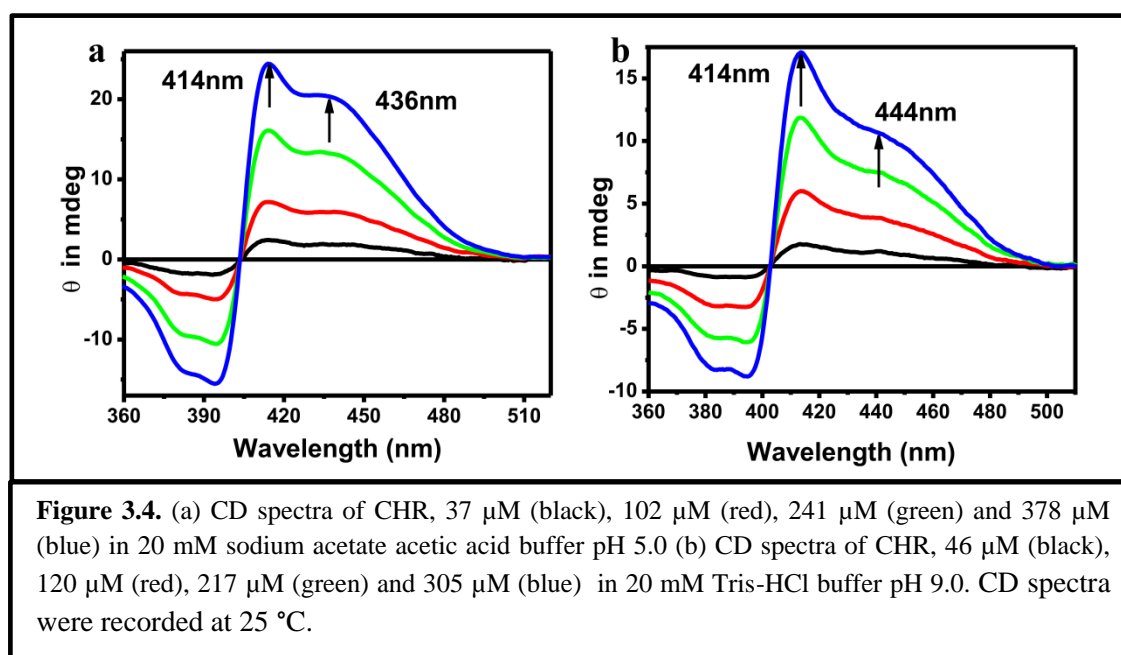


**Figure 3.3.** (a) Fluorescence spectra (normalized per micromolar concentration of CHR) of neutral CHR, 2.5  $\mu\text{M}$  (black), 3.9  $\mu\text{M}$  (red), 5.4  $\mu\text{M}$  (green) and 10  $\mu\text{M}$  (blue) in 20 mM sodium acetate acetic acid buffer pH 5.0. (b) Fluorescence intensity at 540 nm plotted against different CHR concentration in 20 mM sodium acetate acetic acid buffer pH 5.0. (c) Fluorescence spectra (normalized per micromolar concentration of CHR) of anionic CHR, 1  $\mu\text{M}$  (red), 2  $\mu\text{M}$  (black), 3.5  $\mu\text{M}$  (blue) in 20 mM Tris-HCl buffer pH 9.0. (d) Fluorescence intensity at 540nm ( $F_{540}$ ) plotted against different concentration in 20 mM Tris-HCl buffer pH 9.0. All experiments are performed at 25  $^{\circ}\text{C}$ .

Figures 3.3 b and d show that the deviation from linearity of the fluorescence intensity values at 540 nm as a function of CHR concentration. These observations indicate aggregation of the antibiotic in aqueous solution. The difference in the break-points of fluorescence-concentration plots at two different pH values is also noteworthy. Comparison of the data shown in the Figures, 3.3b and d, suggest that aggregation of CHR starts at a lower concentration in case of the anionic antibiotic.

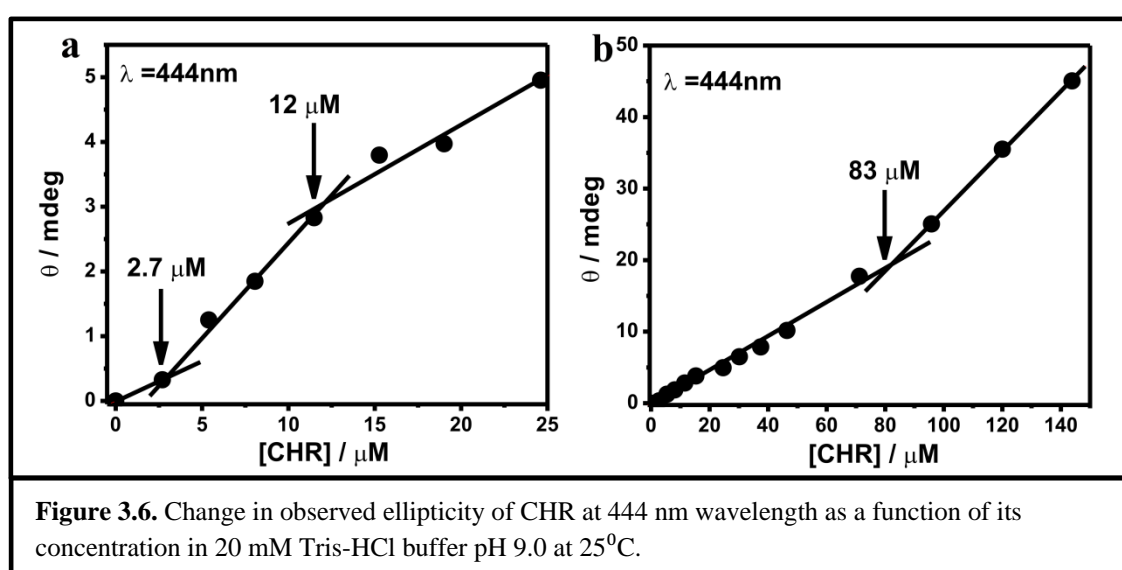
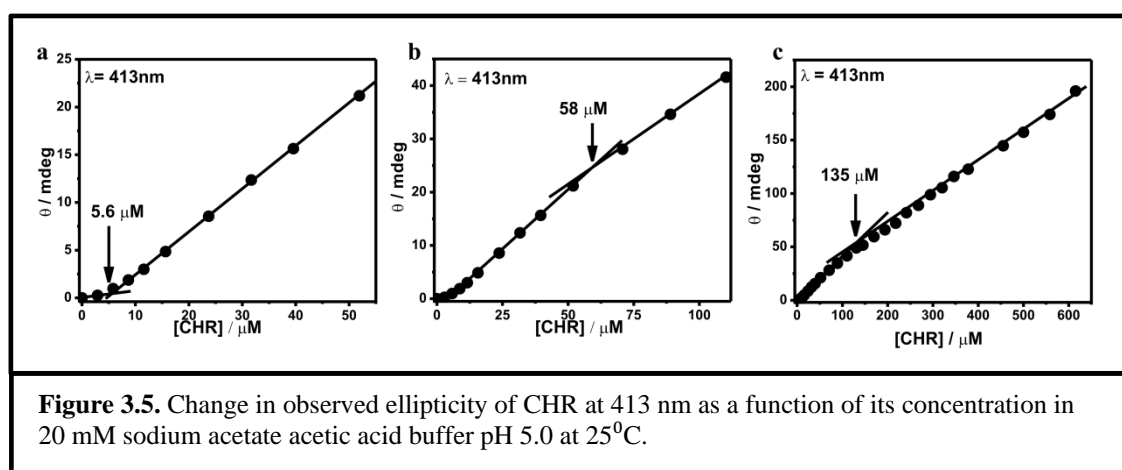
### 3.3.3. CD measurements to determine the mechanism of self-association process

To study the self-association of neutral and anionic CHR, we investigated changes in the chiro-optical properties of CHR in the buffers of pH 5.0 and 9.0 as a function of input CHR concentration. Figures 4a and b show the CD spectra of CHR in the visible range with the increase in concentration of CHR in 20 mM sodium acetate-acetic acid buffer (pH 5.0) and 20 mM Tris-HCl (pH 9.0) buffer, respectively.



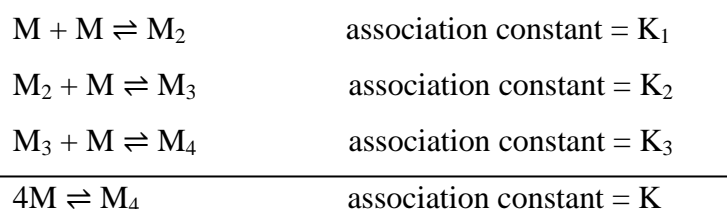
The change in spectral shape is observed with the increase in concentration in both cases (Figure 3.4). At lower concentration broad spectra replace the split into two peaks observed at higher concentrations.

We have plotted the observed ellipticity at 413 nm for the neutral drug and 444 nm for anionic drug as a function of input concentration of CHR (Figures 3.5 and 3.6). The resulting plot shows three breaks over the entire concentration range in each case. The choice of wavelength does not alter the nature of the curves with the break points.





In case of CD spectroscopic study also, the breakpoints as shown in the Figures 3.5 and 3.6 occur at lower concentrations for the anionic antibiotic, thereby suggesting an internal consistency of the results obtained by two different techniques, fluorescence and CD. The results suggest that there are four types of species present over the total concentration range. In analogy to the earlier proposition of a tetrameric model of self-association of MTR (Lahiri et al., 2008), the following multiple equilibria have been proposed to account for the breaks:



with three association constants, denoted as  $K_1$ ,  $K_2$ , and  $K_3$  (where  $K = K_1 \times K_2 \times K_3$ ).  $M$ ,  $M_2$ ,  $M_3$ , and  $M_4$  represent the monomer, dimer, trimer, and tetramer of CHR, respectively. The monomer concentration of CHR ( $[M]$ ) can be expressed in terms of total CHR concentration  $C_0$  and association constant  $K$  as under (Martin, 1980)

$$[M] = \frac{1}{4K} (-1 + \sqrt{1 + 8KC_0}) \quad \dots\dots\dots (1)$$

The molar ellipticity of the monomer and dimer can be connected by the following equation for the dimerization step.

$$\Delta\epsilon = \frac{[M]\Delta\epsilon_M + 0.5\{C_0 - [M]\}\Delta\epsilon_D}{C_0} \quad \dots\dots\dots (2)$$

In equation (2),  $\Delta\epsilon$  = apparent molar CD absorption co-efficient, which is defined as the measured CD, divided by total CHR concentration.  $\Delta\epsilon_M$  and  $\Delta\epsilon_D$  are apparent molar CD absorption co-efficient for the monomer and dimer respectively. Values of  $\Delta\epsilon$ ,  $\Delta\epsilon_M$

and  $\Delta\epsilon_D$  were calculated from measured CD values at different concentrations (Martin, 1980). Apparent molar CD absorption coefficients for the trimerization and tetramerization steps were calculated considering higher concentrations in the CD experiments.

Combining equations (1) and (2) dissociation constants ( $K_d = 1/\text{association constant}$ ) of different aggregation steps have been calculated. For the sake of clarity of comparing the degree of association to form the oligomers,  $K_d$  values representing the different orders of aggregation for neutral and anionic CHR are reported in Table 3.1.

**Table 3.1.** Apparent dissociation constants values for the multiple equilibria of CHR and MTR in both neutral and anionic forms at 25 °C.

Reaction	Dissociation Constant of CHR at pH 5.0 (neutral form)	Dissociation Constant of CHR at pH 9.0 (anionic form)	Dissociation Constant of MTR at pH 3.0 (neutral form)	Dissociation Constant of MTR at pH 8.0 (anionic form)
$M + M \rightleftharpoons M_2$	$K_1^d = 43.4 \text{ nM}$	$K_1^d = 14.5 \text{ nM}$	$K_1^d = 411 \text{ nM}$	$^{[a]}K_1^d = 528 \text{ nM}$
$M_2 + M \rightleftharpoons M_3$	$K_2^d = 212.8 \text{ }\mu\text{M}$	$K_2^d = 204.5 \text{ }\mu\text{M}$	$K_2^d = 11 \text{ nM}$	$^{[a]}K_2^d = 76.9 \text{ nM}$
$M_3 + M \rightleftharpoons M_4$	$K_3^d = 5.78 \text{ }\mu\text{M}$	$K_3^d = 0.33 \text{ }\mu\text{M}$	$K_3^d = 7.4 \text{ nM}$	$^{[a]}K_3^d = 1.7 \text{ nM}$

$^{[a]}$  values are taken from (Lahiri *et al.*, 2008)

The following features characterize the aggregation process. In accordance with the trend mentioned above, the dissociation constant for dimerization process ( $K_d^1$ ) of anionic CHR is three fold lower than that of neutral CHR. It means the ionization leads to oligomerization of CHR at lower concentration. With increase in concentration, the dimer further associates to form trimer and tetramer for both, neutral as well as anionic CHR. Formation of tetramer from trimer is associated with a relatively lower affinity.

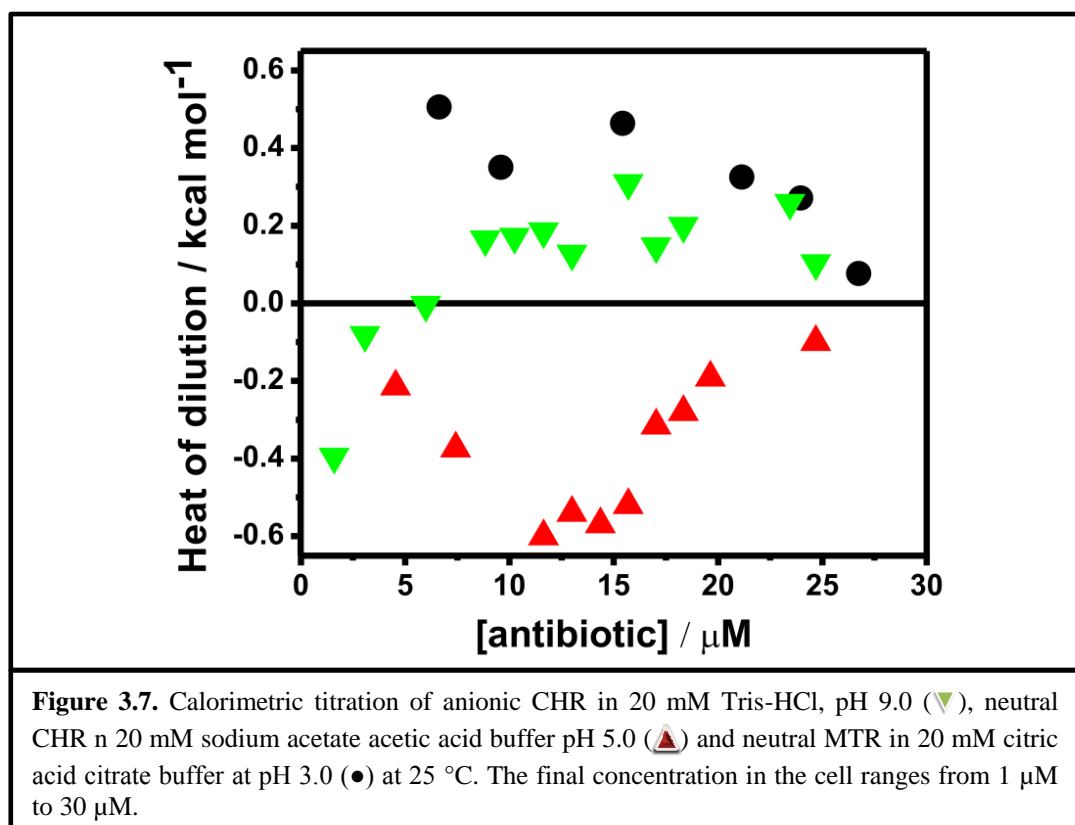
In terms of free energy, the formation of dimer is most favorable followed by the trimer to tetramer formation. Table 3.1 also contains similar data for MTR for comparison, which shows that the lower order oligomerization, namely dimerization, is more favorable in case of CHR compared to that in MTR. The difference among the two antibiotics could be ascribed to difference in the sugar residues with its substituents.

#### **3.3.4. Measurement of heat of dilution by Isothermal titration calorimetry (ITC)**

The differences in the dissociation constant for the dimerization process of the two antibiotics originate from the associated free energy difference characterizing the dimerization. From the energetic perspective, enthalpy-entropy compensation would give rise to the difference in the observed free energy. Therefore, ITC has been used as a tool to investigate the thermodynamics of the dimerization of CHR in buffers at pH values to get neutral and anionic antibiotic. In this method molar heat of dilution has been measured at different concentrations corresponding to dimer and trimer formation. Earlier report from our laboratory shows that, molar heat of dilution is constant within the limits of experimental errors for species which does not aggregate at different concentrations (Lahiri et al., 2008). But for the species which self-aggregates, molar heat of dilution varies with concentration. Figure 3.7 shows the isotherms obtained from the calorimetric titration of neutral and anionic CHR at 25 °C. From the isotherms, we can see that neutral CHR aggregates at ~10 µM concentration whereas the anionic CHR aggregates at much lower concentrations. The enthalpy change is also opposite in direction for neutral and anionic CHR. It is exothermic in the former case, whereas endothermic in the later. The enthalpy change of self-association of both

---

neutral and anionic CHR is smaller in magnitude than the counterparts in MTR as shown here and in an earlier report (Lahiri et al., 2008). The neutral forms of the two antibiotics show opposite trends in the enthalpy change (Figure 3.7).



### 3.3.5. NMR spectroscopic measurements: anionic CHR

While fluorescence, CD and calorimetry throw light on molecular process of self-association, in-depth site specific structural information of the aggregation process can be obtained from NMR spectroscopy. Here we have addressed the following questions. Is the aromatic planar moiety involved in the aggregation via stacking interaction? What is the role of the aglycone moieties? Finally, is there any evidence that the sugars play role in the process, as indirectly suggested from the other methods? To answer

these questions we have identified some protons (listed in Table 3.2) as the markers to procure information about the above structural moieties. From the NMR spectroscopic studies we have also endeavored to propose a geometric orientation of the monomeric units in the dimer and higher order aggregation. The concentration range used in the NMR studies provides an overall process of aggregation instead of specific information at dimer or tetramer levels. Since the NMR spectra of anionic CHR have been reported earlier in the literature (Gao and Patel, 1989, Gao and Patel, 1990, Devi et al., 2007, Lahiri et al., 2012) we have discussed this case followed by neutral CHR.

**Table 3.2.** Chemical shift values of protons of anionic CHR (100  $\mu$ M and 1 mM) in 20 mM sodium phosphate buffer, pH 8.0 at 25 °C

Protons	$\delta$ values (ppm)	
	100 $\mu$ M	1 mM
C3-H	1.215	1.196
C4-H(a, e)	2.8, -	2.786, 3.557
C5-H	6.42	6.396
C7-CH <sub>3</sub>	1.92	1.946
C10-H	6.085	6.058
C1'-OCH <sub>3</sub>	3.240	3.218
C3'-H	3.8	3.785
C4'-H	3.100	3.087
C4'-CH <sub>3</sub>	1.101	1.082
Sugar A C4''-OCOCH <sub>3</sub>	2.059	2.035
Sugar B C4''-OCH <sub>3</sub>	3.200	3.176
Sugar E C4''-OCOCH <sub>3</sub>	2.175	2.159

Chemical shift values ( $\delta$  ppm) of anionic CHR (at pH 8.0) have been assigned using 1D and 2D (through bond connectivity-TOCSY and through space connectivity-NOESY) NMR spectra (Table 3.2) (Gao and Patel, 1989, Gao and Patel, 1990, Lahiri et al., 2012). They were then further compared with the reported values for chemical shifts of different protons in the molecule. In order to understand the mode of self-association,

different parts of the CHR molecule was examined for their possible orientation in the aggregated states (Table 3.3).

**Table 3.3.** NOESY contacts of protons of anionic CHR (1 mM) in 20 mM Phosphate Buffer, pH 8.0 at 25 °C.

Protons	NOESY contacts
<b>C5-H</b>	C10-H (6.058), sugar AC1"-H (5.473), sugar A C5"-CH <sub>3</sub> (1.210)
<b>C10-H</b>	C5-H (6.396), sugar AC5"-CH <sub>3</sub> (1.210), sugar B C5"-CH <sub>3</sub> (1.196), C4'-H (3.087), Sugar protons (1.776, 1.315)
<b>C7-CH<sub>3</sub></b>	1.737
<b>C1'-OCH<sub>3</sub></b>	sugarC 5"-CH <sub>3</sub> (1.196), Sugar A OAc (2.035), 3.005
<b>C3'-H</b>	sugar A C1"-H (5.473), sugar B C1"-H (5.128), , sugar B C5"-CH <sub>3</sub> (1.196), Sugar A OAc (2.035)
<b>C4'-H</b>	C10-H(6.058), sugar A C1"-H (5.473), 2.786, 2.428
<b>C4'-CH<sub>3</sub></b>	3.891, 3.244, 3.389, 2.050
<b>Sugar A C4''-OAc</b>	sugar B C5"-CH <sub>3</sub> (1.196), C1'-OCH <sub>3</sub> (3.218), C3'-H (3.785)
<b>Sugar B C4''-OMe</b>	sugar B C5"-CH <sub>3</sub> (1.196)
<b>Sugar E C4''-OAc</b>	sugar B C5"-CH <sub>3</sub> (1.196)

Chemical shift values of C5-H and C10-H do not show any NOESY contacts apart from those arising from the protons of the same molecule (Figure 3.1, Table 3.3). Involvement of the aromatic region and therefore, role of stacking interactions in the process of aggregation of anionic CHR appears a remote possibility, because there is no concentration dependent upfield shift of the aromatic protons (Table 3.2). Only a single NOESY contact between C10-H ( $\delta = 6.058$ ) and C4'-H ( $\delta = 3.087$ ) is observed (Figure 8a), which could be ascribed to an altered orientation of CHR molecule as discussed later. Involvement of the aliphatic region of the CHR molecule can be determined from the NOESY contacts of different C-atoms of the aliphatic side chain at C3. An examination of table 3.3 shows that C1'-OCH<sub>3</sub> ( $\delta = 3.218$ ) develops NOESY contacts with both C5"-CH<sub>3</sub> ( $\delta = 1.196$ ) and A-ring acetyl group protons ( $\delta = 2.035$ ) (Figure 3.8b). C3'-H ( $\delta = 3.785$ ) builds NOESY contacts with C1"-H (A-ring) ( $\delta = 5.473$ ) as

well as A-ring acetyl group protons ( $\delta = 2.035$ ) (Figure 3.8c) and C4'-CH<sub>3</sub> is spatially close to many sugar atoms (Table 3.3). These NOESY contacts between the protons could not arise from the same molecule as that would involve a severe steric hindrance and conformational stress (Figure 3.1). Therefore the anionic CHR molecules are mutually oriented in such a way that the disaccharide moiety of one molecule lies over the aliphatic side chain at C3. To minimize the electrostatic repulsion arising from two anionic molecules aliphatic chain of one molecule comes close to the aglycone of another molecule. This is probably reflected in the NOESY contact between C10-H and C4'-H (Figure 3.8a).

### 3.3.6. NMR spectroscopic measurements: neutral CHR

Chemical shift values for protons in neutral CHR molecule (at pH 6.0) are assigned from 1D and 2D (through bond connectivity-TOCSY and through space connectivity-NOESY) NMR spectra. The peak assignments were then confirmed by a comparison with those of the anionic CHR molecule. The chemical shift values for the protons in the neutral state are not significantly different from those in the anionic state (Table 3.4). Similar to that in the anionic form, C5-H and C10-H of the neutral molecule do not develop any NOESY cross peaks apart from those arising due to intra-molecular contacts. Here also we do not notice concentration dependent upfield shift of the aromatic protons, thereby ruling out the possibility of aromatic ring stacking mediated association (Table 3.4). The aliphatic side chain develops NOESY contacts with a number of protons of the di- saccharide moiety as is exemplified by NOE cross peaks between C1'-OCH<sub>3</sub> ( $\delta = 3.221$ ) and A-ring acetyl group protons ( $\delta = 2.039$ )

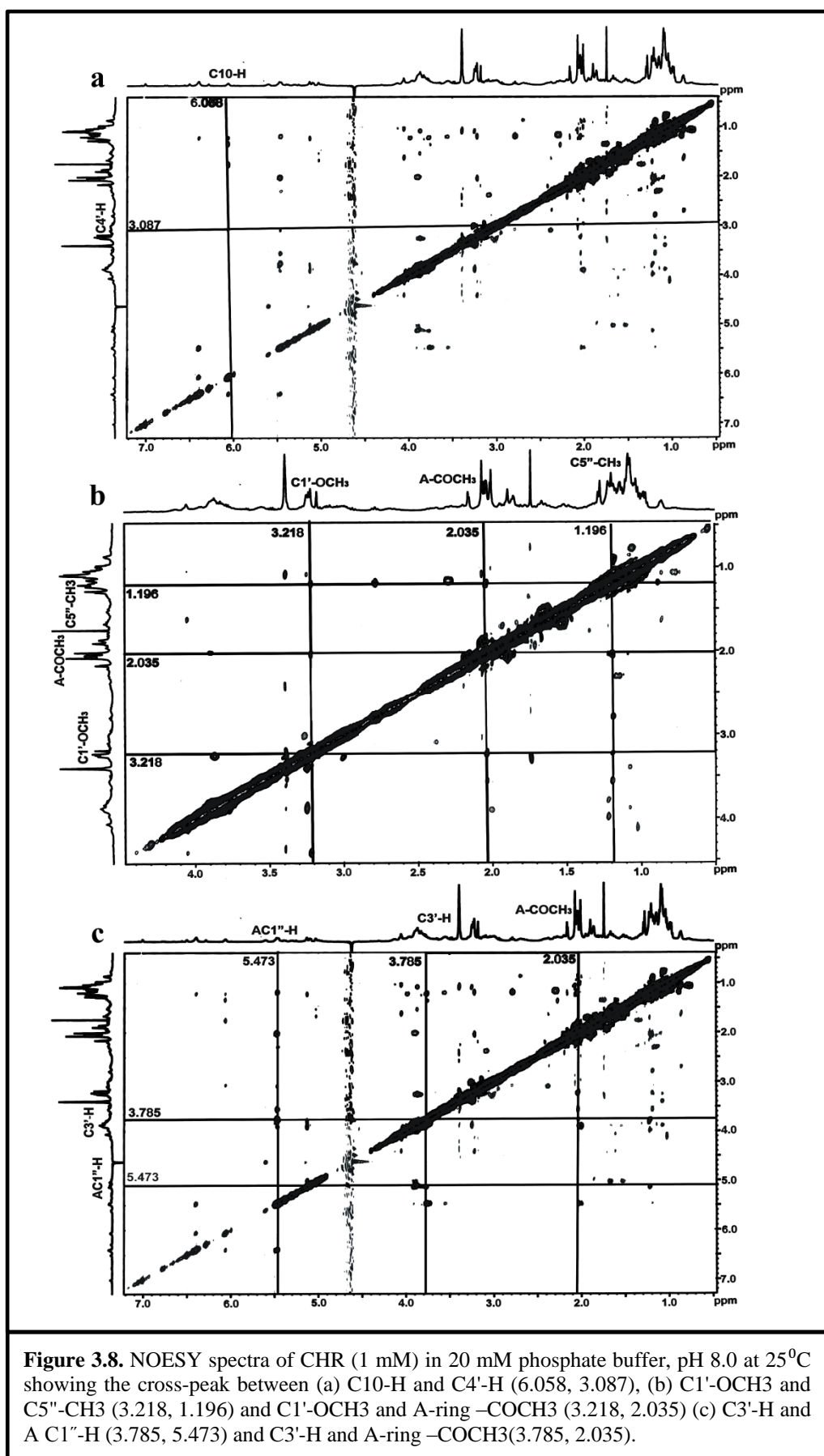




(Figure 3.9a, Table 3.5). In contrast to anionic form of CHR, aliphatic side chain of neutral CHR does not form any NOE contacts with the aglycone. C1'-OCH<sub>3</sub> aliphatic side chain also develops NOE contacts with B- ring C3''-H ( $\delta = 3.763$ ) (Figure 3.9b) and B-ring C5''-CH<sub>3</sub> ( $\delta = 1.198$ ) (Figure 3.9c), which is possible if two neutral CHR molecule arrange themselves such that the aliphatic side chain of one molecule lies over the disaccharide moiety of the other (scheme 3.1).

**Table 3.4.** Chemical shift values of protons of neutral CHR (100  $\mu$ M and 1 mM) in 20 mM sodium phosphate buffer, pH 6.0 at 25 °C

Protons	$\delta$ values (ppm)	
	100 $\mu$ M	1 mM
<b>C3-H</b>	1.23	1.207
<b>C4-H(a, e)</b>	-	2.786, 3.542
<b>C5-H</b>	6.402	6.382
<b>C7-CH<sub>3</sub></b>	1.92	1.907
<b>C10-H</b>	6.063	6.058
<b>C1'-OCH<sub>3</sub></b>	3.237	3.221
<b>C3'-H</b>	-	4.059
<b>C4'-H</b>	-	4.120
<b>C4'-CH<sub>3</sub></b>	1.051	1.035
<b>Sugar A C4''-OCOCH<sub>3</sub></b>	2.059	2.039
<b>Sugar B C4''-OCH<sub>3</sub></b>	3.200	3.185
<b>Sugar E C4''-OCOCH<sub>3</sub></b>	2.181	2.164

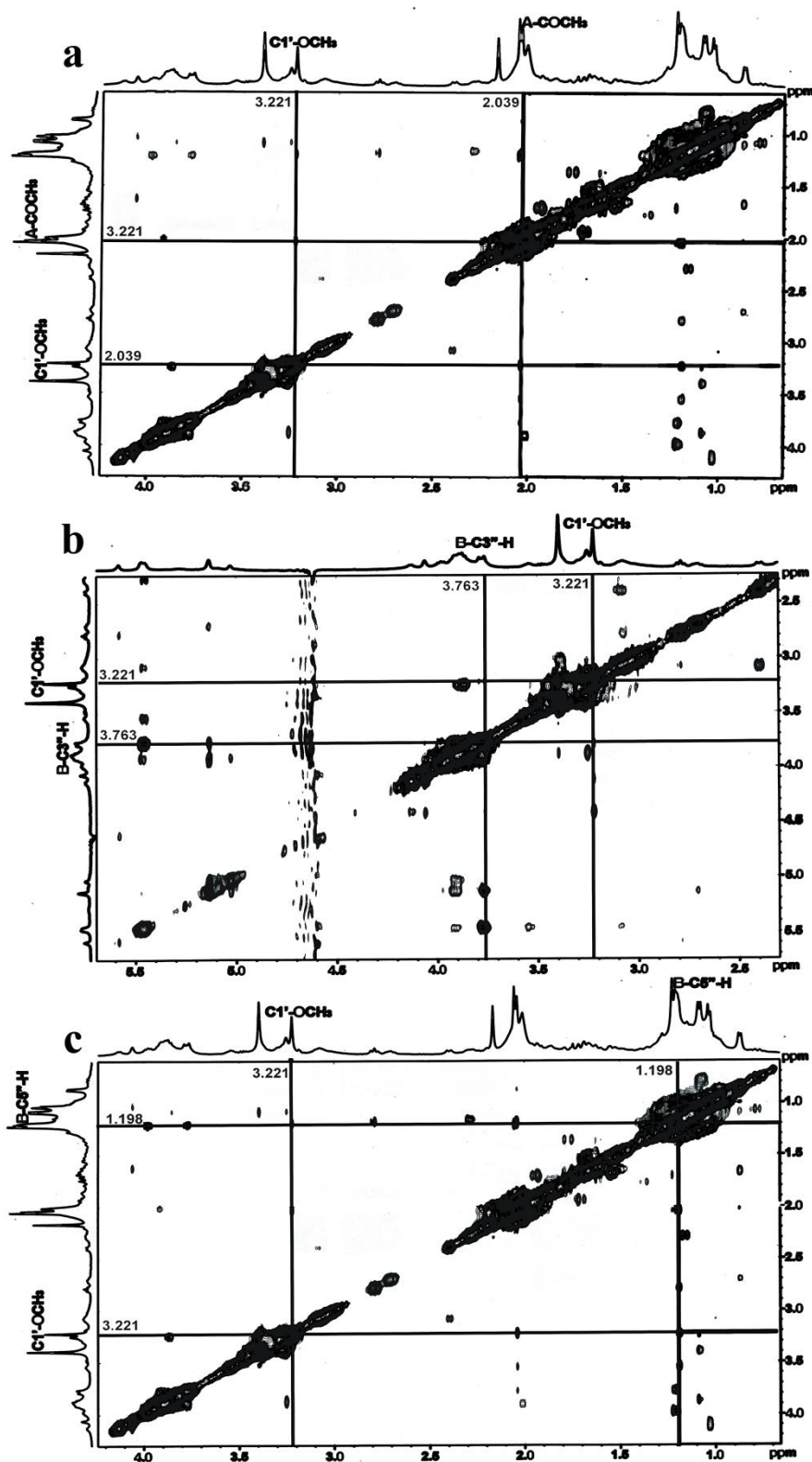
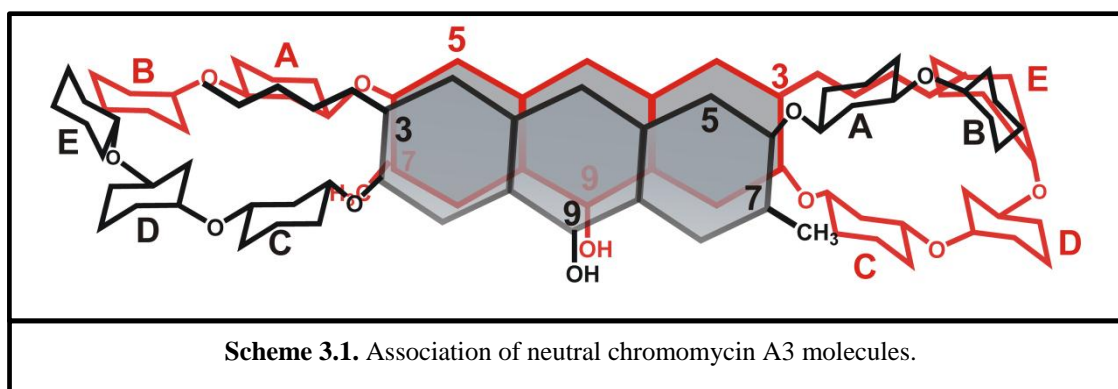


**Figure 3.9.** 2D NMR of neutral form :NOESY spectra of CHR (1 mM) in 20 mM phosphate buffer, pH 6.0 at 25°C showing the cross-peak between (a) C1'-OCH<sub>3</sub> and A-ring -COCH<sub>3</sub> (3.221, 2.039) (b) C1'-OCH<sub>3</sub> and B-ring C3''-H (3.221, 3.763) (c) C1'-OCH<sub>3</sub> and B-ring C5''-H (3.221, 1.198).

**Table 3.5.** Chemical shift values of protons of neutral CHR (100  $\mu$ M and 1 mM) in 20 mM sodium phosphate buffer, pH 6.0 at 25  $^{\circ}$ C

Protons	NOESY contacts
<b>C5-H</b>	C10-H(6.053), sugar A C1''-H (5.470), sugar A C5''-H (3.075), sugar B C5''-CH <sub>3</sub> (1.198), sugar B C3''-H (3.763)
<b>C10-H</b>	C5-H (6.382), sugar A C5''-CH <sub>3</sub> (3.075), sugar B C5''-CH <sub>3</sub> (1.198), Sugar protons (1.785, 1.390)
<b>C7-CH<sub>3</sub></b>	1.785, 1.744, 1.223
<b>C1'-OCH<sub>3</sub></b>	sugar B C5''-CH <sub>3</sub> (1.198), Sugar A OAc (2.039), sugar B C3''-CH <sub>3</sub> (3.763), C4'-H(4.12)
<b>C3'-H</b>	C4'-CH <sub>3</sub> (1.035), 1.663
<b>C4'-H</b>	C1'-OCH <sub>3</sub> (3.221), C4'-CH <sub>3</sub> (1.035)
<b>C4'-CH<sub>3</sub></b>	C3'-H (4.059), C4'-H (4.12)
<b>Sugar A C4''-OAc</b>	sugar B C5''-CH <sub>3</sub> (1.194), sugar B C3''-CH <sub>3</sub> (3.763), sugar B C4''-CH <sub>3</sub> (3.542), sugar A C1''-H (5.470), sugar A C5''-CH <sub>3</sub> (1.145), C1'-OCH <sub>3</sub> (3.221), C3'-H (3.785), 1.685
<b>Sugar E C4''-OAc</b>	sugar B C5''-CH <sub>3</sub> (1.198)



### 3.4. DISCUSSION

Self-association of several antibiotics like CS-088, amithramycin, actinomycin D and amphotericin with diverse biological activity as human medicine has been reported earlier (Chaires et al., 1982, Kikuchi et al., 2005, Lewis et al., 2006, Toledo Grijalba et al., 2006, Veselkov et al., 2002). Our present report has gone in depth to characterize the aggregation behavior of CHR. Previous report on the related antibiotic MTR has been confined to anionic form at which it exists at physiological pH (Lahiri et al., 2008). On the other hand at physiological pH, CHR ( $pK_a = 7.0$ ) is a mixture of anionic and neutral forms. Therefore, in this report, we have employed various spectroscopic and calorimetric techniques to understand the molecular basis of self-association of the antibiotic CHR in its neutral form as well as the anionic form. For comparison among the two antibiotics we have also studied in part the hitherto unreported aggregation of neutral form of MTR. Spectroscopic studies, such as absorbance, fluorescence and circular dichroism, provide evidences for the existence of different molecular species present in wide concentration range. Due to the formation of aggregates, an increase in normalized fluorescence intensity is observed for both neutral and anionic CHR (Figure 3.3), which would otherwise have been unchanged. The aggregation also leads to blue shift of the peak position of the emission spectra, the values being 2 nm and 5 nm for aggregation of neutral and anionic CHR, respectively. These features suggest that the chromophore portion of the molecule enters into an enhanced hydrophobic environment. The self-association process becomes apparent in CD spectroscopy, when the effect of coupling between transition dipoles ( $n \rightarrow \pi^*$ ) of chromophores in aggregates gives rise to the splitting of bands in the visible region at higher concentration (Figure 3.4). The concentration dependence of ellipticity values has

---

---

helped to evaluate the dissociation constant for the three equilibria present over the concentration range reported here. Figures 3.5 and 3.6 show there are three breaks in the plots of ellipticity versus concentration for neutral and anionic CHR in this concentration range. The multiple equilibria as mentioned above to account for the aggregation suggest the formation of a tetramer at the highest concentration. For neutral CHR the trimer to tetramer transition occurs at  $\sim 135 \mu\text{M}$  and for anionic CHR at  $\sim 83 \mu\text{M}$ . No further self-association is observed beyond these concentrations. Among the neutral and anionic forms of CHR, the anionic form has higher association constant in the case of CHR. Quantitative analysis of the CD data (Table 3.1) shows that dimerization is the predominant process followed by weaker association of CHR molecules over the total concentration range. Similar trend in association is also reported for neutral (present study) and anionic MTR from our laboratory (Lahiri et al., 2008). However, a comparative analysis shows that dimer formation is free energy wise most favorable for CHR in contrast to MTR, where tetramer formation is the most favorable process. The overall association constant for the equilibrium:  $4\text{M} \rightleftharpoons \text{M}_4$  is also significantly higher (by a factor of  $10^4$ ) for both forms of MTR (Table 3.1). These results emphasize the role of sugars in the oligomerization process. It also suggests that the state of ionization does not modulate the aggregation property of the antibiotics.

For a molecular species molar heat of dilution depends on its interaction with solvent, which should be independent of its concentration in the solution, if it has not undergone any change during dilution (Lahiri et al., 2008). In this study we have seen a concentration dependent change in molar heat of dilution for neutral CHR (at pH 5.0) and anionic CHR (at pH 9.0), which is possible if CHR molecules self-associate among themselves. But the molar heat of dilution of anionic MTR, which is reported from our

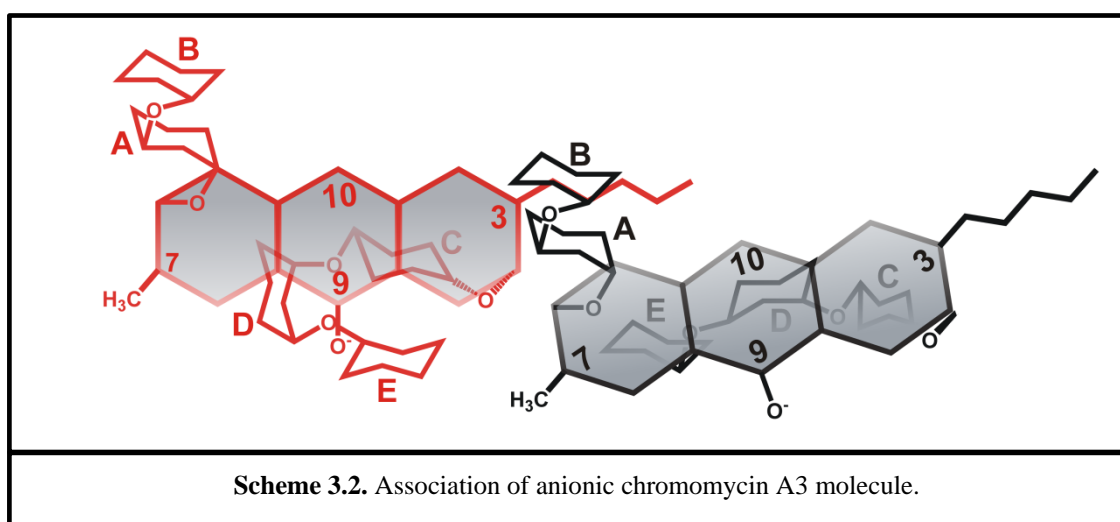
---

laboratory (Lahiri et al., 2008), is greater than the same for neutral and anionic CHR. On the other hand, in case of neutral MTR the enthalpy change is comparable to neutral CHR. Anionic form of MTR has higher free energy of association, as obtained from quantitative analysis of CD data (Table 3.1). The results indicate that self-association process of anionic CHR is mostly entropy driven whereas for anionic MTR it is enthalpy driven. This striking difference between the two molecules with similar structure shows that CHR might form hydrophobic clusters. Such hydrophobic clusters may also characterize the self-association for neutral MTR, because its association is entropy driven as indicated from low value of enthalpy of dissociation. The repulsion of large number of surrounding solvent molecules is a plausible factor contributing to the total entropy of the system.

The mode of self-association is further characterized by NMR spectroscopy. Features suggesting against stacking interactions include, absence of upfield chemical shift of the aromatic protons (Table 3.2) and any intermolecular NOE contacts in the aromatic region (C5-H and C10-H) in both neutral and anionic CHR. Analysis of the NOE spectra of anionic CHR reveals a conformation in which the disaccharide unit of one molecule of anionic CHR lies above the aliphatic side chain at C3 of another molecule (Scheme 3.2). On the other hand, similar analysis of the NOE spectra of neutral CHR reveals an aggregated conformation, where two CHR molecules are probably in a mutually *trans* orientation (Scheme 3.1). Distinct NOE contacts between the disaccharide moiety of one molecule and the aliphatic side chain of another molecule as well as NOE contacts of C7-CH<sub>3</sub> with different sugar protons provide support to our hypothesis. A priori one might assume a similar molecular arrangement for the anionic molecule, due to similar NOE contacts. NOE data shows that there is no significant

---

NOE cross peaks for C7-CH<sub>3</sub> in the anionic CHR, which could therefore rule out such an orientation of the CHR molecules. This altered conformation in case of anionic CHR could be ascribed to the charge repulsion at C9-O, which would be predominant in the *trans* orientation (Scheme 3.2). Similar charge repulsion is not present in the neutral form and hence it can adopt the *trans* orientation (Scheme 3.2). Therefore, it is observed that CHR aggregates both in the neutral as well as in the anionic form with different modes of relative molecular arrangement of the monomer species.



MTR and CHR have different sugar moieties attached to the identical aglycone (Menendez et al., 2004, Bosserman et al., 2011). NMR data analysis had earlier shown that self-aggregation of anionic MTR in aqueous media is mediated by sugar moieties (Lahiri et al., 2008). NMR studies in the present report have also demonstrated that the self-association process in CHR is also sugar mediated; aggregated CHR differs in the structural arrangement from MTR. However, in both cases aromatic moieties do not play a significant role in the stabilization of the aggregates. Sugars are amphiphilic in nature as they have hydrophobic (CH) and hydrophilic (OH) faces (Patel et al., 2007,

Santacroce and Basu, 2004, Yano et al., 1988). Sugars in CHR has more CH-surface compared to MTR, which gives rise to enhanced hydrophobic interaction between CHR molecules in aqueous solvents, which leads to entropy driven self-association for CHR. But in case of MTR due to presence of some extra –OH group there is a possibility of formation of H-bonds between MTR and solvent water molecules, which may be the reason for higher enthalpy change in case of dilution of anionic MTR.

The difference between the two antibiotics can be traced back to the organization of their respective gene clusters, which also suggests different regulatory mechanisms for MTR and CHR in the producer organisms (Lombo et al., 2006). Apart from other differences in chemical properties observed earlier (e.g. acidity, cytotoxicity, etc.), difference in chemical constitution of MTR and CHR, also leads to different characteristics of self-association. CHR aggregates at a much lower concentration (3  $\mu\text{M}$  - 5  $\mu\text{M}$ ) as compared to anionic MTR, which starts aggregating at around 20  $\mu\text{M}$ . This inherent tendency of CHR to dimerize is also reflected in the very low  $K_d$  values of the dimerization process. Although the relative conformations of CHR molecules differ according to the ionization state of the molecule, both forms start to aggregate at relatively lower concentrations. The entropy driven association of CHR also indicates the pre-disposition of the antibiotic to form clusters even at low concentrations, which might therefore lead to altered bioactivity of CHR both in the producer organism as well as an antibiotic.

MTR and CHR have difference in cytotoxicity towards cell lines from different species (Singh and Gupta, 1985, Chan et al., 2004). This suggests that MTR and CHR have differences in cellular uptake and retention rising from the differences present in the structure of these two antibiotics. Different sugar moieties with substituents, present in

---



MTR and CHR, may alter the specific interaction between receptors present on the cell surface and the antibiotics. So, self-aggregation property of these antibiotics plays a role in cellular transportation. Two oligosaccharide moieties and the acetyl-groups which are associated with the sugars (A and E) are major structural contributors to the biological activity of CHR, because it has been established that elimination of acetyl groups leads to the generation of a derivative with significantly decreased antitumor activity (Chakrabarti et al., 2001, Lombo et al., 2006, Menendez et al., 2004). The antibiotics are comparably effective to inhibit DNA dependent RNA synthesis via reversible association of the dimer: metal ion complex with DNA (Singh and Gupta, 1985, Chan et al., 2004). However, in an earlier study we have demonstrated the role of sugars in the association of the antibiotics with DNA and the oligonucleotide fragment (Chakrabarti et al., 2002).

---

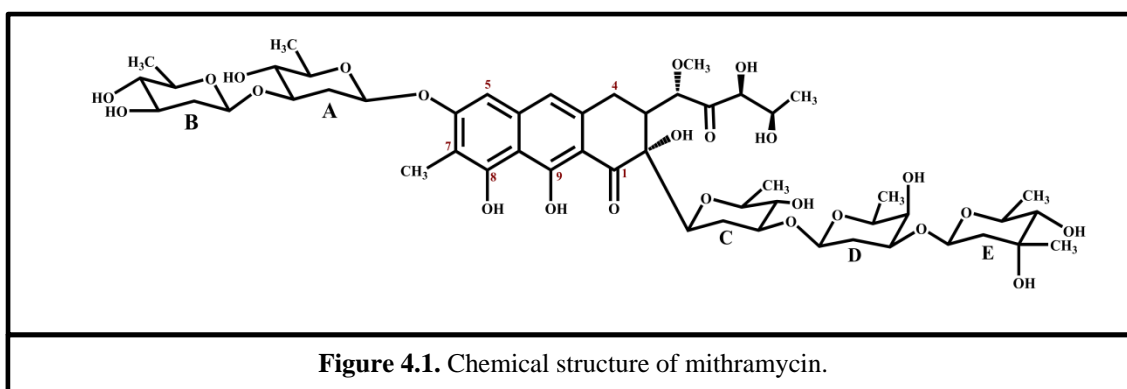
# Chapter 4

---

**Association of Mithramycin  
with  $\text{Mn}^{2+}$  and the potential  
cellular targets of the complex**

## 4.1. INTRODUCTION

Mithramycin (plicamycin, MTR) is a naturally occurring anticancer antibiotic isolated from *Streptomyces plicatus* (Calabresi et al., 1991). It belongs to the aureolic family of drugs, which consists of a chromomycinone moiety, either side of which is linked to sugar residues via *O-glycosidic* linkages (Figure 4.1) (Wohlert et al., 1999). MTR is established as an antibiotic for Gram-positive bacteria (Goldberg and Friedman, 1971). It has been used clinically for many years to treat testicular carcinoma and several types of cancer like leukemia, as well as hypercalcemia in patients with metastatic bone lesions (Lumachi et al., 2008). The anticancer properties were ascribed to the inhibitory



effect of MTR on DNA replication and transcription during macromolecular biosynthesis (Goldberg and Friedman, 1971). The ability of MTR to bind via DNA minor groove and thereby regulating gene expression is the rationale for using it in these pathological cases (Chakraborty et al., 2008, Devi et al., 2009a, Goldberg and Friedman, 1971, Wohlert et al., 1999). MTR was found to inhibit the binding of transcription factor *Sp1* to its promoter, which in turn leads to gene transcription modulation of different genes, including *c-myc*, and *ha-ras*, as well as antiapoptotic genes (Campbell et al., 1994, Jones et al., 1995). Moreover, MTR has been found to

cross the blood-brain barrier and is in its preclinical trials in Huntington's disease (HD) (Ferrante et al., 2004). Structural analysis revealed that, MTR binds to minor groove of DNA around GC-rich sequences in the presence of bivalent metal ions such as  $\text{Mg}^{2+}$ ,  $\text{Zn}^{2+}$ ,  $\text{Co}^{2+}$ ,  $\text{Fe}^{2+}$  etc (Aich and Dasgupta, 1995, Devi et al., 2007, Gochin, 1998, Hou and Wang, 2005, Lu et al., 2009). Previous studies from our laboratory have shown that MTR binds to different types of bivalent metal ions like  $\text{Mg}^{2+}$ ,  $\text{Zn}^{2+}$  and  $\text{Cu}^{2+}$ , of which  $\text{Mg}^{2+}$  belongs to the main group element whereas  $\text{Zn}^{2+}$  and  $\text{Cu}^{2+}$  are transition metal ions (Aich and Dasgupta, 1995, Devi et al., 2007, Lahiri et al., 2012).

Considering the complex formation ability of MTR with the metal ions, we have studied its binding ability with  $\text{Mn}^{2+}$ , an essential micronutrient. Manganese is an important trace element required by all organisms in various cellular processes, including metabolism and oxidative stress defense (Chandra and Shukla, 1981). The most important of them is that it protects against reactive oxygen species (ROS) and increases the fitness of cells by minimizing energy expenditure on the synthesis of a defense mechanism. Manganese superoxide dismutase (MnSOD), a metalloenzyme, is a typical example of such defense mechanism against oxidative damage (Fridovich, 1975, Fridovich, 1997, Zheng et al., 2007). It catalyzes the degradation of toxic superoxide radicals to molecular oxygen and hydrogen peroxide. MnSOD is found in both prokaryotes and mitochondrial matrices.

In human body a very high concentration of  $\text{Mn}^{2+}$  is present in saliva whereas in blood the concentration is in nanomolar range (Horsburgh et al., 2002). Thus,  $\text{Mn}^{2+}$  becomes a potential signal by which bacteria can identify a shift from a mucosal environment to a more invasive site. The homeostasis of  $\text{Mn}^{2+}$  is important, as excess of  $\text{Mn}^{2+}$  is toxic (Mena et al., 1967, Montes et al., 2001). For instance, in humans, exposure to

---

manganese has been associated with a neurological syndrome called ‘manganism’, whose symptoms resemble those of Parkinson’s Disease (Olanow, 2004). Recently it has been shown that  $\text{Mn}^{2+}$  accumulates in brains of cirrhotic patients who also present motor abnormalities.  $\text{Mn}^{2+}$  ion alters dopaminergic transmission promoting an increase in the turnover of dopamine (Pal et al., 1999). Small molecules with the ability to sequester  $\text{Mn}^{2+}$  from the cell with a relatively high affinity might be putative therapeutic agents for these cases to regulate cellular manganese homeostasis pathway.

We have studied by means of different spectroscopic and calorimetric techniques its binding ability with  $\text{Mn}^{2+}$ . These studies have led us to understand its mechanism of binding with  $\text{Mn}^{2+}$ . We have also examined plausible targets of the resultant antibiotic:  $\text{Mn}^{2+}$  complex inside the cell. With the above objectives, we have studied the ability of  $[\text{MTR}:\text{Mn}^{2+}]$  complex to bind double helical DNA as well as chromatin, the protein-DNA complex keeping in view the earlier reports of  $[(\text{MTR})_2:\text{metal ion}]$  complexes as active DNA binding agents. Earlier we have shown the ability of MTR to bind  $\text{Zn}^{2+}$  containing metalloenzymes such as alcohol dehydrogenase (Devi et al., 2009b). We have also examined the association of anionic MTR with MnSOD, an important enzyme containing  $\text{Mn}^{2+}$ .

---

## 4.2. MATERIALS AND METHODS

### 4.2.1. Materials

MTR, Manganese (II) chloride solution (1M), Trizma base, pyrogallol, cacodylic acid, polynucleotides poly (dG-dC), poly (dA-dT)), Manganese superoxide dismutase from *Escherichia Coli* (E.C. 1.15.1.1) and Micrococcal nuclease were purchased from Sigma Chemical Company (U.S.A). Hydrochloric acid (HCl) [ACS grade] was purchased from Merck, Germany.

### 4.2.2. Methods

#### 4.2.2.1. Preparation of buffers for chromatin isolation

Buffers required for the isolation and purification of chromatin are as follows.

**Buffer A:** 0.01M Tris HCl (pH 7.4), 0.31M Sucrose, 5mM Magnesium chloride, 0.2 mM PMSF, 0.4% Triton X 100, 0.04 M Sodium bisulfite;

**Buffer B:** 0.05 M Tris HCl (pH 7.4), 2.2 M Sucrose, 0.01 M Magnesium chloride;

**Buffer C:** 0.05 M Tris HCl (pH 7.4), 1M Sucrose, 0.01 M Magnesium chloride; **Buffer**

**D:** 0.05 M Tris HCl (pH 7.4), 0.34 M Sucrose, 0.01 M Magnesium chloride, 0.8% Triton X 100;

**Digestion Buffer:** 0.05 M Tris HCl (pH 7.4), 0.25 M Sucrose, 3 mM Magnesium chloride, 25 mM Sodium chloride, 1 mM Calcium chloride;

**Lysis Buffer:** 5 mM Tris HCl (pH 7.4), 0.05 mM EDTA, 0.05 mM Sodium bisulfite.

---

#### 4.2.2.2. Preparation of chromatin from chicken liver

Soluble chromatin was isolated from chicken liver kept at -20°C overnight and then transferred to 4°C. Chicken liver nuclei were isolated as described by Blobel and Potter (Blobel and Potter, 1966) with minor modifications. To isolate nuclei from chicken liver it was washed with two volumes of cold buffer A and finely minced using sterile scissors. Minced liver tissue was suspended in one volume of cold buffer A and homogenized using a glass tissue grinder on ice. The homogenate was filtered through four layers of sterile, starch-free cheese cloth and centrifuged at 3000 rpm at 4°C. The supernatant was rejected and the pellet was resuspended in cold buffer B. The suspension was centrifuged for 1 hour 20 minutes at 38,000 rpm in an OTD65B Sorvall Ultracentrifuge at 4°C. Pellet obtained at this step corresponds to nuclei. The pellet obtained was suspended in cold buffer C. The suspension was centrifuged for 10 minutes at 10,000 rpm. The pellet was washed with two changes of buffer D.

Chromatin was prepared from the nuclei by partial micrococcal nuclease digestion (Noll and Kornberg, 1977). Nuclei were suspended in appropriate amount of digestion buffer with calcium chloride (final concentration 2 mM) so as to obtain  $A_{260} = 228$  and incubated at 37°C for 2 minutes. In general, 25 U of micrococcal nuclease was added to 400µl nuclear suspension. Enzymatic digestion was carried out for 30 seconds. The reaction was stopped by addition of 20mM EDTA, followed by chilling on ice. The suspension was centrifuged at 8,000 rpm for 5 minutes, and the supernatant was discarded. Soluble chromatin was extracted by lysis of the micrococcal nuclease-digested nuclei. This was achieved by suspension of the pellet in appropriate amount of lysis buffer and incubation on ice for 30 minutes, followed by centrifugation at 10,000 rpm for 15 minutes. Chromatin was obtained in the supernatant. The soluble chromatin

---

was dialyzed against 20 mM Tris-HCl (pH 8.0) at 4°C overnight. Concentration of chromatin was determined spectrophotometrically using the molar extinction coefficient ( $\epsilon_{260}$ ) of  $6600 \text{ M}^{-1} \text{ cm}^{-1}$  at 260nm.

#### **4.2.2.3. Extraction of chromosomal DNA**

Chromosomal DNA was extracted from soluble chromatin isolated from chicken liver. Chromatin samples were treated with 1/7<sup>th</sup> volume of 10% SDS, and mixed well. 5M sodium chloride (2/7<sup>th</sup> volume) was added, and the mixture was incubated for 4 hours. This step ensured the denaturation of proteins present in chromatin, and their subsequent separation from chromosomal DNA. Equal volume of phenol: chloroform: isoamyl alcohol (25:24:1 v/v) was added, and vortexed vigorously. The emulsion was then centrifuged at 10,000rpm for 10 minutes at room temperature. The aqueous (top) layer was carefully removed into a clean tube and re-extracted in a similar manner. After 3 extractions with phenol: chloroform: isoamyl alcohol, the aqueous layer was extracted with an equal volume of chloroform. For precipitation of DNA, the pH of the solution was adjusted to 5.2 by addition of 1/10<sup>th</sup> volume of 3M sodium acetate (pH 5.2). 3 volumes of isopropanol were added, and the mixture was chilled at -20°C overnight or at -80°C for 1 hour. The DNA was collected by centrifugation at full speed for 15 minutes at 4°C. The DNA pellet was washed with 70% ethanol and dried in air. It was dissolved in appropriate amount of TE buffer and checked for purity spectrophotometrically, as well as by agarose gel electrophoresis. The mononucleotide concentration was determined spectrophotometrically, using the molar extinction coefficient of  $\epsilon_{260} = 6600 \text{ M}^{-1} \text{ cm}^{-1}$ .

---



#### 4.2.2.4. Absorption spectroscopy

Absorbance spectra were recorded in a Cecil CE7500 spectrophotometer fitted with a water circulation system to maintain a constant temperature using 1 cm path length quartz cuvettes. Concentration of MTR was calculated from a known molar absorption coefficient of  $10,000 \text{ M}^{-1}\text{cm}^{-1}$  at 400 nm wavelength (Aich and Dasgupta, 1995). Similarly, concentrations of the polynucleotides were measured from the molar extinction coefficients, which are  $8400 \text{ M}^{-1} \text{ cm}^{-1}$  at 254 nm for poly (dG–dC) and  $6800 \text{ M}^{-1} \text{ cm}^{-1}$  at 260 nm poly (dA–dT) (Wells et al., 1970). All the spectroscopic studies were carried out in 20 mM Tris–HCl buffer pH 8.0 at 25 °C. Fixed amount of MTR (20  $\mu\text{M}$ ) was titrated with increasing concentration of  $\text{Mn}^{2+}$ . Each reading was an average of four runs. Readings were noted 4 minutes after each addition to ensure complete complex formation.

#### 4.2.2.5 Steady State Fluorescence spectroscopy

Fluorescence spectra were recorded in a Perkin-Elmer LS55 luminescence spectrometer fitted with a water circulation system to maintain a constant temperature using a quartz cuvette of 1cm path length. Fixed amount of MTR (20  $\mu\text{M}$ ) was titrated with increasing concentration of metal ion. Reported spectra were an average of four runs and corrected for buffer contribution. In order to avoid photo-degradation of MTR, the fluorescence excitation wavelength was 470 nm instead of the absorption maximum and the emission was recorded over the range of 500-700 nm (Aich and Dasgupta, 1995). During fluorescence measurements, care was taken to ensure that the absorbance of the

---

samples does not exceed 0.05 at the excitation wavelength. Therefore, we did not correct the emission intensity for optical filtering effects.

#### **4.2.2.6. Circular Dichroism (CD) spectroscopy**

The CD spectra were recorded in a JASCO J715 spectropolarimeter (Jasco Cooperation, Tokyo, Japan) at 25°C. The CD scans were recorded within the wavelength range of 220-520 nm with scan speed 200 nm per minute and step size of 0.1 nm. The time constant was 2 seconds and bandwidth was 1 nm. CD spectra in the near UV and visible region were recorded on the addition of increasing concentration of  $\text{Mn}^{2+}$  to a fixed concentration of MTR (20  $\mu\text{M}$ ). Reported spectra were an average of four scans. The observed data points were smoothened by Jasco CD Standard Analysis Software.

#### **4.2.2.7. Isothermal Titration Calorimetry (ITC)**

Isothermal Titration Calorimetry (ITC) experiments were done in VP-ITC microcalorimeter (MicroCal Inc., U.S.A.) at 25°C. Samples were extensively degassed prior to titration. The single injection mode (SIM) was used to determine the apparent binding constant for the association of MTR with  $\text{Mn}^{2+}$ . A single shot of 250  $\mu\text{l}$   $\text{Mn}^{2+}$  solution (2.5 mM) was injected over a span of 500 seconds into the cell containing 75  $\mu\text{M}$  of MTR and the resultant enthalpy change was monitored for 2000 seconds. The stirring speed of the syringe was 546 rpm. For the control experiments, the same amount of  $\text{Mn}^{2+}$  was added to the buffer (20mM Tris-HCl, pH 8.0) present in the cell.

---

The heat released due to addition of single aliquot of  $\text{Mn}^{2+}$  to MTR solution was measured by a thermoelectric device between the sample and reference cells. The heat associated with the injection was observed as a peak which corresponds to the power required to maintain the sample and reference cells at identical temperatures. The peaks produced over the course of titration can be converted to heat output per injection by integration and correcting for cell volume and sample concentration. The heat released for the  $i$ -th injection,  $\Delta Q(i)$  is given by (Ladbury and Doyle, 2005)

$$\Delta Q(i) = Q(i) + \frac{dV_i}{V_0} \left[ \frac{Q(i) + Q(i-1)}{2} \right] - Q(i-1) \dots \dots \dots (1)$$

where  $V_i$  is the injection volume and  $V_0$  is the cell volume. The total heat released ( $Q(t)$ ) was fit by non-linear least square minimization method using the equation (Ladbury and Doyle, 2005)

$$Q(t) = \frac{nM_t \Delta H V_0}{2} \left[ 1 + \frac{X_t}{nM_t} + \frac{1}{nkM_t} - \sqrt{\left( 1 + \frac{X_t}{nM_t} + \frac{1}{nkM_t} \right)^2 - \frac{4X_t}{nM_t}} \right] \dots \dots \dots (2)$$

where  $n$  is the number of binding sites,  $k$  is the binding constant,  $M_t$  is the bulk concentration of macromolecule in active cell volume ( $V_0$ ),  $X_t$  is the bulk concentration of the ligand and  $\Delta H$  is the molar enthalpy of ligand binding. Corrected isotherm was obtained by subtracting the molar heat change upon addition of  $\text{Mn}^{2+}$  into buffer from the heat change due to addition of  $\text{Mn}^{2+}$  into the same buffer containing MTR (75  $\mu\text{M}$ ). The resultant enthalpy changes were then analyzed using ‘one set of sites’ model in the inbuilt MicroCal LLC SIM software to obtain the apparent dissociation constant,  $K_d^{app}$ , and other thermodynamic parameters ( $\Delta H$  and  $\Delta S$ ). The Gibbs Energy was calculated using the equation

$$\Delta G = \Delta H - T\Delta S \dots \dots \dots (3)$$

#### **4.2.2.8. Enzymatic Assay of Manganese Superoxide Dismutase**

Inhibition of pyrogallol autoxidation by MnSOD (Marklund and Marklund, 1974) has been used to determine the activity of MnSOD in presence and absence of MTR. The autoxidation was followed from the increase in absorbance of pyrogallol at 420 nm for 30 minutes in 50 mM Tris-cacodylic acid buffer, pH 8.20 at 25°C. To study the effect of MTR upon the enzyme activity of MnSOD, the solution containing MnSOD (100 nM) was pre-incubated with different concentrations of MTR (10, 20, and 50 µM, respectively) for 1 hour at 25°C and mixed with 0.2 mM pyrogallol.

---

### 4.3. ANALYSIS

#### 4.3.1. Determination of binding stoichiometry

The method of continuous variation (Job plot) was employed to determine the stoichiometry of the complex between MTR and  $\text{Mn}^{2+}$  (Huang, 1982). Absorbance of MTR at 400nm wavelength was recorded at 25°C for the reaction mixtures, in which the number of moles of  $\text{Mn}^{2+}$  and MTR were varied in fixed volume keeping the total number of moles of  $\text{Mn}^{2+}$  and MTR constant. Under these conditions the absorbance at 400nm ( $A_{400}$ ) was plotted against the mole fraction of MTR in the respective solutions. The break point in the resulting plot corresponds to the mole fraction of MTR in the MTR:  $\text{Mn}^{2+}$  complex. The stoichiometry was obtained as follows

$$\text{MTR}:\text{Mn}^{2+} = \chi_{\text{ligand}} : (1 - \chi_{\text{ligand}})$$

where,  $\chi_{\text{ligand}}$  is the mole fraction of MTR calculated as the ratio of molar concentration of antibiotics to the total molar concentration of MTR and  $\text{Mn}^{2+}$ .

#### 4.3.2. Estimation of apparent dissociation constant ( $K_d^{app}$ )

Apparent dissociation constant ( $K_d^{app}$ ) was determined for the complex between MTR and  $\text{Mn}^{2+}$  by fluorescence, absorbance and circular dichroism methods. In all these methods fixed concentration of MTR (20  $\mu\text{M}$ ) in a cuvette was titrated with increasing concentration of  $\text{Mn}^{2+}$ . We employed two methods to determine the affinity constant for association of MTR and  $\text{Mn}^{2+}$ .

**Method 1:** The apparent dissociation constant ( $K_d^{app}$ ) for the interaction of ligand (L) (MTR or  $[(MTR)_2Mn^{2+}]$ ) with polynucleotide (D) was obtained by monitoring the change in absorbance, fluorescence and CD spectra of ligand upon addition of polynucleotide. The experimental data points are fitted to a non-linear equation based on the equilibrium (Chakrabarti et al., 2000)



where L, D and LD denote ligand ( MTR or  $[(MTR)_2 Mn^{2+}]$ ), DNA (  $Mn^{2+}$  or chromatin or chromosomal DNA) and ligand-DNA /  $Mn^{2+}$  complex respectively. For an initial concentration  $C_0$  of the ligand and an input concentration  $C_p$  of DNA/ $Mn^{2+}$ , the concentration of LD is given by x, such that  $K_d^{app}$  takes the form,

$$K_d^{app} = \frac{(C_0-x)(C_p-x)}{x} \dots\dots\dots(2)$$

Replacing “x” by the spectroscopic signal in the above equation, we get

$$K_d^{app} = \frac{[C_0-(\Delta S_{obs}/\Delta S_{max}).C_0][C_p-(\Delta S_{obs}/\Delta S_{max}).C_0]}{[(\Delta S_{obs}/\Delta S_{max}).C_0]} \dots\dots\dots(3)$$

where  $\Delta S_{obs}$  is the change in spectroscopic signal due to each addition of DNA/chromatin and  $\Delta S_{max}$  is the same parameter when the ligand is totally bound to the DNA.  $\Delta S_{max}$  was determined from the double reciprocal plot of  $1/\Delta S$  against  $1/(C_p-C_0)$  using the equation (Chakrabarti et al., 2000)

$$\frac{1}{\Delta S} = \frac{1}{\Delta S_{max}} + \frac{1}{(C_p-C_0)} \dots\dots\dots(4)$$

The experimental points for the binding isotherm were fitted by least-square analysis using the equation(Chakrabarti et al., 2000)

$$C_0 \cdot \left( \frac{\Delta S}{\Delta S_{\max}} \right)^2 - (C_0 + C_p + K_d) \cdot \left( \frac{\Delta S}{\Delta S_{\max}} \right) + C_p = 0 \dots\dots\dots (5)$$

obtained from Eq. 3. The X-intercept value at  $\Delta S/\Delta S_{\max} = 0.5$  (corresponding to 50 % binding) gives  $K_d^{app}$  for ligand-DNA/  $Mn^{2+}$  interaction.

**Method 2:** In this method the true dissociation constant ( $K_D$ ) was determined taking in to account the 2:1 stoichiometry (in terms of MTR:  $Mn^{2+}$ ) of the complex. The method of analysis is described below(Devi et al., 2007, Lahiri et al., 2012):



According to the law of mass action at equilibrium  $K_D$  can be given by

$$K_D = \frac{[D]_f^2 [Mn^{2+}]_f}{[(D)_2 Mn^{2+}]} \dots\dots\dots (7)$$

where, species in square brackets indicate the respective molar concentrations at equilibrium. Therefore the concentrations of the unbound drug and metal ions at equilibrium can be expressed as

$$[D]_f = [D]_0 - 2[(D)_2 Mn^{2+}] \dots\dots\dots (8)$$

$$[Mn^{2+}]_f = [Mn^{2+}]_i - [(D)_2 Mn^{2+}] \dots\dots\dots (9)$$

where,  $[D]_0$  is the initial drug concentration and  $[Mn^{2+}]_i$  is the added  $Mn^{2+}$  concentration in solution. So, the fraction of antibiotics bound ( $\alpha$ ) is given by

---


$$\alpha = \frac{2[(D)_2 Mn^{2+}]}{D_0} \dots\dots\dots(9)$$

therefore, substituting the value of  $2[(D)_2 Mn^{2+}]$  into the Eq.8 and Eq.9, we obtain

$$[D]_f = [D]_0(1 - \alpha) \dots\dots\dots(11)$$

and,

$$[Mn^{2+}]_f = [Mn^{2+}]_i - \frac{\alpha[D]_0}{2} \dots\dots\dots(12)$$

Substituting Eq. 10 and Eq. 11 in equation (2), we get

$$K_D = \frac{[D]_0(1-\alpha)^2(2[Mn^{2+}]_i - \alpha[D]_0)}{\alpha} \dots\dots\dots(13)$$

**Scatchard plot:** Results from absorbance titration to study association of  $[(MTR)_2 Mn^{2+}]$  with chromosomal DNA and chromatin were also analyzed by the Scatchard plot(Scatchard, 1949).

$$\frac{r}{C_f} = K'(n - r) \dots\dots\dots(14)$$

where,  $r = C_b/C_p$  ( $C_b$  is the concentration of bound drug and  $C_p$  the concentration of DNA/chromatin);  $n$  is the binding stoichiometry in terms of bound drug per nucleotide;  $C_f$  is the molar concentration of the free ligand and  $K'$  is the intrinsic binding constant.

---



### 4.3.3.Determination of kinetic parameters for [(MTR)<sub>2</sub>Mn<sup>2+</sup>] formation

**Rate constant (*k*):** The kinetics of association of MTR with Mn<sup>2+</sup> was followed by different spectroscopic properties, such as absorbance at 440nm, fluorescence at 540nm and CD at 275nm. In all these methods a fixed concentration of Mn<sup>2+</sup> is mixed with different concentrations of MTR at 25°C. The formation of the complex with time is monitored by change in absorbance intensity at 440nm as well as change in fluorescence intensity at 540nm ( $\lambda_{\text{ex}} = 470\text{nm}$ ). To determine the rate constant '*k*', four independent runs are accumulated in the final data analysis. The association kinetics of MTR and Mn<sup>2+</sup> was also observed from the change in ellipticity at 275nm. The rate constant of the complex formation was determined by fitting the observed kinetic traces to a curve generated on the basis of pseudo-first order rate equation (where  $[\text{Mn}^{2+}] \gg [\text{MTR}]$ ) (Devi et al., 2007)

$$\frac{S_t - S_\infty}{S_0 - S_\infty} = e^{-kt} \quad \dots\dots\dots(15)$$

where, *S*<sub>0</sub>, *S*<sub>*t*</sub> and *S*<sub>∞</sub> denote the spectroscopic property at the start of the reaction, after time '*t*' (in seconds) and at the end of the reaction respectively. '*k*' denote the rate constant of the reaction. Measurement of change in the spectroscopic property (*S*<sub>*t*</sub>) was started after an initial time lag of 10-12 seconds.

**Activation energy (*E<sub>a</sub>*):** The change in rate constant (*k*) is measured at various temperatures and the activation energy (*E<sub>a</sub>*) for the association of MTR with Mn<sup>2+</sup> was determined using Arrhenius equation as follows

$$\ln k = -\frac{E_a}{RT} + \text{constant} \quad \dots\dots\dots(16)$$

From the slope of Arrhenius plot ( $\ln k$  vs  $1/T$ ) the value of activation energy ( $E_a$ ) was calculated.

**Order of the reaction (n):** The methods of isolation and initial rates were used to determine the order of the association reaction between MTR and  $Mn^{2+}$ . The initial rates were obtained from the slope of the linear portion of the kinetic trace for the first 50 seconds of the association reaction. To obtain the order of the reaction, one of the reactant concentration was kept constant and in large excess. At different concentrations of the other reactant (R), if the reaction has an order 'n' with respect to R; then the rate of the reaction (r) can be written as (Devi et al., 2007)

$$r = k_{obs}[R]^n \quad \dots\dots\dots(17)$$

Therefore,

$$\ln r = \ln k_{obs} + n \ln[R] \quad \dots\dots\dots(18)$$

where,  $k_{obs} = k[X]$

[X] is the reactant whose concentration is kept constant. A double-logarithmic plot of  $\ln r$  vs  $\ln[R]$  gives a straight line of slope 'n', which is the order of the reaction.

#### 4.3.4. Estimation of thermodynamic parameters

**van't Hoff's method:** The thermodynamic parameters,  $\Delta H$  (change in van't Hoff's enthalpy),  $\Delta S$  (change in entropy) and  $\Delta G$  (change in Gibb's free energy) for the association of MTR with  $Mn^{2+}$  were calculated from the following equations:

$$\Delta G = -RT \ln K_a \quad \dots\dots\dots(19)$$

---

$$\ln K_a = -\frac{\Delta H}{RT} + \frac{\Delta S}{R} \dots\dots\dots(2)$$

where, R is the universal gas constant and T is the absolute temperature. The plot of  $\ln (1/K_d^{\text{app}})$  vs  $1/T$  gives a straight line, the slope of which gives the van't Hoff's enthalpy change and change in entropy is obtained from the intercept of the plot, where  $K_a=1/K_d^{\text{app}}$ .

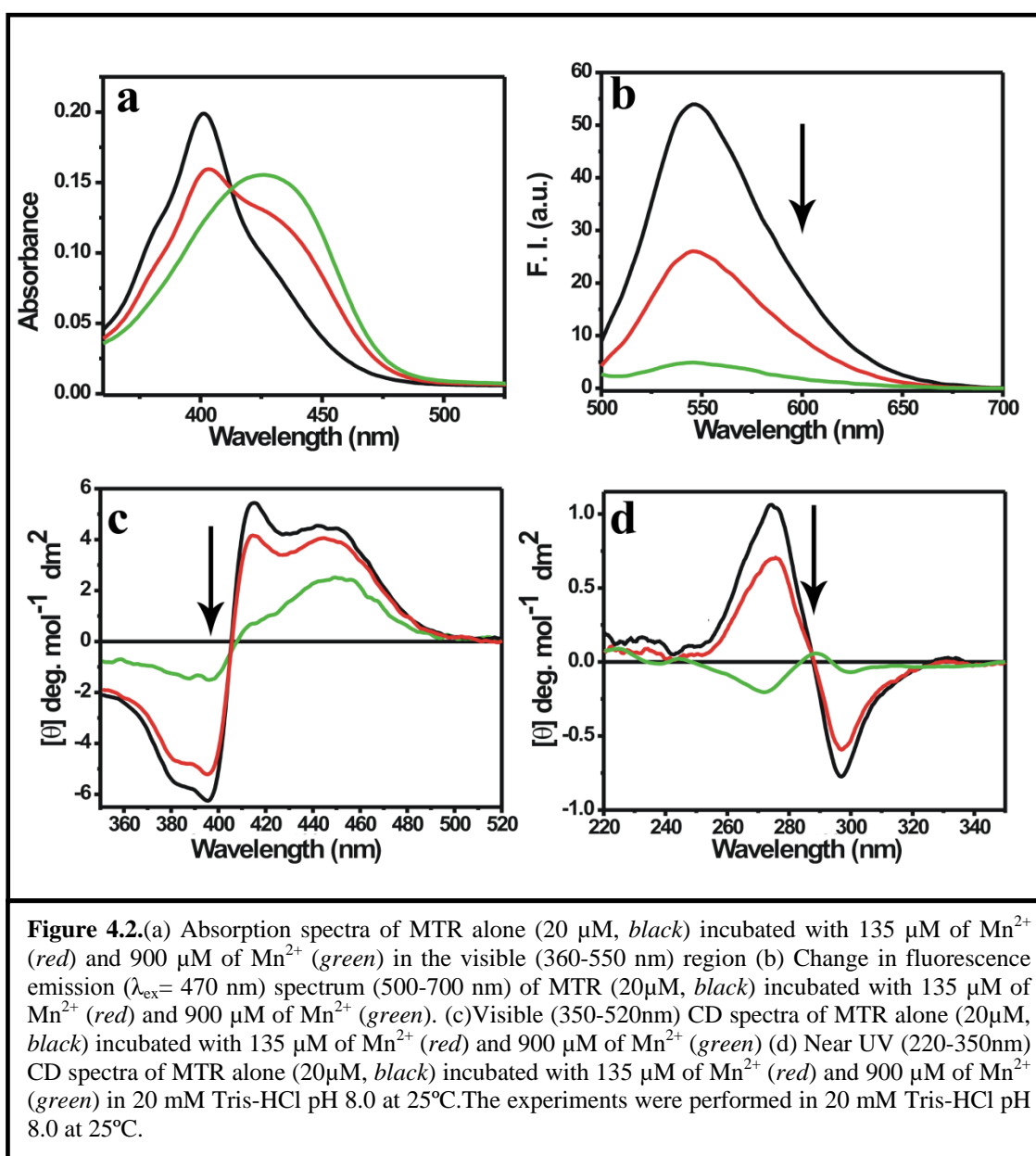
---

## 4.4. RESULTS

### 4.4.1. Characterization of MTR:Mn<sup>2+</sup> complex

Association of MTR with Mn<sup>2+</sup> was demonstrated by absorption, fluorescence and CD spectroscopy (Figure 4.2). Upon addition of Mn<sup>2+</sup> there is a decrease in absorbance at 400 nm. As shown in figure 4.2a, with the increase in concentration of Mn<sup>2+</sup> there is a broadening of the peak associated with a red shift in the visible spectrum of MTR. The appearance of a new absorption band at around 440nm is a signature of complex formation of MTR with the metal ion. The presence of an isosbestic point at 413nm suggests the formation of a single type of complex. Quenching of fluorescence intensity as shown in figure 4.2b, is associated with broadening of the fluorescence emission spectrum of MTR upon addition of increasing concentrations of Mn<sup>2+</sup>. This result further validates the formation of complex between MTR and Mn<sup>2+</sup>. The conformational change of MTR upon binding to Mn<sup>2+</sup> was characterized using CD spectroscopy. Figures 4.2c and 4.2d show the change in CD spectra of MTR in the visible and near UV range. In the visible CD spectra, the peak due to free MTR at 415nm disappears and a broad band appears at around 450 nm as a result of an increase in concentration of Mn<sup>2+</sup>. In the near UV CD spectra there is an inversion of the signature CD band of MTR at 274nm as the concentration of Mn<sup>2+</sup> increases. The presence of an isoelliptic point at 405 nm in the visible region, and at 287 nm in the UV region corroborates the proposition of a single complex between Mn<sup>2+</sup> and MTR. These well-defined spectroscopic signatures characterize the association of antibiotic (MTR) with Mn<sup>2+</sup>. Additionally, [(MTR)<sub>2</sub> Mn<sup>2+</sup>] exhibits two strong Cotton effects at 274 nm ( $\Delta\epsilon_2$ ) and 285 nm ( $\Delta\epsilon_1$ ).

---



**Binding stoichiometry:** The plot obtained from the method of continuous variation for the formation of MTR:  $\text{Mn}^{2+}$  complex is shown in Figure 4.3b. The inflection point occurs at  $\chi_{\text{ligand}} = 0.71$  suggesting a stoichiometry of 2.4:1 with respect to MTR:  $\text{Mn}^{2+}$ . Therefore the composition of the complex is  $[(\text{MTR})_2\text{Mn}^{2+}]$ .

**Binding parameters:** The stability constant for the complex of MTR with  $\text{Mn}^{2+}$  was evaluated using the method described in the section 4.3.2. Figure 4.3a represents the plot of the fraction bound against the input concentration of  $\text{Mn}^{2+}$ . A mean curve fits the data satisfactorily. The dissociation constant values ( $K_d^{app}$  and  $K_D$ ) evaluated from the spectroscopic methods is summarized in Table 4.1.

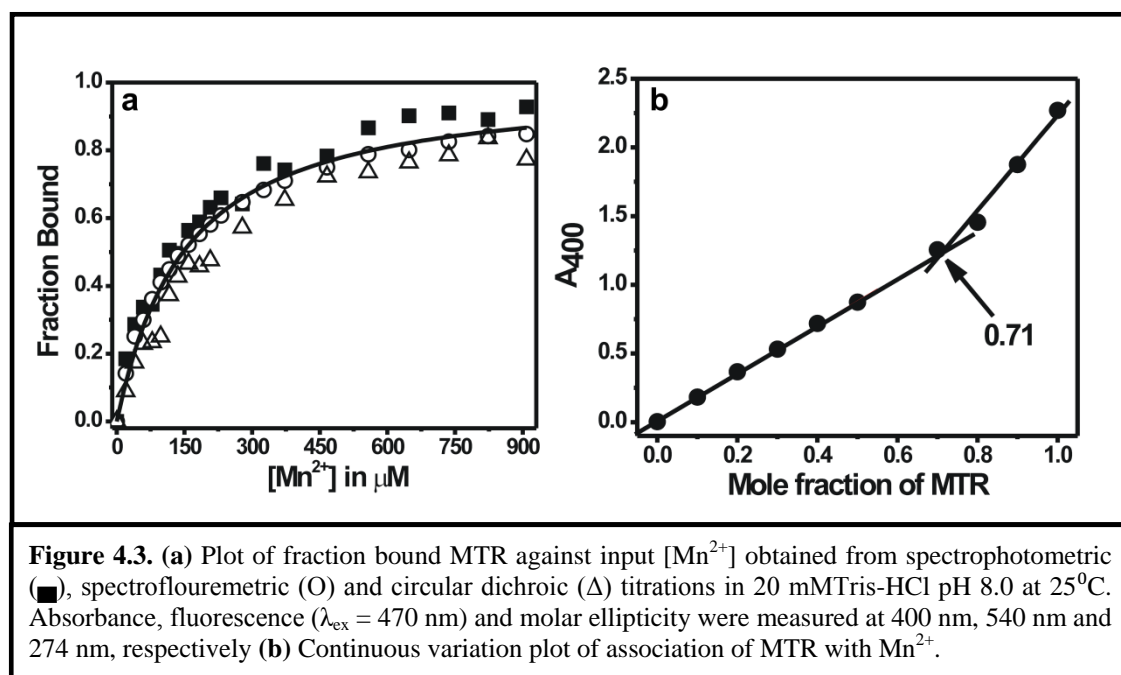


**Figure 4.3.** (a) Plot of fraction bound MTR against input  $[\text{Mn}^{2+}]$  obtained from spectrophotometric (■), spectrofluorimetric (O) and circular dichroic ( $\Delta$ ) titrations in 20 mM Tris-HCl pH 8.0 at  $25^\circ\text{C}$ . Absorbance, fluorescence ( $\lambda_{\text{ex}} = 470 \text{ nm}$ ) and molar ellipticity were measured at 400 nm, 540 nm and 274 nm, respectively (b) Continuous variation plot of association of MTR with  $\text{Mn}^{2+}$ .

**Table 4.1. Affinity of MTR for  $\text{Mn}^{2+}$  in vitro:** Apparent dissociation constant ( $K_d^{app}$ ) and true dissociation constant ( $K_D$ ) values for the association of MTR with  $\text{Mn}^{2+}$ .  
 $2(\text{MTR}) + \text{Mn}^{2+} \rightleftharpoons [(\text{MTR})_2\text{Mn}^{2+}]$

Complex	Method used	Apparent dissociation constant, $K_d^{app} (\mu\text{M})$	True dissociation constant, $K_D (\text{M}^2) \times 10^{-10}$
$[(\text{MTR})_2 \text{Mn}^{2+}]$	Absorbance at 440nm	$111.1 \pm 4.3$	$17.4 \pm 2.4$
	Fluorescence at 540nm	$137.0 \pm 2.7$	$22.9 \pm 2.1$
	CD at 275 nm	$193.4 \pm 5.3$	$40 \pm 4.7$
	ITC	$132 \pm 3.2$	-

#### 4.4.2. Kinetics of association of MTR with $\text{Mn}^{2+}$

Association of MTR with  $\text{Mn}^{2+}$  follows first-order kinetics with comparable rate constants obtained from the time dependent changes in absorbance at 440 nm, fluorescence emission intensity at 540 nm and ellipticity at 275 nm (Figure 4.4a). This is further corroborated from the linear plot for determining the order of the reaction (using Eq. 17 and Eq. 18), which was found to be one with respect to MTR (Figure 4.4b) and zero order with respect to  $\text{Mn}^{2+}$  (Figure 4.4c).

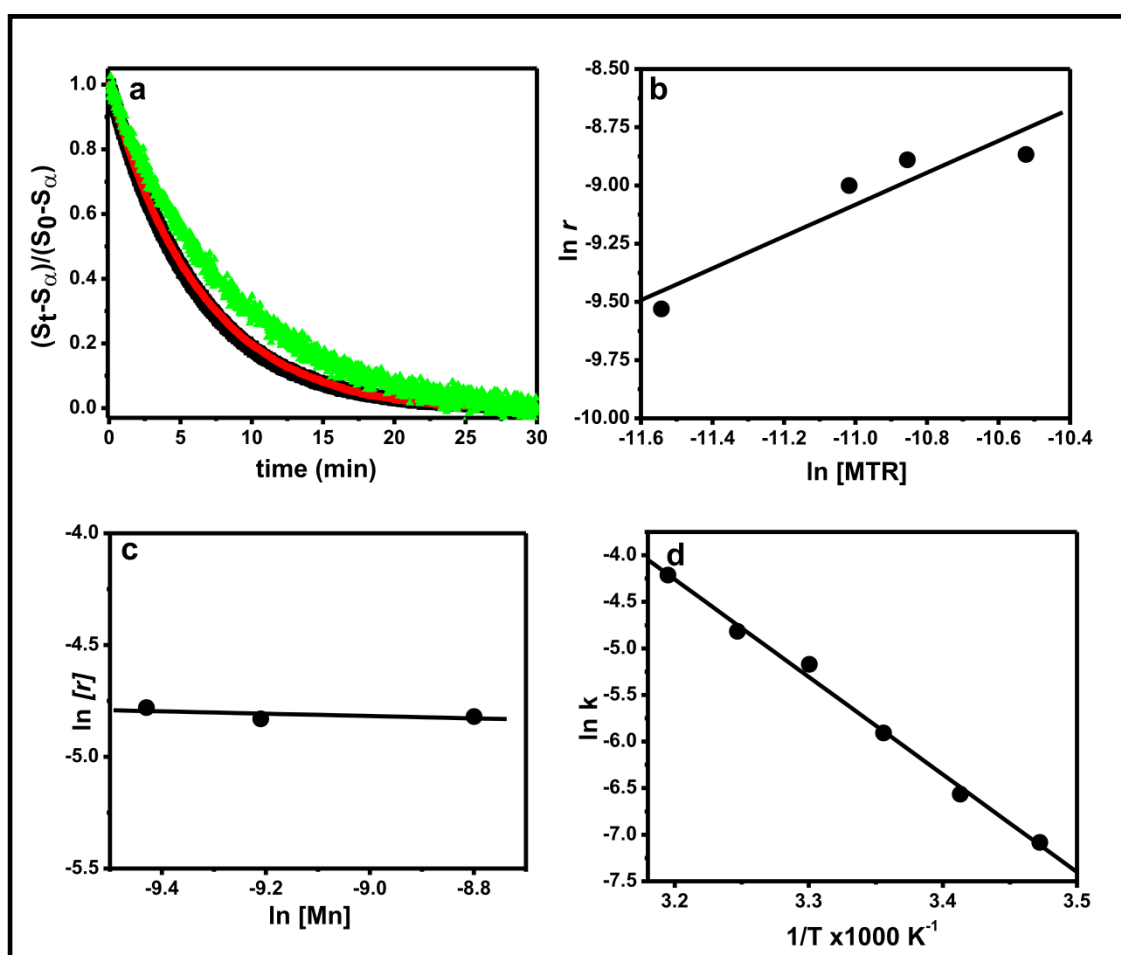


**Figure 4.4.** (a) Overlay of the kinetic traces of MTR (10  $\mu\text{M}$ ) with  $\text{Mn}^{2+}$  (300  $\mu\text{M}$ ) measured by absorption ( $\lambda=440 \text{ nm}$ , *black*), fluorescence ( $\lambda=540 \text{ nm}$ , *red*) and circular dichroism ( $\lambda=275 \text{ nm}$ , *green*) spectroscopy. (b) Plot of logarithm of initial rate against the logarithm of different concentrations of MTR (5, 10, 15 and 20  $\mu\text{M}$ ) for the complex formation with  $\text{Mn}^{2+}$  (300  $\mu\text{M}$ ) (c) Plot of logarithm of initial rate against the logarithm of different concentrations of  $\text{Mn}^{2+}$  (80, 100 and 150  $\mu\text{M}$ ) for the complex formation with MTR (10  $\mu\text{M}$ ) (d) Plot of logarithm of rate constant  $\ln k$  against  $1/T$  at different temperatures (15, 20, 25, 30 and 35 $^{\circ}\text{C}$ ) in 20 mM Tris-HCl pH 8.0.

These results indicate that the same structural alteration step of the reaction is monitored by all the three spectroscopic methods. The relevant kinetic data are summarized in Table 4.2. Figure 4.4d shows a linear plot of  $\ln k$  versus  $1/T$ , which suggests a single step reaction for the association of MTR with  $\text{Mn}^{2+}$ . Energy of activation for the association of MTR with  $\text{Mn}^{2+}$  (obtained from Arrhenius plot, Eq. 16) is  $20.73 \pm 0.37 \text{ kcal mol}^{-1} \text{K}^{-1}$ .

**Table 4.2.** Rate constant ( $k$ ) for the association of MTR ( $10 \mu\text{M}$ ) with  $\text{Mn}^{2+}$  ( $300 \mu\text{M}$ ) at  $25^\circ\text{C}$

Complex	Method	$k$ (second <sup>-1</sup> )
[(MTR) <sub>2</sub> Mn <sup>2+</sup> ]	Absorbance	$2.7 \pm 0.10$
	Fluorescence	$2.8 \pm 0.01$
	CD	$2.1 \pm 0.02$

#### 4.4.3. Thermodynamic parameters for the complex formation

ITC profile for the association of MTR with  $\text{Mn}^{2+}$  is shown in Figure 4.5. The thermodynamic parameters for the association are summarized in table 4.3. Apparent dissociation constant obtained from ITC and spectroscopic methods are comparable ( $137 \mu\text{M}$  from spectroscopic method and  $132 \mu\text{M}$  from ITC). van't Hoff enthalpy was determined from fluorescence measurements at different temperatures. Changes in enthalpy ( $\Delta H$ ) and entropy ( $\Delta S$ ) determined from ITC show that the association is predominantly enthalpy driven. However, thermodynamic parameters obtained from van't Hoff's method show that the reaction is entropy driven, with positive enthalpy change.



**Table 4.3.** Thermodynamic parameters for the association of MTR with  $Mn^{2+}$  in 20mMTrisHCl buffer, pH 8.0 at 25 °C

ITC			van't Hoff's		
$\Delta H_{cal}$ (kcal mol <sup>-1</sup> )	$\Delta S_{cal}$ (kcal mol <sup>-1</sup> K <sup>-1</sup> )	$\Delta G_{cal}$ (kcal mol <sup>-1</sup> )	$\Delta H_{vH}$ (kcal mol <sup>-1</sup> )	$\Delta S_{vH}$ (kcal mol <sup>-1</sup> K <sup>-1</sup> )	$\Delta G_{vH}$ (kcal mol <sup>-1</sup> )
-4.58	2.38	-5.3	9.65	50.2	-5.3

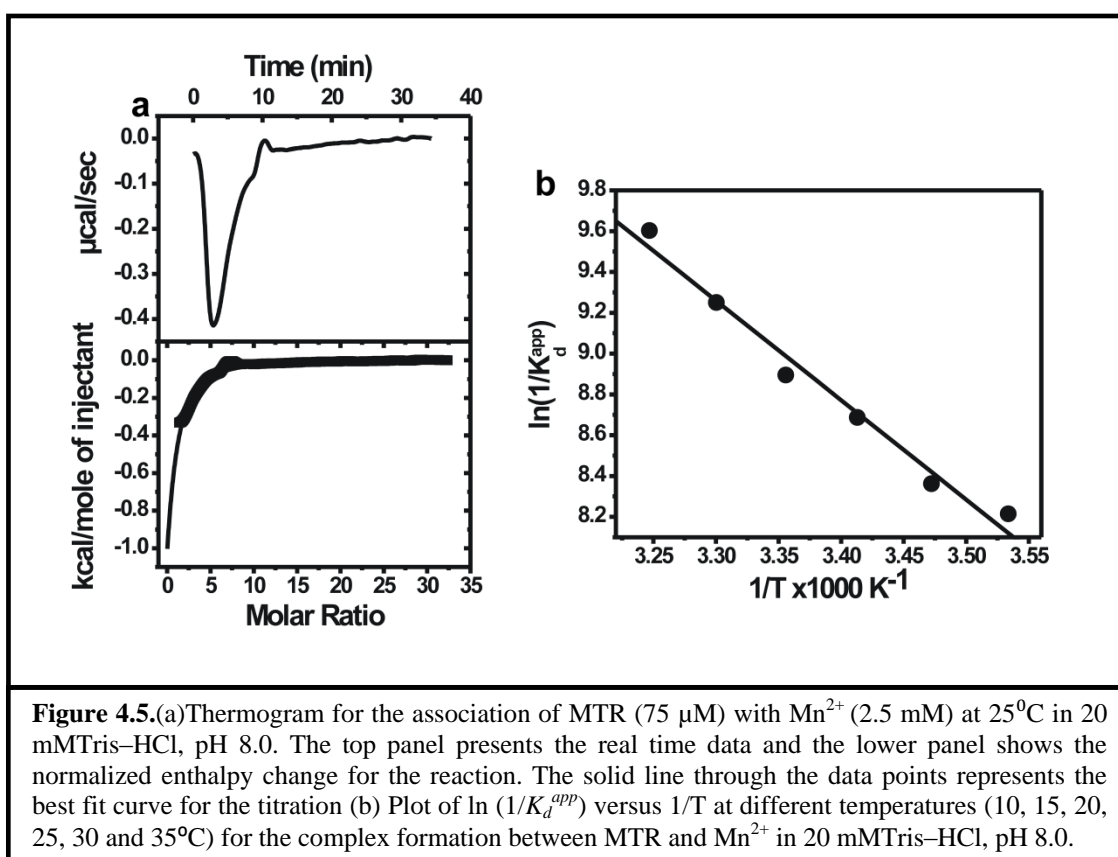
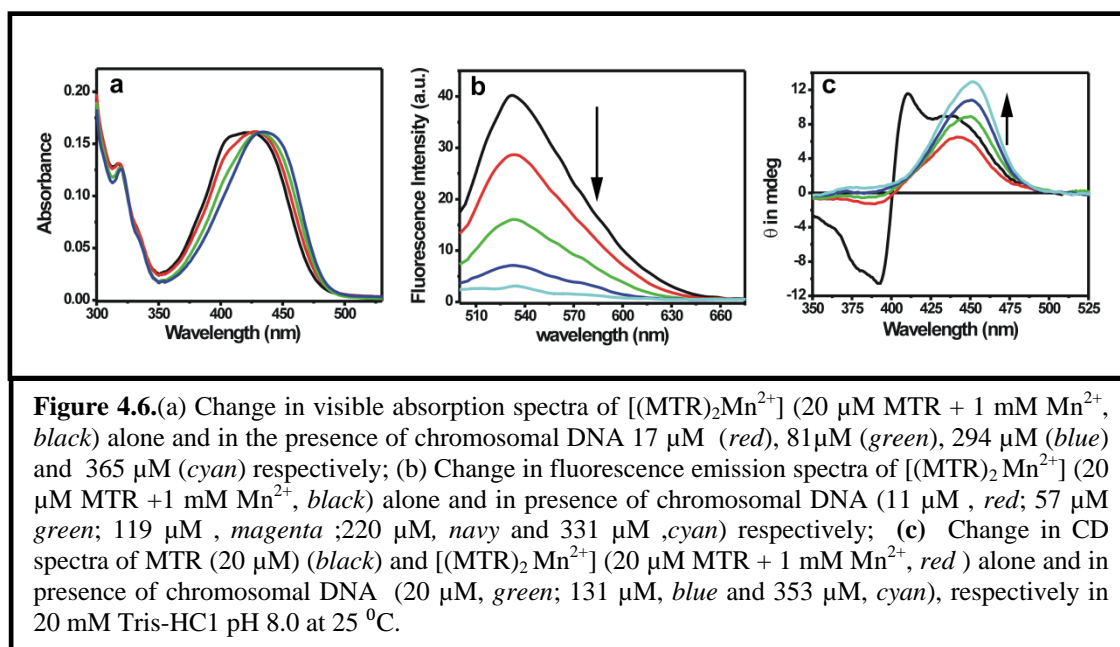


**Figure 4.5.** (a) Thermogram for the association of MTR (75 μM) with  $Mn^{2+}$  (2.5 mM) at 25°C in 20 mMTris–HCl, pH 8.0. The top panel presents the real time data and the lower panel shows the normalized enthalpy change for the reaction. The solid line through the data points represents the best fit curve for the titration (b) Plot of  $\ln(1/K_d^{app})$  versus  $1/T$  at different temperatures (10, 15, 20, 25, 30 and 35°C) for the complex formation between MTR and  $Mn^{2+}$  in 20 mMTris–HCl, pH 8.0.

#### 4.4.4. Interaction of $[(\text{MTR})_2 \text{Mn}^{2+}]$ with chromosomal DNA

Spectroscopic methods were employed to determine the interaction of  $[(\text{MTR})_2 \text{Mn}^{2+}]$  with chromosomal DNA. Upon addition of DNA, there was a decrease in absorbance of  $[(\text{MTR})_2 \text{Mn}^{2+}]$  at 440 nm decreases with concomitant red shift and broadening of the spectra (Figure 4.6a). The fluorescence intensity of  $[(\text{MTR})_2 \text{Mn}^{2+}]$  decreased upon complexation with DNA (Figure 4.6b). The positive CD band for  $[(\text{MTR})_2 \text{Mn}^{2+}]$  at 450 nm increases upon binding to DNA (Figure 4.6c).



The binding affinity of  $[(\text{MTR})_2\text{Mn}^{2+}]$  with chromosomal DNA was determined from Figure 4.7.  $K_d^{\text{app}}$ , and stoichiometry determined from non-linear curve fitting analysis and from Scatchard plot are comparable and are summarized in Table 4.4. Linearity of the Scatchard plot indicates that the binding is non-cooperative. Fluorescence studies indicate a higher binding affinity of poly (dG-dC) with  $[(\text{MTR})_2\text{Mn}^{2+}]$  as compared to

poly (dA-dT) (43  $\mu\text{M}$  for poly(dG-dC) and 466  $\mu\text{M}$  for poly(dA-dT)). This suggests that the complex binds selectively to poly(dG-dC) (Figure 4.7c).

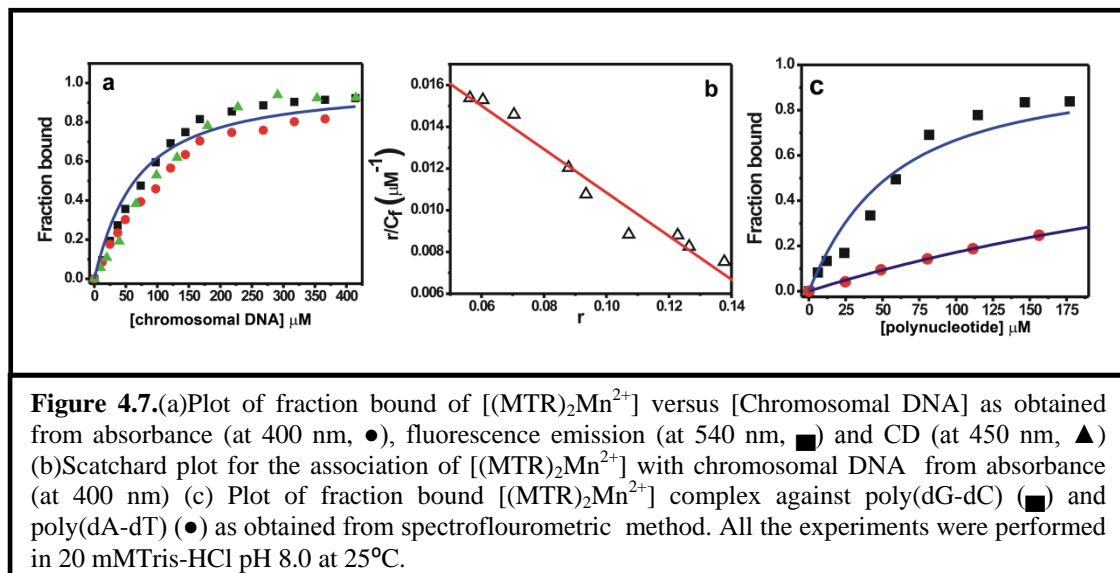


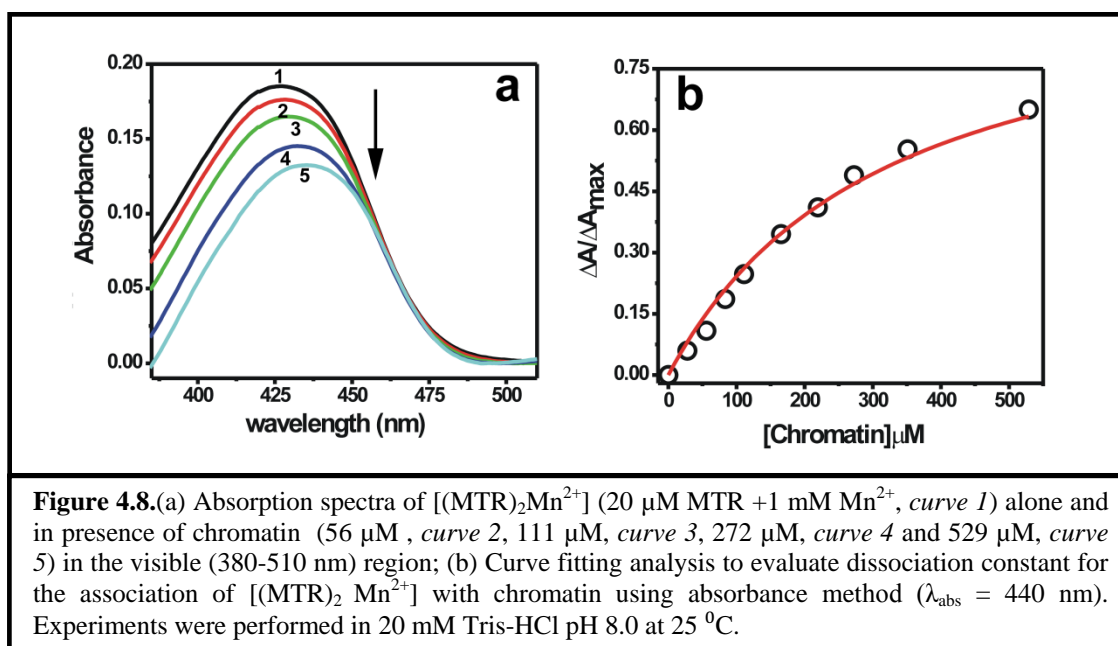
**Table 4.4.** Binding parameters for the interaction of  $(\text{MTR})_2\text{Mn}^{2+}$  with chromatin and chromosomal DNA in 20 mM Tris-HCl buffer, pH 8.0 at 25 °C

Complex	System	$K_d^{\text{appa}}$ ( $\mu\text{M}$ )	$n^b$ (ligand / nucleotide)
$[(\text{MTR})_2\text{Zn}^{2+}]^c$	ct DNA	19	$0.18 \pm 0.02$
	Chromatin	75	$0.10 \pm 0.01$
$[(\text{MTR})_2\text{Mg}^{2+}]^d$	Chromosomal DNA	32	$0.13 \pm 0.01$
	Chromatin	184	$0.03 \pm 0.01$
$[(\text{MTR})_2\text{Mn}^{2+}]$	Chromosomal DNA	$32 \pm 2.9$	$0.22 \pm 0.03$
	Chromatin	$298 \pm 10.6$	$0.15 \pm 0.01$

<sup>a</sup> Dissociation constants ( $K_d^{\text{app}}$ ) were determined from spectrophotometric titration using non-linear curve fitting analysis as stated in Materials and methods. <sup>b</sup>  $n$  values are obtained from Scatchard plot described in Materials and methods. <sup>c</sup>  $K_d^{\text{app}}$  and  $n$  values for the association of  $[(\text{MTR})_2\text{Zn}^{2+}]$  with free DNA and chromatin are cited from (Das and Dasgupta, 2005). The standard deviation from three sets of experiment is 15%. <sup>d</sup>  $K_d^{\text{app}}$  and  $n$  values for the association of  $[(\text{MTR})_2\text{Mg}^{2+}]$  with free DNA and chromatin are cited from (Mir et al., 2004). The standard deviation from three sets of experiment is 15%.

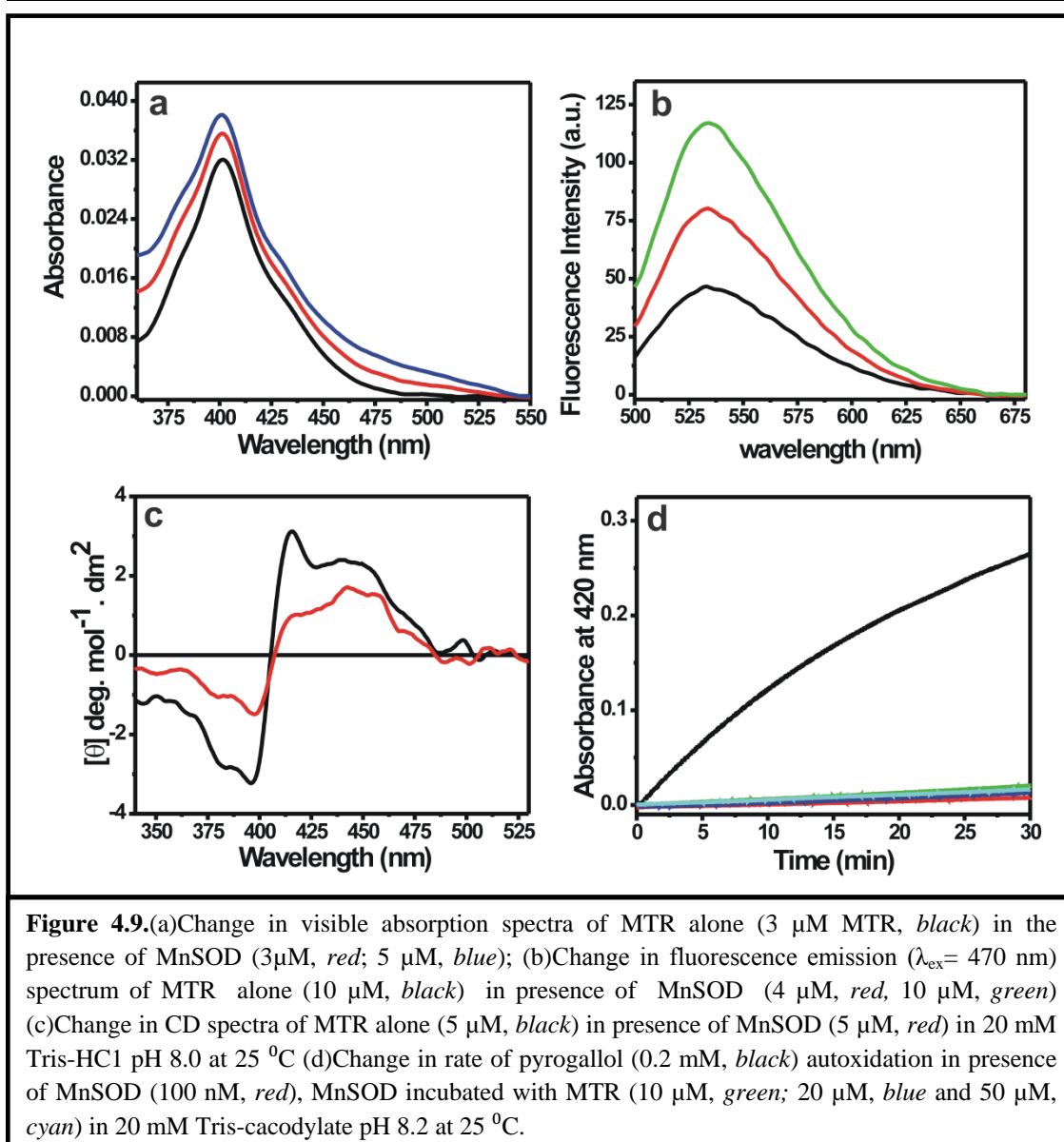
#### 4.4.5. Association of $[(\text{MTR})_2\text{Mn}^{2+}]$ with Chromatin

Change in absorption spectra of  $[(\text{MTR})_2\text{Mn}^{2+}]$  upon binding to chromatin is shown in figure 4.8a. The binding affinity of  $[(\text{MTR})_2\text{Mn}^{2+}]$  for chromatin was calculated from figure 4.8b and the value is lower than that for chromosomal DNA as evident from the dissociation constants (Table 4.4).



#### 4.4.6. Interaction of MTR with MnSOD

Spectroscopic studies (absorption, fluorescence and CD) suggest association of MTR with MnSOD as shown in figure 4.9 (a-c). Contrary to the quenching of fluorescence intensity of MTR upon binding to  $\text{Mn}^{2+}$ , the emission intensity of MTR increases on association with MnSOD (Figure 4.9b). The pyrogallol autoxidation assay shows that the enzymatic activity of MnSOD remains unaltered upon binding to MTR (Figure 4.9d).



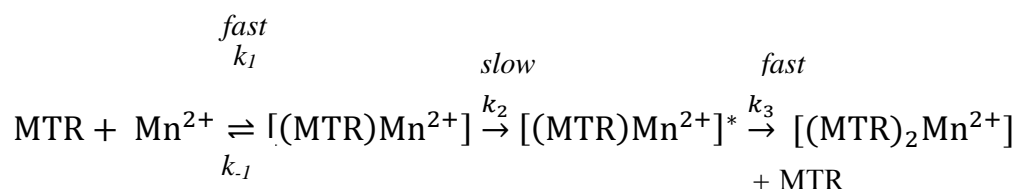
## 4.5. DISCUSSION

The current study proposes the mechanism of association of MTR with the essential micronutrient,  $\text{Mn}^{2+}$ . The biological significance of this association has been demonstrated in the chromatin context. Like other bivalent metal ions  $\text{Zn}^{2+}$ ,  $\text{Fe}^{2+}$  and  $\text{Co}^{2+}$ , MTR forms only one type of complex with  $\text{Mn}^{2+}$  with the stoichiometry of 2:1 (MTR:  $\text{Mn}^{2+}$ ) (Devi et al., 2007, Hou et al., 2009, Hou and Wang, 2005). However, the association of MTR with  $\text{Mg}^{2+}$  is different from these metal ions ( $\text{Zn}^{2+}$ ,  $\text{Fe}^{2+}$  and  $\text{Co}^{2+}$ ) (Aich and Dasgupta, 1995). MTR forms two type of complex with  $\text{Mg}^{2+}$ , namely complex-I (1:1 complex with respect to MTR:  $\text{Mg}^{2+}$ ) and complex-II (2:1 complex with respect to MTR:  $\text{Mg}^{2+}$ ), depending on the concentration of  $\text{Mg}^{2+}$  ion.  $\text{Mg}^{2+}$  is an alkaline earth metal with ionic radius  $0.65\text{\AA}$  and is a hard cation. In aqueous medium it forms stable  $[(\text{Mg}(\text{H}_2\text{O})_6)]^{2+}$  complex with octahedral coordination (Helm and Merbach, 2005). Formation of complex-I is attributed to electrostatic attraction of cationic  $[(\text{Mg}(\text{H}_2\text{O})_6)]^{2+}$  with anionic MTR present in the solution, where the inner hydration shell of  $\text{Mg}^{2+}$  remains intact. On the other hand,  $\text{Mn}^{2+}$  is a first row transition metal ion with higher ionic radius,  $0.8\text{\AA}$  (Yavuz et al., 2003). It has variable coordination number and prefers to form coordination bond with oxygen/nitrogen atoms of incoming ligands (Millonig et al., 2009). Hence,  $\text{Mn}^{2+}$  and other transition metal ions like  $\text{Zn}^{2+}$ ,  $\text{Fe}^{2+}$ , and  $\text{Co}^{2+}$  forms coordinate bond with O1 and O9 atoms of MTR with the removal of water molecules from its hydration shell and forms only one type of complex (2:1 with respect to MTR:  $\text{M}^{2+}$ ).

The red shift of MTR absorption peak upon complex formation with  $\text{Mn}^{2+}$  can be ascribed to the changes in electronic environment of the chromophore (chromomycinone moiety) present in MTR. Due to the complexation with  $\text{Mn}^{2+}$ ,  $\pi^*$

orbital of the chromomycinone moiety might be stabilized via charge transfer to the positively charged metal center (ligand to metal charge transfer, LMCT) thereby reducing the energy gap between  $\pi \rightarrow \pi^*$  transition (Huheey et al., 1983). Broadening of both absorption and fluorescence emission spectra might occur due to the distortion of chromophore, which perturbs the energy levels of the molecule. Quenching of the emission spectrum could be an outcome of the deactivation of the singlet excited state of the chromomycinone moiety (Aich and Dasgupta, 1995). Similar changes in CD spectra for  $\text{Mg}^{2+}$ ,  $\text{Zn}^{2+}$ ,  $\text{Mn}^{2+}$  and  $\text{Fe}^{2+}$  suggest a single type of conformational change of MTR due to complexation (Aich and Dasgupta, 1995, Devi et al., 2007, Hou and Wang, 2005).

The kinetic mechanism for the formation of  $[(\text{MTR})_2\text{Mn}^{2+}]$  has been followed by different spectroscopic methods, like absorption, fluorescence, and CD. From all these methods, we see that the reaction follows a first-order kinetics with respect to both MTR and  $\text{Mn}^{2+}$ , similar to the kinetics of  $[(\text{MTR})_2\text{Zn}^{2+}]$  (Devi et al., 2007). Association of two bulky antibiotics with one metal center in a single step might face steric hindrance. So, we propose that the formation of  $[(\text{MTR})_2\text{Mn}^{2+}]$  might go through the following steps:



First and third steps of the proposed mechanism are either spectroscopically silent or too fast to be monitored by the spectroscopic methods employed. Linear nature of the

Arrhenius plot favors the first explanation. In the second step, structural alteration of the complex takes place. A transient species  $[(MTR)Mn^{2+}]^*$  is formed, which is monitored spectroscopically. This step is comparatively slower and therefore the rate-determining step of the reaction. Once the conformational alteration has occurred, the second antibiotic binds rapidly to the transient species to form  $[(MTR)_2 Mn^{2+}]$ . The overall rate for the above mechanism can be written as (Devi et al., 2007):

$$rate = \frac{\{k_2[MTR][Mn^{2+}]\}}{\{\frac{k_{-1}+k_2}{k_1}+[Mn^{2+}]\}} \dots\dots\dots(21)$$

The concentration of  $Mn^{2+}$  was kept in large excess (300  $\mu$ M) such that the contribution of  $(k_{-1}+k_2)/k_1$  becomes negligible. Under this condition, the overall rate for the complexation reduces to:

$$rate = \frac{\{k_2[MTR][Mn^{2+}]\}}{[Mn^{2+}]} = k_2[MTR] \dots\dots\dots(22)$$

This is consistent with the observed kinetic data obtained from different spectroscopic methods employed in this study.

While van't Hoff analysis suggests that association of MTR with  $Mn^{2+}$  is entropy driven, calorimetry suggests that the association is enthalpy driven (Table 4.3). ITC provides the heat change involving the entire process of complex formation. On the other hand, van't Hoff gives the energetics corresponding to the spectroscopically apparent step only. The multistep association of MTR with  $Mn^{2+}$  might thus be a plausible reason for the observed discrepancy.



Paramagnetic  $\text{Mn}^{2+}$  leads to line broadening in  $^1\text{H}$  NMR spectrum. This prevented us from obtaining clean 1D-spectrum of  $[(\text{MTR})_2 \text{Mn}^{2+}]$ . The structures of other MTR-metal complexes such as  $[(\text{MTR})_2 \text{Mg}^{2+}]$ ,  $[(\text{MTR})_2 \text{Zn}^{2+}]$ , and  $[(\text{MTR})_2 \text{Co}^{2+}]$  have been validated from both NMR and CD studies. In all these complexes, the metal ion is octahedrally coordinated to O1 and O9 of the chromophore, which serves as a bidentate ligand and the two water molecules act as the fifth and sixth ligand. To comment upon the probable coordination geometry of the metal center in  $[(\text{MTR})_2 \text{Mn}^{2+}]$ , we have compared the CD spectral features of  $[(\text{MTR})_2 \text{Mn}^{2+}]$  with the previously reported MTR-metal complexes. The CD spectra of all these complexes are characterized by the appearance of a broad band around 450 nm and a negative peak around 274 nm. Available reports have suggested that these spectral features are evidence for an octahedral coordination sphere around the metal ion which have also been validated from the NMR spectra of the complexes (Hou et al., 2009, Hou and Wang, 2005). We can thus propose that the metal center in  $[(\text{MTR})_2 \text{Mn}^{2+}]$  has an octahedral coordination. The positive value of the difference in the amplitudes of the observed Cotton effects ( $A = \Delta\epsilon_1 - \Delta\epsilon_2$ ) suggests that this octahedral geometry has a right handed screw conformation (Demicheli et al., 1991, Lu et al., 2009).

Having characterized the association of MTR with  $\text{Mn}^{2+}$  and the structure of the complex we went on to study the interaction of  $[(\text{MTR})_2 \text{Mn}^{2+}]$  with chromatin and chromosomal DNA. In eukaryotes, DNA is wrapped with histones to form a nucleoprotein complex, chromatin.  $[(\text{MTR})_2 \text{Mn}^{2+}]$  binds to chromatin with a relatively lower affinity and lower binding stoichiometry (in terms of ligand / nucleotide) compared to chromosomal DNA (Table 4.4). This may be ascribed to the histone(s) present in chromatin, which hinders the accessibility of DNA minor groove to

$[(\text{MTR})_2\text{Mn}^{2+}]$ . The association of the  $[(\text{MTR})_2\text{Mg}^{2+}]$  and  $[(\text{MTR})_2\text{Zn}^{2+}]$  with chromatin and chromosomal DNA follow a similar trend (Das and Dasgupta, 2005, Mir et al., 2004, Mir and Dasgupta, 2001). The right-handed twist conformation of  $[(\text{MTR})_2\text{Mn}^{2+}]$  facilitates the binding of the complex via DNA minor groove. The binding affinity and stoichiometry for the association of chromatin and chromosomal DNA with  $[(\text{MTR})_2\text{Mn}^{2+}]$  is comparable to the earlier reported values of their interaction with other MTR-metal complexes. The red shift of the absorption peaks of  $[(\text{MTR})_2\text{Mn}^{2+}]$  upon binding to chromatin and chromosomal DNA could be ascribed to perturbation of the  $\pi \rightarrow \pi^*$  transition by the chromomycinone ring upon interaction with DNA.

Fluorescence intensity of  $[(\text{MTR})_2\text{Mn}^{2+}]$  is quenched in the presence of DNA. On the contrary, the fluorescence intensity of other MTR-metal ( $\text{Mg}^{2+}$  and  $\text{Zn}^{2+}$ ) complexes is enhanced upon binding to DNA. This difference could be attributed to the inherent properties of the metal ions. Affinity of a metal ion for a specific site on DNA is a general function of its charge, hydration-free energy, coordination geometry, and coordinate bond-forming capacity (Subirana and Soler-Lopez, 2003). In aqueous medium, the transition metal ion  $\text{Mn}^{2+}$  has a loosely bound hydration sphere with a distorted octahedral geometry. In the inner hydration sphere the distance between water and  $\text{Mn}^{2+}$  is 2.3 Å (Millonig et al., 2009). It has been reported that  $\text{Mn}^{2+}$  interacts with DNA through major groove by forming direct bonds with N7 and O6 atoms of guanine bases at GG and GC steps (van de Sande et al., 1982). It can also form direct bonds with N7 of guanine and O atoms of phosphate back bone. Thus, it can either unwind the DNA helix or change the water structure around the helix. Therefore, the change in conformation of DNA mixed with 1 mM  $\text{Mn}^{2+}$ , may not lead to the excited-state- proton

transfer to  $[(\text{MTR})_2\text{Mn}^{2+}]$  bound in the minor groove. Upon association with DNA,  $[(\text{MTR})_2\text{Mn}^{2+}]$  may lose any of the two coordinated water molecules present in the complex to form a direct bond to nitrogen atom present in the nearby guanine base, without any radical alteration in the structure of DNA. In this condition the central metal ion becomes more electron deficient, which, in turn, can induce LMCT. This phenomenon might lead to the quenching of fluorescence intensity of  $[(\text{MTR})_2\text{Mn}^{2+}]$  upon binding to DNA.

In order to check the sequence selectivity of binding of  $[(\text{MTR})_2\text{Mn}^{2+}]$  if any, we have determined the binding affinity of  $[(\text{MTR})_2\text{Mn}^{2+}]$  with poly (dG-dC) and poly(dA-dT) (Figure 4.7d). Results indicate that  $[(\text{MTR})_2\text{Mn}^{2+}]$  has a higher affinity towards poly (dG-dC) than poly(dA-dT). It has been reported that  $[(\text{MTR})_2\text{Mg}^{2+}]$  also binds specifically to the GC rich sequence of DNA (Goldberg and Friedman, 1971). The molecular basis of sequence specific recognition of DNA was attributed to the H-bonding of phenolic group of MTR and the amino group present in the guanine base in the minor groove of DNA (Banville et al., 1990, Keniry et al., 1993, Keniry et al., 1987, Sastry et al., 1995, Sastry and Patel, 1993). This suggests that change in the metal centre of the dimeric complex of MTR does not alter sequence specificity of the complex.

To investigate whether the  $\text{Mn}^{2+}$  binding ability of MTR alters the activity of  $\text{Mn}^{2+}$ -containing metalloenzymes we have studied the effect of MTR on Manganese superoxide dismutase (MnSOD) using various spectroscopic methods. MnSOD is a metalloenzyme which deals with the defense mechanism against the toxic effects of reactive oxygen species by catalyzing the dismutation of the superoxide radical anion ( $\text{O}_2^{\cdot -}$ ) into  $\text{O}_2$  and  $\text{H}_2\text{O}_2$  (Zheng et al., 2007). MnSOD from *E. coli* as well as from many

prokaryotes is a dimer (Lah et al., 1995, Smith and Doolittle, 1992). The active site of MnSOD contains one  $\text{Mn}^{2+}$  which is coordinated in trigonal bipyramidal geometry by three histidines, one aspartate and a bound solvent molecule (Fridovich, 1975, Bannister et al., 1987, Yamakura et al., 1998). Change in absorption spectrum and increase in fluorescence quantum yield can be attributed to the change in transition dipole of the chromophore of MTR due to hydrophobic environment within the protein. This arises as a result of binding of MTR in the hydrophobic backbone of MnSOD. A close inspection of CD spectra of MTR in presence of MnSOD shows certain similarity in its feature with the CD spectrum of  $[(\text{MTR})_2 \text{Mn}^{2+}]$ . Binding of MTR to the  $\text{Mn}^{2+}$  in MnSOD could be a plausible reason for the similarity. However, the notable feature is that the association of the antibiotic with MnSOD does not alter its activity.

The affinity of MTR towards various bivalent metal ions may have important roles in different pathological conditions.  $\text{Mn}^{2+}$  is an important trace element required by all organisms in various cellular processes. It is a transition metal with variable oxidation states ( $\text{Mn}^{2+}$ ,  $\text{Mn}^{3+}$ ). Therefore, it can participate in disproportionation reaction with the reactive oxygen species (ROS) produced in several biochemical reactions. But excess of free  $\text{Mn}^{2+}$  is toxic, as it gets accumulated in basal ganglia of brain leading to a diseased condition. Removal of excess  $\text{Mn}^{2+}$  is thus necessary. Since MTR can cross the blood brain barrier (Ferrante et al., 2004), it could specifically bind to  $\text{Mn}^{2+}$  present there. In this chapter we have also shown that MTR does not inhibit the free radical scavenging activity of MnSOD upon binding to it. MTR might be used in the treatment of various brain pathologies as a metal ion chelator with reduced toxicity. So the present data suggest a potential use of the antibiotic as a metal chelating class of medicine. Moreover, the complex forming ability of MTR with  $\text{Mn}^{2+}$  under

---

physiological conditions and the association of  $[(\text{MTR})_2 \text{Mn}^{2+}]$  with DNA, may provide an additional pathway for the antitumor activity of MTR in brain tumor cells. Thus MTR has the potential as an anticancer agent with low toxicity as compared to other metal based chemotherapeutics.

---

# Chapter 5

---

**Association of Chelerythrine  
with DNA and chromatin**

**Figure 5.1.** Chemical structure of cationic/iminium and neutral /alkanolamine forms of chelerythrine.

However, a number of recent studies indicate that PKC-independent mechanisms might be also responsible for its potential anticancer property (Ansari et al., 2006, Zhang et al., 2011). Among them, its DNA-binding potential has been suggested as a plausible factor. This is further reinforced from the observation that a structurally similar alkaloid, sanguinarine (SGR) binds to both duplex and quadruplex DNA leading to inhibition of transcription and down regulation of telomerase activity (Maiti and Nandi, 1987, Maiti et al., 1982, Maiti et al., 1984, Maiti et al., 2002, Pradhan et al., 2011, Ghosh et al., 2013). Therefore, we felt the necessity to examine in depth the binding modes of the compound to different types of DNA. There are preliminary reports of interaction of CHL with calf thymus DNA using spectroscopic techniques (Li et al., 2012, Urbanova et al., 2009, Bai et al., 2008, Bai et al., 2006, Basu et al., 2013). However none of the existing reports has studied the effect of base sequence upon the intercalation potential of CHL. In order to gain an insight of the molecular and structural basis of the recognition we have employed chromosomal DNA extracted from chicken liver chromatin, which contains comparable percentage of (G.C) and (A.T) base pairs (LaDeana W. Hillier, 2004) along with four synthetic polynucleotides with homopolymeric and alternate copolymer sequence of (G.C) and (A.T) base pairs.

In cell DNA is wrapped around histone proteins to form a hierarchically packaged assembly, chromatin (Horn and Peterson, 2002). It consists of chromatosome, the asymmetric mono-nucleosomal particle containing a single linker histone, connected through linker DNA. Earlier studies have shown that passage of CHL through cytoplasm to the cell nucleus (Slaninova et al., 2001). It suggests the possibility of interaction of CHL with different levels of chromatin. Till date, there are no reports which demonstrate the interaction of CHL with chromatin. In this chapter we have

---



reported the association of CHL with soluble chromatin and its components-chromatosome, nucleosome and chromosomal DNA. Structurally, CHL changes from iminium to alkanolamine form at pH 7.5 (Kulp et al., 2011) as shown in Figure 5.1. Positive charge present in the iminium form may facilitate the binding of CHL to double helical DNA (Urbanova et al., 2009). Optical spectroscopic methods such as absorption, fluorescence and CD spectroscopy have been employed to detect the association of CHL with chromatin and various DNA sequences and characterize them in terms of the structural basis. Coupled with these methods an in-depth isothermal titration calorimetric approach has been used to further characterize the molecular basis of the association of CHL with DNA with different base sequences and chromatin.

---

## 5.2. MATERIALS AND METHODS

### 5.2.1. Materials

Chelerythrine chloride (CHL), potassium phosphate monobasic, potassium phosphate dibasic, polynucleotides - poly(dG-dC), poly(dA-dT), poly(dG).poly(dC) and poly(dA).poly(dT), magnesium chloride solution (1M), calcium chloride, phenyl methyl sulphonyl fluoride (PMSF), ethylene diamino tetra acetic acid disodium salt (EDTA), Triton X-100, CM-Sephadex C-25 and micrococcal nuclease were purchased from Sigma Chemical Corporation, USA. All buffers were prepared in MilliQ water from Millipore Water System, Millipore, USA and filtered through 0.1  $\mu\text{m}$  filters (Millipore, USA) prior to use. Unless mentioned otherwise, all studies were done in 10 mM potassium phosphate buffer pH 6.8. A stock solution of  $4.0 \times 10^{-3}$  mol/L CHL was prepared by directly dissolving it in 10 mM potassium phosphate buffer of pH 6.8 and kept in dark until further use. The concentrations of polynucleotides were determined from the known molar extinction coefficients (Wells et al., 1970).

### 5.2.2. Methods

#### 5.2.2.1. Preparation of chromatin components and chromosomal DNA

Soluble chromatin was isolated from chicken livers following standard protocol (Blobel and Potter, 1966) described in-details in the previous chapter (section 4.2.2). Partial MNase digestion of the nuclear pellet was carried out to prepare long chromatin and chromatosome (Mir and Dasgupta, 2001, Banerjee et al., 2014). Soluble chromatin/ chromatosome thus obtained, was purified by centrifugation through a 5–25% linear

---

sucrose density gradient. Nucleosome was prepared after removal of histone H1 from chromatosome. CM-Sephadex C-25 (60 mg dry resin/ml of chromatosome) was used to remove histone H1 from chromatosome (Garcia-Ramirez et al., 1990). Chromosomal DNA was isolated from soluble chromatin by phenol – chloroform – isoamyl alcohol extraction followed by precipitation with isopropanol (Majumder and Dasgupta, 2011). All samples, prior to experiment were dialyzed extensively against 10 mM K-phosphate buffer (pH 6.8). Chromatin, chromatosome and chromosomal DNA were estimated in terms of nucleotides using molar extinction coefficient,  $\epsilon_{260} = 6600 \text{ M}^{-1} \text{ cm}^{-1}$  (Majumder and Dasgupta, 2011).

#### **5.2.2.2. Spectrophotometric and spectrofluorimetric studies**

Absorption and fluorescence measurements were performed with CECIL 7500 spectrophotometer and PerkinElmer LS55 luminescence spectrometer using 1 cm path length quartz cuvettes. Both the instruments are fitted with a water circulation system to maintain a constant temperature, 25 °C. Absorption spectra were recorded in the region 300 nm to 550 nm and fluorescence emission spectra of CHL were taken in the region 380 nm to 640 nm corresponding to an excitation wavelength of 340 nm (Li et al., 2012). To determine the dissociation constant of the complex of DNA/ chromatin components with CHL, a fixed concentration of CHL was titrated with increasing concentrations of DNA/ polynucleotides/ chromatin (subsequently referred to as polymers). To ensure complete complex formation, data was collected till there is no change in the absorbance and fluorescence of CHL upon addition of the polymers.  $\Delta F$  is the change in fluorescence intensity at 540 nm for each addition of polymers;  $\Delta F_{\text{max}}$

---

is the same parameter when CHL is completely bound to polymers.  $\Delta F_{\max}$  was obtained from the following equation(Chakrabarti et al., 2002):

$$\frac{1}{\Delta F} = \frac{1}{\Delta F_{\max}} + \frac{1}{(C_p - C_0)} \dots \dots \dots (1)$$

Here  $C_0$  is the initial concentration of CHL and  $C_p$  is the concentration of the polymer. The binding isotherm was obtained from the fluorescence data by plotting  $\Delta F/\Delta F_{\max}$  at 540 nm against polymer concentration. The binding isotherm was fitted with the equation to obtain the dissociation constant(Chakrabarti et al., 2002):

$$C_0 \cdot \left( \frac{\Delta F}{\Delta F_{\max}} \right)^2 - (C_0 + C_p + K_d) \cdot \left( \frac{\Delta F}{\Delta F_{\max}} \right) + C_p = 0 \dots \dots \dots (2)$$

Binding stoichiometry for the interaction was obtained from the above isotherm by fitting the data points with two straight lines. Concentration of polymer corresponding to the break point obtained from the straight lines was divided by the fixed concentration of CHL, to get the DNA: CHL binding stoichiometry (Majee et al., 1997).

### 5.2.2.3. Calorimetric studies:

Isothermal calorimetric measurements were performed in iTC200 microcalorimeter (Microcal Inc.) under constant stirring at 300 rpm at 25 °C. In case of chromatin, chromatosome and nucleosome fixed concentration of CHL (50 µM) present in cell was titrated against aliquots of 3.5 mM either chromatin or chromatosome or nucleosome (in syringe). However, for chromosomal DNA and other polynucleotides, 25 µM of

CHL was titrated against DNA/ polynucleotides by injecting DNA/ polynucleotides (1.5 mM) from syringe. Samples were degassed prior to titration. Each injection is associated with a heat change due to interaction of polymer with small molecule. Blank experiments, where polymers were injected into buffer, were done to get the heat change due to dilution and these heats of dilution were appropriately subtracted to get the corrected thermogram. The thermograms were analyzed using the in-built Microcal LLC ITC software to get the binding isotherm. The “one set of sites” model yielded the best fit curve for the obtained data points in all cases (described in details in the previous chapter, section 4.2.7). Equilibrium association constant ( $K_a$ ), change in enthalpy ( $\Delta H$ ) and entropy ( $\Delta S$ ) for CHL- DNA/polynucleotides interactions were determined by fitting the isotherms in ‘one set of sites’ model provided with the software. Gibbs free energy ( $\Delta G$ ) was calculated using the equation

$$\Delta G = \Delta H - T\Delta S \quad \dots\dots\dots(3)$$

Specific heat capacity change ( $\Delta C_p$ ) for CHL- DNA/ polynucleotides interaction was derived from the plot of the enthalpy change ( $\Delta H$ ) versus temperature (T), at constant pressure using the following relation (Majumder and Dasgupta, 2011):

$$\Delta C_p = \left[ \frac{\partial(\Delta H)}{\partial(\Delta T)} \right]_P \quad \dots\dots\dots (4)$$

Enthalpy– entropy compensation was determined from the slope of  $\Delta H$  versus  $T\Delta S$  (Ghosh et al., 2013).

#### 5.2.2.4. Circular dichroism studies

Circular dichroism (CD) spectra were recorded in a Spectropolarimeter from BioLogic Science Instruments, France equipped with Bio-Kine 32 V4.49-1 software. Wavelength range of 220 nm to 400 nm was scanned with an acquisition step size of 0.5 nm at 25 °C. All measurements were carried out in a quartz cuvette of 1 cm path length. Fixed concentration of polymers (100 µM) were titrated with increasing concentrations of CHL. Convex constraint analysis (CCA) was performed on the spectral set in order to extract the basis spectra and their associated coefficients (Pradhan et al., 2011, Ghosh et al., 2013, Perczel et al., 1992). It gives the number of components contributing to the observed spectra of the mixture of CHL and DNA/ chromatin components.

**Convex Constraint Analysis:** It is an algorithm to analyze and deconvolute a set of CD spectra and extract the common features of the data set in terms of pure curves and conformational weights for the corresponding curves. The algorithm is based on the following three constraints:

1. The sum of the weight coefficients,  $C(i, j)$ , for each conformer must be unity,

$$\sum_{i=1}^p C(i, j) = 1$$

Where  $j = 1, 2, \dots, N$ , representing the number of the analyzed CD spectra

2.  $C(i, j) \geq 0$
3. The points of  $\{C(i, j), I = 1, 2, \dots, p\}, j = 1, 2, \dots, N$ , must be embedded in a simplex of the P-dimensional Euclidean space with the smallest volume.

The ideal application of this method is to deconvolute a data set obtained by fixing all other variables except the targeted one. In this case we have varied CHL concentration keeping the polymer concentration and reaction volume fixed. The obtained spectra

were deconvoluted using CCA analysis to obtain the basis spectra for each pair of polymer-CHL interaction.

#### **5.2.2.5. Ethidium bromide displacement assay**

Ethidium bromide (EtBr) displacement assays were performed with LS 55 luminescence spectrometer (Perkin-Elmer) at 25 °C. Excitation and emission slits were kept at 5 nm each. CHL was added to a pre-equilibrated mixture of DNA/ polynucleotide (100  $\mu$ M) and EtBr (7  $\mu$ M) (Banerjee et al., 2013). The fluorescence intensity at 590 nm ( $\lambda_{\text{ex}} = 520$  nm) was recorded upon each addition of CHL. CHL concentration required to quench the fluorescence of DNA/ polynucleotide-EtBr complex by 50% ( $\text{IC}_{50}$ ) was obtained from the plot of fluorescence intensity at 590 nm versus CHL concentration.

#### **5.2.2.6. Dynamic light scattering measurements**

Zetasizer Nano S particle analyzer (Malvern Instruments, UK) was used to perform dynamic light scattering (DLS) measurements. The light source was a He-Ne laser (632.8 nm) that utilizes 4 mW power at the same wavelength. Scattered light from the samples was collected at an angle of 173° and the intensity autocorrelation function was utilized to generate a correlation curve. Translational diffusion coefficient (D) was obtained from the homodyne autocorrelation function defined by (Majumder and Dasgupta, 2011):

---

---


$$G(\tau) = A\{1 + Be^{-2\Gamma\tau}\} \dots\dots\dots(6)$$

Where  $G(\tau)$  is the correlation coefficient,  $A$  is the amplitude of the correlation function,  $B$  is the baseline and  $\Gamma$  is defined by:

$$\Gamma = Dq^2 \dots\dots\dots(7)$$

Where  $D$  is the Stokes-Einstein diffusion coefficient and  $q$  is the scattering vector. Intensity weighted mean hydrodynamic diameter ( $Z_{av}$ ) was obtained from the cumulants analysis of the correlation curve. To study the effect of CHL on the hydrodynamic size of chromatin, 500  $\mu$ M of chromatin was treated with CHL in ligand to DNA base ratio ranging from 0 to 0.2 at 25 °C and subjected to DLS measurements.

#### **5.2.2.7. Chromatosome stability assay**

Chromatosome, isolated from chicken liver, was incubated with CHL in ligand to DNA base ratio of 0, 0.1 and 0.2 for 1 hour to 3 hours at 37 °C. Agarose gel electrophoresis (1.5 % in 0.5X TBE) was used to analyze the samples, followed by post staining with SYBR green (Majumder et al., 2013, Banerjee et al., 2014).

---



---

## 5.3. RESULTS

### 5.3.1. Association of chelerythrine with chromosomal DNA and polynucleotides

Association of CHL with chromosomal DNA and various polynucleotides such as, poly(dG-dC), poly(dG).poly(dC), poly(dA-dT) and poly(dA).poly(dT), were indicated from the change in the absorption spectrum of the ligand upon addition of DNA/ polynucleotide ( Figure 5.2). Free CHL had three absorption peaks in the visible region at 316, 338 and 402 nm. On titration with DNA/ polynucleotides, hypochromic effects and bathochromic shifts were observed in the three peaks. The sets of spectra are characterized by the presence of isosbestic points originating from the equilibrium between free and bound CHL molecule. The alterations in the spectral features of free CHL in presence of the different polynucleotides are summarized in Table 5.1. The bathochromic shift, a common feature in all cases, can be ascribed to intercalation of the chromophore moiety of the ligand in the DNA base pairs. The extent of bathochromic shift is dependent upon the base sequence and maximum ( $\Delta\lambda = 11$  nm) in case of poly(dG).poly(dC).

Fluorescence spectrum of CHL undergoes an alteration both in terms of emission maximum and intensity in presence of chromosomal DNA / polynucleotides (Figure 5.3). In contrast to the absorption spectral change, alteration in fluorescence property of the ligand is sensitive to the nature of the DNA/ polynucleotide. Fluorescence intensity of CHL enhances upon association with chromosomal DNA, poly(dA-dT) and poly(dA).poly(dT) [Figure 5.3 a, d, and e)]. On the other hand, quenching of the fluorescence entails the association of the ligand with poly(dG-dC) and

---

poly(dG).poly(dC) [ Figure 5.3 b and c)]. Table 5.2 summarizes the major features of the change in emission spectrum of CHL upon association with DNA/ polynucleotide.

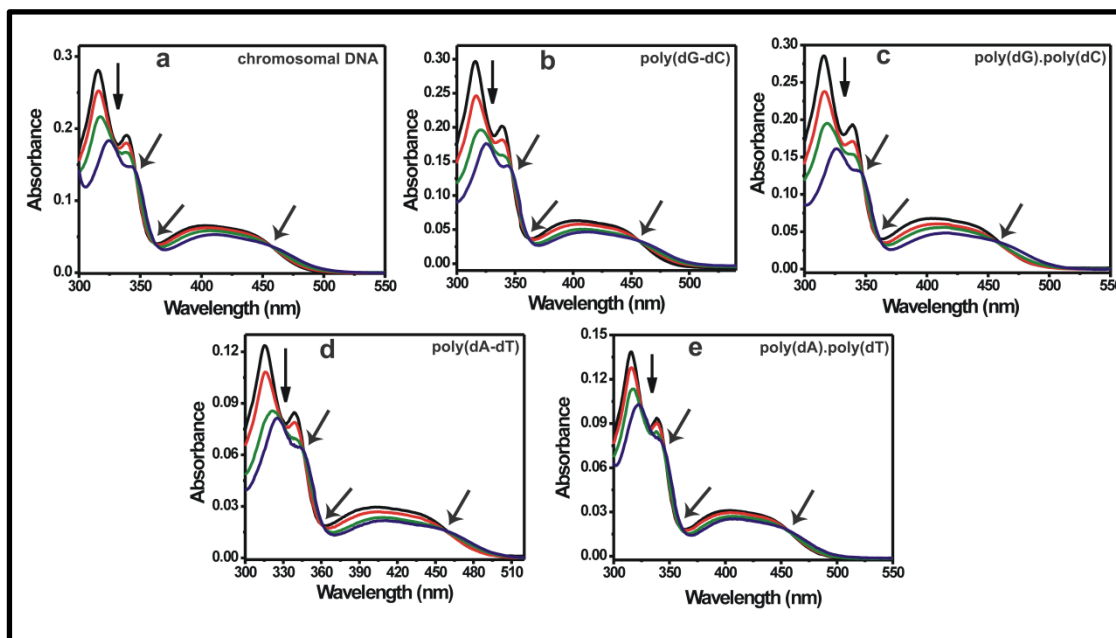


**Figure 5.2.** (a) Absorption spectra of CHL alone (10  $\mu$ M, *black*) and in presence of increasing concentrations of chromosomal DNA, 10  $\mu$ M (*red*), 24  $\mu$ M (*green*) and 104  $\mu$ M (*blue*); (b) Absorption spectra of CHL alone (10  $\mu$ M, *black*) in presence of increasing concentrations of poly(dG-dC), 10  $\mu$ M (*red*), 24  $\mu$ M (*green*) and 104  $\mu$ M (*blue*); (c) Absorption spectra of CHL alone (10  $\mu$ M, *black*) upon addition of poly(dG).poly(dC), 10  $\mu$ M (*red*), 24  $\mu$ M (*green*) and 104  $\mu$ M (*blue*); (d) Absorption spectra of CHL alone (5  $\mu$ M, *black*) upon addition of poly(dA-dT), 10  $\mu$ M (*red*), 24  $\mu$ M (*green*) and 104  $\mu$ M (*blue*); (e) Absorption spectra of CHL alone (5  $\mu$ M, *black*) upon addition of poly(dA).poly(dT), 10  $\mu$ M (*red*), 24  $\mu$ M (*green*) and 104  $\mu$ M (*blue*). Experiments were performed in 10 mM potassium phosphate buffer pH 6.8 at 25°C.

**Table 5.1.** Summary of absorption properties of CHL after binding with DNA/polynucleotides in 10 mM potassium phosphate pH 6.8 at 25 °C

Polynucleotide	$\lambda_{\text{max}}$ free CHL/nm	$\lambda_{\text{max}}$ bound CHL/nm	$\Delta\lambda$ nm	$\lambda_{\text{isosbestic}}$ /nm
Chromosomal DNA	316	325	9	345, 362, 455
Poly(dG-dC).poly(dG-dC)	316	325	9	347, 361, 458
Poly(dG).poly(dC)	316	327	11	347, 361, 458
Poly(dA-dT).poly(dA-dT)	316	325	9	345, 361, 458
Poly(dA).poly(dT)	316	323	7	344, 362, 455

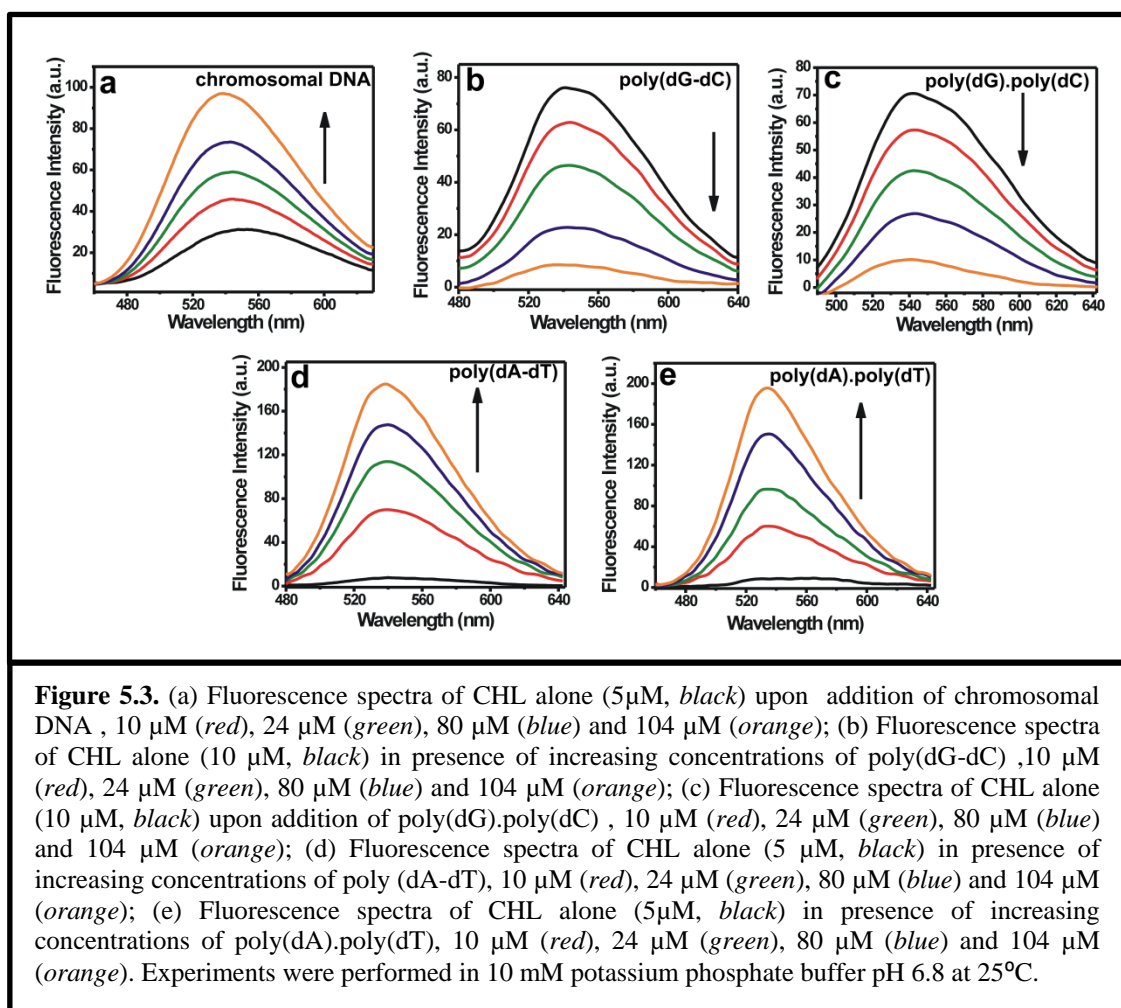


**Table 5.2.** Summary of fluorescence properties of CHL after binding with DNA/ polynucleotides in 10 mM K-Phosphate pH 6.8 at 25 °C.

Polynucleotide	Blue Shift of fluorescence maximum (nm)	$\Delta F_{\max}$ (normalized with respect to ligand concentration) <sup>a</sup>
Chromosomal DNA	8	8.3
Poly(dG-dC)	7	-7.4
Poly(dG).poly(dC)	7	-6.9
Poly(dA-dT)	4	41.24
Poly(dA).poly(dT)	6	39.5

<sup>a</sup>  $\Delta F_{\max}$  values are obtained from  $1/\Delta F$  versus  $1/(C_p - C_0)$  plot described in material and methods.

$\Delta F = F_{540}$  (free CHL) -  $F_{540}$  (bound CHL).

As described in the materials and methods section, changes in fluorescence intensity of CHL at 540 nm ( $\Delta F_{540}$ ) were employed for the determination of stoichiometry and apparent dissociation constant ( $K_d^{\text{app}}$ ) for CHL- DNA/ polynucleotide interaction. Apparent dissociation constants were estimated by nonlinear curve-fitting analysis as shown in Figure 5.4. Each isotherm has been fitted to two straight lines which give the value of binding stoichiometry from the point of intersection (*Insets* of Figure 5.4). Apparent dissociation constants ( $K_d^{\text{app}}$ ), binding stoichiometries ( $n$ ) and free energy changes ( $\Delta G$ ) for the association of CHL with DNA/ polynucleotides are summarized in Table 5.5.

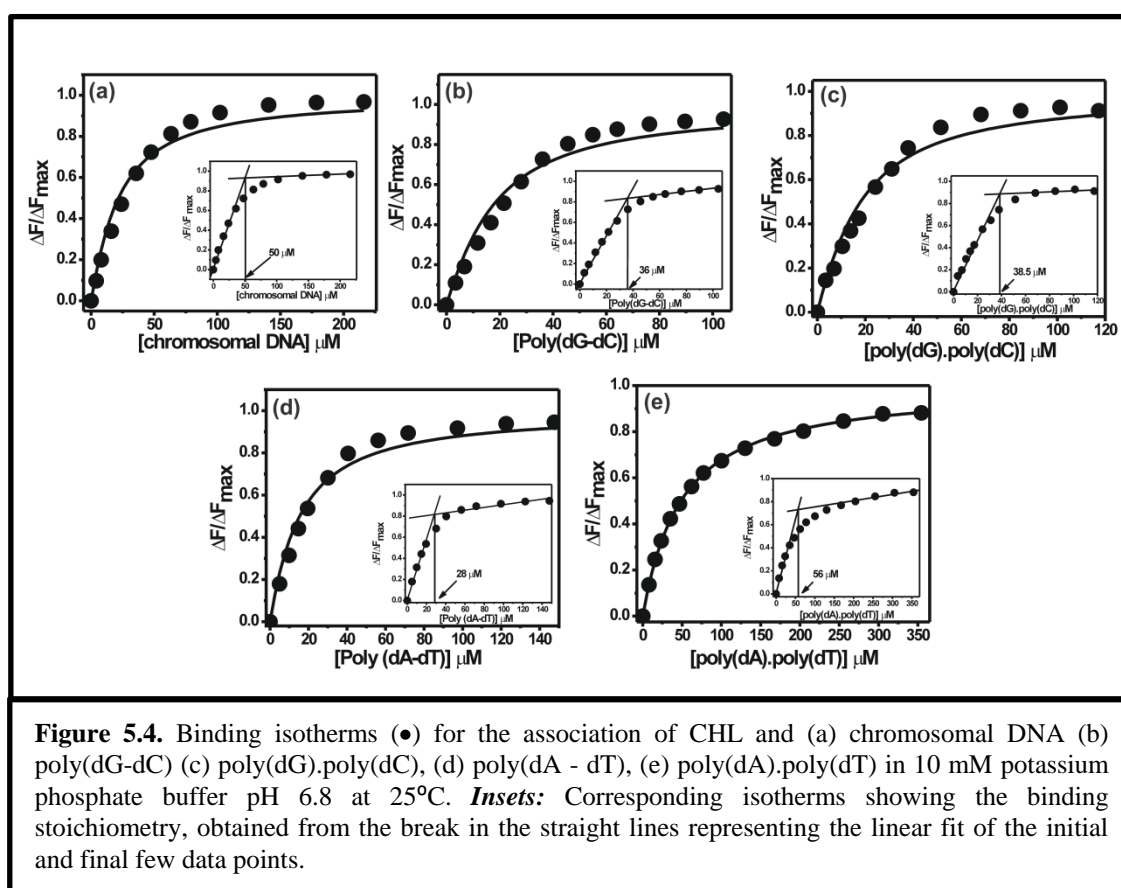


**Table 5.3.** Dissociation constant, stoichiometry and free energy change for the interaction of different DNA sequences with CHL in 10 mM potassium phosphate pH 6.8 at 25 °C obtained from spectrofluorimetric titration.

System	Apparent dissociation constant, $K_d^{app}$ ( $\mu$ M)	Stoichiometry <sup>a</sup>	$\Delta G$ (kcal/mol) <sup>b</sup>
<b>Chromosomal DNA - CHL</b>	$16.6 \pm 1.6$	5.0	$-(5.13 \pm 0.5)$
<b>Poly(dG-dC) - CHL</b>	$12.6 \pm 1.1$	3.4	$-(6.68 \pm 0.4)$
<b>Poly(dG).poly(dC) - CHL</b>	$13.01 \pm 1.1$	3.8	$-(6.66 \pm 0.3)$
<b>Poly(dA-dT) - CHL</b>	$12.9 \pm 1.0$	5.6	$-(6.67 \pm 0.3)$
<b>Poly(dA).poly(dT) - CHL</b>	$46.1 \pm 0.02$	11.6	$-(5.91 \pm 0.01)$

<sup>a</sup>Binding stoichiometry in terms of number of nucleotide bases bound per CHL molecule, is reported from point of intersection of the two straight lines fitted to a plot of normalized increase in fluorescence against the ratio of molar concentration of DNA/polynucleotides as described in Material and Methods.

<sup>b</sup> $\Delta G = -RT \ln (K_a)$ , where  $K_a = 1 / K_d^{app}$

### 5.3.2. Thermodynamics of binding of chelerythrine with different polynucleotides

The representative ITC profiles and corresponding binding isotherms for the association of CHL with DNA/ polynucleotides are shown in Figure 5.5. With the exception of poly(dA).poly(dT) which has an endothermic ITC profile for the association with CHL, other polynucleotides/ DNA exhibit an exothermic ITC profile. The binding parameters obtained from ITC are summarized in Table 5.4. Figure 5.6 is the graphical representation of enthalpy ( $\Delta H$ ) and entropy ( $T\Delta S$ ) contributions towards free energy change ( $\Delta G$ ) for the binding of CHL to DNA/ polynucleotides. With the exception of poly(dA).poly(dT), enthalpy and entropy contribute favorably for binding of CHL with DNA/polynucleotides. Figure 5.7 shows the temperature dependence of enthalpy ( $\Delta H$ ), entropy ( $T\Delta S$ ) and free energy change ( $\Delta G$ ) due to the association of CHL with DNA/ polynucleotides. The slope of  $\Delta H$  versus temperature ( $T$ ) yields  $\Delta C_p$

values, summarized in Table 5.6, for the association of CHL with different DNA/polynucleotides. In all cases we have observed non- zero  $\Delta C_p$  and  $\Delta C_p > \Delta S$ . The linear plots of  $\Delta H$  versus  $T\Delta S$  for CHL-DNA/polynucleotide interaction have a slope of  $\sim 1.0$  (Figure 5.7), which indicates the complete enthalpy –entropy compensation.

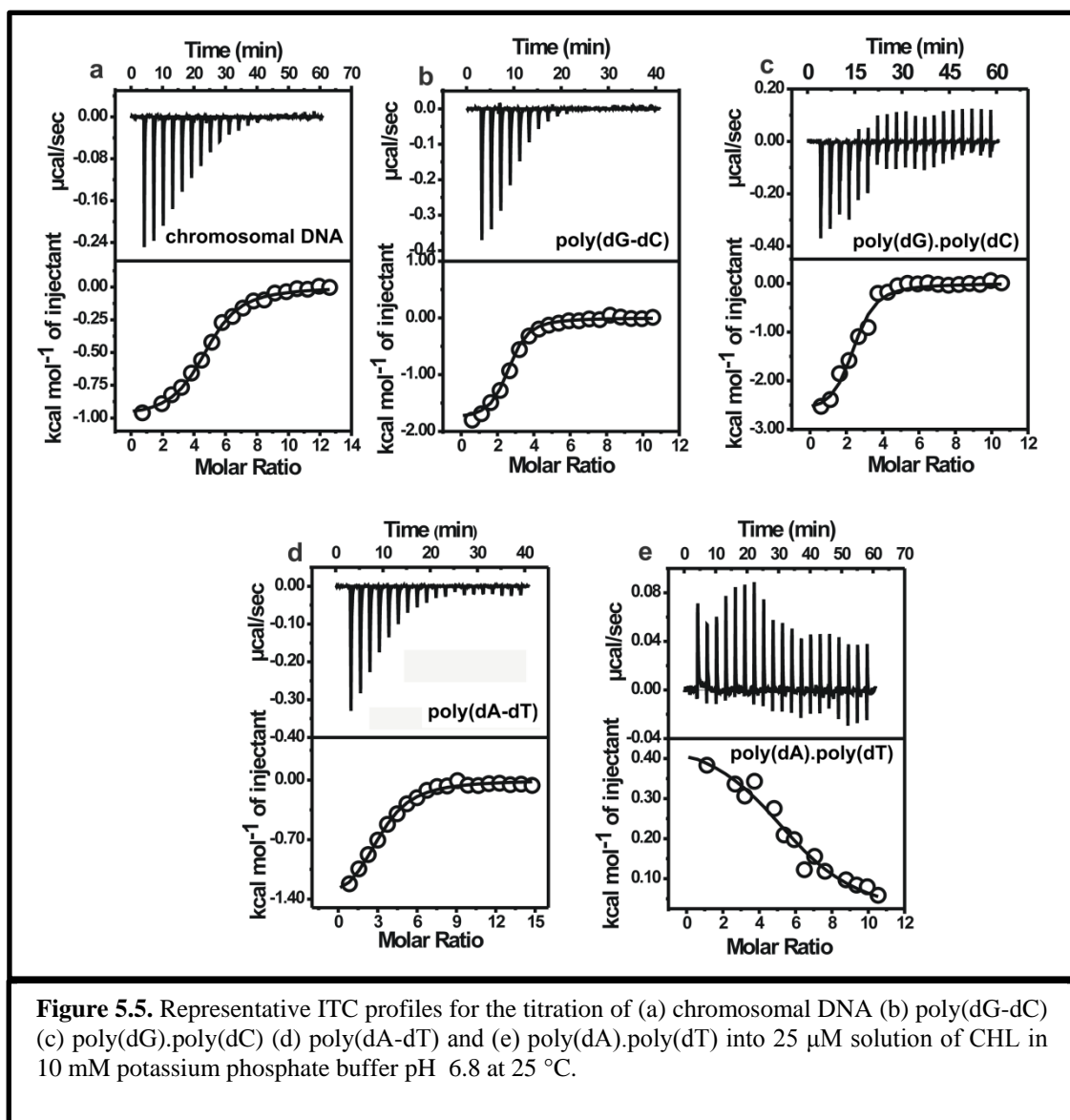


**Table 5.4.** Thermodynamic parameters for the association DNA/ polynucleotide with CHL by isothermal titration calorimetry in 10 mM potassium phosphate buffer pH 6.8 at 25°C.

System	$K_d^{app}(\mu M)^a$	$\Delta H$ (kcal/mol) <sup>a</sup>	$\Delta S$ (cal/mol/K) <sup>a</sup>	$T\Delta S$ (kcal/mol) <sup>a</sup>	$\Delta G$ (kcal/mol) <sup>a</sup>	$\Delta C_p$ (cal mol <sup>-1</sup> K <sup>-1</sup> ) <sup>b</sup>
Chromosomal DNA- CHL	1.41 ± 0.02	-4.71 ± 0.02	11.0	3.28	-7.9	-106.4 ± 17.5
Poly(dG-dC) - CHL	1.16 ± 0.02	-4.48 ± 0.11	12.1	3.60	-8.1	-102.8 ± 25.2
Poly(dG).poly(dC)- CHL	1.84 ± 0.05	-6.28 ± 0.24	5.16	1.54	-7.8	-21.5 ± 7.0
Poly(dA-dT) - CHL	2.58 ± 0.14	-2.42 ± 0.18	17.5	5.21	-7.6	-101.6 ± 18.6
Poly(dA).poly(dT) - CHL	5.71 ± 1.04	3.25 ± 0.09	34.9	10.40	-7.1	211.7 ± 62.1

<sup>a</sup> binding parameters obtained from ITC experiments performed at 25°C.  $K_d^{app} = 1/K_a$ .  $K_a$  is the equilibrium association constant. <sup>b</sup>  $\Delta C_p$  values are determined from the linear plot of enthalpy values obtained from ITC experiments against temperatures.

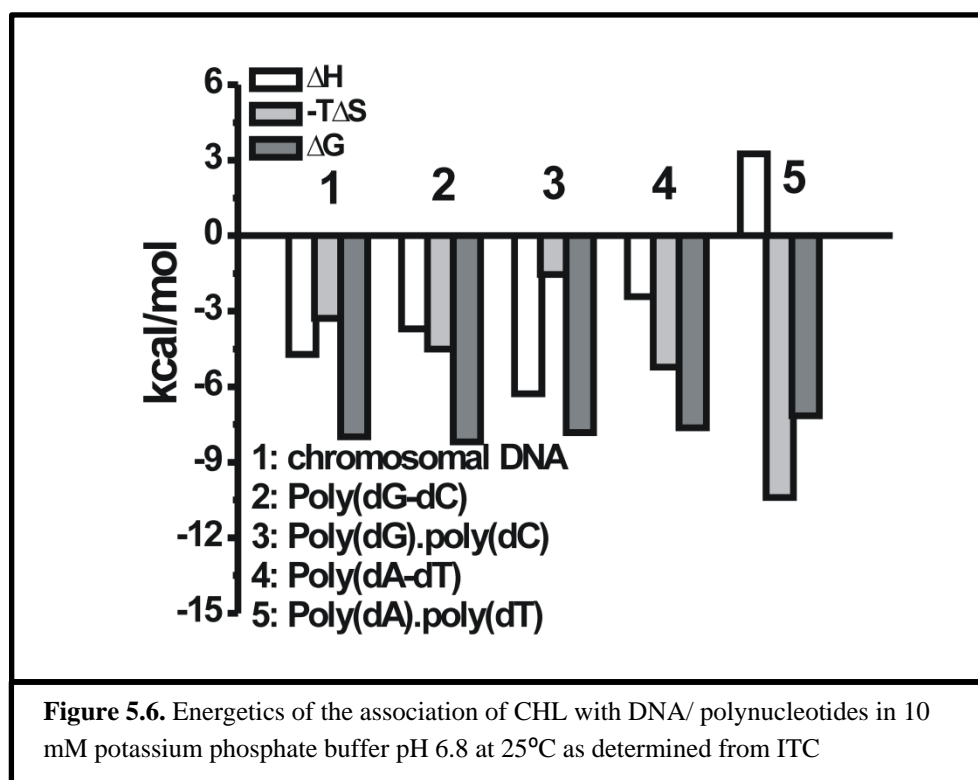


**Figure 5.6.** Energetics of the association of CHL with DNA/ polynucleotides in 10 mM potassium phosphate buffer pH 6.8 at 25°C as determined from ITC

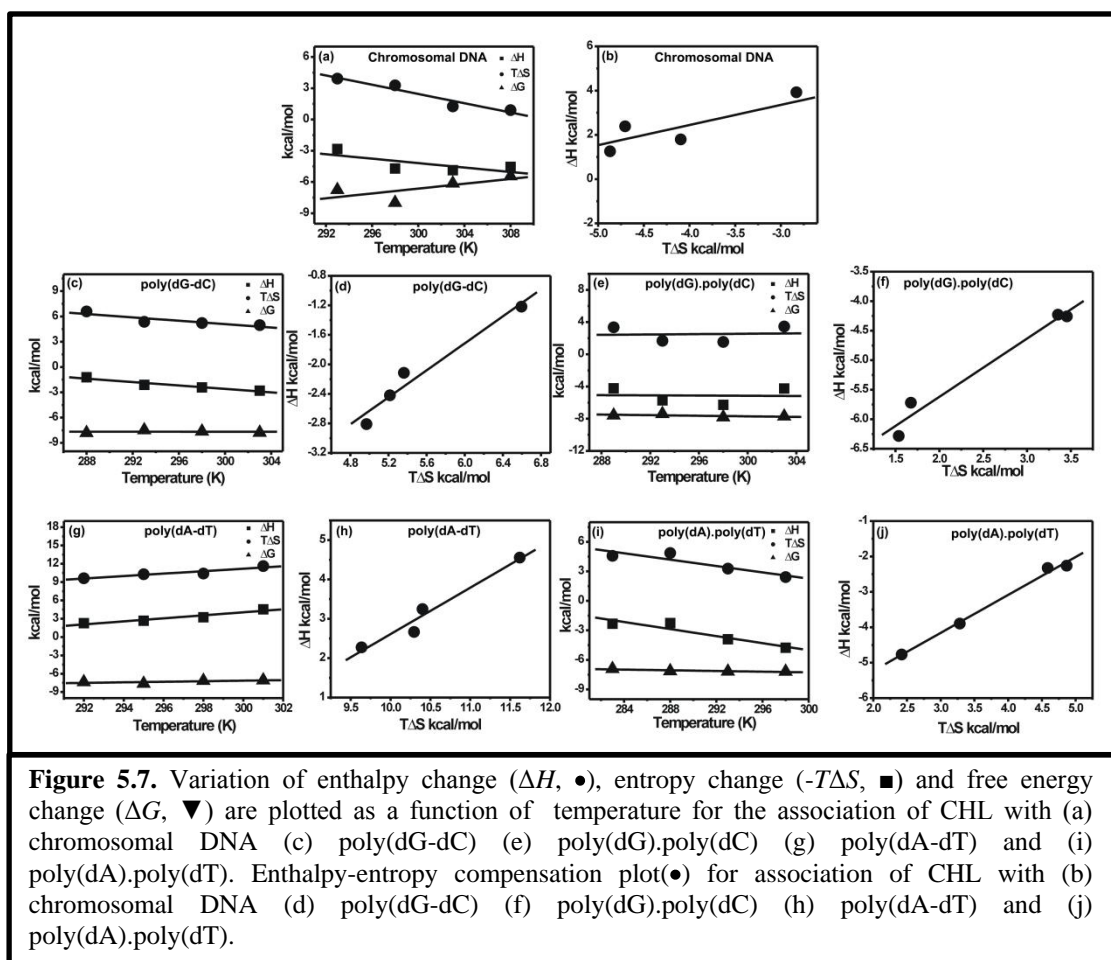


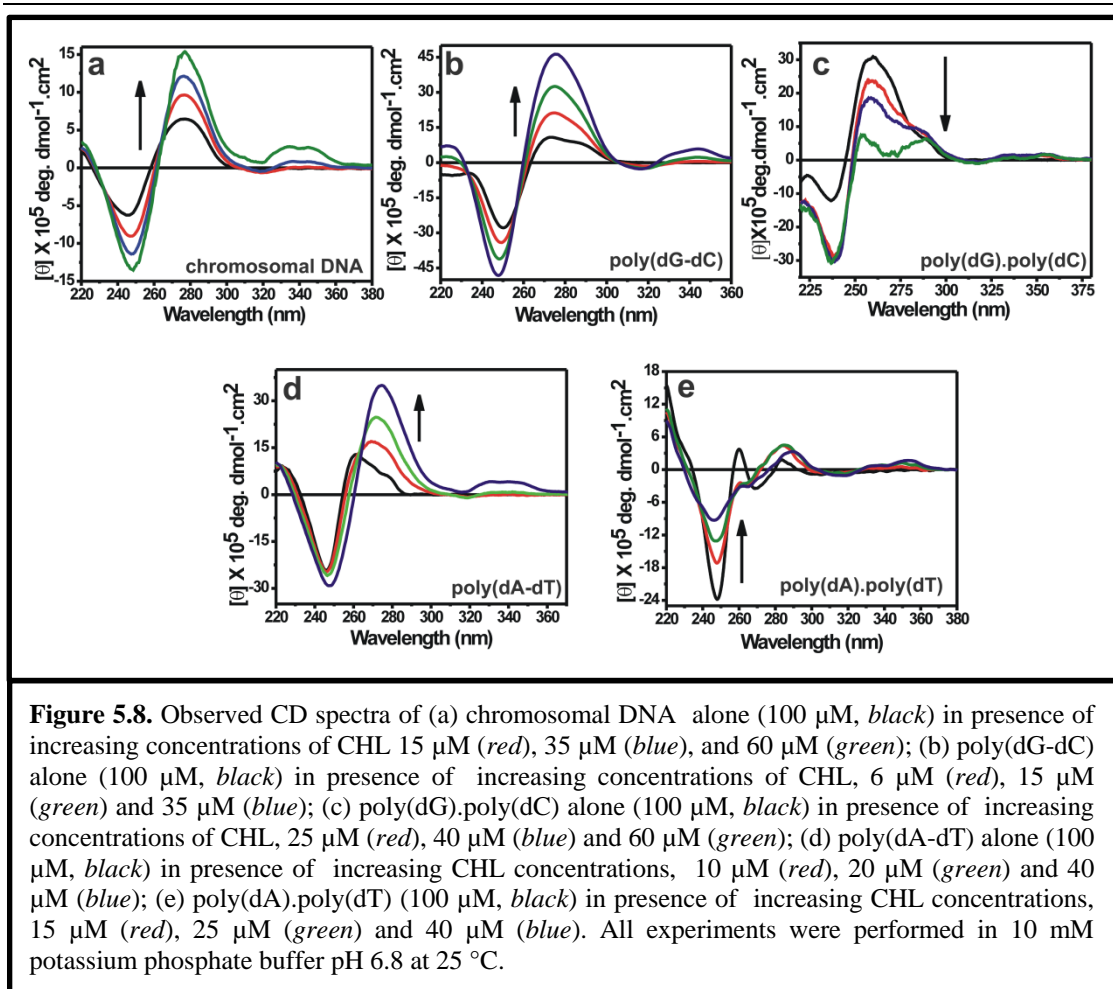
**Figure 5.7.** Variation of enthalpy change ( $\Delta H$ , ●), entropy change ( $-T\Delta S$ , ■) and free energy change ( $\Delta G$ , ▼) are plotted as a function of temperature for the association of CHL with (a) chromosomal DNA (c) poly(dG-dC) (e) poly(dG).poly(dC) (g) poly(dA-dT) and (i) poly(dA).poly(dT). Enthalpy-entropy compensation plot(●) for association of CHL with (b) chromosomal DNA (d) poly(dG-dC) (f) poly(dG).poly(dC) (h) poly(dA-dT) and (j) poly(dA).poly(dT).



### 5.3.3. Structural alteration of polynucleotides upon association with chelerythrine

Conformational changes induced in the DNA/ polynucleotide structure due to association with CHL molecule have been monitored by CD experiments (Figure 5.8). In all cases binding to CHL led to an induced CD band at the absorption region of CHL. In case of chromosomal DNA, poly(dG-dC) and poly(dA-dT) characteristic CD spectra of B-form of duplexes with large positive bands in 260-290nm region and a negative band at 248nm result from the association. Binding to CHL led to significant increase in ellipticity of both positive and negative bands of chromosomal DNA and poly(dG-dC) (Figure 5.8 a and b). In case of poly(dA-dT) significant red shift ( $\Delta\lambda=15$  nm) was associated with enhanced ellipticity of the positive band upon binding to CHL (Figure 5.8d). However, ellipticity of negative band of poly(dA-dT) remains unaltered upon binding to CHL. CHL decreases the ellipticity of the positive and negative bands of poly(dG).poly(dC) and poly(dA).poly(dT) upon binding to them (Figure 5.8 c and e).

To detect the conformational change of different polynucleotide structure due to association with CHL we deconvoluted the CD spectra of DNA/ polynucleotide by CCA method. In all cases the CD spectra could be best deconvoluted into two basis spectra: component 1 and component 2 (right hand panel, Figure 5.9). In all cases component 1 matched with native/ unbound CD spectra of the DNA/ polynucleotides and component 2 represents the CHL-bound CD spectra of the polymers. The variation in percentage population of each component with increasing CHL (left hand panel, Figure 5.9) shows a decrease in component 1 population with a concomitant increase in component 2 population.



#### 5.3.4. Ethidium Bromide displacement assay of DNA and chromatin

In order to ascertain the binding modes of CHL to double stranded DNA we have carried out EtBr displacement assay by fluorescence titration method. The fluorescence intensity of the pre-equilibrated EtBr-DNA/ polynucleotide mixture decreases with addition of CHL (Figure 5.10a). This indicates the CHL accesses double stranded DNA via minor groove. The  $\text{IC}_{50}$  values obtained are graphically presented in Figure 5.10b.

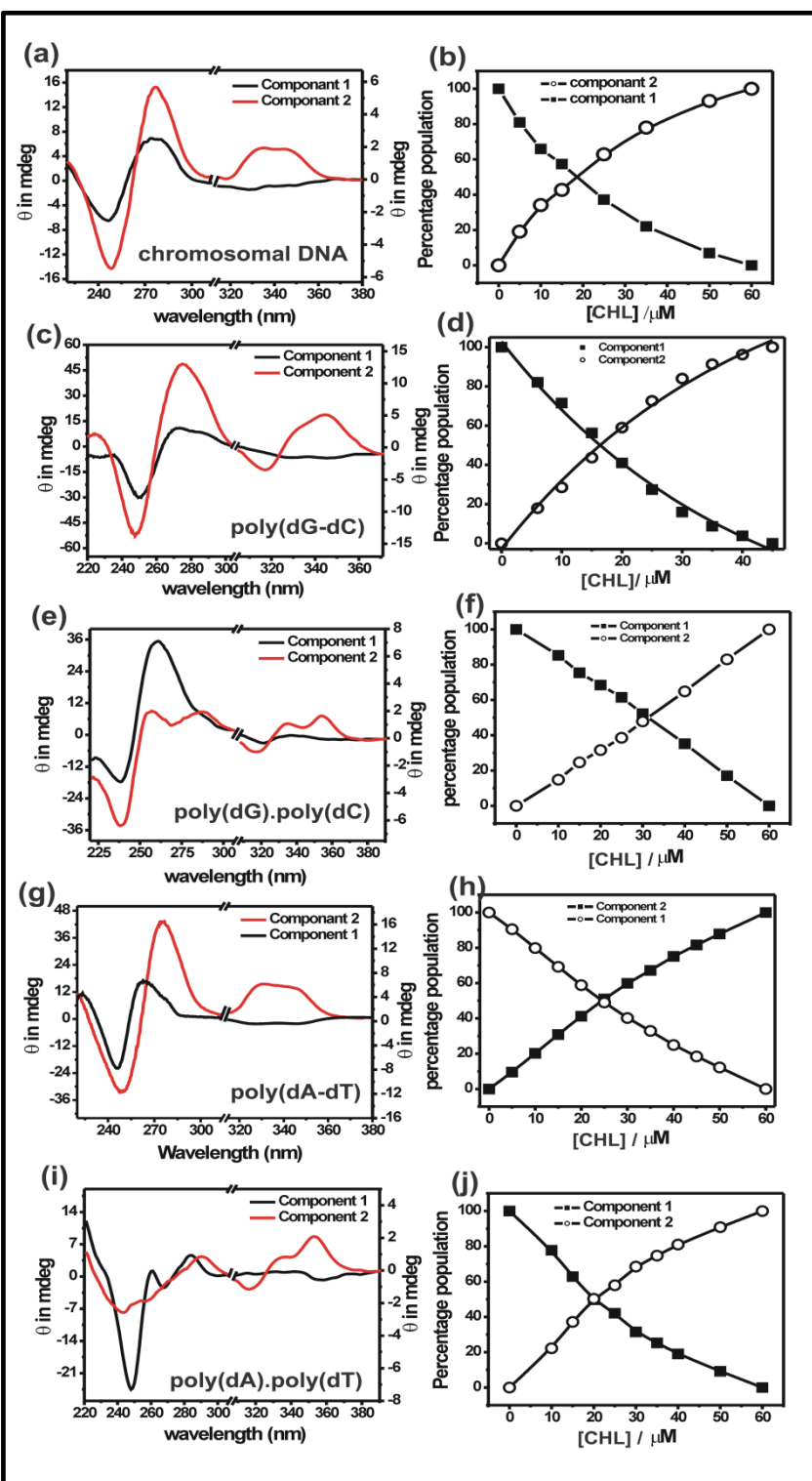
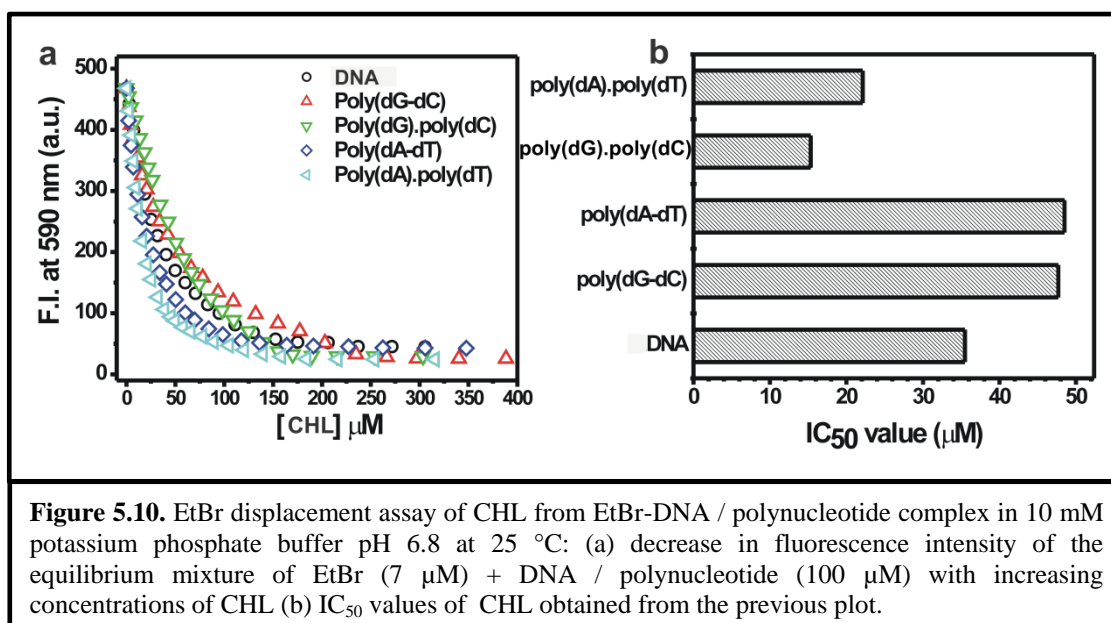


**Figure 5.9.** Basis spectra obtained from CCA analysis of CD spectra of DNA / polynucleotide in 10 mM potassium phosphate buffer pH 6.8 at 25 °C: left hand panel (a, c, e, g and i) are components 1 and 2 obtained from the CCA analysis of the observed CD spectrum. **Note:** Right hand scales of these plots show the observed ellipticity of induced CD band from CHL. Percentage populations of the components 1 and 2 for (b) chromosomal DNA (d) poly(dG-dC) (f) poly(dG).poly(dC) (h) poly(dA-dT) and (j) poly(dA).poly(dT) are plotted as a functions of CHL concentration.

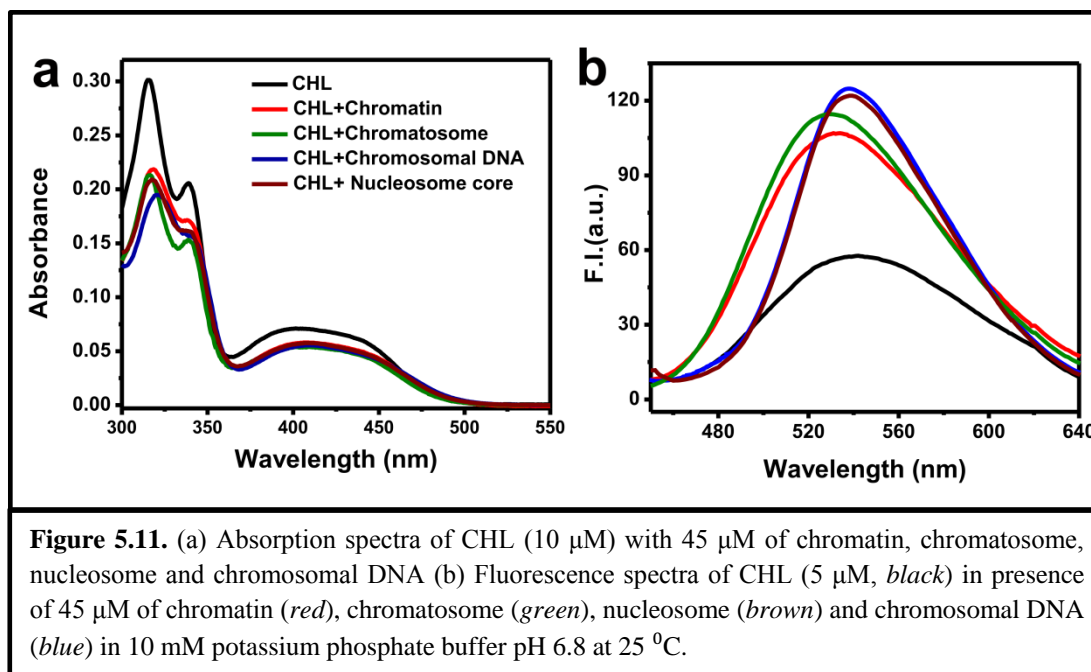


### 5.3.5. Association of chelerythrine and with chromatin

The association of CHL with chromatin and its components (chromatosome, nucleosome and chromosomal DNA) have been characterized by absorbance and fluorescence studies. The absorption spectra of CHL in absence and presence of chromatin and its components are shown in Figure 5.11a. Upon addition of these polymer samples the intensity of the three peaks in free CHL decreases. Another feature of the changes of the absorbance spectra are red shift and broadening of the peaks in 300 nm -350 nm region. Both features are maximum in case of chromosomal DNA (shift of 316 nm to 321 nm) and minimum in case of chromatosome.

Association of CHL with different levels of chromatin structure is further probed with fluorescence spectroscopy. Increase in fluorescence intensity with a blue shift is observed when fixed concentration of CHL is titrated with chromatin and its

components (Figure 5.11b). Extent of blue shift of the fluorescence intensity peak of CHL bound to the polymers follows the following order: chromosomal DNA > chromatin > nucleosome > chromatosome. Binding isotherms are generated from fluorescence titration experiments using method described in material and methods (Figure 5.12). Binding stoichiometry and apparent dissociation constant values, evaluated from nonlinear curve fitting of binding isotherms, are summarized in Table 5.5. CHL has higher binding affinity and lower stoichiometry for chromosomal DNA compared to chromatin, chromatosome and nucleosome.



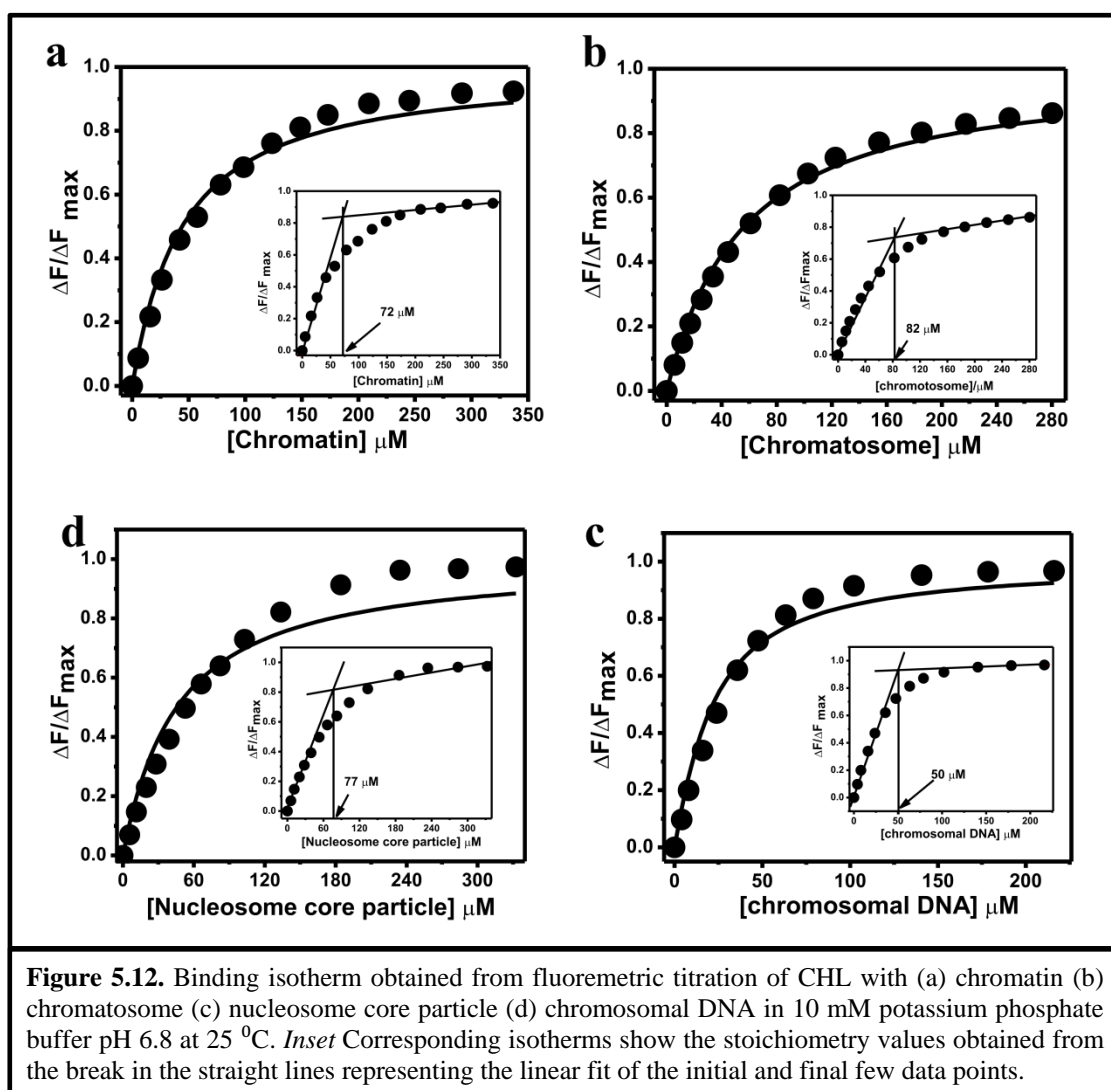


**Table 5.5.** Binding parameters obtained from fluorescence studies for the association of CHL with chromatin, chromatosome, nucleosome and chromosomal DNA at 25°C.

	$K_d^{\text{app}}$ ( $\mu\text{M}$ )	$n$ (Bases/ligand )
Chromatin	$41.6 \pm 2.2$	$14.4 \pm 0.5$
Chromatosome	$51.6 \pm 1.5$	$16.4 \pm 0.2$
Nucleosome	$42.9 \pm 2.4$	$15.4 \pm 0.5$
Chromosomal DNA	$16.6 \pm 1.6$	$5.0 \pm 0.1$

---

### 5.3.6. Binding energetics of chelerythrine with chromatin and its components

Isothermal titration calorimetry (ITC) was used to evaluate the binding parameters and associated energetics of association of CHL with different levels of chromatin. Representative thermograms for CHL-chromatin/ chromatosome/ nucleosome / chromosomal DNA association at 25 °C are shown in upper panels of Figure 5.13. Dissociation constants, enthalpy ( $\Delta H$ ) and entropy ( $\Delta S$ ) values obtained from the resulting binding isotherms are summarized in Table 5.6. Apparent dissociation constants ( $K_d^{app}$ ) for chromatin and chromatosome are comparable at 25 °C. Trend in the change of enthalpy and entropy values for the formation of CHL-chromatin complex shows that the binding is entropy driven in case of chromatin, chromatosome and nucleosome.

### 5.3.7. Circular dichroism studies for chelerythrine - chromatin complex

We have monitored the CD spectra (300-220 nm) of chromatin, chromatosome and chromosomal DNA in absence of CHL and they agree well with previous reports in the literature (Figure 5.6). Addition of CHL leads to change in CD spectra of chromatin and chromatosome in the region 300 - 220 nm. In case of chromatin and chromatosome positive CD band at 272 nm increased in presence of CHL. Induced CD bands of CHL (380-310 nm) are also observed in case of chromatin, chromatosome and chromosomal DNA [Fig. 4(D)]. Shape of induced CD bands obtained from the association of CHL with chromatin and chromatosome are comparable. However, molar ellipticity of the induced CD band for chromatosome – CHL is less compared to chromatin- CHL.

---

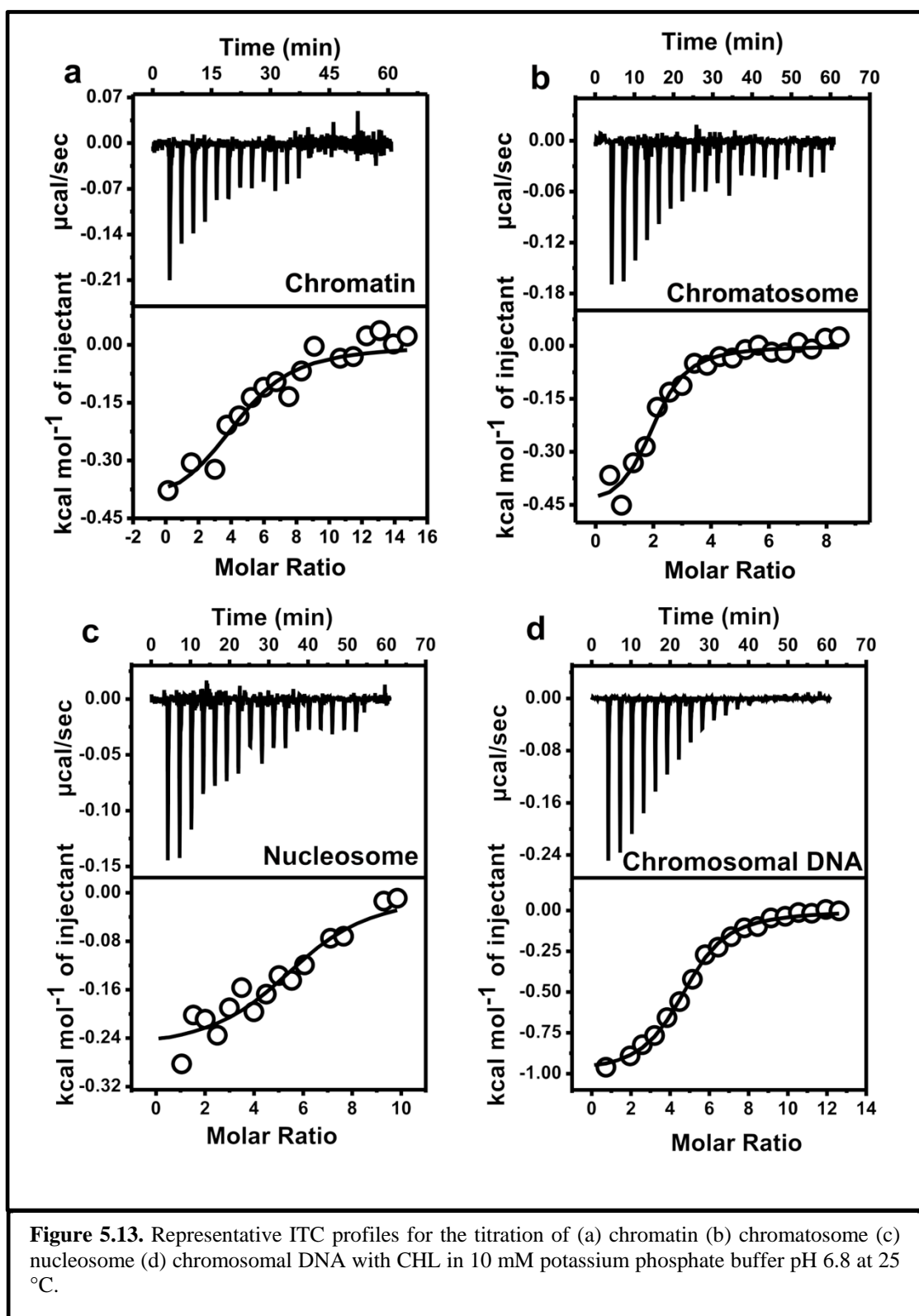
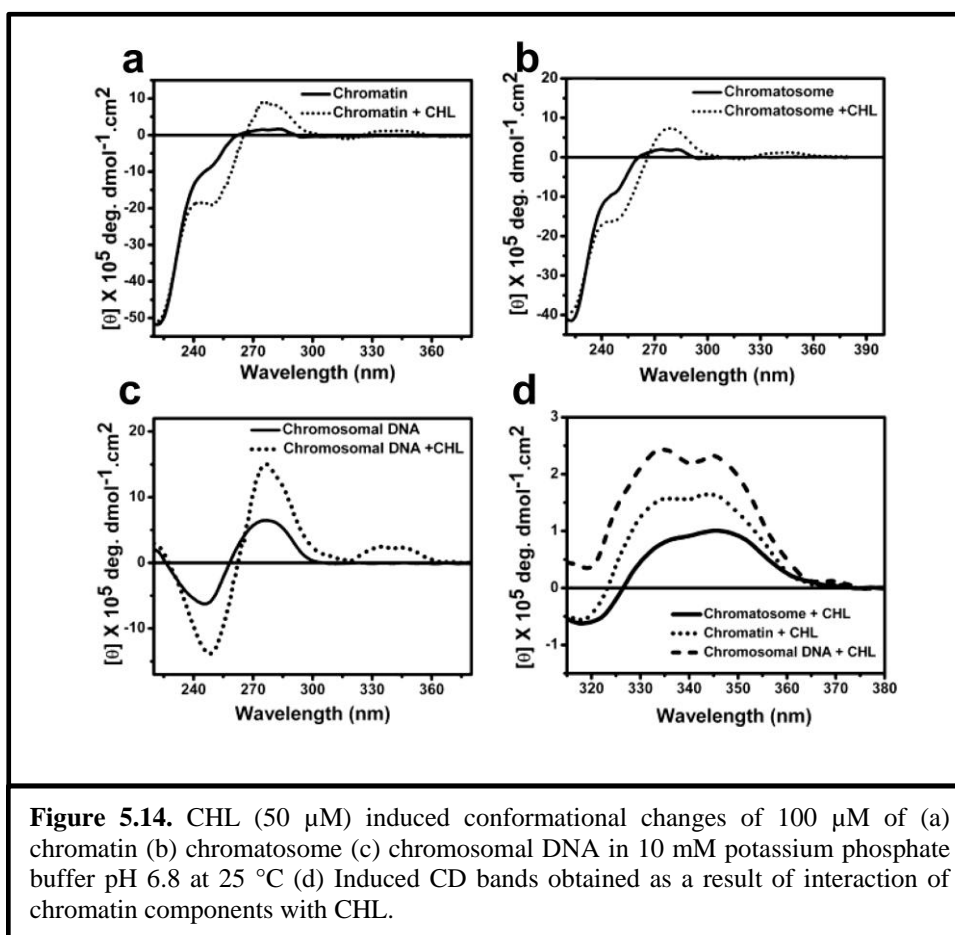




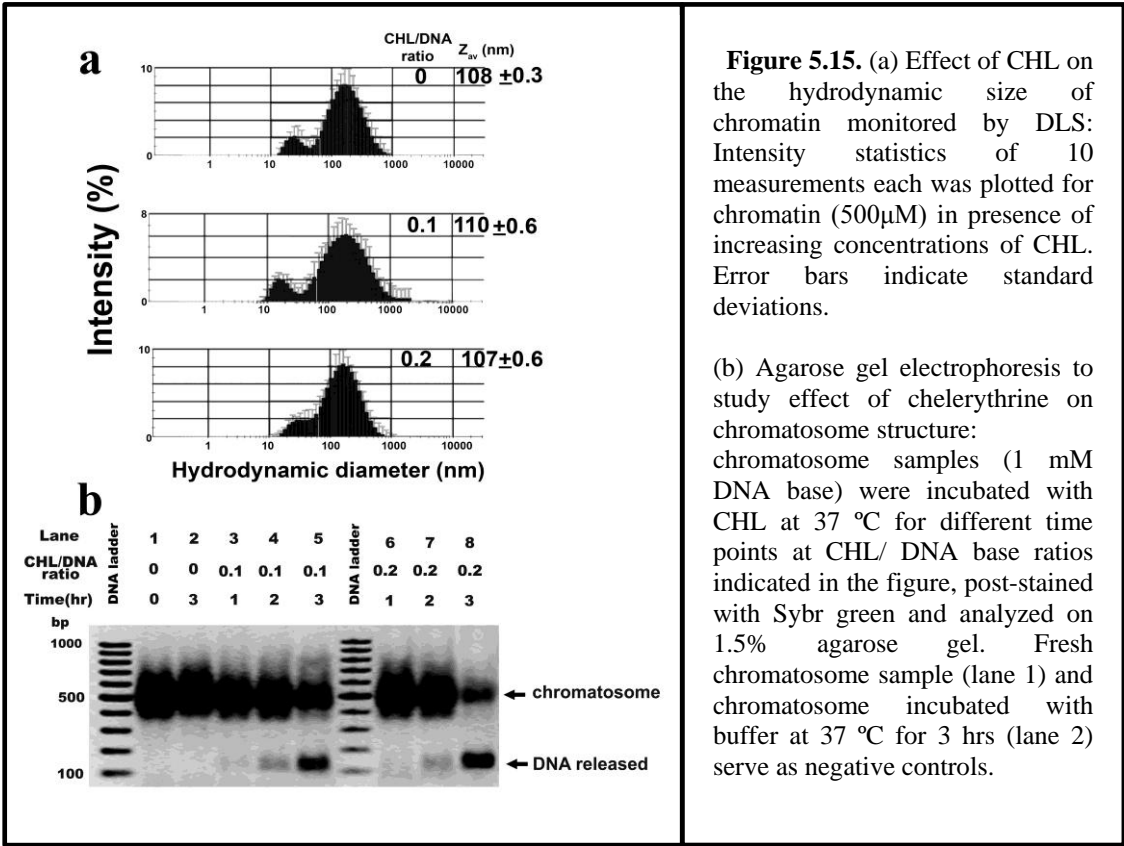
**Table 5.6.** Thermodynamic parameters obtained from ITC experiments for the association of CHL with chromatin and its components in 10 mM K-phosphate (pH 6.8) at 25 °C.

	$K_d^{app}$ ( $\mu$ M)	$\Delta H$ (kcal mol <sup>-1</sup> )	$\Delta S$ (cal mol <sup>-1</sup> K <sup>-1</sup> )	$\Delta G$ (kcal mol <sup>-1</sup> )
Chromatin	$8.2 \pm 0.6$	$-2.0 \pm 0.2$	16.6	-6.9
Chromatosome	$8.4 \pm 0.4$	$-1.0 \pm 0.1$	19.9	-6.9
Nucleosome	$6.4 \pm 0.1$	$-1.5 \pm 0.1$	18.6	-7.1
Chromosomal DNA	$1.4 \pm 0.1$	$-4.7 \pm 0.1$	8.83	-7.3



5.3.8. Dynamic light scattering measurements of chelerythrine treated chromatin

DLS measurements show that the hydrodynamic radius of chromatin does not change significantly upon CHL treatment. The  $Z_{av}$  diameter of untreated chromatin changed from  $108 \pm 0.3$  nm to  $107 \pm 0.6$  nm at a ligand to DNA base ratio of 0.2 (Figure 5.7a). Thus the hydrodynamic diameter of chromatin was practically unchanged in presence of CHL suggesting no significant alteration at the gross structural level.



5.3.9. Chromosome mobility assay with chelerythrine

The difference in electrophoretic mobilities of CHL treated and untreated chromosome has been analyzed on agarose gel (Figure 5.7b). Appearance of single

bands was observed at around 200 bp in case of CHL treated chromatosome which was absent in untreated chromatosome (~500 bp). The faster migrating single band corresponds to the DNA wrapped around histone octamer in intact chromatosome indicating that CHL affects the stability of chromatosome structure. Partial destabilization of chromatosome structure with initiation of DNA release was evident at CHL to DNA base ratio 0.1 when incubated for 2 hrs at 37°C which became more pronounced at CHL to DNA base ratio of 0.2 after incubation for 3 hrs under similar condition.

---

---

## 5.4. DISCUSSION

There are only a few preliminary reports on the interaction of CHL with dsDNA (Li et al., 2012, Urbanova et al., 2009, Bai et al., 2008, Bai et al., 2006, Basu et al., 2013). In this chapter, we have reported an in-depth study of the molecular and structural basis of the recognition of DNA by the alkaloid at a pH where it is in its positively charged imminium form (Urbanova et al., 2009). Use of the four synthetic polynucleotides could be appreciated from the consideration that they contain the following sequences at the dinucleotide levels: (G.C), (G.G), (A.T) and (A.A). We have also compared the results of the polynucleotides with chromosomal DNA which is the combination of all of these sequences.

Changes in absorption spectrum of CHL demonstrate the association of CHL with DNA / polynucleotides (Figure 5.2). The figure supports the earlier report that the association is not base pair selective, that is normally a characteristic feature of the binding of small DNA binding intercalators and groove binders (Li et al., 2012). However, as summarized in Table 5.3, the absorption properties are dependent upon the sequence of the synthetic polynucleotides. Hypochromic effects and bathochromic shifts in absorption spectra of CHL-DNA/ polynucleotide complex can be attributed to the stabilization of singlet excited state of CHL upon interaction with the  $\pi$  electrons of nucleotide bases. Energy difference corresponding to  $\pi \rightarrow \pi^*$  transition between the ground and excited states diminishes due to increased hydrophobicity induced in the micro environment of CHL upon association with DNA (Bai et al., 2006). The bathochromic shift, in particular, is consistent with the proposition of intercalative mode of association of CHL. The aromatic moiety stacks between the base pairs of DNA and polynucleotide. From the same viewpoint the differences in  $\Delta\lambda$  values in

---

---

Table 5.3 may be ascribed to base sequence dependent variation in the intercalation geometry when the ligand binds to the synthetic polynucleotides.

The sequence dependent nature at the dinucleotide level of the association is further corroborated from a comparative analysis of the fluorescence spectral changes of CHL upon addition of DNA / polynucleotides (Figure 5.3). The enhancement of fluorescence intensity of CHL upon association with poly(dA-dT) and poly(dA).poly(dT) is typical for intercalator like EtBr (Garbett et al., 2004). Hydrophobic environment of the chromophore of the ligand when it stacks between the base pair and the alteration in its structure are the two potential factors for the enhancement in fluorescence. On the other hand, fluorescence quenching of CHL upon association with poly(dG-dC) and poly(dG).poly(dC) can be attributed to the electron transfer of guanine base to singlet excited state of CHL. This type of quenching of fluorescence intensity has been explained in literature by excited state reductive reaction mechanism coupled with ground state complex formation (Jasuja et al., 1997). Guanine, being the most reducing among the four bases, is able to decrease the energy level of the singlet excited state of CHL. It culminates in non-radiative relaxation pathway of the excited state of the fluorophore in the ligand thereby quenching the fluorescence intensity of CHL upon association with G-C containing nucleotide. Similar feature of fluorescence quenching in presence of (G.C) base pair is also observed in case of SGR (Maiti et al., 2002, Ghosh et al., 2013). This is a characteristic feature of these two intercalators not commonly observed in case of a majority of the intercalating ligands. In case of chromosomal DNA, CHL binds to both base pair. Since the increase in fluorescence quantum yield in presence of (A.T) base pair overrides the decrease upon binding to

---

(G.C) base pair, the emission intensity increases upon association with chromosomal DNA.

The apparent dissociation constants for chromosomal DNA, poly(dG-dC), poly(dG).poly(dC) and poly(dA-dT) complexed with CHL are comparable (Table 5.3). In contrast, the same is ~3.5 fold higher for poly(dA).poly(dT)- CHL complex. Binding stoichiometry for the association of CHL and (G.C) rich polynucleotides are comparable (Table 5.3) whereas those are higher for (A.T) rich polynucleotides. Weak affinity of CHL towards poly(dA).poly(dT) is further corroborated from higher stoichiometry value (11.6). Differences in the binding stoichiometry of CHL-DNA/ polynucleotide complexes can be explained as follows. Structural dissimilarities linked to helical twist, strand and sugar puckering vary at each dinucleotide step for the polynucleotides, which in turn influence inter-nucleotide distances and base stacking. The relatively smaller inter base distance in (G.C) specific polynucleotides influences base stacking interactions favorably in CHL-bound complexes resulting in complexes with lower stoichiometry (Chandrasekaran and Arnott, 1989, Chandrasekaran et al., 1989, Bhattacharyya and Bansal, 1990).

The results pertaining to CD spectroscopy is discussed for two regions: the induced band region from 300 nm to 360 nm and the DNA region from 300 nm to 250 nm (Figure 5.14 and 5.15). CHL is an achiral molecule; hence it does not possess any intrinsic CD signal. But upon association with DNA/ polynucleotide an induced band appears. Based on theoretical and experimental CD and X-ray crystallography data, the induced CD signals obtained for small molecule-DNA complex is attributed to the interactions between the chromophore transition dipole moment and the transition moments of the chiral arrangement surrounding DNA bases (Monnot et al., 1992). We

---

propose that the induced CD band seen in the CHL-DNA/ polynucleotide complex originates either from CHL molecules bound in the proximity of the chiral deoxyribose moieties on DNA or from CHL molecules intercalated into DNA base pairs (Monnot et al., 1991). It provides indirect information to compare the stacking geometry of the chromophore of CHL when it is intercalated into the base pairs. We have noticed that the induced CD bands with positive ellipticity vary in shape and magnitude of ellipticity depending upon both the nature of the base and its sequence (Lyng et al., 1987). Therefore, differences between the induced CD spectra are likely to reflect different geometry of intercalation for the different dinucleotide sequences. On the other hand, the observed induced band in case of natural DNA is base composition weighted average. The alteration of the CD spectra in the range 250-300 nm originates from the CHL induced changes in the structure of the synthetic homo and hetero polynucleotides (Monnot et al., 1992). The comparison of the free and bound component of the spectra in this region suggests that the structural alteration as a sequel to ligand binding is more pronounced in case of the homopolymer, poly(dA).poly(dT). This aspect is discussed in greater details in the last paragraph, where we have compared the ligand induced structural alterations at the dinucleotide level to elaborate the structural basis of the recognition.

From ITC experiments we have observed that with the notable exception of poly(dA).poly(dT), both enthalpy and entropy contribute in a favorable way to the negative free energy change associated with the complex formation (Table 5.4 and Figure 5.6). The association with poly(dA).poly(dT) stands alone as the entropy driven binding. Negative enthalpic contribution indicates non-covalent interaction such as stacking and hydrogen bonding which stabilizes the complex between DNA/ polynucleotides and

---

---

CHL (Haq, 2002, Ren et al., 2000). The net enthalpy change ( $\Delta H_{\text{obs}}$ ) can be parsed into the following contributions (Majee et al., 1997):

$$\Delta H_{\text{obs}} = \Delta H_{\text{ligand-DNA}} + \Delta H_{\text{DNA}} + \Delta H_{\text{ligand}}$$

$\Delta H_{\text{ligand-DNA}}$  is the DNA binding enthalpy of CHL with DNA/ polynucleotide,  $\Delta H_{\text{DNA}}$  is the conformational enthalpy change of DNA at the ligand binding site and  $\Delta H_{\text{ligand}}$  is the conformational enthalpy change of CHL upon binding to DNA/ polynucleotide. The last term ( $\Delta H_{\text{ligand}}$ ) is not expected to vary much for the different polynucleotides and natural DNA used. A comparison of the  $\Delta H$  –values presented in Table 5.6 indicate that the first two terms contribute to a major degree to the overall enthalpy changes. Since stacking interaction is a common feature in all the complexes, it may be proposed that its contribution is offset by the enthalpy change due to conformational change in the polynucleotide and DNA. The relatively higher magnitude of negative  $\Delta H$  –value in case of poly(dG).poly(dC) may arise from additional hydrogen bonding or lesser degree of ligand – induced conformational alteration in this polynucleotide.

In case of all DNA/ polynucleotides, entropy is found to play a positive role in the association with CHL. Positive entropic contribution could be ascribed to the release of water molecules present in the minor groove of the DNA/ polynucleotides through which CHL access the macromolecule which has been proved from the EtBr displacement assay experiments. The notable difference in the energetic of binding of CHL to poly(dA).poly(dT) is a result of non-classical B-DNA structure of the polynucleotide (Premilat and Albiser, 1997, Chan et al., 1997). Poly(dA). poly(dT) has a very narrow minor groove and wide major groove as compared to classical B-DNA. Higher propeller twist present in the poly(dA).poly(dT) structure entails its structural

---



rigidity. Positive enthalpic contribution for the binding of CHL to poly(dA).poly(dT) can be attributed to the structural rigidity of the polynucleotide. Moreover, it has a unique water of hydration in the minor groove, which can be replaced during its association with CHL. It is reflected in the higher entropic contribution towards free energy of the reaction (Bhadra et al., 2007).

Consistent with the results from fluorescence spectroscopy, the results from ITC studies show that CHL has comparable affinity towards chromosomal DNA and all other polynucleotides except poly(dA).poly(dT). Similar thermodynamic features were also reported with SGR and EtBr (Hossain and Suresh Kumar, 2010). However, there is a discrepancy in the values of dissociation constant obtained by the two methods (spectroscopy and ITC) similar to that is observed in case of CHL-chromatin interaction. It can be attributed to the higher concentration of the ligand employed in ITC experiments to obtain reliable values of enthalpy changes during the calorimetric titration. Similar discrepancy has earlier been reported for the interaction of Hoechst 33258 to the d(CGCAAATTTGCG)<sub>2</sub> duplex (Haq et al., 1997).

Heat capacity ( $\Delta C_p$ ) values are indicative of structural alterations that occur in the DNA/ polynucleotide due to ligand binding (Haq, 2002, Ren et al., 2000, Ha et al., 1989). Negative  $\Delta C_p$  values are observed for association of CHL with chromosomal DNA, poly(dG-dC), poly(dG).poly(dC) and poly(dA-dT). Negative  $\Delta C_p$  values are associated with release of structured water molecule present in the hydrophobic region of the nucleic acid with transfer of hydrophobic aromatic groups into interior of the helix (Haq, 2002, Ren et al., 2000). The strikingly low magnitude of  $\Delta C_p$  in case of poly(dG).poly(dC) indicates that no major structural change takes place when the ligand intercalates into it via the minor groove. Since poly(dG).poly(dC), has a A-DNA

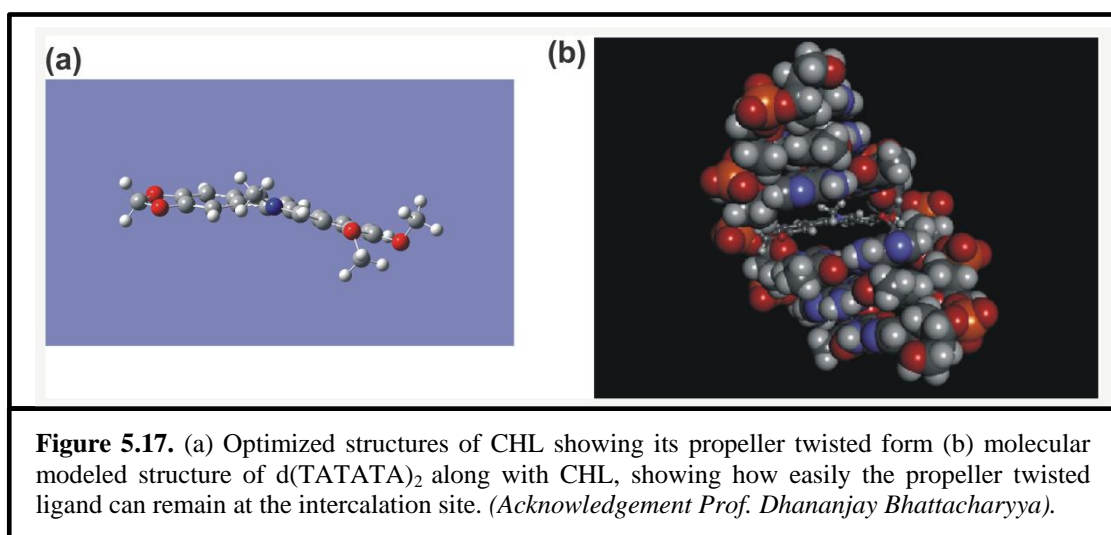
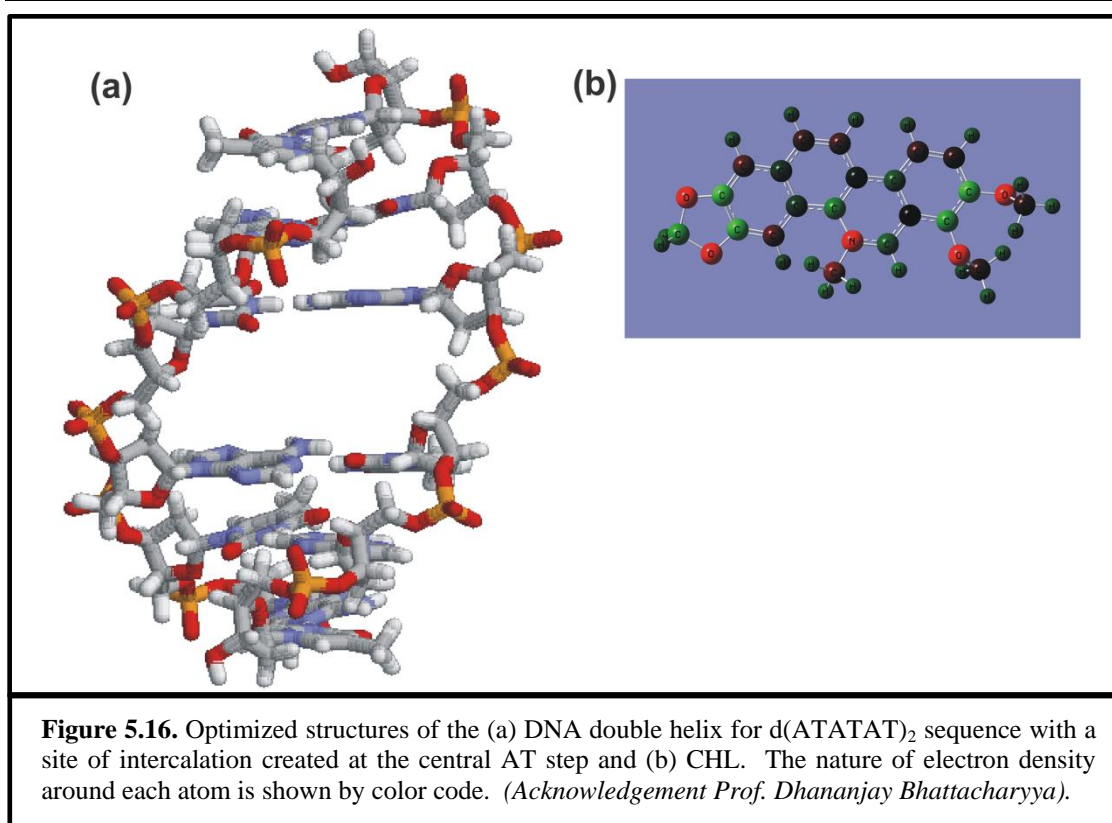
structure, characterized by a C3'-endo furanose ring and a wider (about 11 Å) and shallower minor groove (Majee et al., 1997) which easily accommodates CHL without any significant structural alteration. The negative  $\Delta H$ -value is maximum for poly(dG).poly(dC) because the contribution from  $\Delta H_{\text{DNA}}$  is comparatively less. On the other hand in case of poly(dA).poly(dT), it requires considerable structural alteration to accommodate CHL approaching from minor groove as it has very narrow minor groove with high structural rigidity, hence the reverse trend of  $\Delta C_p$  in case of association with this polynucleotide.

Spectroscopic and calorimetric studies show that similar type of interaction occurs between CHL and chromosomal DNA, poly(dG-dC) and poly(dA-dT). This can be attributed to the fact that they all possess a similar structure which is the classical B-DNA structure. On the contrary the interaction of poly(dG).poly(dC) and poly(dA).poly(dT) with CHL is strikingly different. Poly(dG).poly(dC) has a higher affinity for CHL as compared to the other macromolecules used. Additionally, CHL can displace EtBr from the EtBr- poly (dG).poly(dC) complex at very low concentration as evident from the low  $IC_{50}$  value (Figure 5.10b). Poly(dA).poly(dT) on the other hand has a lower affinity for CHL with distinctly different thermodynamic features. But it has an  $IC_{50}$  value for EtBr displacement comparable to that of poly(dG).poly(dC). This difference in the association features can also be attributed to the structures adopted by poly(dG).poly(dC) and poly(dA).poly(dT). The wide shallow minor groove of poly(dG).poly(dC) facilitates easy access of CHL through minor groove resulting in (a) higher affinity (b) higher  $\Delta H$  (c) lower  $\Delta C_p$  (d) least structural perturbation in DNA and (e) low  $IC_{50}$  value. On the contrary for poly (dA).poly(dT) which has a very narrow minor groove in a rigid bent structure. CHL binding through minor groove is

unfavorable leading to low affinity. This binding phenomena alters the structure of poly (dA).poly(dT) which is manifested in CD and also the high  $\Delta C_p$  value. The alteration in the structure of poly (dA).poly(dT) due to CHL accessing through the minor groove enables easy EtBr displacement and concurrent low  $IC_{50}$  value.

Based on the results obtained from the above mentioned experiments, we have followed a preliminary model to propose the geometry at the site of the intercalation. DNA double helical structures generally have base pairs with negative propeller twist and hence we generated the structures having -20 degree propeller twist. The base pairs at the intercalation site also is expected to have such propeller twist values, hence, the site is not uniform (Figure 16a). The optimized structure of the ligand also has a negative propeller like motion, to avoid steric clash between the N-CH<sub>3</sub> with the neighboring C-H groups (Figure 5.17a). Thus, the ligand can freely get inserted into the site of interest, as shown in Figure 5.17b. Analysis of partial charge, calculated by various methods, indicates that the extra positive charge is distributed throughout the molecule and most of the hydrogen atoms have reasonably high positive charge (Figure 5.16a). So, the ligand molecule can be easily attracted by the negative electrostatic potential of minor groove of DNA.

After characterization of the binding of CHL with naked chromosomal DNA, we went on to study the association of CHL with different structural levels of chromatin by employing various spectroscopic methods. Change in absorption spectrum of free CHL upon addition of chromatin, chromatosome, nucleosome and chromosomal DNA originates from the complex formation between them (Figure 5.17a). Broadening and red shifting of the absorption spectra of CHL may be ascribed to the delocalization of



$\pi$ - electrons in CHL as a result of binding between the base pairs of DNA (Li et al., 2012). Observed blue shift of fluorescence peak of CHL could be attributed to the

---

stabilization of ground and/or excited-state of CHL upon intercalation with DNA base pairs (Figure 5.17b)(Selvi B et al., 2009, Luger et al., 1997).

The binding parameters for the association of CHL with chromatin and its components (Table 5.6) imply that the presence of histone proteins in chromatin, chromatosome and nucleosome reduces the accessibility of CHL for DNA. The minor grooves of DNA in chromatosome are occupied by the side chains of histone, which reduces the accessibility of CHL molecule that intercalates into the DNA base pair accessing via the minor groove (Luger et al., 1997). Comparison of the binding affinity and stoichiometry of CHL among chromatin, chromatosome and nucleosome suggest that CHL binds to linker DNA as well, although it does not bind to linker histone H1. This feature of the association is similar to other DNA-binding intercalator like EtBr and groove binder such as mithramycin (Mir and Dasgupta, 2001, Banerjee et al., 2014). A similar trend in apparent dissociation constants ( $K_d^{app}$ ) is also observed from ITC measurements. Release of bound water molecules present in the chromatin/ chromatosome / nucleosome structure accounts for the entropy driven binding of CHL with them. Conformational entropy change of chromatin/ chromatosome / nucleosome as a result of association with CHL could be another potential source of positive enthalpy change. However, for chromosomal DNA the association with CHL is favored by both enthalpy and entropy contributions. Difference in the thermodynamic feature of the association can be ascribed to the presence of associated histones in chromatin, chromatosome and nucleosome. The negative enthalpy change from intercalation into the DNA base pair is offset by the positive enthalpy change arising from the alteration in the histone-DNA interaction as a sequel to the intercalation of CHL molecule in the base pairs of chromosomal DNA.

---

The effect of CHL on the structure of chromatin and its components has also been studied by CD spectroscopy (Figure 5.14). The increase in positive CD bands of chromatin at 272 nm with the increasing concentrations of CHL, could be ascribed to the intercalation of CHL molecule into DNA pair present in the chromatin/chromatosome (Selvi B et al., 2009, Vergani et al., 1994). Optically asymmetric and non-identical environment of naked DNA and DNA wrapped with histone octamer (chromatin and chromatosome) gives rise to the different shape and intensity of induced CD band (Figure 5.14d) (Selvi B et al., 2009). Presence of linker DNA give rise to higher molar ellipticity of the induced CD bands for chromatin-CHL complex compared to the same for chromatosome. At chromatosome level CHL disrupts DNA-histone integrity triggering DNA release (Figure 5.15). In this chapter we have reported the association of CHL with different structural levels of chromatin and various polynucleotides with different base sequences, emphasizing the necessity for exploring additional biological potential of CHL.

---

# Chapter 6

**Summary**

---

The present thesis is an attempt to understand the chemical biology of action of two aureolic acid antibiotics, mithramycin (MTR) and chromomycin A3 (CHR) and one plant alkaloid chelerythrine (CHL). Physico-chemical properties of antibiotics play important roles in absorption and distribution of them across cell membranes. The following factors control the mechanism by which antibiotics pass through membranes: size and shape of the antibiotic, degree of ionization, state of aggregation and relative lipid solubility of its ionized and neutral forms. In **chapter 2** we have studied the difference in the ionization properties of the antibiotics, MTR and CHR. We have estimated by means of optical spectroscopic methods, the ionization constants ( $pK_a$ ) of MTR and CHR. MTR and CHR are weak acids of  $pK_a$  5.5 and 7.0 respectively. Despite the presence of two phenol groups (C8 and C9 positions) only one  $pK_a$  was observed for MTR and CHR. This is ascribed to the fact that intra molecular hydrogen bonding stabilizes the mono-anionic form of the antibiotics. We have also estimated the heat of ionization of MTR and CHR by employing calorimetric techniques. Heat of ionization of MTR is higher from that of CHR. Broadening of NMR spectra of MTR and CHR at pH 3.0 supports our proposition of protonation at C1 carbonyl oxygen, which leads to the exchange of aromatic proton with solvent water molecule. Different sugars and specific modifications of the sugars are responsible for the different ionization property of MTR and CHR. Many bioactive natural products are glycosylated compounds in which the sugar moieties are essential for their biological activity. Biosynthesis of chromomycin A3 requires two acetylation steps and one methylation step which contribute to the biological activity of it. Different sugars and modifications like acetylation and methylation in CHR are proposed to be responsible for the difference in the ionization properties of the two antibiotics.

---



---

Previous reports from our laboratory have shown that anionic form of MTR self-associates in physiological condition (pH 7.4). CHR has mixed population of anionic and neutral forms at pH 7.4. In **chapter 3** we have examined the self-association of both in neutral and in anionic forms of CHR by means of spectroscopic and calorimetric techniques. Our study has characterized the oligomerization ( $n = 2$  to  $4$ ) of neutral and anionic forms of CHR in buffers of pH 5.0 and 9.0. Dimerization of neutral and anionic forms of CHR starts at much lower concentrations ( $< 10 \mu\text{M}$ ) compared to MTR; in contrast tetramerisation is the predominant process for MTR in both neutral as well as anionic forms. From  $^1\text{H}$  NMR studies it was observed that, sugar moieties attached to their aglycone part in CHR and MTR play key roles in the self association process. The difference in the sugar substituents present in CHR and MTR give rise to the alteration of self aggregation pattern in aqueous solution. The most important feature emerging from the present study shows that the different carbohydrate moieties present in the same class of antibiotics might give rise to a difference in intracellular state of molecular forms (monomer or aggregate) and hence altered biological activity.

In **chapter 4** we have focused our studies to understand the divalent transition metal ion binding property of MTR. After analyzing the results obtained from **chapter 4**, we have concluded that MTR forms single type of complex with  $\text{Mn}^{2+}$ , which has a stoichiometry of 2:1 with respect to  $\text{MTR}:\text{Mn}^{2+}$  with an apparent binding affinity in the micro molar range.  $[(\text{MTR})_2 \text{Mn}^{2+}]$  has similar structures with those of  $[(\text{MTR})_2 \text{Mg}^{2+}]$  and  $[(\text{MTR})_2 \text{Zn}^{2+}]$ , where the metal ion has octahedral coordination. Calorimetric study shows that the reaction between MTR and  $\text{Mn}^{2+}$  is exothermic in nature and enthalpy driven at room temperature.  $[(\text{MTR})_2 \text{Mn}^{2+}]$  bind to chromatin and chromosomal DNA, the affinity of association being higher for DNA.  $[(\text{MTR})_2 \text{Mn}^{2+}]$

---

---

complex could access the double helical DNA via minor groove with GC base specificity. Presence of histone proteins in chromatin hinders the accessibility of the complex for minor groove of DNA. Our study also shows that MTR binds to  $Mn^{2+}$ -containing metalloenzyme manganese superoxide dismutase without inhibiting its enzymatic activity. The significance of these results from the perspective of mode of action of MTR inside the cell has been discussed.

Nature, particularly the plant kingdom is an important resource as human medicine. Quaternary benzo[c]phenanthridine alkaloids (QBA) from the plant source exhibit various bioactivities such as anti-inflammatory, antitumor, SH-enzymes inhibition, and antiplaque effect. These alkaloids are potential DNA-targeting agents as they possess poly-aromatic planar structure with quaternary nitrogen atoms attached to them. Chelerythrine (CHL), a member of QBA group of alkaloids, is known as a specific protein kinase C inhibitor and putative anticancer agent. In **chapter 5** we have shown that CHL binds to chromosomal DNA and different DNA sequences namely poly(dG-dC), poly(dG).poly(dC), poly(dA-dT), poly(dA).poly(dT). The results show that association of CHL with polynucleotide is sequence dependent. CHL exhibits different fluorescence properties in presence of (A.T) and (G.C) containing polynucleotides. Thermodynamic parameters for the association of CHL with different sequences of DNA except poly(dA).pol(dT), suggest that both enthalpy and entropy contribute in a favorable way to the negative free energy change associated with complex formation. Since in physiological condition chromosomal DNA is present in association with various proteins in the form of chromatin, we have extended our studies in the context of association of CHL with different structural levels of chromatin. We have observed that CHL binds with chromatin long fragment, chromatosome, nucleosome and

---

chromosomal DNA. Presence of associated histone proteins in chromatin and chromatosome has a negative effect upon DNA-binding potential of CHL. Therefore our present work helps us to understand an alternate mode of action of CHL for exhibiting antitumor property. Overall, the results of present work suggest that CHL is a putative anticancer agent.

---

# References

- 
- A**ICH, P. & DASGUPTA, D. 1995. Role of magnesium ion in mithramycin-DNA interaction: binding of mithramycin-Mg<sup>2+</sup> complexes with DNA. *Biochemistry*, 34, 1376-85.
- AICH, P., SEN, R. & DASGUPTA, D. 1992. Role of magnesium ion in the interaction between chromomycin A3 and DNA: binding of chromomycin A3-Mg<sup>2+</sup> complexes with DNA. *Biochemistry*, 31, 2988-97.
- ALBERTINI, V., JAIN, A., VIGNATI, S., NAPOLI, S., RINALDI, A., KWEE, I., NUR-E-ALAM, M., BERGANT, J., BERTONI, F., CARBONE, G. M., ROHR, J. & CATAPANO, C. V. 2006. Novel GC-rich DNA-binding compound produced by a genetically engineered mutant of the mithramycin producer *Streptomyces argillaceus* exhibits improved transcriptional repressor activity: implications for cancer therapy. *Nucleic Acids Res*, 34, 1721-34.
- ANSARI, K. M., DHAWAN, A., KHANNA, S. K. & DAS, M. 2006. Protective effect of bioantioxidants on argemone oil/sanguinarine alkaloid induced genotoxicity in mice. *Cancer Lett*, 244, 109-18.
- ASCHNER, M., ERIKSON, K. M. & DORMAN, D. C. 2005. Manganese dosimetry: species differences and implications for neurotoxicity. *CRC Critical Reviews in Toxicology*, 35, 1-32.
- ASCHNER, M., GUILARTE, T. R., SCHNEIDER, J. S. & ZHENG, W. 2007. Manganese: recent advances in understanding its transport and neurotoxicity. *Toxicology and applied pharmacology*, 221, 131-147.
- AU, C., BENEDETTO, A. & ASCHNER, M. 2008. Manganese transport in eukaryotes: the role of DMT1. *Neurotoxicology*, 29, 569-576.
- AULD, D. S. 2001. Zinc coordination sphere in biochemical zinc sites. *Zinc Biochemistry, Physiology, and Homeostasis*. Springer.
- B**AI, L. P., CAI, Z., ZHAO, Z. Z., NAKATANI, K. & JIANG, Z. H. 2008. Site-specific binding of chelerythrine and sanguinarine to single pyrimidine bulges in hairpin DNA. *Anal Bioanal Chem*, 392, 709-16.
- BAI, L. P., ZHAO, Z. Z., CAI, Z. & JIANG, Z. H. 2006. DNA-binding affinities and sequence selectivity of quaternary benzophenanthridine alkaloids sanguinarine, chelerythrine, and nitidine. *Bioorg Med Chem*, 14, 5439-45.
- BALTZ, R. 2005. Antibiotic discovery from actinomycetes: will a renaissance follow the decline and fall. *SIM News*, 55, 186-196.
- BALTZ, R. H. 2006. Marcel Faber Roundtable: is our antibiotic pipeline unproductive because of starvation, constipation or lack of inspiration? *Journal of Industrial Microbiology and Biotechnology*, 33, 507-513.
- BANERJEE, A., MAJUMDER, P., SANYAL, S., SINGH, J., JANA, K., DAS, C. & DASGUPTA, D. 2014. The DNA intercalators ethidium bromide and propidium iodide also bind to core histones. *FEBS open bio*, 4, 251-259.
-

- BANERJEE, A., SINGH, J. & DASGUPTA, D. 2013. Fluorescence spectroscopic and calorimetry based approaches to characterize the mode of interaction of small molecules with DNA. *J Fluoresc*, 23, 745-52.
- BANNISTER, J. V., BANNISTER, W. H. & ROTILIO, G. 1987. Aspects of the structure, function, and applications of superoxide dismutase. *Critical Reviews in Biochemistry and Molecular Biology*, 22, 111-180.
- BANVILLE, D. L., KENIRY, M. A., KAM, M. & SHAFER, R. H. 1990. NMR studies of the interaction of chromomycin A3 with small DNA duplexes. Binding to GC-containing sequences. *Biochemistry*, 29, 6521-34.
- BASU, P., BHOWMIK, D. & SURESH KUMAR, G. 2013. The benzophenanthridine alkaloid chelerythrine binds to DNA by intercalation: Photophysical aspects and thermodynamic results of iminium versus alkanolamine interaction. *Journal of Photochemistry and Photobiology B: Biology*, 129, 57-68.
- BEAM, M. P., BOSSERMAN, M. A., NOINAJ, N., WEHENKEL, M. & ROHR, J. 2009a. Crystal structure of Baeyer-Villiger monooxygenase MtmOIV, the key enzyme of the mithramycin biosynthetic pathway. *Biochemistry*, 48, 4476-87.
- BEAM, M. P., BOSSERMAN, M. A., NOINAJ, N., WEHENKEL, M. & ROHR, J. R. 2009b. Crystal structure of Baeyer-Villiger monooxygenase MtmOIV, the key enzyme of the mithramycin biosynthetic pathway. *Biochemistry*, 48, 4476.
- BERG, J. M. & GODWIN, H. A. 1997. Lessons from zinc-binding peptides. *Annual review of biophysics and biomolecular structure*, 26, 357-371.
- BHADRA, K., MAITI, M. & KUMAR, G. S. 2007. Molecular recognition of DNA by small molecules: AT base pair specific intercalative binding of cytotoxic plant alkaloid palmatine. *Biochim Biophys Acta*, 1770, 1071-80.
- BHATTACHARYYA, D. & BANSAL, M. 1990. Local variability and base sequence effects in DNA crystal structures. *Journal of Biomolecular Structure and Dynamics*, 8, 539-572.
- BIANCHI, N., CHIARABELLI, C., BORGATTI, M., MISCHIATI, C., FIBACH, E. & GAMBARI, R. 2001. Accumulation of  $\gamma$ -globin mRNA and induction of erythroid differentiation after treatment of human leukaemic K562 cells with tallimustine. *British journal of haematology*, 113, 951-961.
- BIANCHI, N., ONGARO, F., CHIARABELLI, C., GUALANDI, L., MISCHIATI, C., BERGAMINI, P. & GAMBARI, R. 2000. Induction of erythroid differentiation of human K562 cells by cisplatin analogs. *Biochemical pharmacology*, 60, 31-40.
- BLACK, A. R., BLACK, J. D. & AZIZKHAN-CLIFFORD, J. 2001. Sp1 and kruppel-like factor family of transcription factors in cell growth regulation and cancer. *J Cell Physiol*, 188, 143-60.
- BLACKBURN, G. M. 2006. *Nucleic acids in chemistry and biology*, Royal Society of Chemistry.
-

BLANCO, G., FERNÁNDEZ, E., FERNÁNDEZ, M. J., BRAÑA, A., WEISSBACH, U., KÜNZEL, E., ROHR, J., MÉNDEZ, C. & SALAS, J. 2000. Characterization of two glycosyltransferases involved in early glycosylation steps during biosynthesis of the antitumor polyketide mithramycin by *Streptomyces argillaceus*. *Molecular and General Genetics MGG*, 262, 991-1000.

BLANCO, G., FU, H., MENDEZ, C., KHOSLA, C. & SALAS, J. A. 1996. Deciphering the biosynthetic origin of the aglycone of the aureolic acid group of anti-tumor agents. *Chemistry & biology*, 3, 193-196.

BLOBEL, G. & POTTER, V. R. 1966. Nuclei from rat liver: isolation method that combines purity with high yield. *Science*, 154, 1662-1665.

BLUMAUEROVÁ, M., LIPAVSKÁ, H., STAJNER, K. & VANĚK, Z. 1976. The study of variability and strain selection in *Streptomyces atroolivaceus*. *Folia microbiologica*, 21, 285-293.

BLUME, S. W., SNYDER, R. C., RAY, R., THOMAS, S., KOLLER, C. A. & MILLER, D. M. 1991. Mithramycin inhibits SP1 binding and selectively inhibits transcriptional activity of the dihydrofolate reductase gene in vitro and in vivo. *J Clin Invest*, 88, 1613-21.

BOSSERMAN, M. A., FLOREZ, A. B., SHAABAN, K. A., BRANA, A. F., SALAS, J. A., MENDEZ, C. & ROHR, J. R. 2011. Characterization of the terminal activation step catalyzed by oxygenase CmmOIV of the chromomycin biosynthetic pathway from *Streptomyces griseus*. *Biochemistry*, 50, 1421-1428.

BRAZHNIKOVA, M., KRUGLIAK, E., KOVSHAROVA, I., KONSTANTINOVA, N. & PROSHLIAKOVA, V. 1962. Isolation, purification and study on some physico-chemical properties of a new antibiotic olivomycin. *Antibiotiki*, 7, 39.

CALABRESI, P., CHABNER, B. A., HARDMAN, L. E. & LIMBARD, L. E. 1991. *Goodman and Gilman's the pharmacological basis of therapeutics: Chemotherapy of neoplastic disease*, New York, Macmillan.

CALABRESI, P. & PARKS, R. E. 1985. *Goodman and Gilman's the pharmacological basis of therapeutics*, New York, Macmillan.

CAMPBELL, V. W., DAVIN, D., THOMAS, S., JONES, D., ROESEL, J., TRAN-PATTERSON, R., MAYFIELD, C. A., RODU, B., MILLER, D. M. & HIRAMOTO, R. A. 1994. The G-C specific DNA binding drug, mithramycin, selectively inhibits transcription of the C-MYC and C-HA-RAS genes in regenerating liver. *The American Journal of the Medical Sciences*, 307, 167-72.

CHAIRES, J. B. 1997. Energetics of drug–DNA interactions. *Biopolymers*, 44, 201-215.

CHAIRES, J. B., DATTAGUPTA, N. & CROTHERS, D. M. 1982. Self-association of daunomycin. *Biochemistry*, 21, 3927-32.

CHAKRABARTI, S., BHATTACHARYYA, B. & DASGUPTA, D. 2002. Interaction of Mithramycin and Chromomycin A3 with d (TAGCTAGCTA)<sub>2</sub>: Role of Sugars in Antibiotic-DNA Recognition. *The Journal of Physical Chemistry B*, 106, 6947-6953.

- 
- CHAKRABARTI, S., BHATTACHARYYA, D. & DASGUPTA, D. 2000. Structural basis of DNA recognition by anticancer antibiotics, chromomycin A3, and mithramycin: Roles of minor groove width and ligand flexibility. *Biopolymers*, 56, 85-95.
- CHAKRABARTI, S., BHATTACHARYYA, D. & DASGUPTA, D. 2001. Structural basis of DNA recognition by anticancer antibiotics, chromomycin A3, and mithramycin: Roles of minor groove width and ligand flexibility. *Biopolymers*, 56, 85-95.
- CHAKRABORTY, H., DEVI, P. G., SARKAR, M. & DASGUPTA, D. 2008. Multiple functions of generic drugs: future perspectives of aureolic acid group of anti-cancer antibiotics and non-steroidal anti-inflammatory drugs. *Mini Reviews in Medicinal Chemistry*, 8, 331-49.
- CHAN, J., KKAN, S., HARVEY, I., MERRICK, W. & PELLETIER, J. 2004. Eukaryotic protein synthesis inhibitors identified by comparison of cytotoxicity profiles. *Rna*, 10, 528-543.
- CHAN, S. L., LEE, M. C., TAN, K. O., YANG, L. K., LEE, A. S., FLOTOW, H., FU, N. Y., BUTLER, M. S., SOEJARTO, D. D., BUSS, A. D. & YU, V. C. 2003. Identification of chelerythrine as an inhibitor of BclXL function. *J Biol Chem*, 278, 20453-6.
- CHAN, S. S., AUSTIN, R. H., MUKERJI, I. & SPIRO, T. G. 1997. Temperature-dependent ultraviolet resonance Raman spectroscopy of the premelting state of dA.dT DNA. *Biophys J*, 72, 1512-20.
- CHANDRA, S. & SHUKLA, G. 1981. Concentrations of striatal catecholamines in rats given manganese chloride through drinking water. *Journal of neurochemistry*, 36, 683-687.
- CHANDRASEKARAN, R. & ARNOTT, S. 1989. The structures of DNA and RNA helices in oriented fibers. *Landolt-Börnstein Numerical Data and Functional Relationships in Science and Technology*, 7, 31-170.
- CHANDRASEKARAN, R., WANG, M., HE, R.-G., PUIGJANER, L., BYLER, M., MILLANE, R. & ARNOTT, S. 1989. A re-examination of the crystal structure of A-DNA using fiber diffraction data. *Journal of Biomolecular Structure and Dynamics*, 6, 1189-1202.
- CHATTERJEE, S., ZAMAN, K., RYU, H., CONFORTO, A. & RATAN, R. R. 2001. Sequence-selective DNA binding drugs mithramycin A and chromomycin A3 are potent inhibitors of neuronal apoptosis induced by oxidative stress and DNA damage in cortical neurons. *Ann Neurol*, 49, 345-54.
- CHMURA, S. J., DOLAN, M. E., CHA, A., MAUCERI, H. J., KUFE, D. W. & WEICHELBAUM, R. R. 2000. In vitro and in vivo activity of protein kinase C inhibitor chelerythrine chloride induces tumor cell toxicity and growth delay in vivo. *Clin Cancer Res*, 6, 737-42.
- CLARDY, J., FISCHBACH, M. A. & WALSH, C. T. 2006. New antibiotics from bacterial natural products. *Nature biotechnology*, 24, 1541-1550.
- CONDON, J. R., REITH, S., NASSIM, J., MILLARD, F., HILB, A. & STAINTHORPE, E. 1971. Treatment of Paget's disease of bone with mithramycin. *British medical journal*, 1, 421.
- COQUERET, O. 2003. New roles for p21 and p27 cell-cycle inhibitors: a function for each cell compartment? *Trends in cell biology*, 13, 65-70.
-



COUPER, J. 1837. On the effects of black oxide of manganese when inhaled into the lungs. *Br Ann Med Pharmacol*, 1, 41-42.

CRAGG, G. M. 1998. Paclitaxel (Taxol®): A success story with valuable lessons for natural product drug discovery and development. *Medicinal research reviews*, 18, 315-331.

CRAGG, G. M. & NEWMAN, D. J. 2004. A tale of two tumor targets: topoisomerase I and tubulin. The Wall and Wani contribution to cancer chemotherapy. *Journal of Natural Products*, 67, 232-244.

CRAGG, G. M. & NEWMAN, D. J. 2005. Plants as a source of anti-cancer agents. *Journal of ethnopharmacology*, 100, 72-79.

CROSSGROVE, J. S., ALLEN, D. D., BUKAVECKAS, B. L., RHINEHEIMER, S. S. & YOKEL, R. A. 2003. Manganese distribution across the blood-brain barrier: I. Evidence for carrier-mediated influx of manganese citrate as well as manganese and manganese transferrin. *Neurotoxicology*, 24, 3-13.

CSEKE, L. J., KIRAKOSYAN, A., KAUFMAN, P. B., WARBER, S., DUKE, J. A. & BRIELMANN, H. L. 2006. *Natural products from plants*, CRC Press.

**D**A ROCHA, A. B., LOPES, R. M. & SCHWARTSMANN, G. 2001. Natural products in anticancer therapy. *Current Opinion in Pharmacology*, 1, 364-369.

DAS, S. & DASGUPTA, D. 2005. Binding of  $(\text{MTR})_2\text{Zn}^{2+}$  complex to chromatin: a comparison with  $(\text{MTR})_2\text{Mg}^{2+}$  complex. *Journal of Inorganic Biochemistry*, 99, 707-15.

DEMICHELI, C., ALBERTINI, J. P. & GARNIER-SUILLEROT, A. 1991a. Interaction of mithramycin with DNA. Evidence that mithramycin binds to DNA as a dimer in a right-handed screw conformation. *European Journal of Biochemistry*, 198, 333-8.

DEMICHELI, C., ALBERTINI, J. P. & GARNIER-SUILLEROT, A. 1991b. Interaction of mithramycin with DNA. Evidence that mithramycin binds to DNA as a dimer in a right-handed screw conformation. *Eur J Biochem*, 198, 333-8.

DENNY, W. A. 1989. DNA-intercalating ligands as anti-cancer drugs: prospects for future design. *Anticancer Drug Des*, 4, 241-63.

DEVI, P. G., CHAKRABORTY, P. K. & DASGUPTA, D. 2009a. Inhibition of a Zn (II)-containing enzyme, alcohol dehydrogenase, by anticancer antibiotics, mithramycin and chromomycin A 3. *Journal of Biological Inorganic Chemistry*, 14, 347-359.

DEVI, P. G., CHAKRABORTY, P. K. & DASGUPTA, D. 2009b. Inhibition of a Zn(II)-containing enzyme, alcohol dehydrogenase, by anticancer antibiotics, mithramycin and chromomycin A3. *Journal of Biological Inorganic Chemistry*, 14, 347-59.

DEVI, P. G., PAL, S., BANERJEE, R. & DASGUPTA, D. 2007. Association of antitumor antibiotics, mithramycin and chromomycin, with Zn(II). *J Inorg Biochem*, 101, 127-37.

DEWICK, P. M. 2011. *Medicinal natural products: a biosynthetic approach*, John Wiley & Sons.

DIAS, D. A., URBAN, S. & ROESSNER, U. 2012. A historical overview of natural products in drug discovery. *Metabolites*, 2, 303-336.

**E**GOROV, N. S. 1985. *Antibiotic, a Scientific Approach* Moscow, MIR Publisher.

ELDER, A. L. 1970. History of penicillin production.

ELDIN, S. & JENCKS, W. P. 1995. Lifetimes of iminium ions in aqueous solution. *Journal of the American Chemical Society*, 117, 4851-4857.

ERMLER, U., GRABARSE, W., SHIMA, S., GOUBEAUD, M. & THAUER, R. K. 1998. Active sites of transition-metal enzymes with a focus on nickel. *Current opinion in structural biology*, 8, 749-758.

ESBRIT, P. & HURTADO, J. 2002. Treatment of malignant hypercalcaemia. *Expert opinion on pharmacotherapy*, 3, 521-527.

EVANS, W. C. 2009. *Trease and Evans' pharmacognosy*, Elsevier Health Sciences.

**F**ABRE, N., CLAPAROLS, C., RICHELME, S., ANGELIN, M.-L., FOURASTÉ, I. & MOULIS, C. 2000. Direct characterization of isoquinoline alkaloids in a crude plant extract by ion-pair liquid chromatography–electrospray ionization tandem mass spectrometry: example of *Eschscholtzia californica*. *Journal of Chromatography A*, 904, 35-46.

FARINA, M., AVILA, D. S., DA ROCHA, J. B. T. & ASCHNER, M. 2013. Metals, oxidative stress and neurodegeneration: a focus on iron, manganese and mercury. *Neurochemistry international*, 62, 575-594.

FERRANTE, R. J., RYU, H., KUBILUS, J. K., D'MELLO, S., SUGARS, K. L., LEE, J., LU, P., SMITH, K., BROWNE, S. & BEAL, M. F. 2004. Chemotherapy for the brain: the antitumor antibiotic mithramycin prolongs survival in a mouse model of Huntington's disease. *The Journal of neuroscience*, 24, 10335-10342.

FIBACH, E., BIANCHI, N., BORGATTI, M., PRUS, E. & GAMBARI, R. 2003. Mithramycin induces fetal hemoglobin production in normal and thalassemic human erythroid precursor cells. *Blood*, 102, 1276-1281.

FLEMING, A. 1929. On the antibacterial action of cultures of a penicillium, with special reference to their use in the isolation of *B. influenzae*. *British journal of experimental pathology*, 10, 226.

FLETCHER, T. M. & HANSEN, J. C. 1996. The nucleosomal array: structure/function relationships. *Critical Reviews™ in Eukaryotic Gene Expression*, 6.

FLETCHER, W. 1973. Chemotherapy of testicular germinal tumors. *Oncology*, 28, 147-163.

FRIDOVICH, I. 1975. Superoxide dismutases. *Annual Review of Biochemistry*, 44, 147-59.

FRIDOVICH, I. 1997. Superoxide Anion Radical ( $\text{O}_2^{\cdot-}$ ), Superoxide Dismutases, and Related Matters. *Journal of Biological Chemistry*, 272, 18515-18517.

FRIEDMAN, B., FREELAND-GRAVES, J. H., BALES, C. W., BEHMARDI, F., SHOREY-KUTSCHKE, R. L., WILLIS, R. A., CROSBY, J. B., TRICKETT, P. C. & HOUSTON, S. D. 1987. Manganese balance and clinical observations in young men fed a manganese-deficient diet. *The Journal of nutrition*, 117, 133-143.

**G**AO, X. & PATEL, D. J. 1989. Solution structure of the chromomycin-DNA complex. *Biochemistry*, 28, 751-762.

GAO, X. & PATEL, D. J. 1990. Chromomycin dimer-DNA oligomer complexes. Sequence selectivity and divalent cation specificity. *Biochemistry*, 29, 10940-10956.

GAO, Y., JIA, Z., KONG, X., LI, Q., CHANG, D. Z., WEI, D., LE, X., SUYUN, H., HUANG, S., WANG, L. & XIE, K. 2011. Combining betulinic acid and mithramycin a effectively suppresses pancreatic cancer by inhibiting proliferation, invasion, and angiogenesis. *Cancer Res*, 71, 5182-93.

GARBETT, N. C., HAMMOND, N. B. & GRAVES, D. E. 2004. Influence of the amino substituents in the interaction of ethidium bromide with DNA. *Biophys J*, 87, 3974-81.

GARCIA-RAMIREZ, M., LEUBA, S. H. & AUSIO, J. 1990. One-step fractionation method for isolating H1 histones from chromatin under nondenaturing conditions. *Protein expression and purification*, 1, 40-44.

GASPAR, N., DI GIANNATALE, A., GEOERGER, B., REDINI, F. O., CORRADINI, N. G., ENZ-WERLE, N., TIRODE, F., MAREC-BERARD, P., GENTET, J.-C. & LAURENCE, V. R. 2012. Bone sarcomas: from biology to targeted therapies. *Sarcoma*, 2012, 1-18.

GAVIN, C. E., GUNTER, K. K. & GUNTER, T. E. 1992.  $Mn^{2+}$  sequestration by mitochondria and inhibition of oxidative phosphorylation. *Toxicology and applied pharmacology*, 115, 1-5.

GHOSH, S., MAJUMDER, P., PRADHAN, S. K. & DASGUPTA, D. 2010. Mechanism of interaction of small transcription inhibitors with DNA in the context of chromatin and telomere. *Biochim Biophys Acta*, 1799, 795-809.

GHOSH, S., PRADHAN, S. K., KAR, A., CHOWDHURY, S. & DASGUPTA, D. 2013. Molecular basis of recognition of quadruplexes human telomere and c-myc promoter by the putative anticancer agent sanguinarine. *Biochimica et Biophysica Acta (BBA)-General Subjects*, 1830, 4189-4201.

GIANNI, L., CORDEN, B. J. & MYERS, C. E. 1983. The biochemical basis of anthracycline toxicity and antitumor activity. *Rev. Biochem. Toxicol*, 5.

GIBSON, M., NUR-E-ALAM, M., LIPATA, F., OLIVEIRA, M. A. & ROHR, J. 2005. Characterization of Kinetics and Products of the Baeyer-Villiger Oxygenase MtmOIV, The Key Enzyme of the Biosynthetic Pathway toward the Natural Product Anticancer Drug Mithramycin from *Streptomyces aegilaceus*. *Journal of the American Chemical Society*, 127, 17594-17595.

GIEDROC, D. P. & ARUNKUMAR, A. I. 2007. Metal sensor proteins: nature's metalloregulated allosteric switches. *Dalton Transactions*, 3107-3120.

GILLESPIE, S. K., ZHANG, X. D. & HERSEY, P. 2004. Ingenol 3-angelate induces dual modes of cell death and differentially regulates tumor necrosis factor-related apoptosis-inducing ligand-induced apoptosis in melanoma cells. *Molecular cancer therapeutics*, 3, 1651-1658.

GIRIJASHANKER, K., HE, L., SOLEIMANI, M., REED, J. M., LI, H., LIU, Z., WANG, B., DALTON, T. P. & NEBERT, D. W. 2008. Slc39a14 gene encodes ZIP14, a metal/bicarbonate symporter: similarities to the ZIP8 transporter. *Molecular pharmacology*, 73, 1413-1423.

GOCHIN, M. 1998. Nuclear magnetic resonance characterization of a paramagnetic DNA-drug complex with high spin cobalt; assignment of the <sup>1</sup>H and <sup>31</sup>P NMR spectra, and determination of electronic, spectroscopic and molecular properties. *Journal of Biomolecular NMR*, 12, 243-57.

GOLDBERG, I. H. & FRIEDMAN, P. 1971. Antibiotics and nucleic acids. *Annual review of biochemistry*, 40, 775-810.

GOLDSTEIN, S., MEYERSTEIN, D. & CZAPSKI, G. 1993. The fenton reagents. *Free Radical Biology and Medicine*, 15, 435-445.

GONZALEZ, A., REMSING, L., LOMBÓ, F., FERNÁNDEZ, M., PRADO, L., BRAÑA, A., KÜNZEL, E., ROHR, J., MÉNDEZ, C. & SALAS, J. A. 2001. The mtmVUC genes of the mithramycin gene cluster in *Streptomyces argillaceus* are involved in the biosynthesis of the sugar moieties. *Molecular and General Genetics MGG*, 264, 827-835.

GRAHAM, D. G. 1978. Oxidative pathways for catecholamines in the genesis of neuromelanin and cytotoxic quinones. *Molecular pharmacology*, 14, 633-643.

GRUNDY, W. E., GOLDSTEIN, A. W., RICKHER, C. J., HANES, M. E., VARREN, H. B., JR. & SYLVESTER, J. C. 1953. Aureolic acid, a new antibiotic. I. Microbiologic studies. *Antibiot Chemother (Northfield Ill)*, 3, 1215-7.

GUERITTE, F. & FAHY, J. 2005. The vinca alkaloids. *Anticancer agents from natural products*, 10, 123-135.

GUILARTE, T. R., MCGLOTHAN, J. L., DEGAONKAR, M., CHEN, M.-K., BARKER, P. B., SYVERSEN, T. & SCHNEIDER, J. S. 2006. Evidence for cortical dysfunction and widespread manganese accumulation in the nonhuman primate brain following chronic manganese exposure: a <sup>1</sup>H-MRS and MRI study. *Toxicological Sciences*, 94, 351-358.

**H**A, J. H., SPOLAR, R. S. & RECORD, M. T., JR. 1989. Role of the hydrophobic effect in stability of site-specific protein-DNA complexes. *J Mol Biol*, 209, 801-16.

HAGIWARA, H., IYO, M. & HASHIMOTO, K. 2009. Mithramycin protects against dopaminergic neurotoxicity in the mouse brain after administration of methamphetamine. *Brain research*, 1301, 189-196.

HAJIHASSAN, Z. & RABBANI-CHADEGANI, A. 2011. Interaction of mitoxantrone, as an anticancer drug, with chromatin proteins, core histones and H1, in solution. *Int J Biol Macromol*, 48, 87-92.

---

- 
- HALL, T., SCHAEUBLIN, M. & CHAMBERS, T. 1993. The Majority of Osteoclasts Require mRNA and Protein Synthesis for Bone Resorption *in vitro*. *Biochemical and biophysical research communications*, 195, 1245-1253.
- HANDELSMAN, J., RONDON, M. R., BRADY, S. F., CLARDY, J. & GOODMAN, R. M. 1998. Molecular biological access to the chemistry of unknown soil microbes: a new frontier for natural products. *Chemistry & biology*, 5, R245-R249.
- HAQ, I. 2002. Thermodynamics of drug-DNA interactions. *Arch Biochem Biophys*, 403, 1-15.
- HAQ, I., LADBURY, J. E., CHOWDHRY, B. Z., JENKINS, T. C. & CHAIRES, J. B. 1997. Specific binding of hoechst 33258 to the d(CGCAAATTTGCG)<sub>2</sub> duplex: calorimetric and spectroscopic studies. *J Mol Biol*, 271, 244-57.
- HARTWELL, J. L. 1982. *Plants used against cancer: a survey*, Quarterman Publications.
- HE, L., GIRIJASHANKER, K., DALTON, T. P., REED, J., LI, H., SOLEIMANI, M. & NEBERT, D. W. 2006. ZIP8, member of the solute-carrier-39 (SLC39) metal-transporter family: characterization of transporter properties. *Molecular pharmacology*, 70, 171-180.
- HELM, L. & MERBACH, A. E. 2005. Inorganic and bioinorganic solvent exchange mechanisms. *Chemical Review*, 105, 1923-59.
- HERBERT, J., AUGEREAU, J., GLEYE, J. & MAFFRAND, J. 1990. Chelerythrine is a potent and specific inhibitor of protein kinase C. *Biochemical and biophysical research communications*, 172, 993-999.
- HOPWOOD, D. A. 1997. Genetic contributions to understanding polyketide synthases. *Chemical reviews*, 97, 2465-2498.
- HOPWOOD, D. A. & SHERMAN, D. H. 1990. Molecular genetics of polyketides and its comparison to fatty acid biosynthesis. *Annual review of genetics*, 24, 37-62.
- HORN, P. J. & PETERSON, C. L. 2002. Molecular biology. Chromatin higher order folding--wrapping up transcription. *Science*, 297, 1824-7.
- HORSBURGH, M. J., WHARTON, S. J., KARAVOLOS, M. & FOSTER, S. J. 2002. Manganese: elemental defence for a life with oxygen. *Trends in Microbiology*, 10, 496-501.
- HOSSAIN, M. & SURESH KUMAR, G. 2010. Thermodynamic profiles of the DNA binding of benzophenanthridines sanguinarine and ethidium: A comparative study with sequence specific polynucleotides. *The Journal of Chemical Thermodynamics*, 42, 1273-1280.
- HOU, M. H., LU, W. J., HUANG, C. Y., FAN, R. J. & YUANN, J. M. 2009. Effects of polyamines on the DNA-reactive properties of dimeric mithramycin complexed with cobalt(II): implications for anticancer therapy. *Biochemistry*, 48, 4691-8.
- HOU, M. H. & WANG, A. H. 2005. Mithramycin forms a stable dimeric complex by chelating with Fe(II): DNA-interacting characteristics, cellular permeation and cytotoxicity. *Nucleic Acids Research*, 33, 1352-61.
-

HUANG, C. C., CHU, N. S., LU, C. S. & CALNE, D. B. 1997. Cock gait in manganese intoxication. *Movement disorders*, 12, 807-808.

HUANG, C. Y. 1982. Determination of binding stoichiometry by the continuous variation method: the Job plot. *Methods Enzymol*, 87, 509-25.

HUHEEY, J. E., KEITER, E. A., KEITER, R. L. & MEDHI, O. K. 1983. *Inorganic chemistry: principles of structure and reactivity*, New York, Harper & Row

HURLEY, L. H. 2002. DNA and its associated processes as targets for cancer therapy. *Nat Rev Cancer*, 2, 188-200.

HUTCHINSON, C. R. & FUJII, I. 1995. Polyketide synthase gene manipulation: a structure-function approach in engineering novel antibiotics. *Annual Reviews in Microbiology*, 49, 201-238.

**I**SHIKAWA, T. 2001. Benzo[c]phenanthridine bases and their antituberculosis activity. *Medicinal research reviews*, 21, 61-72.

**J**ASUJA, R., JAMESON, D. M., NISHIJO, C. K. & LARSEN, R. W. 1997. Singlet excited state dynamics of tetrakis (4-N-methylpyridyl) porphine associated with DNA nucleotides. *The Journal of Physical Chemistry B*, 101, 1444-1450.

JAYASURIYA, H., LINGHAM, R. B., GRAHAM, P., QUAMINA, D., HERRANZ, L., GENILLOU, O., GAGLIARDI, M., DANZEISEN, R., TOMASSINI, J. E., ZINK, D. L., GUAN, Z. & SINGH, S. B. 2002. Durhamycin A, a potent inhibitor of HIV Tat transactivation. *J Nat Prod*, 65, 1091-5.

JIA, Z., GAO, Y., WANG, L., LI, Q., ZHANG, J., LE, X., WEI, D., YAO, J. C., CHANG, D. Z., HUANG, S. & XIE, K. 2010. Combined treatment of pancreatic cancer with mithramycin A and tolfenamic acid promotes Sp1 degradation and synergistic antitumor activity. *Cancer Res*, 70, 1111-9.

JIA, Z., ZHANG, J., WEI, D., WANG, L., YUAN, P., LE, X., LI, Q., YAO, J. & XIE, K. 2007. Molecular basis of the synergistic antiangiogenic activity of bevacizumab and mithramycin A. *Cancer Res*, 67, 4878-85.

JONES, D. E. J., CUI, D.-M. & MILLER, D. M. 1995. Expression of beta-galactosidase under the control of the human c-myc promoter in transgenic mice is inhibited by mithramycin. *Oncogene*, 10, 2323-2330.

**K**AMINSKYY, V. O., LOOTSIK, M. D. & STOIKA, R. S. 2006. Correlation of the cytotoxic activity of four different alkaloids, from *Chelidonium majus* (greater celandine), with their DNA intercalating properties and ability to induce breaks in the DNA of NK/Ly murine lymphoma cells. *Central European Journal of Biology*, 1, 2-15.

KATAHIRA, R., YAMASHITA, Y., OGAWA, H., YOSHIDA, M., KATAHIRA, M. & KYOGOKU, Y. 1998. Solution structure of the novel antitumor drug UCH9 complexed with d (TTGGCCAA)<sub>2</sub> as determined by NMR. *Nucleic Acids Research*, 26, 744-755.

- 
- KATZ, L. & DONADIO, S. 1993. Polyketide synthesis: prospects for hybrid antibiotics. *Annual Reviews in Microbiology*, 47, 875-912.
- KEDEI, N., LUNDBERG, D. J., TOTH, A., WELBURN, P., GARFIELD, S. H. & BLUMBERG, P. M. 2004. Characterization of the interaction of ingenol 3-angelate with protein kinase C. *Cancer research*, 64, 3243-3255.
- KEEN, C., ENSUNSA, J., WATSON, M., BALY, D., DONOVAN, S., MONACO, M. & CLEGG, M. 1998. Nutritional aspects of manganese from experimental studies. *Neurotoxicology*, 20, 213-223.
- KEMENY-BEKE, A., ARADI, J., DAMJANOVICH, J., BECK, Z., FACSKO, A., BERTA, A. & BODNAR, A. 2006. Apoptotic response of uveal melanoma cells upon treatment with chelidonine, sanguinarine and chelerythrine. *Cancer Lett*, 237, 67-75.
- KENIRY, M. A., BANVILLE, D. L., SIMMONDS, P. M. & SHAFER, R. 1993. Nuclear magnetic resonance comparison of the binding sites of mithramycin and chromomycin on the self-complementary oligonucleotide d(ACCCGGGT)<sub>2</sub>. Evidence that the saccharide chains have a role in sequence specificity. *Journal of Molecular Biology*, 231, 753-67.
- KENIRY, M. A., BROWN, S. C., BERMAN, E. & SHAFER, R. H. 1987. NMR studies of the interaction of chromomycin A3 with small DNA duplexes I. *Biochemistry*, 26, 1058-67.
- KENIRY, M. A., OWEN, E. A. & SHAFER, R. H. 2000. The three-dimensional structure of the 4:1 mithramycin:d(ACCCGGGT)<sub>2</sub> complex: evidence for an interaction between the E saccharides. *Biopolymers*, 54, 104-14.
- KENNEDY, B. & TORKELOSON, J. L. 1995. Long-Term Follow-Up of Stage III Testicular Carcinoma Treated With Mithramycin (Plicamycin). *Medical and pediatric oncology*, 24, 327-328.
- KENNEDY, B. J., YARBRO, J. W., KICKERTZ, V. & SANDBERG-WOLLHEIM, M. 1968. Effect of mithramycin on a mouse glioma. *Cancer Res*, 28, 91-7.
- KIKUCHI, T., ITO, N., SUZUKI, M., KUSAI, A., ISEKI, K. & SASAKI, H. 2005. Self-association properties of 4-[1-hydroxy-1-methylethyl]-2-propyl-1-[4-[2-[tetrazole-5-yl]phenyl]phenyl] methylimidazole-5-carboxylic acid monohydrate (CS-088), an antiglaucoma ophthalmic agent. *Int J Pharm*, 299, 100-6.
- KINGSTON, D. 2005. Taxol and its analogs. CRC Press/Taylor & Francis, Boca Raton, London.
- KOLLER, C. A., CAMPBELL, V. W., POLANSKY, D. A., MULHERN, A. & MILLER, D. M. 1985. In vivo differentiation of blast-phase chronic granulocytic leukemia. Expression of c-myc and c-abl protooncogenes. *J Clin Invest*, 76, 365-9.
- KOLLER, C. A. & MILLER, D. M. 1986. Preliminary observations on the therapy of the myeloid blast phase of chronic granulocytic leukemia with plicamycin and hydroxyurea. *New England Journal of Medicine*, 315, 1433-1438.
- KORNBERG, R. D. 1977. Structure of chromatin. *Annu Rev Biochem*, 46, 931-54.
-

KORNBERG, R. D. & LORCH, Y. 1999. Twenty-five years of the nucleosome, fundamental particle of the eukaryote chromosome. *Cell*, 98, 285-294.

KOSUGE, Y., TANIGUCHI, Y., IMAI, T., ISHIGE, K. & ITO, Y. 2011. Neuroprotective effect of mithramycin against endoplasmic reticulum stress-induced neurotoxicity in organotypic hippocampal slice cultures. *Neuropharmacology*, 61, 252-261.

KRANE, B. D., FAGBULE, M. O., SHAMMA, M. & GÖZLER, B. 1984. The benzophenanthridine alkaloids. *Journal of Natural Products*, 47, 1-43.

KULP, M., BRAGINA, O., KOGERMAN, P. & KALJURAND, M. 2011. Capillary electrophoresis with led-induced native fluorescence detection for determination of isoquinoline alkaloids and their cytotoxicity in extracts of *Chelidonium majus* L. *Journal of Chromatography A*, 1218, 5298-5304.

KÜNZEL, E., WOHLERT, S. E., BENINGA, C., HAAG, S., DECKER, H., HUTCHINSON, C. R., BLANCO, G., MENDEZ, C., SALAS, J. A. & ROHR, J. 1997. Tetracenomycin M, a novel genetically engineered tetracenomycin resulting from a combination of mithramycin and tetracenomycin biosynthetic genes. *Chemistry-A European Journal*, 3, 1675-1678.

KURSINSZKI, L., SÁRKÖZI, Á., KÉRY, Á. & SZÖKE, É. 2006. Improved RP-HPLC method for analysis of isoquinoline alkaloids in extracts of *Chelidonium majus*. *Chromatographia*, 63, S131-S135.

**L**ADBURY, J. E. & DOYLE, M. L. 2005. *Biocalorimetry 2: applications of calorimetry in the biological sciences*, John Wiley & Sons.

LADEANA W. HILLIER, W. M., EWAN BIRNEY, WESLEY WARREN, ROSS C. HARDISON, CHRIS P. PONTING, PEER BORK, DAVID W. BURT, MARTIEN A. M. GROENEN, MARY E. DELANY, JERRY B. DODGSON 2004. Sequence and comparative analysis of the chicken genome provide unique perspectives on vertebrate evolution. *Nature*, 432, 695-716.

LAH, M. S., DIXON, M. M., PATTRIDGE, K. A., STALLINGS, W. C., FEE, J. A. & LUDWIG, M. L. 1995. Structure-function in *Escherichia coli* iron superoxide dismutase: comparisons with the manganese enzyme from *Thermus thermophilus*. *Biochemistry*, 34, 1646-60.

LAHIRI, S., DEVI, P. G., MAJUMDER, P., DAS, S. & DASGUPTA, D. 2008. Self-association of the anionic form of the DNA-binding anticancer drug mithramycin. *J Phys Chem B*, 112, 3251-8.

LAHIRI, S., TAKAO, T., DEVI, P. G., GHOSH, S., GHOSH, A., DASGUPTA, A. & DASGUPTA, D. 2012. Association of aureolic acid antibiotic, chromomycin A3 with  $\text{Cu}^{2+}$  and its negative effect upon DNA binding property of the antibiotic. *Biometals*, 25, 435-50.

LAX, E. 2004. *The Mold in Dr. Florey's Coat: The Story of the Penicillin Miracle*, Macmillan.

LEE, S. S., LAI, Y. C., CHEN, C. K., TSENG, L. H. & WANG, C. Y. 2007. Characterization of isoquinoline alkaloids from *Neolitsea sericea* var. *aurata* by HPLC-SPE-NMR. *J Nat Prod*, 70, 637-42.



- LENFELD, J., KROUTIL, M., MARŠÁLEK, E., SLAVIK, J., PREININGER, V. & ŠIMÁNEK, V. 1981. Antiinflammatory Activity of Quaternary Benzophenanthridine Alkaloids from *Chelidonium majus*. *Planta medica*, 43, 161-165.
- LERMAN, L. S. 1961. Structural considerations in the interaction of DNA and acridines. *J Mol Biol*, 3, 18-30.
- LEWIS, R. J., HUGHES, R. A., ALCARAZ, L., THOMPSON, S. P. & MOODY, C. J. 2006. Solution structures of thiopeptide antibiotics. *Chemical communications*, 4215-4217.
- LI, J., LI, B., WU, Y., SHUANG, S., DONG, C. & CHOI, M. M. 2012. Luminescence and binding properties of two isoquinoline alkaloids chelerythrine and sanguinarine with ctDNA. *Spectrochimica Acta Part A: Molecular and Biomolecular Spectroscopy*, 95, 80-85.
- LIACINI, A., SYLVESTER, J., LI, W. Q. & ZAFARULLAH, M. 2005. Mithramycin downregulates proinflammatory cytokine-induced matrix metalloproteinase gene expression in articular chondrocytes. *Arthritis Res Ther*, 7, 777-783.
- LIN, R. K., HSU, C. H. & WANG, Y. C. 2007. Mithramycin A inhibits DNA methyltransferase and metastasis potential of lung cancer cells. *Anticancer Drugs*, 18, 1157-64.
- LOMBÓ, F., BLANCO, G., FERNÁNDEZ, E., MÉNDEZ, C. & SALAS, J. 1996. Characterization of *Streptomyces argillaceus* genes encoding a polyketide synthase involved in the biosynthesis of the antitumor mithramycin. *Gene*, 172, 87-91.
- LOMBÓ, F., BRAÑA, A. F., MÉNDEZ, C. & SALAS, J. A. 1999. The mithramycin gene cluster of *Streptomyces argillaceus* contains a positive regulatory gene and two repeated DNA sequences that are located at both ends of the cluster. *Journal of bacteriology*, 181, 642-647.
- LOMBO, F., MENENDEZ, N., SALAS, J. A. & MENDEZ, C. 2006a. The aureolic acid family of antitumor compounds: structure, mode of action, biosynthesis, and novel derivatives. *Applied Microbiology and Biotechnology*, 73, 1-14.
- LOMBO, F., MENENDEZ, N., SALAS, J. A. & MENDEZ, C. 2006b. The aureolic acid family of antitumor compounds: structure, mode of action, biosynthesis, and novel derivatives. *Appl Microbiol Biotechnol*, 73, 1-14.
- LOMBO, F., SIEMS, K., BRAÑA, A. F., MÉNDEZ, C., BINDSEIL, K. & SALAS, J. A. 1997. Cloning and insertional inactivation of *Streptomyces argillaceus* genes involved in the earliest steps of biosynthesis of the sugar moieties of the antitumor polyketide mithramycin. *Journal of bacteriology*, 179, 3354-3357.
- LOZANO, M. J. F., REMSING, L. L., QUIRÓS, L. M., BRAÑA, A. F., FERNÁNDEZ, E., SÁNCHEZ, C., MÉNDEZ, C., ROHR, J. & SALAS, J. A. 2000. Characterization of two polyketide methyltransferases involved in the biosynthesis of the antitumor drug mithramycin by *Streptomyces argillaceus*. *Journal of Biological Chemistry*, 275, 3065-3074.
- LU, W. J., WANG, H. M., YUANN, J. M., HUANG, C. Y. & HOU, M. H. 2009. The impact of spermine competition on the efficacy of DNA-binding Fe(II), Co(II), and Cu(II) complexes of dimeric chromomycin A(3). *Journal of Inorganic Biochemistry*, 103, 1626-33.

LUGER, K., MADER, A. W., RICHMOND, R. K., SARGENT, D. F. & RICHMOND, T. J. 1997a. Crystal structure of the nucleosome core particle at 2.8 Å resolution. *Nature*, 389, 251-60.

LUGER, K., MÄDER, A. W., RICHMOND, R. K., SARGENT, D. F. & RICHMOND, T. J. 1997b. Crystal structure of the nucleosome core particle at 2.8 Å resolution. *Nature*, 389, 251-260.

LUMACHI, F., BRUNELLO, A., ROMA, A. & BASSO, U. 2008. Medical treatment of malignancy-associated hypercalcemia. *Current Medicinal Chemistry*, 15, 415-21.

LYNG, R., HARD, T. & NORDEN, B. 1987. Induced CD of DNA intercalators: electric dipole allowed transitions. *Biopolymers*, 26, 1327-1345.

MADEJCZYK, M. S. & BALLATORI, N. 2012. The iron transporter ferroportin can also function as a manganese exporter. *Biochimica et Biophysica Acta (BBA)-Biomembranes*, 1818, 651-657.

MAITI, M., DAS, S., SEN, A., DAS, A., KUMAR, G. S. & NANDI, R. 2002. Influence of DNA structures on the conversion of sanguinarine alkanolamine form to iminium form. *J Biomol Struct Dyn*, 20, 455-64.

MAITI, M. & KUMAR, G. S. 2007a. Molecular aspects on the interaction of protoberberine, benzophenanthridine, and aristolochia group of alkaloids with nucleic acid structures and biological perspectives. *Med Res Rev*, 27, 649-95.

MAITI, M. & KUMAR, G. S. 2007b. Protoberberine alkaloids: physicochemical and nucleic acid binding properties. *Top Heterocycl Chem*, 10, 155-209.

MAITI, M. & NANDI, R. 1987. Circular dichroism of sanguinarine-DNA complexes: effect of base composition, pH and ionic strength. *J Biomol Struct Dyn*, 5, 159-75.

MAITI, M., NANDI, R. & CHAUDHURI, K. 1982. Sanguinarine: a monofunctional intercalating alkaloid. *FEBS Lett*, 142, 280-4.

MAITI, M., NANDI, R. & CHAUDHURI, K. 1984. Interaction of sanguinarine with natural and synthetic deoxyribonucleic acids. *Indian J Biochem Biophys*, 21, 158-65.

MAJEE, S., SEN, R., GUHA, S., BHATTACHARYYA, D. & DASGUPTA, D. 1997. Differential interactions of the  $Mg^{2+}$  complexes of chromomycin A3 and mithramycin with poly(dG-dC) . poly(dC-dG) and poly(dG) . poly(dC). *Biochemistry*, 36, 2291-9.

MAJUMDER, P. & DASGUPTA, D. 2011. Effect of DNA groove binder distamycin A upon chromatin structure. *PLoS One*, 6, e26486.

MALIKOVA, J., ZDARILOVA, A. & HLOBILKOVA, A. 2006a. Effects of sanguinarine and chelerythrine on the cell cycle and apoptosis. *Biomed Pap Med Fac Univ Palacky Olomouc Czech Repub*, 150, 5-12.

- 
- MALIKOVA, J., ZDAŘILOVÁ, A., HLOBILKOVA, A. & ULRICHOVA, J. 2006b. The effect of chelerythrine on cell growth, apoptosis, and cell cycle in human normal and cancer cells in comparison with sanguinarine. *Cell biology and toxicology*, 22, 439-453.
- MANCINI, M., NICHOLSON, D. W., ROY, S., THORNBERRY, N. A., PETERSON, E. P., CASCIOLA-ROSEN, L. A. & ROSEN, A. 1998. The caspase-3 precursor has a cytosolic and mitochondrial distribution: implications for apoptotic signaling. *The Journal of cell biology*, 140, 1485-1495.
- MANN, J. 1999. *The elusive magic bullet: the search for the perfect drug*, Oxford University Press, USA.
- MARKLUND, S. & MARKLUND, G. 1974. Involvement of the superoxide anion radical in the autoxidation of pyrogallol and a convenient assay for superoxide dismutase. *European Journal Biochemistry*, 47, 469-74.
- MARTIN, S. R. 1980. Absorption and circular dichroic spectral studies on the self-association of daunorubicin. *Biopolymers*, 19, 713-21.
- MARTINEZ-FINLEY, E. J., GAVIN, C. E., ASCHNER, M. & GUNTER, T. E. 2013. Manganese neurotoxicity and the role of reactive oxygen species. *Free Radical Biology and Medicine*, 62, 65-75.
- MATKAR, S. S., WRISCHNIK, L. A. & HELLMANN-BLUMBERG, U. 2008. Production of hydrogen peroxide and redox cycling can explain how sanguinarine and chelerythrine induce rapid apoptosis. *Archives of biochemistry and biophysics*, 477, 43-52.
- MAULIK, N., YOSHIDA, T. & DAS, D. K. 1999. Regulation of cardiomyocyte apoptosis in ischemic reperfused mouse heart by glutathione peroxidase. *Mol Cell Biochem*, 196, 13-21.
- MCCONKEY, D. J., ZHIVOTOVSKY, B. & ORRENIUS, S. 1996. Apoptosis—molecular mechanisms and biomedical implications. *Molecular aspects of medicine*, 17, 1-110.
- MCGHEE, J. D. & FELSENFELD, G. 1980. Nucleosome structure. *Annu Rev Biochem*, 49, 1115-56.
- MENA, I., MARIN, O., FUENZALIDA, S. & COTZIAS, G. C. 1967. Chronic manganese poisoning. Clinical picture and manganese turnover. *Neurology*, 17, 128-36.
- MENÉNDEZ, N., NUR-E-ALAM, M., BRAÑA, A. F., ROHR, J., SALAS, J. A. & MÉNDEZ, C. 2004. Biosynthesis of the Antitumor Chromomycin A<sub>3</sub> in *Streptomyces griseus*: Analysis of the Gene Cluster and Rational Design of Novel Chromomycin Analogs. *Chemistry & biology*, 11, 21-32.
- MENENDEZ, N., NUR-E-ALAM, M., FISCHER, C., BRANA, A. F., SALAS, J., ROHR, J. & MENDEZ, C. 2006a. Deoxysugar transfer during chromomycin A<sub>3</sub> biosynthesis in *Streptomyces griseus* subsp. *griseus*: new derivatives with antitumor activity. *Applied and environmental microbiology*, 72, 167-177.
- MENENDEZ, N., NUR-E-ALAM, M., FISCHER, C., BRANA, A. F., SALAS, J. A., ROHR, J. & MENDEZ, C. 2006b. Deoxysugar transfer during chromomycin A<sub>3</sub> biosynthesis in
-

*Streptomyces griseus* subsp. *griseus*: new derivatives with antitumor activity. *Appl Environ Microbiol*, 72, 167-77.

MENENDEZ, N., NUR, E. A. M., BRANA, A. F., ROHR, J., SALAS, J. A. & MENDEZ, C. 2004. Tailoring modification of deoxysugars during biosynthesis of the antitumour drug chromomycin A by *Streptomyces griseus* ssp. *griseus*. *Mol Microbiol*, 53, 903-15.

MIAO, F., YANG, X.-J., ZHOU, L., HU, H.-J., ZHENG, F., DING, X.-D., SUN, D.-M., ZHOU, C.-D. & SUN, W. 2011. Structural modification of sanguinarine and chelerythrine and their antibacterial activity. *Natural Product Research*, 25, 863-875.

MILLONIG, H., POUS, J., GOUYETTE, C., SUBIRANA, J. A. & CAMPOS, J. L. 2009. The interaction of manganese ions with DNA. *Journal of Inorganic Biochemistry*, 103, 876-80.

MIR, M. A., DAS, S. & DASGUPTA, D. 2004. N-terminal tail domains of core histones in nucleosome block the access of anticancer drugs, mithramycin and daunomycin, to the nucleosomal DNA. *Biophysical Chemistry*, 109, 121-35.

MIR, M. A. & DASGUPTA, D. 2001. Interaction of antitumor drug, mithramycin, with chromatin. *Biochemical and Biophysical Research Communications*, 280, 68-74.

MITSCHER, L., PARK, Y., CLARK, D., CLARK 3RD, G., HAMMESFAHR, P., WU, W. & BEAL, J. 1977. Antimicrobial agents from higher plants. An investigation of *Hunnemannia fumariaefolia* pseudoalcoholates of sanguinarine and chelerythrine. *Lloydia*, 41, 145-150.

MONNOT, M., MAUFFRET, O., LESCOT, E. & FERMANDJIAN, S. 1992. Probing intercalation and conformational effects of the anticancer drug 2-methyl-9-hydroxyellipticinium acetate in DNA fragments with circular dichroism. *Eur J Biochem*, 204, 1035-9.

MONNOT, M., MAUFFRET, O., SIMON, V., LESCOT, E., PSAUME, B., SAUCIER, J., CHARRA, M., BELEHRADEK, J. & FERMANDJIAN, S. 1991. DNA-drug recognition and effects on topoisomerase II-mediated cytotoxicity. A three-mode binding model for ellipticine derivatives. *Journal of Biological Chemistry*, 266, 1820-1829.

MONTANARI, A. & ROSAZZA, J. 1990. Biogenesis of chromomycin A3 by *Streptomyces griseus*. *The Journal of antibiotics*, 43, 883.

MONTES, S., ALCARAZ-ZUBELDIA, M., MURIEL, P. & RIOS, C. 2001. Striatal manganese accumulation induces changes in dopamine metabolism in the cirrhotic rat. *Brain Research*, 891, 123-9.

MYERS, C., MIMNAUGH, E., YEH, G. & SINHA, B. 1988. Biochemical mechanisms of tumor cell kill by the anthracyclines. *Anthracycline and anthracenedione-based anticancer agents*, 6, 527-569.

NAKANISHI, T., MASUDA, A., SUWA, M., AKIYAMA, Y., HOSHINO-ABE, N. & SUZUKI, M. 2000. Synthesis of derivatives of NK109, 7-OH Benzo [c] phenanthridine alkaloid, and evaluation of their cytotoxicities and reduction-resistant properties. *Bioorganic & medicinal chemistry letters*, 10, 2321-2323.

NAKANISHI, T., SUZUKI, M., MASHIBA, A., ISHIKAWA, K. & YOKOTSUKA, T. 1998. Synthesis of NK109, an anticancer benzo [c] phenanthridine alkaloid. *The Journal of Organic Chemistry*, 63, 4235-4239.

NAVARRO, V. & DELGADO, G. 1999. Two antimicrobial alkaloids from *Bocconia arborea*. *Journal of ethnopharmacology*, 66, 223-226.

NAYAK, R., SIRSI, M. & PODDER, S. K. 1975. Mode of action of antitumour antibiotics: Spectrophotometric studies on the interaction of chromomycin A3 with DNA and chromatin of normal and neoplastic tissue. *Biochimica et Biophysica Acta (BBA)-Nucleic Acids and Protein Synthesis*, 378, 195-204.

NEWMAN, D. J., CRAGG, G. M. & SNADER, K. M. 2003. Natural products as sources of new drugs over the period 1981-2002. *Journal of Natural Products*, 66, 1022-1037.

NOLL, M. & KORNBERG, R. D. 1977. Action of micrococcal nuclease on chromatin and the location of histone H1. *Journal of Molecular Biology*, 109, 393-404.

**O**DEBIYI, O. & SOFOWORA, E. 1979. Antimicrobial alkaloids from a Nigerian chewing stick (*Fagara zanthoxyloides*). *Planta medica*, 36, 204-207.

OGAWA, H., YAMASHITA, Y., KATAHIRA, R., CHIBA, S., IWASAKI, T., ASHIZAWA, T. & NAKANO, H. 1998. UCH9, a new antitumor antibiotic produced by *Streptomyces*: I. Producing organism, fermentation, isolation and biological activities. *The Journal of antibiotics*, 51, 261.

OLANOW, C. W. 2004. Manganese-induced parkinsonism and Parkinson's disease. *Annals of New York Academy of Science*, 1012, 209-23.

ORRENIUS, S. 1995. Apoptosis: molecular mechanisms and implications for human disease. *Journal of internal medicine*, 237, 529-536.

**P**AL, P. K., SAMII, A. & CALNE, D. B. 1999. Manganese neurotoxicity: a review of clinical features, imaging and pathology. *Neurotoxicology*, 20, 227-38.

PALOMA, L. G., SMITH, J. A., CHAZIN, W. J. & NICOLAOU, K. 1994. Interaction of calicheamicin with duplex DNA: role of the oligosaccharide domain and identification of multiple binding modes. *Journal of the American Chemical Society*, 116, 3697-3708.

PARENTY, A. D., SMITH, L. V., PICKERING, A. L., LONG, D.-L. & CRONIN, L. 2004. General one-pot, three-step methodology leading to an extended class of N-heterocyclic cations: spontaneous nucleophilic addition, cyclization, and hydride loss. *The Journal of Organic Chemistry*, 69, 5934-5946.

PATEL, T. R., HARDING, S. E., EBRINGEROVA, A., DESZCZYNSKI, M., HROMADKOVA, Z., TOGOLA, A., PAULSEN, B. S., MORRIS, G. A. & ROWE, A. J. 2007. Weak self-association in a carbohydrate system. *Biophys J*, 93, 741-9.

PERCZEL, A., PARK, K. & FASMAN, G. 1992. Analysis of the circular dichroism spectrum of proteins using the convex constraint algorithm: a practical guide. *Analytical biochemistry*, 203, 83-93.

PERRY, J., SHIN, D., GETZOFF, E. & TAINER, J. 2010. The structural biochemistry of the superoxide dismutases. *Biochimica et Biophysica Acta (BBA)-Proteins and Proteomics*, 1804, 245-262.

PRADHAN, S. K., DASGUPTA, D. & BASU, G. 2011. Human telomere d [(TTAGGG)<sub>4</sub>] undergoes a conformational transition to the Na<sup>+</sup>-form upon binding with sanguinarine in presence of K<sup>+</sup>. *Biochemical and biophysical research communications*, 404, 139-142.

PRADO, L., FERNÁNDEZ, E., WEIBBACH, U., BLANCO, G., QUIRÓS, L. M., BRAÑA, A. F., MÉNDEZ, C., ROHR, J. & SALAS, J. A. 1999a. Oxidative cleavage of premithramycin B is one of the last steps in the biosynthesis of the antitumor drug mithramycin. *Chemistry & biology*, 6, 19-30.

PRADO, L., LOMBO, F., BRANA, A. F., MENDEZ, C., ROHR, J. & SALAS, J. A. 1999b. Analysis of two chromosomal regions adjacent to genes for a type II polyketide synthase involved in the biosynthesis of the antitumor polyketide mithramycin in *Streptomyces argillaceus*. *Mol Gen Genet*, 261, 216-25.

PREMILAT, S. & ALBISER, G. 1997. X-ray fibre diffraction study of an elevated temperature structure of poly(dA).poly(dT). *J Mol Biol*, 274, 64-71.

**R**ABBANI, A., ISKANDAR, M. & AUSIO, J. 1999. Daunomycin-induced unfolding and aggregation of chromatin. *J Biol Chem*, 274, 18401-6.

RAO, K., CULLEN, W. & SOBIN, B. 1962. A new antibiotic with antitumor properties. *Antibiotics and chemotherapy*, 12, 182-186.

RAO, K. V. R. & NORENBURG, M. D. 2004. Manganese induces the mitochondrial permeability transition in cultured astrocytes. *Journal of Biological Chemistry*, 279, 32333-32338.

REMSING, L. L., BAHADORI, H. R., CARBONE, G. M., MCGUFFIE, E. M., CATAPANO, C. V. & ROHR, J. 2003. Inhibition of c-src transcription by mithramycin: structure-activity relationships of biosynthetically produced mithramycin analogues using the c-src promoter as target. *Biochemistry*, 42, 8313-8324.

REMSING, L. L., GARCIA-BERNARDO, J., GONZALEZ, A., KÜNZEL, E., RIX, U., BRAÑA, A. F., BEARDEN, D. W., MÉNDEZ, C., SALAS, J. A. & ROHR, J. 2002. Ketopremithramycins and Ketomithramycins, Four New Aureolic Acid-Type Compounds Obtained upon Inactivation of Two Genes Involved in the Biosynthesis of the Deoxysugar Moieties of the Antitumor Drug Mithramycin by *Streptomyces Argillaceus*, Reveal Novel Insights into Post-PKS Tailoring Steps of the Mithramycin Biosynthetic Pathway. *Journal of the American Chemical Society*, 124, 1606-1614.

REN, J., JENKINS, T. C. & CHAIRES, J. B. 2000. Energetics of DNA intercalation reactions. *Biochemistry*, 39, 8439-47.

- 
- REYES-CABALLERO, H., CAMPANELLO, G. C. & GIEDROC, D. P. 2011. Metalloregulatory proteins: metal selectivity and allosteric switching. *Biophysical chemistry*, 156, 103-114.
- REYNOLDS, R. D., FISHER, J. I., JENSEN, P. A., PAJAK, T. F. & BATEMAN, J. R. 1976. Phase I alternate-day dose study of chromomycin A3. *Cancer Treat Rep*, 60, 1251-5.
- RODIER, J. 1955. Manganese poisoning in Moroccan miners. *British journal of industrial medicine*, 12, 21.
- RODRÍGUEZ, D., QUIRÓS, L. M., BRAÑA, A. F. & SALAS, J. A. 2003. Purification and characterization of a monooxygenase involved in the biosynthetic pathway of the antitumor drug mithramycin. *Journal of bacteriology*, 185, 3962-3965.
- RODRIGUEZ, L., RODRIGUEZ, D., OLANO, C., BRANA, A. F., MENDEZ, C. & SALAS, J. A. 2001. Functional analysis of OleY L-oleandrosyl 3-O-methyltransferase of the oleandomycin biosynthetic pathway in *Streptomyces antibioticus*. *J Bacteriol*, 183, 5358-63.
- ROHR, J. 1992. Comparison of multicyclic polyketides by folding analysis: a novel approach to recognize biosynthetic and/or evolutionary interrelationships of the natural products or intermediates and its exemplification on hepta-, octa-, and decaketides. *The Journal of Organic Chemistry*, 57, 5217-5223.
- ROHR, J. R., MENDEZ, C. & SALAS, J. A. 1999. The biosynthesis of aureolic acid group antibiotics. *Bioorganic Chemistry*, 27, 41-54.
- ROTH, J. A. 2009. Are there common biochemical and molecular mechanisms controlling manganism and parkinsonism. *Neuromolecular medicine*, 11, 281-296.
- ROTH, J. A., LI, Z., SRIDHAR, S. & KHOSHBOUEI, H. 2013. The effect of manganese on dopamine toxicity and dopamine transporter (DAT) in control and DAT transfected HEK cells. *Neurotoxicology*, 35, 121-128.
- RUSSELL, A. S. & LENTLE, B. C. 1974. Mithramycin therapy in Paget's disease. *Canadian Medical Association Journal*, 110, 397.
- RYU, H., LEE, J., HAGERTY, S. W., SOH, B. Y., MCALPIN, S. E., CORMIER, K. A., SMITH, K. M. & FERRANTE, R. J. 2006. ESET/SETDB1 gene expression and histone H3 (K9) trimethylation in Huntington's disease. *Proceedings of the National Academy of Sciences*, 103, 19176-19181.
- S**ACHER, A., COHEN, A. & NELSON, N. 2001. Properties of the mammalian and yeast metal-ion transporters DCT1 and Smf1p expressed in *Xenopus laevis* oocytes. *Journal of Experimental Biology*, 204, 1053-1061.
- SAENGER, W. 1984. *Principles of nucleic acid structure*, Springer-Verlag.
- SAHAR, E. & LATT, S. A. 1978. Enhancement of banding patterns in human metaphase chromosomes by energy transfer. *Proc Natl Acad Sci U S A*, 75, 5650-4.
-

- 
- SANTACROCE, P. V. & BASU, A. 2004. Studies of the carbohydrate-carbohydrate interaction between lactose and GM3 using Langmuir monolayers and glycolipid micelles. *Glycoconjugate journal*, 21, 89-95.
- SASTRY, M., FIALA, R. & PATEL, D. J. 1995. Solution structure of mithramycin dimers bound to partially overlapping sites on DNA. *Journal of Molecular Biology*, 251, 674-89.
- SASTRY, M. & PATEL, D. J. 1993. Solution structure of the mithramycin dimer-DNA complex. *Biochemistry*, 32, 6588-604.
- SATO, K., OKAMURA, N., UTAGAWA, K., ITO, Y. & WATANABE, M. 1960. Studies on the antitumor activity of chromomycin A3. *The science reports of the research institutes, Tohoku University. Ser. C, Medicine. Tōhoku Daigaku*, 9, 224.
- SCATCHARD, G. 1949. The attractions of proteins for small molecules and ions. *Annals of the New York Academy of Sciences*, 51, 660-672.
- SELVI B, R., PRADHAN, S. K., SHANDILYA, J., DAS, C., SAILAJA, B. S., SHANKAR G, N., GADAD, S. S., REDDY, A., DASGUPTA, D. & KUNDU, T. K. 2009. Sanguinarine interacts with chromatin, modulates epigenetic modifications, and transcription in the context of chromatin. *Chemistry & biology*, 16, 203-216.
- SÉNÈQUE, O., BONNET, E., JOUMAS, F. L. & LATOUR, J. M. 2009. Cooperative Metal Binding and Helical Folding in Model Peptides of Treble- Clef Zinc Fingers. *Chemistry-A European Journal*, 15, 4798-4810.
- SENSI, P., GRECO, A. & PAGANI, H. 1958. Isolation and properties of a new antibiotic, LA 7017. *Antibiotics & chemotherapy*, 8, 241-244.
- SETHI, M. L. 1979. Inhibition of reverse transcriptase activity by benzophenanthridine alkaloids. *Journal of Natural Products*, 42, 187-196.
- SHERR, C. J. & ROBERTS, J. M. 1999. CDK inhibitors: positive and negative regulators of G1-phase progression. *Genes & development*, 13, 1501-1512.
- SIDORYK-WEGRZYNOWICZ, M., LEE, E., MINGWEI, N. & ASCHNER, M. 2011. Disruption of astrocytic glutamine turnover by manganese is mediated by the protein kinase C pathway. *Glia*, 59, 1732-1743.
- SINGH, B. & GUPTA, R. S. 1985. Species-specific differences in the toxicity and mutagenicity of the anticancer drugs mithramycin, chromomycin A3, and olivomycin. *Cancer Res*, 45, 2813-20.
- SLANINOVA, I., TABORSKA, E., BOCHORAKOVA, H. & SLANINA, J. 2001. Interaction of benzo[c]phenanthridine and protoberberine alkaloids with animal and yeast cells. *Cell Biol Toxicol*, 17, 51-63.
- SMITH, M. W. & DOOLITTLE, R. F. 1992. A comparison of evolutionary rates of the two major kinds of superoxide dismutase. *Journal of molecular evolution*, 34, 175-184.
- SNYDER, R. C., RAY, R., BLUME, S. & MILLER, D. M. 1991. Mithramycin blocks transcriptional initiation of the c-myc P1 and P2 promoters. *Biochemistry*, 30, 4290-7.
-



---

SOUTHON, I. W. & BUCKINGHAM, J. 1989. *Dictionary of Alkaloids, with CD-ROM*, CRC Press.

SPOLAR, R. S. & RECORD JR, M. T. 1994. Coupling of local folding to site-specific binding of proteins to DNA. *Science-AAAS-Weekly Paper Edition-including Guide to Scientific Information*, 263, 777-784.

STERMITZ, F. R., GILLESPIE, J. P., AMOROS, L. G., ROMERO, R., STERMITZ, T. A., LARSON, K. A., EARL, S. & OGG, J. E. 1975. Synthesis and biological activity of some antitumor benzophenanthridinium salts. *Journal of Medicinal Chemistry*, 18, 708-713.

STERMITZ, F. R., LARSON, K. A. & KIM, D. K. 1973. Structural relations among cytotoxic and antitumor benzophenanthridine alkaloid derivatives. *Journal of Medicinal Chemistry*, 16, 939-940.

SUBIRANA, J. A. & SOLER-LOPEZ, M. 2003. Cations as hydrogen bond donors: a view of electrostatic interactions in DNA. *Annual Review of Biophysics and Biomolecular Structure*, 32, 27-45.

**T**AKEDA, A. 2003. Manganese action in brain function. *Brain Research Reviews*, 41, 79-87.

THORNBERRY, N. A. & LAZEBNIK, Y. 1998. Caspases: enemies within. *Science*, 281, 1312-1316.

TOLEDO GRIJALBA, M., CHERON, M., BOROWSKI, E., BOLARD, J. & SCHREIER, S. 2006. Modulation of polyene antibiotics self-association by ions from the Hofmeister series. *Biochim Biophys Acta*, 1760, 973-9.

**U**ESUGI, M. & SUGIURA, Y. 1993. New insights into sequence recognition process of esperamicin A1 and calicheamicin gamma 1I.: origin of their selectivities and "induced fit" mechanism. *Biochemistry*, 32, 4622-7.

UPADRASHTA, S. M. & WURSTER, D. E. 1988. Spectroscopic Analysis of the Ionization Behavior of Anthralin. *Spectroscopy Letters*, 21, 147-155.

URBANOVA, J., LUBAL, P., SLANINOVA, I., TABORSKA, E. & TABORSKY, P. 2009. Fluorescence properties of selected benzo[c]phenanthridine alkaloids and studies of their interaction with CT DNA. *Anal Bioanal Chem*, 394, 997-1002.

**V**AN DE SANDE, J. H., MCINTOSH, L. P. & JOVIN, T. M. 1982. Mn<sup>2+</sup> and other transition metals at low concentration induce the right-to-left helical transformation of poly[d(G-C)]. *The EMBO Journal*, 1, 777-82.

VERGANI, L., GAVAZZO, P., MASCETTI, G. & NICOLINI, C. 1994. Ethidium bromide intercalation and chromatin structure: a spectropolarimetric analysis. *Biochemistry*, 33, 6578-6585.

---

VESELKOV, D., LANTUSHENKO, A., DAVIES, D. & VESELKOV, A. 2002. The Self-Association of Antibiotic Actinocyl-bis (3-dimethylaminopropylamine) in Aqueous Solution: A  $^1\text{H}$  NMR Analysis. *Russian Journal of Bioorganic Chemistry*, 28, 342-347.

VON HARSDORF, R., LI, P.-F. & DIETZ, R. 1999. Signaling pathways in reactive oxygen species-induced cardiomyocyte apoptosis. *Circulation*, 99, 2934-2941.

WAINWRIGHT, M. 1990. *Miracle cure: The story of penicillin and the golden age of antibiotics*, Blackwell Oxford, UK.

WAKISAKA, G., UCHINO, H., NAKAMURA, T., SOTOVAYASHI, H., SHIRAKAWA, S., ADACHI, A. & SAKURAI, M. 1963. Selective incells by chromomycin A3. *Nature*, 198, 385-6.

WAKSMAN, S. A. 1941. Antagonistic Relations of Microorganisms. *Bacteriol Rev*, 5, 231-91.

WAKSMAN, S. A., KATZ, E. & VINING, L. C. 1958. Nomenclature of the Actinomycins. *Proc Natl Acad Sci U S A*, 44, 602-12.

WALBERG, M., GAUSTAD, P. & STEEN, H. B. 1999. Uptake kinetics of nucleic acid targeting dyes in *S. aureus*, *E. faecalis* and *B. cereus*: a flow cytometric study. *J Microbiol Methods*, 35, 167-76.

WANG, G., PAHARI, P., KHAREL, M. K., CHEN, J., ZHU, H., VAN LANEN, S. G. & ROHR, J. 2012. Cooperation of two bifunctional enzymes in the biosynthesis and attachment of deoxysugars of the antitumor antibiotic mithramycin. *Angewandte Chemie International Edition*, 51, 10638-10642.

WARD, D. C., REICH, E. & GOLDBERG, I. H. 1965. Base specificity in the interaction of polynucleotides with antibiotic drugs. *Science*, 149, 1259-63.

WARING, M. J. 1981. DNA modification and cancer. *Annual Review of Biochemistry*, 50, 159-192.

WATVE, M. G., TICKOO, R., JOG, M. M. & BHOLE, B. D. 2001. How many antibiotics are produced by the genus *Streptomyces*? *Archives of microbiology*, 176, 386-390.

WELLS, R. D., LARSON, J. E., GRANT, R. C., SHORTLE, B. E. & CANTOR, C. R. 1970. Physicochemical studies on polydeoxyribonucleotides containing defined repeating nucleotide sequences. *Journal of Molecular Biology*, 54, 465-97.

WOHLERT, S. E., KUNZEL, E., MACHINEK, R., MENDEZ, C., SALAS, J. A. & ROHR, J. 1999. The structure of mithramycin reinvestigated. *Journal of Natural Products*, 62, 119-21.

WYLLIE, A. 1997. Apoptosis and carcinogenesis. *European journal of cell biology*, 73, 189.

YAMAKURA, F., RARDIN, R. L., PETSKE, G. A., RINGE, D., HIRAOKA, B. Y., NAKAYAMA, K., FUJIMURA, T., TAKA, H. & MURAYAMA, K. 1998. Inactivation and destruction of conserved Trp159 of Fe-superoxide dismutase from *Porphyromonas gingivalis* by hydrogen peroxide. *European Journal of Biochemistry*, 253, 49-56.

YAMAMOTO, S., SETA, K., MORISCO, C., VATNER, S. F. & SADOSHIMA, J. 2001. Chelerythrine rapidly induces apoptosis through generation of reactive oxygen species in cardiac myocytes. *J Mol Cell Cardiol*, 33, 1829-48.

YANO, Y., TANAKA, K., DOI, Y. & JANADO, M. 1988. The polystyrene affinity of methylglycosides, deoxysugars and glucooligosaccharides. *Journal of solution chemistry*, 17, 347-358.

YAVUZ, O., ALTUNKAYNAK, Y. & GUZEL, F. 2003. Removal of copper, nickel, cobalt and manganese from aqueous solution by kaolinite. *Water Research*, 37, 948-52.

YOKEL, R. A. & CROSSGROVE, J. S. 2004. Manganese toxicokinetics at the blood-brain barrier. *Research Report (Health Effects Institute)*, 7-58; discussion 59-73.

YOON, H., KIM, D.-S., LEE, G.-H., KIM, K.-W., KIM, H.-R. & CHAE, H.-J. 2011. Apoptosis induced by manganese on neuronal SK-N-MC cell line: endoplasmic reticulum (ER) stress and mitochondria dysfunction. *Environmental health and toxicology*, 26.

YOSHIDA, J.-I., SUGA, S., SUZUKI, S., KINOMURA, N., YAMAMOTO, A. & FUJIWARA, K. 1999. Direct Oxidative Carbon-Carbon Bond Formation Using the "Cation Pool" Method. 1. Generation of Iminium Cation Pools and Their Reaction with Carbon Nucleophiles. *Journal of the American Chemical Society*, 121, 9546-9549.

YUAN, P., WANG, L., WEI, D., ZHANG, J., JIA, Z., LI, Q., LE, X., WANG, H., YAO, J. & XIE, K. 2007. Therapeutic inhibition of Sp1 expression in growing tumors by mithramycin a correlates directly with potent antiangiogenic effects on human pancreatic cancer. *Cancer*, 110, 2682-90.

**Z**DARLOVA, A., MALIKOVA, J., DVORAK, Z., ULRICHOVA, J. & SIMANEK, V. 1997. Quaternary isoquinoline alkaloids sanguinarine and chelerythrine. In vitro and in vivo effects. *Feedback*, 91, 30-41.

ZHANG, M., MATHUR, A., ZHANG, Y., XI, S., ATAY, S., HONG, J. A., DATRICE, N., UPHAM, T., KEMP, C. D. & RIPLEY, R. T. 2012. Mithramycin Represses Basal and Cigarette Smoke-Induced Expression of ABCG2 and Inhibits Stem Cell Signaling in Lung and Esophageal Cancer Cells. *Cancer research*, 72, 4178-4192.

ZHANG, Z. F., GUO, Y., ZHANG, J. B. & WEI, X. H. 2011. Induction of apoptosis by chelerythrine chloride through mitochondrial pathway and Bcl-2 family proteins in human hepatoma SMMC-7721 cell. *Arch Pharm Res*, 34, 791-800.

ZHENG, J., DOMSIC, J. F., CABELLI, D., MCKENNA, R. & SILVERMAN, D. N. 2007. Structural and kinetic study of differences between human and Escherichia coli manganese superoxide dismutases. *Biochemistry*, 46, 14830-14837.

---